

Imperial College London

Calculation of the free energy of crystalline solids

Manolis Vasileiadis

A thesis submitted for the Doctor of Philosophy degree of Imperial College London and for
the Diploma of Imperial College

Centre for Process Systems Engineering
Department of Chemical Engineering
Imperial College London
London SW7 2AZ
United Kingdom

28th of November 2013

Abstract

The prediction of the packing of molecules into crystalline phases is a key step in understanding the properties of solids. Of particular interest is the phenomenon of *polymorphism*, which refers to the ability of one compound to form crystals with different structures, which have identical chemical properties, but whose physical properties may vary tremendously. Consequently the control of the polymorphic behavior of a compound is of scientific interest and also of immense industrial importance. Over the last decades there has been growing interest in the development of crystal structure prediction algorithms as a complement and guide to experimental screenings for polymorphs.

The majority of existing crystal structure prediction methodologies is based on the minimization of the static lattice energy. Building on recent advances, such approaches have proved increasingly successful in identifying experimentally observed crystals of organic compounds. However, they do not always predict satisfactorily the relative stability among the many predicted structures they generate. This can partly be attributed to the fact that temperature effects are not accounted for in static calculations. Furthermore, existing approaches are not applicable to enantiotropic crystals, in which relative stability is a function of temperature.

In this thesis, a method for the calculation of the free energy of crystals is developed with the aim to address these issues. To ensure reliable predictions, it is essential to adopt highly accurate molecular models and to carry out an exhaustive search for putative structures. In view of these requirements, the harmonic approximation in lattice dynamics offers a good balance between accuracy and efficiency. In the models adopted, the intra-molecular interactions are calculated using quantum mechanical techniques; the electrostatic inter-molecular interactions are modeled using an *ab-initio* derived multipole expansion; a semi-empirical potential is used for the repulsion/dispersion interactions. Rapidly convergent expressions for the calculation of the conditionally and poorly convergent series that arise in the electrostatic model are derived based on the Ewald summation method.

Using the proposed approach, the phonon frequencies of argon are predicted successfully using a simple model. With a more detailed model, the effects of temperature on the predicted lattice energy landscapes of imidazole and tetracyanoethylene are investigated. The experimental structure of imidazole is

correctly predicted to be the most stable structure up to the melting point. The phase transition that has been reported between the two known polymorphs of tetracyanoethylene is also observed computationally. Furthermore, the predicted phonon frequencies of the monoclinic form of tetracyanoethylene are in good agreement with experimental data. The potential to extend the approach to predict the effect of temperature on crystal structure by minimizing the free energy is also investigated in the case of argon, with very encouraging results.

Declaration

I confirm that the work presented in this thesis is my own. Any information derived from other sources is appropriately referenced.

Manolis Vasileiadis

The copyright of this thesis rests with the author and is made available under a Creative Commons Attribution-Non Commercial-No Derivatives licence. Researchers are free to copy distribute or transmit the thesis on the condition that they attribute it, that they do not use it for commercial purposes and that they do not alter, transform or build upon it. For any reuse or distribution, researchers must make clear to others the licence terms of this work.

Acknowledgments

The past four years have been a unique experience in my life. Without doubt completing this Ph.D. would have not been possible without the support of many people. I am grateful and I would like to thank my supervisors Prof. Claire Adjiman and Prof. Costas Pantelides for their effort and support all these years, the “crystal prediction” team and especially Panos and Andrei, the Molecular Systems Engineering group, my friends Vasilis, Esther, Apostolis, Thomas and Evangelia, my “koumparous” and close friends Xenia and George, their son Leuteris, my parents Michalis and Fotini and my brother Vasilis. Finally I am more than grateful to Eirini, whose multiple contributions to this work and presence in my life are invaluable.

Manolis

Στους γονείς μου, Φωτεινή και Μιχάλη

Contents

Abstract	i
Declaration	iii
Acknowledgments	iv
Contents	vi
List of tables	ix
List of figures	xi
1. Introduction	1
1.1. Polymorphism	1
1.2. Scope and outline	4
2. Crystals and free energy	6
2.1. Structure and classifications of crystals	6
2.2. Free energy—Definition	7
2.3. Challenges in the calculation of the free energy	9
2.4. Methods for the calculation of the free energy	11
2.4.1. Overlap methods	11
2.4.2. Thermodynamic integration	15
2.4.3. Expanded ensemble methods	23
2.4.4. Other methods	23
3. Lattice dynamics	25
3.1. Harmonic approximation	25
3.2. Assumptions and necessary conditions	30
3.3. The permissible wave vectors	32
3.4. Normal modes & dispersion curves	34
3.5. Calculation of the free energy	35
3.6. The density of vibrational states	40
3.7. Evaluation of the free energy expression	41

3.8. The quasi-harmonic approximation	45
3.9. Applications of lattice dynamics	47
3.9.1. Inorganic crystals	47
3.9.2. Organic molecular crystals	49
4. Molecular models	55
4.1. Intra-molecular interactions	57
4.2. Pairwise additive potentials.....	58
4.2.1. Energy	58
4.2.2. Dynamical matrix.....	62
4.3. Repulsion/dispersion interactions	64
4.4. Electrostatic interactions	66
4.4.1. Electrostatic interactions using distributed multipoles	68
4.4.2. Orientation dependence of distributed multipoles	71
4.4.3. Derivatives of the electrostatic contributions	73
4.5. Summary	74
5. Evaluation of lattice sums.....	75
5.1. The need for a “lattice sum method”	75
5.2. Lattice sum methods.....	77
5.3. Generalized Ewald summation method.....	84
5.3.1. Calculation of the lattice energy of molecular crystals.....	90
5.3.2. Efficient summation scheme for the dynamical matrix	98
5.4. The Γ -point in the reciprocal space sum	107
6. Results	110
6.1. The Lennard-Jones solid; Dispersion curves and density of states	110
6.2. Crystal structure prediction methodology	114
6.2.1. Overview of the approach.....	114
6.2.2. Comparison of crystal structures	115

6.3.	Imidazole	116
6.3.1.	Experimental information	116
6.3.2.	Crystal structure prediction.....	117
6.3.3.	Temperature effects in crystal structure prediction	120
6.4.	Tetracyanoethylene	125
6.4.1.	Experimental information	125
6.4.2.	Crystal structure prediction.....	127
6.4.3.	Calculation of the dispersion curves	129
6.4.4.	Temperature effects in crystal structure prediction	133
6.4.5.	The effect of the molecular model on the lattice energy calculation ...	141
6.5.	Quasi-harmonic free energy minimisation; Argon example revisited	150
7.	Conclusion and Perspectives	153
7.1.	Summary	153
7.2.	Future work	157
	Conference presentations & publication	160
8.	Bibliography	162
	Appendix A—Relations for the $S_{l_i l_j l}^{m_{Ii} m_{Jj}}$ tensor	195
	Appendix B—The term $T_s^2 \left(l_{Ii}, l_{Jj}, m_{Ii}, m_{Jj}, \frac{1}{2} \right)$	199

List of tables

Table 2-1 Summary of the most widely used thermodynamic potentials.....	9
Table 3-1 The coefficients and corresponding abscissas for Gauss-Legendre quadrature. The density of sampling is limited to four nodes per direction.	45
Table 4-1 Summary of all the contributions that are included in the electrostatic interactions, when the multipole expansion is truncated at interactions of fourth order.	71
Table 5-1 The self correction term for the different components of the various contributions to the electrostatic energy gradient (equation 5-31).	99
Table 6-1 Basic characteristics of the unit cell of the two resolved forms of imidazole. Lattice angles α and γ are equal to 90° for all forms at all temperature because of symmetry constraints.	117
Table 6-2 Summary of the lattice energy, rank and the Helmholtz free energy of the α and β forms of imidazole, as function of temperature.	121
Table 6-3 Basic characteristics of the unit cell of the two resolved forms of TCNE. Lattice angles α and γ are equal to 90° for all forms at all temperatures because of symmetry constraints.	126
Table 6-4 The Helmholtz free energy \mathcal{A} and rank of the cubic and monoclinic forms of TCNE, as function of temperature T . The value of the global minimum free energy is presented in the last column for comparison. In the bottom, the lattice energy \bar{U} and rank of the relevant structures are also presented. Quantum mechanical calculations were performed at the HF/6-31G(d,p) level.	135

Table 6-5 Comparison of the unit cells of the two predicted forms of TCNE at M06 and HF level of theory. Lattice angle α is equal to 90° for all forms because of symmetry constraints.	143
Table 6-6 The Helmholtz free energy \mathcal{A} and rank of the cubic and monoclinic forms of TCNE, as function of temperature T . The value of the global minimum free energy is presented in the last column for comparison. In the bottom, the lattice energy \bar{U} and rank of the relevant structures are also presented. Quantum mechanical calculations were performed at the M06/6-31G(d,p) level.	144
Table 8-1 The self correction term for the different components of the contributions up to second order to the electrostatic energy hessian (equation 5-34).	201
Table 8-2 The self correction term for the different components of the contributions from the third order to the electrostatic energy hessian (equation 5-34).	202

List of figures

Figure 1-1 Two views of the crystal of α -glycine (Marsh, 1958), with the unit cell indicated by a box	1
Figure 1-2 The chemical diagram and unit cell of (a) paracetamol and (b) ibuprofen, two widely known pharmaceuticals.....	3
Figure 5-1 (a) The chemical diagram of tetracyanoethylene and (b) the experimental unit cell of the monoclinic form at 298K.....	93
Figure 5-2 The value of the charge-charge contribution to the electrostatic energy of the calculated monoclinic form of tetracyanoethylene, as a function of the Ewald convergence parameter. The direct space sum, the reciprocal space sum, the molecular correction, and the self correction are also presented. Distributed multipoles were derived at the M06/6-31G(d,p) level.	94
Figure 5-3 The value of the charge-dipole contribution to the electrostatic energy of the calculated monoclinic form of tetracyanoethylene, as function of the Ewald convergence parameter. The direct space sum, the reciprocal space sum, and the molecular correction are also presented. Distributed multipoles were derived at the M06/6-31G(d,p) level.	95
Figure 5-4 The value of the charge-quadrupole contribution to the electrostatic energy of the calculated monoclinic form of tetracyanoethylene, as function of the Ewald convergence parameter. The direct space sum, the reciprocal space sum, and the molecular correction are also presented. Distributed multipoles were derived at the M06/6-31G(d,p) level.	96
Figure 5-5 The value of the dipole-dipole contribution to the electrostatic energy of the calculated monoclinic form of tetracyanoethylene, as function of the Ewald convergence parameter. The direct space sum, the reciprocal space sum, and the molecular correction are also presented. Distributed multipoles were derived at the M06/6-31G(d,p) level.	97

Figure 5-6 (a) The $\widehat{\mathbf{D}}_{13,12}$ element of the dynamical matrix is related the interaction of the red atom ($Ii = 13$) with the $Jj = 12$ atom and its periodic images (green). (b) The $\widehat{\mathbf{D}}_{11,11}$ element of the dynamical matrix is related to the self-interaction of the green atoms ($Ii, Jj = 11$)	101
Figure 5-7 The value of the component (0,1s) of the charge-dipole contribution to the element (x, x) of matrix $\widehat{\mathbf{D}}_{13,12}$ (defined in equation 4-22, page 63), for $\mathbf{k} = (0.2, 0, 0)$ as function of the Ewald convergence parameter α . The calculation is performed for the predicted structure that corresponds to the monoclinic form of tetracyanoethyelene (see section 6.4.2). The quantum mechanical calculations were performed at the M06/6-31G(d,p) level. The direct space sum and the reciprocal space sum are also shown.	103
Figure 5-8 A projection onto the complex plane of the dynamical matrix element shown in Figure 5-7. The correction term and the direct and reciprocal space sums are also shown.....	104
Figure 5-9 The value of the component (0,2c) of the charge-quadruple contribution to the element (x, x) of matrix $\widehat{\mathbf{D}}_{11,11}$ (defined in equation (4-22), page 63), for $\mathbf{k} = (0.2, 0, 0)$ as a function of the Ewald convergence parameter α . The calculation is performed for the predicted structure that corresponds to the monoclinic form of tetracyanoethyelene (see section 6.4.2). The quantum mechanical calculations were performed at the M06/6-31G(d,p) level. The direct space sum and the reciprocal space sum are also shown.	105
Figure 5-10 A projection onto the plane defined by the real part of the dynamical matrix element shown in Figure 5-9, and the α parameter. The correction term and the direct and reciprocal space sums are also shown.....	106
Figure 6-1 Dispersion curves of Argon when the wave vectors vary along three directions $(\xi, 0, 0)$, $(\xi, \xi, 0)$, and (ξ, ξ, ξ) , as a function of the reduced wave vector coordinate ξ . The dots are the calculated points, while the triangles are experimental data (Fujii et al., 1974).....	112

Figure 6-2 (a) Normalized density of vibrational sates as a function of frequency; (b) a close-up of the normalized density of states in the low frequency region. A quadratic trend curve is also fitted to the low frequency region and shown in red.....	113
Figure 6-3 The molecular diagram of imidazole.	116
Figure 6-4 Visualisation of the experimental unit cells of the two forms of imidazole a) the unit cell of the α -form at 103 K and ambient pressure (McMullan et al., 1979) ; b) the unit cell of the β -form at 298K and 0.8GPa (Paliwoda et al., 2012).	117
Figure 6-5 Final lattice energy landscape of imidazole. Red dot and diamond represent the experimentally known α and β forms. Quantum mechanical calculations were performed at M06/6-31G(d,p) level.....	119
Figure 6-6 Overlay between the predicted (green) and experimental (coloured by element) forms of imidazole. a) the α -form, with $rms_{15}=0.133\text{\AA}$, b) the β -form, with $rms_{15}=0.425\text{\AA}$. Quantum mechanical calculations were performed at the M06/6-31G(d,p) level.. ..	119
Figure 6-7 The Helmholtz free energy landscape of imidazole at (a) 0 K ; (b) 100 K. All necessary quantum mechanical (charge density and geometry) calculations were performed at M06/6-31G(d,p) level. The colour scale describes the difference in the rank of each structure before and after the vibrational contributions are included. ..	122
Figure 6-8 The Helmholtz free energy landscape of imidazole at (a) 200K ; (b) 300K. All necessary quantum mechanical (charge density and geometry) calculations were performed at M06/6-31G(d,p) level. The colour scale describes the difference in the rank of each structure before and after the vibrational contributions are included. ..	123
Figure 6-9 The Helmholtz free energy landscape of imidazole at 350K. All necessary quantum mechanical (charge density and geometry) calculations were performed at M06/6-31G(d,p) level. The colour scale describes the difference in the rank of each structure before and after the vibration contributions are included. ..	124

Figure 6-10 a) The molecular diagram of tetracyanoethylene ; b) A visualisation of the geometry of the isolated molecule of TCNE obtained by quantum mechanical calculations at MP2/6-31G(d,p) level.....	125
Figure 6-11 Visualization of the experimental unit cells of the two forms of tetracyanoethylene. a) the unit cell of the cubic form at 298K (Little et al., 1971); b) the unit cell of the monoclinic form also at 298K (Chaplot et al., 1984).	126
Figure 6-12 Final lattice energy landscape of TCNE. The red dot and diamond represent the monoclinic and cubic experimentally known forms. Quantum mechanical calculation were performed at HF/6-31G(d,p) level.....	128
Figure 6-13 Overlay of the two known experimental forms of TCNE (coloured by element) and the corresponding predicted structures (green). a) the cubic form compares to the experimental with an $r_{ms}^{15}=0.039\text{\AA}$; b) the predicted monoclinic form is different from the experimental by an $r_{ms}^{15}=0.285\text{\AA}$. Quantum mechanical calculations were performed at the HF/6-31G(d,p) level.	129
Figure 6-14 Dispersion curves of TCNE. The three panels correspond to different wave vectors as indicated at the top. The 12 lowest energy branches represent the external modes of vibration while the remaining branches represent the internal modes.....	131
Figure 6-15 Comparison of the 8 experimentally determined lowest frequency modes of vibration of TCNE (in red) with the corresponding calculated modes (in black). The wave vector varies along directions $(\xi, 0, 0)$, $(0, \xi, 0)$ and $(0, 0, \xi)$	132
Figure 6-16 Comparison of the 4 experimentally determined highest frequency external modes of vibration of TCNE (in red) with the corresponding calculated modes (in black). The wave vector varies along directions $(\xi, 0, 0)$, $(0, \xi, 0)$ and $(0, 0, \xi)$	133

Figure 6-17 The Helmholtz free energy landscape of tetracyanoethylene at (a) 0 K ; (b) 50 K. All necessary quantum mechanical (charge density and geometry) calculations were performed at HF/6-31G(d,p) level. The colour scale describes the difference in the rank of each structure before and after the vibrational contributions are included.....	136
Figure 6-18 The Helmholtz free energy landscape of tetracyanoethylene at (a) 100 K ; (b) 200 K. All necessary quantum mechanical (charge density and geometry) calculations were performed at HF/6-31G(d,p) level. The colour scale describes the difference in the rank of each structure before and after the vibrational contributions are included.....	137
Figure 6-19 The Helmholtz free energy landscape of tetracyanoethylene at (a) 300 K ; (b) 400 K. All necessary quantum mechanical (charge density and geometry) calculations were performed at HF/6-31G(d,p) level. The colour scale describes the difference in the rank of each structure before and after the vibrational contributions are included.....	138
Figure 6-20 The Helmholtz free energy landscape of tetracyanoethylene at (a) 450 K (b) 500 K. All necessary quantum mechanical (charge density and geometry) calculations were performed at HF/6-31G(d,p) level. The colour scale describes the difference in the rank of each structure before and after the vibrational contributions are included.....	139
Figure 6-21 The free energy difference between the cubic and monoclinic forms of TCNE as function of temperature. The red dashed line is a linear interpolation of the free energy difference in the region of temperatures between 60K and the melting point. The transition temperature is obtained as the solution of the equation on the plot, setting y to 0.....	140
Figure 6-22 The free energy difference between the structure that corresponds to the monoclinic form and structure #24 as a function of temperature. The red dashed line is a linear interpolation of the free energy difference in the region of temperatures	

between 60K and the melting point. The transition temperature is obtained as solution of the equation on the plot setting y to 0.....	140
Figure 6-23 Overlay of the predicted and experimental forms of TCNE. a) the cubic form matches the experimental with an $\text{rms}_{15}=0.103\text{\AA}$, b) the predicted monoclinic form matches the experimental form with an $\text{rms}_{15}=0.299\text{\AA}$. Quantum mechanical calculations were performed at the M06/6-31G(d,p) level of theory.	142
Figure 6-24 Final lattice energy landscape of TCNE. Red dot and diamond represent the monoclinic and cubic experimentally known forms. Quantum mechanical calculation were performed at M06/6-31G(d,p) level.	142
Figure 6-25 Dispersion curves of TCNE. The 12 lowest energy branches represent the external modes of vibration while the remaining branches represent the internal modes. Quantum mechanical calculations were performed at the M06/6-31G(d,p) level of theory.	145
Figure 6-26 Comparison of the 8 experimentally determined lowest frequency modes of vibration of TCNE (in red) with the corresponding calculated modes (in black). The wave vector varies along directions $(\xi, 0, 0)$, $(0, \xi, 0)$ and $(0, 0, \xi)$. Calculations were carried out at the M06/6-31G(d,p) level of theory	146
Figure 6-27 Comparison of the 4 experimentally determined highest frequency external modes of vibration of TCNE (in red) with the corresponding calculated modes (in black). The wave vector varies along directions $(\xi, 0, 0)$, $(0, \xi, 0)$ and $(0, 0, \xi)$. Calculations were carried out at the M06/6-31G(d,p) level of theory.....	147
Figure 6-28 The Helmholtz free energy landscape of tetracyanoethylene at (a) 0 K ; (b) 100 K. All necessary quantum mechanical (charge density and geometry) calculations were performed at M06/6-31G(d,p) level. The colour scale describes the difference in the rank of each structure before and after the vibrational contributions are included.....	148

Figure 6-29 The Helmholtz free energy landscape of tetracyanoethylene at (a) 200 K ; (b) 300 K. All necessary quantum mechanical (charge density and geometry) calculations were performed at M06/6-31G(d,p) level. The colour scale describes the difference in the rank of each structure before and after the vibration contributions are included.....	149
Figure 6-30 The lattice constant of argon as function of temperature.....	152
Figure 6-31 The thermal expansion coefficient of argon as function of temperature.	152

1. Introduction

1.1. Polymorphism

Solid materials can be either *amorphous* or *crystalline*. Crystals are unique because they exhibit long range spatial order in all directions, in contrast to amorphous solids. An example is shown in Figure 1-1, where the crystal of α -glycine (Marsh, 1958) can be seen. The ordered packing of crystals is a key characteristic that essentially distinguishes the crystalline phases from other types of phases such as liquid and gas. In addition, the ordered packing is the reason why most of the physical properties of crystalline solids are anisotropic, i.e., depend on direction. The other major states (liquids and gases), with the notable exception of liquid crystals which exhibit a degree of order, have an isotropic structure and thus also have isotropic properties.

A phenomenon related to the crystalline state is *polymorphism*. This term describes the ability of any compound, inorganic or organic, to arrange itself in more than one crystal structure; these different structures are referred to as the *polymorphs* of the compound. The most common and one of the earliest examples of

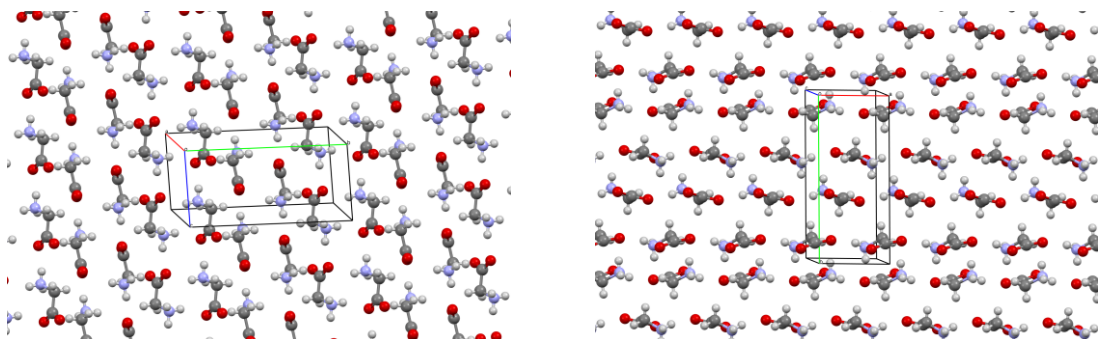


Figure 1-1 Two views of the crystal of α -glycine (Marsh, 1958), with the unit cell indicated by a box.

polymorphism, dating back to the early 19th century, is the discovery of the existence of two allotropic forms of carbon, diamond and graphite (McCrone, 1965). The importance, industrial and academic, of polymorphism arises from the fact that different polymorphs have different physical properties. For example the melting point of diamond is close to 3900°C, while graphite disintegrates above 700°C. Furthermore, graphite is an electric conductor along a specific direction, while diamond is not. As McCrone noted in a widely quoted statement (McCrone, 1965):

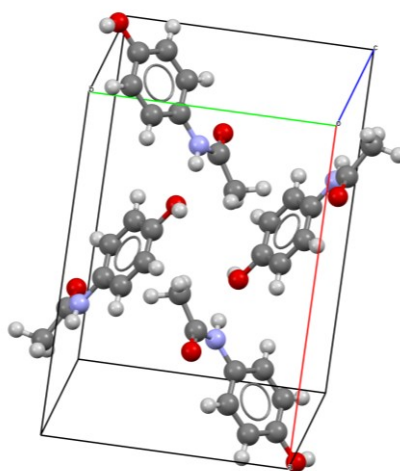
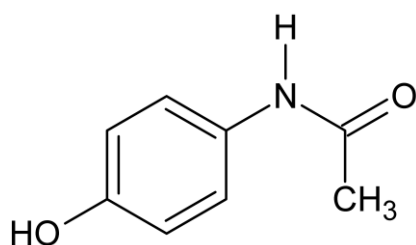
“It is at least this author’s opinion that every compound has different polymorphic forms and that, in general the number of forms known for a given compound is proportional to the time and money spent in research on that compound.”

I believe the following is an equally important and instructive phrase in McCrone’s (1965) text:

“...different polymorphs of a given compound are, in general, as different in structure and properties as the crystals of two different compounds...”

Many solid state industrial products such as agrochemicals and pharmaceuticals are produced in crystalline form. Pharmaceuticals such as paracetamol (Figure 1-2, a) or ibuprofen (Figure 1-2, b) are common examples of organic molecular crystals of industrial relevance. The understanding of the dependence of the properties of the product on its structure is key for the design and manufacturing of crystalline products. The implications of polymorphism in pharmaceutical development have been described by many authors (Campeta et al., 2010; Chekal et al., 2009; Hilfiker 2006). The most notorious example of the impact of polymorphism in the production of pharmaceuticals is that of ritonavir (Chemburkar et al, 2000; Bauer et al., 2001), a novel anti-HIV drug developed by Abbott Laboratories, for which a more stable polymorph appeared years after the start of production. The new form was much less soluble, and much more stable. The significantly different solubility required a new design for both product formulation and production. This incident threatened the supply of the drug to patients. There are also other examples of the appearance of a new polymorph during the late stage of drug development (Desikan et al. 2005), albeit with less impact on drug development and production.

(a)



(b)

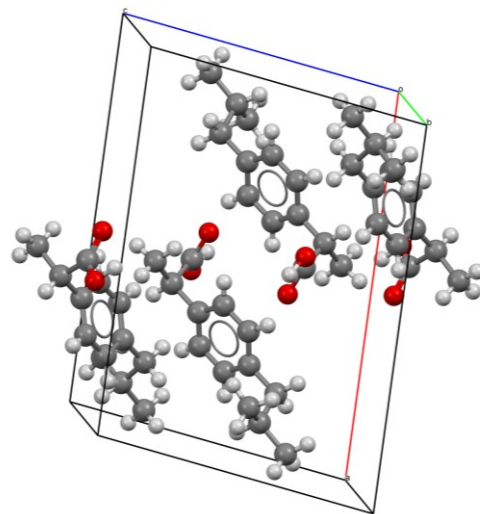
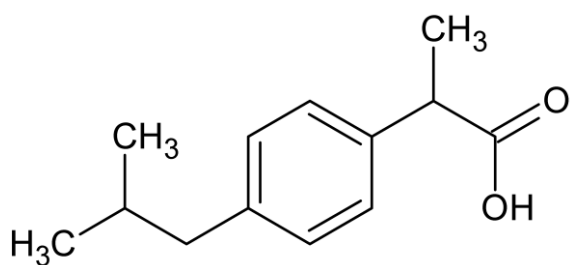


Figure 1-2 The chemical diagram and unit cell of (a) paracetamol and (b) ibuprofen, two widely known pharmaceuticals.

It is evident that the control and prediction of the polymorphic landscape, i.e. the relative stability of different polymorphs, is not only academically interesting, but is also crucial for industry. The exploration of the polymorphic landscape is usually done through experimental screening for polymorphs. Unfortunately this task, in addition to being costly, cannot guarantee that all polymorphs (stable and metastable) have been found, nor that the thermodynamically most stable polymorph for a given compound for given temperature and pressure conditions is known. Therefore there has been a growing interest in the development of *crystal structure prediction*

techniques as a tool complementary to the experimental screening for polymorphs. In *crystal structure prediction* the aim is to identify all (stable and metastable) polymorphs into which a compound may crystallise. The determination of the relative thermodynamic stability of the polymorphs of the compound is also required as part of the investigation of the polymorphic landscape.

1.2. Scope and outline

The vast majority of the methods that aim to tackle the problem of crystal structure prediction are based on static lattice energy minimisation algorithms (Day, 2011; Price 2008). Based on these algorithms, it is in general possible to predict the structure of small molecules with limited flexibility (Bardwell et al., 2010; Day et al., 2005, 2009; Motherwell et al. 2002; Lommerse et al. 2000). Furthermore recent advances, mainly in the handling of flexibility (Kazantsev et al., 2010, 2011:a), have allowed the successful prediction of the crystal of a large flexible molecule that resembles those of pharmaceutical interest (Bardwell et al., 2010; Kazantsev et al., 2011:b). Despite their success the applicability of these algorithms is limited to monotropically-related polymorphs. The relative stability of enantiotropically-related polymorphs is a function of temperature (McCrone, 1965), and therefore they cannot be studied by consideration of the lattice energy only, as this restricts the calculations to 0 K.

In this thesis a method for the calculation of the free energy of crystal structures is presented, and integrated into a lattice energy based crystal structure prediction technique. The purpose of the work is to design a methodology that would allow the prediction of the thermodynamically stable crystal structure as function of temperature without dependence on experimentally available structures for the compound of interest.

Some fundamentals of crystallography and a brief survey of the most widely used free energy methods are presented in chapter 2. In chapter 3 the calculation of the free energy using the method of lattice dynamics under harmonic approximation is described in detail. Furthermore useful concepts of the dynamical theory of crystal lattices are introduced.

The molecular models adopted in the calculations involved in this thesis are presented in chapter 4. The modeling approach is chosen as a compromise between the conflicting requirements of high accuracy and reasonable computational cost.

When static or dynamical calculations are performed in crystals usually one encounters the problem of the evaluation of lattice sums, i.e. infinite summations over all the unit cells of the crystal. In chapter 5 a method based on the Ewald summation technique is developed to perform the necessary lattice sums.

Lattice dynamics and free energy calculations are performed on computationally generated crystals including argon and two small rigid organic molecules, imidazole and tetracyanoethylene. The crystal structures are generated by the CrystalPredictor algorithm and, for the organic molecules, ranked using the more sophisticated electrostatic models in the DMACRYS package. Furthermore the free energy of the fcc crystal of argon is minimised at various temperatures from 0 K to 84 K. The results of these calculations are presented in chapter 6.

Finally some concluding remarks are presented in chapter 7. Directions for future work are also suggested.

2. Crystals and free energy

2.1. Structure and classifications of crystals

The structure of crystals is periodic, allowing their description by means of a unit cell, usually defined by three lattice vectors (or equivalently by three lattice lengths and three lattice angles), the number of molecules in the unit cell, and the positions of all the atoms in the cell. By translation of the unit cell along the three lattice vectors, it is possible to obtain the coordinates of all the remaining atoms in the crystal. The unit cell for α -glycine is shown as a box in Figure 1-1. The atomic positions within the unit cell can be defined in many equivalent ways; this has been extensively discussed elsewhere (Karamertzanis, 2004).

In crystallography crystals are categorized based on the symmetry properties they exhibit. Here I briefly describe those terms that are useful for the purpose of this thesis. More detailed information on the subject of symmetry can be found in several textbooks e.g. (McWeeny, 1963). There are two kinds of symmetry properties. In the first kind are operations that leave only one point of the crystal unmoved. Such symmetry operations are the so-called *proper and improper* rotations, which form groups that are commonly known as *point groups*. Reflection and inversion are special cases of improper rotations. The other kind of symmetry operations that is found in crystals does not leave any point of the crystal at its original position. Those are *translations* along the three vectors that define the crystal lattice. Sets that are composed of point group operations and translations are called *space groups*. Space groups can describe fully the symmetry properties of crystalline solids, and therefore crystals are classified based on their space group. One important concept is that of the

symmetry element, which should not be confused with the symmetry operation. The symmetry element is the “reference” with respect to which a symmetry operation is defined. For example if rotation is performed about the y-axis, the y-axis is the symmetry element. Another example of a symmetry element is the point with respect to which an inversion is performed.

The symmetry operations that form a point group within a space group must be compatible with each other. For example the rotations that compose a point group must be such that, when an operation is performed, the symmetry elements of the object must be transformed into new symmetry elements. As a result, only 32 of the possible point groups can be sub-groups of a space group as a consequence of the presence of translational symmetry. Each of these point groups defines a *crystal class*. Each of the crystal classes may belong to one of the 7 *crystal systems* and one of the 14 *Bravais lattices*. The term “crystal system” is defined by the point group associated with the empty lattice of a crystal if it is described by a primitive unit cell (i.e. only one point is included in each unit cell). There are seven point groups that are compatible with an empty lattice and they define the following crystal systems: cubic, tetragonal, hexagonal, rhombohedral, orthorhombic, monoclinic, and triclinic. The 14 Bravais lattices include the 7 primitive lattices in each crystal system and 7 more lattices described by non-primitive (off-centred) unit cells. The seven non primitive lattices are the body centred cubic (bcc), the face centred cubic (fcc), the body centred rhombohedral, the face centred orthorhombic, the base centred orthorhombic, the body centred orthorhombic, and the base centred monoclinic. In general not all 32 point groups defining a crystal class are compatible with every one of the 14 Bravais lattices. As a result it can be proven that only 230 space groups can be formed.

2.2. Free energy—Definition

The general framework of chemical thermodynamics can be used to describe any system by means of the so-called characteristic function:

$$dU = TdS - PdV + \sum_{i=1}^N \mu_i dn_i \quad (2-1)$$

Equation (2-1) gives the internal energy, U , of a system of N components as function of the entropy S , volume V and the number of particles of each component n_i , its natural variables. T , P and μ_i are the temperature, pressure and chemical potential of component i respectively. They are related to the natural variables of U by:

$$\begin{aligned} T &= \left. \frac{\partial U}{\partial S} \right|_{N,V} \\ -P &= \left. \frac{\partial U}{\partial V} \right|_{S,n_i} \\ \mu_i &= \left. \frac{\partial U}{\partial n_i} \right|_{V,S,n_j \neq n_i} \quad \forall i = 1, \dots, N \end{aligned} \tag{2-2}$$

Although the characteristic function provides information that allows the full description of the system by means of the formalism of the chemical thermodynamics, in most cases this function is not known. For example, the lack of a direct method for the measurement of entropy hinders its use.

As a result it is common practice to work using a *thermodynamic potential* or *fundamental equation* instead of the internal energy (McQuarrie, 2000; Sandler, 1999). A thermodynamic potential is a function that contains all the information included in the characteristic function but whose natural variables are different. The most convenient choice of thermodynamic potential function depends on the application. Thermodynamic potentials are constructed as Legendre transforms of the internal energy (McQuarrie, 2000):

$$\Psi = U - \left. \frac{\partial U}{\partial x} \right|_{x' \neq x} x \tag{2-3}$$

where x and x' represent any of the natural variables of the internal energy and Ψ is the thermodynamic potential obtained. The most widely used thermodynamic potentials are summarized in Table 3-1.

Thermodynamic potential	Symbol	Legendre transform	Natural Variables
Helmholtz free energy	\mathcal{A}	$\mathcal{A}=U-TS$	$N V T$
Enthalpy	H	$H=U-(-P)V$	$N P S$
Gibbs free energy	G	$G=H-TS$	$N P T$
Grand potential	Ω	$\Omega = \mathcal{A} - \sum_{i=1}^N \mu_i n_i$	$V T \mu_i , i = 1, \dots, N$

Table 2-1 Summary of the most widely used thermodynamic potentials.

According to chemical thermodynamics, for a system at equilibrium each thermodynamic potential is minimum when its natural variables have been constrained (Sandler, 1999). If for example the volume, temperature and particle numbers are specified for a closed system then the Helmholtz free energy is at a minimum when the system reaches equilibrium. On the other hand if pressure, temperature and particle numbers are specified the Gibbs free energy is at a minimum when the system reaches equilibrium.

2.3. Challenges in the calculation of the free energy

Statistical mechanics (Hill, 1986; McQuarrie, 2000) provides the formalism for the macroscopic description of a system using information on its microscopic states. The *ensemble* is the core concept of statistical thermodynamics. An ensemble is a virtual collection of a large number of replicas of the system, each one compatible with the macroscopic state of the system being studied. Some of the most common ensembles are the *canonical ensemble* (or $N V T$ ensemble) defined by specification of the number of particles, volume and temperature, the *grand canonical ensemble* (or $V T \mu$ ensemble) where volume, temperature and chemical potential are constrained and the *isothermal isobaric ensemble* (or $N P T$ ensemble), where the macroscopic properties specified are the number of particles, the pressure and the temperature. The number of times each microscopic state is found in an ensemble is proportional to its probability, which is defined by statistical mechanics. Details of the probability distribution in each ensemble can be found in the standard textbooks (Allen &

Tildesley, 1987; Frenkel & Smit, 2002; Hill, 1986; McQuarrie, 2000). The normalization factor of the probability distribution is known as the *partition function*, Q .

In general the free energy, whose natural variables are the defining quantities of a statistical ensemble, is associated with the partition function of the ensemble with an equation of the form (Allen & Tildesley, 1987; Hill, 1986; McQuarrie, 2000):

$$\Psi \sim \ln(Q) \quad (2-4)$$

In the canonical ensemble for example the Helmholtz free energy is given by:

$$\mathcal{A} = -k_B T \ln(Q_{NVT}) \quad (2-5)$$

while the Gibbs free energy is given by:

$$\mathcal{G} = -k_B T \ln(Q_{NPT}) \quad (2-6)$$

where k_B is the Boltzmann constant.

Thus in principle the “absolute” free energy could be calculated with a standard molecular simulation. Unfortunately this is not the case. The canonical partition function for example can be expressed as an ensemble average (Allen & Tildesley, 1987; Lyubartsev et al., 1992):

$$Q_{NVT} \sim \left(\langle e^{\frac{U}{k_B T}} \rangle_{NVT} \right)^{-1}, \quad (2-7)$$

where the notation $\langle \rangle_{NVT}$ indicates a canonical ensemble average, obtained in a Metropolis Monte Carlo or a molecular dynamics simulation (Allen & Tildesley, 1987; Frenkel & Smit, 2002). Since the configuration space is sampled proportionally to the Boltzmann factor:

$$e^{-\frac{U}{k_B T}} \quad (2-8)$$

the quantity $e^{\frac{U}{k_B T}}$ (which is the reciprocal to the Boltzmann factor) in the configurations that are sampled more often is small. In contrast the configurations whose $e^{\frac{U}{k_B T}}$ value is high are only rarely sampled, and therefore the estimate of the average in equation (2-7) would be very poor.

2.4. Methods for the calculation of the free energy

In order to overcome the difficulties in the calculation of the free energy many ingenious algorithms have been designed. Their common characteristic is that they aim to calculate a free energy difference instead of an “absolute” free energy. The various free energy methods are going to be categorized in a way similar to Kofke & Cummings (1998). Three broad categories are identified, (a) the overlap methods (b) the thermodynamic integration methods and (c) the expanded ensemble methods. In this section some of the methods that can be found in the literature and can be potentially used for the calculation of the free energy of a crystal are summarized.

2.4.1. Overlap methods

Zwanzig (1954) proposed the *free energy perturbation* method for the calculation of free energy differences. The method was originally presented as a perturbation theory for the calculation of the thermodynamic properties of a system. The free energy difference between two systems “0” (the reference) and “1” (the system of interest) is calculated as:

$$\mathcal{A}_1 - \mathcal{A}_0 = -k_B T \ln \left(\langle e^{-\frac{\Delta U}{k_B T}} \rangle_0 \right) \quad (2-9)$$

where $\Delta U = U_1 - U_0$ and $\langle \cdots \rangle_0$ denotes an average over the ensemble of the reference system. It is important to note that in equation (2-9) the subscripts may be interchanged, having as a consequence the requirement of sampling the distribution of system “1”.

The calculation of the free energy by means of equation (2-9) is often very difficult. Free energy perturbation offers an efficient calculation method for the free energy if the important region of the configuration space of the reference system and the system of interest overlap sufficiently (Allen & Tildesley, 1987; Frenkel & Smit, 2002). A method that was proposed in order to tackle this problem is *umbrella sampling* (Torrie & Valleau, 1974, 1976; Valleau & Card, 1972). In umbrella sampling, a calculation of the free energy is performed via an average $\langle \dots \rangle_w$ according to a distribution modified by a weighting function w . The bias introduced is then removed and the calculation of the free energy is performed as:

$$\mathcal{A}_1 - \mathcal{A}_0 = -k_B T \ln \left(\frac{\langle e^{-\frac{\Delta U}{k_B T}} w^{-1} \rangle_w}{\langle w^{-1} \rangle_w} \right) \quad (2-10)$$

The modified distribution is necessary to have a “bridging” property i.e. to overlap (almost completely) with both the distributions of the systems “0” and “1”. It is adjusted so that it is nearly uniform. Umbrella sampling can also be applied in a multistage fashion (Valleau & Card, 1972).

Bennett in 1976 proposed the *acceptance ratio method* in order to overcome the difficulties associated with the calculation of the free energy differences. He wrote the ratio of the configurational integral of the two systems “0” and “1” as:

$$\mathcal{A}_1 - \mathcal{A}_0 = -k_B T \ln \left(\frac{\langle e^{-\frac{U_1}{k_B T}} w \rangle_0}{\langle e^{-\frac{U_0}{k_B T}} w \rangle_1} \right) \quad (2-11)$$

and determined the weighting function w that minimizes the variance of the free energy calculation. The functional form of the optimal w comprises a parameter, C , that has the physical significance of a shift of the potential energy. The determination of the optimal parameter C is done in a self-consistent, iterative, way. Note that in contrast to umbrella sampling, the acceptance ratio method requires the performance of two simulations for the estimation of the free energy difference.

In the same paper (Bennett, 1976) the *interpolation or curve fitting method* is also presented. In this method during the two Monte Carlo runs necessary for the

evaluation of (2-11) the histograms $h_0(\Delta U)$ and $h_1(\Delta U)$ are stored. These show the probability of generating microstates with energy difference ΔU when sampling the Boltzmann distributions of systems “0” and “1” respectively. Nearly identical polynomials are then fitted to both histograms, with the only difference being the constant terms. The free energy is then estimated as the difference of the constant terms. The method of Bennett is also found in literature under the name *overlapping distribution method* (Frenkel & Smit, 2002). Bennett uses the term “*overlap methods*” to describe all the methods mentioned so far in this section as a general category within free energy methods.

Kofke and co-workers (Kofke & Cummings, 1997, 1998; Lu & Kofke, 1999) adopted a different point of view from the previously mentioned methods. They pointed out the similarities between them and classified umbrella sampling and acceptance ratio methods as *staged versions* of the free energy perturbation method, where an intermediate system is used to facilitate the calculation. They also suggested that it is more efficient to adopt a free energy method where sampling is performed according to the distribution of the higher entropy system. The authors call this approach sampling in the “insertion” direction by analogy to Widom’s test particle insertion method (Widom, 1963). When the distribution of the lower entropy system is sampled they refer to sampling in the “deletion” direction. Based on this way of thinking they also proposed two analogous schemes for the calculation of the free energy, namely *staged deletion* (or *annihilation*) and *staged insertion*. In the former scheme, the energy difference is obtained as:

$$\mathcal{A}_1 - \mathcal{A}_0 = -k_B T \ln \left(\frac{1}{\langle e^{\frac{\Delta U}{k_B T}} w \rangle_1 \langle w^{-1} \rangle_w} \right) \quad (2-12)$$

where “1” is assumed to be the system of lower entropy and in *staged insertion*, it is given by:

$$\mathcal{A}_1 - \mathcal{A}_0 = -k_B T \ln \left(\langle e^{-\frac{\Delta U}{k_B T}} w^{-1} \rangle_w \langle w \rangle_0 \right) \quad (2-13)$$

Tan et al. (2010) proposed a method for the calculation of the free energy of crystalline solids using the overlap sampling methods described before. The reference system is chosen to be the solid with harmonically coupled particles (as in the harmonic approximation which will be described in chapter 3), with a constrained centre of mass. The system of interest is linked to the reference via a path passing thorough (a) the crystal of interest, (b) the crystal of interest with a constrained centre of mass, and (c) the harmonic crystal with a constrained centre of mass. The free energy of the system of interest is expressed as:

$$\frac{\widehat{\mathcal{A}}_1}{k_B T} = \frac{\widehat{\mathcal{A}}_{CM}^{harm}}{k_B T} + \frac{\Delta\widehat{\mathcal{A}}_{CM}}{k_B T} - \frac{3}{2} \frac{\ln(N)}{N} + \frac{\ln(\rho)}{N} \quad (2-14)$$

N is number of atoms in the crystal, ρ is the number density, $\widehat{\mathcal{A}}_{CM}^{harm}$ is the free energy of the harmonic solid with constrained centre of mass (reference), and $\Delta\widehat{\mathcal{A}}_{CM}$ is the free energy difference between the reference, and the solid of interest with a constrained centre of mass. The last two terms in equation (2-14) are the free energy difference between the centre of mass constrained and the unconstrained crystal of interest. The free energy of the harmonic solid is known analytically:

$$\frac{\widehat{\mathcal{A}}_{CM}^{harm}}{k_B T} = \frac{\widehat{U}_{latt}}{k_B T} + \frac{k_B T}{2N} \sum_{i=1}^{3N-3} \ln\left(\frac{\lambda_i}{2\pi k_B T}\right) \quad (2-15)$$

In Equation (2-15) the classical description of the harmonic oscillator is used. The λ_i 's are the eigenvalues of the “force constant matrix”. The force constant matrix is obtained in two ways (Tan et al., 2010). It is either the Hessian matrix of the potential energy, a choice that the authors describe as “derivative based (DB) harmonic system”, or the second order correlation matrix of the displacements obtained during an ordinary Monte Carlo simulation. The last approach is referred to as “correlation based” (CB). The term $\Delta\widehat{\mathcal{A}}_{CM}$ is then calculated using the acceptance ratio method of Bennett or the umbrella sampling method.

Multiple histogram reweighting (MHR) of Ferrenberg and Swendsen (1988, 1989) is a method closely related to the acceptance ratio method of Bennet. Essentially the method is a way to combine information from different simulations at

more than two state points so that the free energy difference between any two points can be calculated. In the limit of two simulations (two different state points) this method reduces to the acceptance ratio method. The method was originally used in MC simulations in the canonical ensemble. The method has also been used in Grand canonical Monte Carlo (GCMC) simulations of Stockmayer fluids (Kiyohara et al., 1997) and Lennard-Jones fluids (Shi & Johnson, 2001). Conrad & De Pablo (1998) studied a Lennard-Jones fluid and water using MHR within GCMC and isothermal-isobaric Monte Carlo.

Other free energy methods exist, such as the test particle insertion method of Widom (1963), the method of Shing & Gubbins (1982) and its multistage extension (Mon & Griffiths, 1985). These methods depend on inserting a particle in a configuration of the system of interest. Another method whose success depends strongly on successful particle insertions is the *Gibbs ensemble method* of Panagiotopoulos (1987). Theodorou (2006) proposed a general method for the calculation of free energy difference of two systems by establishing a bijective mapping between disjoint subsets of the two configuration spaces. The way to establish this mapping in the general case of two arbitrary systems is not clarified. Furthermore he proposed a realization of the bijective mapping methodology in the special case of the calculation of the chemical potential based on gradual particle insertion/deletion. Particle insertion and deletion procedure is inefficient in dense systems and produce a defective crystal. For these reasons, methods that depend on the insertion/deletion of particles are not appropriate for the calculation of the relative stability of crystalline phases and therefore they are not discussed in detail.

2.4.2. Thermodynamic integration

Thermodynamic integration (Allen & Tildesley, 1987; Frenkel & Smit, 2002) is another class of methods for the calculation of free energy differences. In these methods a mechanical quantity which is a derivative of the free energy is calculated using molecular simulations as an ensemble average. The free energy is then obtained by integration of its derivative. In general we have:

$$\Psi(x_1) = \Psi(x_0) + \int_{x_0}^{x_1} \frac{\partial \Psi}{\partial x} dx \quad (2-16)$$

Of course there is a large number of ways in which this equation can be exploited. Some common options are *integration along an isotherm*:

$$\frac{\widehat{\mathcal{A}}(V_1, T)}{k_B T} = \frac{\widehat{\mathcal{A}}(V_0, T)}{k_B T} + \int_{V_0}^{V_1} \frac{P(V)}{N k_B T} dV \quad (2-17)$$

or *integration along an isochore*:

$$\frac{\widehat{\mathcal{A}}(V, T_1)}{k_B T} = \frac{\widehat{\mathcal{A}}(V, T_0)}{k_B T} + \int_{T_0}^{T_1} \frac{\widehat{U}(T)}{k_B T^2} dT \quad (2-18)$$

The pressure as function of volume, $P(V)$, and potential energy per molecule as function of temperature, $\widehat{U}(T)$, can be calculated as canonical ensemble averages in multiple Monte Carlo or molecular dynamics simulations. The integration of equations (2-17) and (2-18) can then be performed using standard numerical integration techniques, such as the trapezoidal rule or the Gauss-Legendre quadrature. Thermodynamic integration can also be performed *along an isobar*:

$$\frac{\widehat{\mathcal{G}}(T_1, P)}{k_B T} = \frac{\widehat{\mathcal{G}}(T_0, P)}{k_B T} + \int_{T_0}^{T_1} \frac{\widehat{H}(T)}{k_B T^2} dT \quad (2-19)$$

The enthalpy per molecule as a function of temperature is obtained as an average in the isothermal-isobaric ensemble via multiple molecular dynamics or Monte Carlo simulations. The configurational entropy has also been calculated using the same method (Herrero & Ramírez, 2013):

$$\frac{\hat{S}(T_1, V)}{k_B T} = \frac{\hat{S}(T_0, V)}{k_B T} + \int_{T_0}^{T_1} \frac{\hat{C}_v(T)}{k_B T^2} dT \quad (2-20)$$

Here the heat capacity at constant volume is obtained as a canonical ensemble average of the fluctuations of energy in a molecular simulation.

The main requirement for thermodynamic integration to be performed is that the path connecting the two states, the free energy difference being calculated, is reversible. Consequently no phase transition should occur.

Thermodynamic integration can also be performed along a path connecting two different systems in the same state, and is known as *integration along a Hamiltonian path*. This idea was first introduced by Kirkwood in 1935. In general if both systems can be described by a Hamiltonian containing a parameter $\lambda \in [0,1]$, the extreme values of which define each system, the free energy difference between the two systems can be obtained as:

$$\hat{\mathcal{A}}(V, T, \lambda = 1) = \hat{\mathcal{A}}(V, T, \lambda = 0) + \int_0^1 \langle \frac{\partial U_\lambda}{\partial \lambda} \rangle_{NVT\lambda} d\lambda \quad (2-21)$$

The integral of equation (2-21) is also evaluated using standard numerical techniques, for values of the integrand that have been obtained as *NVT* ensemble averages using ordinary simulation techniques for different values of the parameter λ .

To the best of my knowledge Hoover and Ree (1967, 1968) were the first to try to calculate the free energy of solids. Their method is based on the *single occupancy cell* (SOC) model that had been introduced earlier (Kirkwood, 1950) and is essentially an extension of the “cell model” that had been proposed for liquids (Lennard-Jones & Devonshire, 1937). Each particle in the solid is confined to a private cell, and is allowed to collide both with the cell walls and the other particles. A single occupancy system can be extended to arbitrarily low densities without melting. Furthermore, at sufficiently low density, the free energy of the SOC system can be calculated analytically, therefore serving as a reference state for the calculation of the “absolute” free energy of solids. Integration along an isotherm was employed in the work of Hoover and Ree (1967, 1968). The authors also used a similar method for the calculation of the free energy difference between the solid and the liquid phases

by constructing an artificial reversible path between liquid and solid, within a Hamiltonian path thermodynamic integration scheme. Hoover and Ree studied the hard sphere system in this way. The SOC method was later used by other authors together with the histogram reweighting method for the study of the hard sphere system (Nayhouse et al., 2011:a), the Lennard-Jones system (Nayhouse et al., 2011:b) and a system of repulsive particles (Nayhouse et al., 2012)

Thermodynamic integration has also been used to calculate anharmonic effects on the harmonically coupled approximation to the real crystal (Hoover et al., 1970). The free energy difference between the crystal at the state of interest and a state in which harmonic approximation is accurate enough is calculated using thermodynamic integration (equation 2-17). Then the “absolute” free energy at the high density (harmonic) state is calculated analytically using lattice dynamics theory.

The *Einstein Crystal method* (Frenkel & Ladd, 1984; Polson et al., 2000) is another method for the calculation of the free energy of solids via thermodynamic integration. The reference state here is the Einstein crystal in which the atoms do not interact but vibrate around their equilibrium position via harmonic springs (ideal Einstein crystal). Another option could be the interacting Einstein crystal where the atoms are harmonically held around their equilibrium position while interacting with the other atoms of the crystal. The latter option is more appropriate for discontinuous potentials such as the hard sphere model (Frenkel & Ladd, 1984). The free energy of the Einstein crystal is obtained by a correction to the free energy of the interacting Einstein crystal. The method has also been used for ellipsoid particles (Frenkel & Mulder, 2002), and hard dumbbells (Vega et al., 1992).

In the case of continuous potentials (Polson et al., 2000) the ideal Einstein crystal is more appropriate. The “absolute” free energy of the solid of interest is calculated via a path connecting four systems (a) the solid of interest (free energy $\widehat{\mathcal{A}}$), (b) the solid of interest with constrained centre of mass ($\widehat{\mathcal{A}}_{CM}$), (c) the Einstein crystal with constrained centre of mass ($\widehat{\mathcal{A}}_{CM}^{Ein}$) and (d) the unconstrained ideal Einstein crystal ($\widehat{\mathcal{A}}^{Ein}$). The free energy is then obtained as (Polson et al., 2000):

$$\widehat{\mathcal{A}} = (\widehat{\mathcal{A}} - \widehat{\mathcal{A}}_{CM}) + (\widehat{\mathcal{A}}_{CM} - \widehat{\mathcal{A}}_{CM}^{Ein}) + (\widehat{\mathcal{A}}_{CM}^{Ein} - \widehat{\mathcal{A}}^{Ein}) + \widehat{\mathcal{A}}^{Ein} \quad (2-22)$$

Apart from the difference $\widehat{\mathcal{A}}_{CM} - \widehat{\mathcal{A}}_{CM}^{Ein}$ the remaining terms are known analytically. The term $\widehat{\mathcal{A}}_{CM} - \widehat{\mathcal{A}}_{CM}^{Ein}$ is obtained via integration along a Hamiltonian path. The final expression for the free energy in the case of a single component system of N particles is:

$$\frac{\widehat{\mathcal{A}}}{k_B T} = -\frac{3}{2} \ln \left(\frac{4\pi^2 k_B^2 T^2 m}{\alpha} \right) - \frac{1}{2k_B T} \int_0^1 \langle \Delta U \rangle_{\lambda}^{CM} d\lambda - \frac{3}{2N} \ln \left(\frac{\alpha}{2\pi k_B T} \right) - \frac{3 \ln(N)}{2} + \frac{\ln(\rho)}{N} \quad (2-23)$$

where m is the mass of the particles, k_B is the Boltzmann constant, T is temperature, and α is a constant associated with the spring constants of the ideal Einstein crystal. The integral in equation (2-23) is performed by averaging based on the potential energy given by:

$$\tilde{U}(\lambda) = (\lambda - 1)U + \lambda U^{Ein} \quad (2-24)$$

where U is the potential energy of the crystal of interest and U^{Ein} is the potential energy of the Einstein crystal:

$$U^{Ein} = \frac{\alpha}{2} \sum_{i=1}^N (r_i - r_i^0)^2 \quad (2-25)$$

r_i^0 being the equilibrium positions of the particles of the crystal. It is important to note that the centre of mass constraint is adopted so that the integration of equation (2-23) can be performed more efficiently and more accurately. A similar method had been used earlier for the calculation of the absolute free energy of a modified Lennard-Jones crystal (Broughton & Gilmer, 1983). The major difference was that in their method Broughton & Gilmer did not impose the centre of mass constraint but they allowed it to move within a box of 0.05σ (σ being the Lennard-Jones unit of length), with periodic boundary conditions.

The *lattice-coupling expansion method* (Meijer et al., 1990) is a variant of the Einstein crystal method. The reference state here is also the Einstein crystal, but it is reached in two stages, via the intermediate state of the interacting Einstein crystal. Both stages are performed using Hamiltonian thermodynamic integration. In the first stage, the free energy difference between the interacting Einstein crystal and the crystal of interest is calculated. Then, with the aid of another parameter, the solid is expanded to the limit of zero density so that the inter-atomic interactions vanish, and the crystal becomes an Einstein crystal. During these stages the crystal does not melt. Both integrals involved are well-behaved and there is no need for the centre of mass constraint. The method was applied to the crystal of N₂.

Vega and Noya (2007) proposed a modified version of the Einstein crystal method. They called their method *Einstein molecule* to distinguish it from Frenkel & Ladd's method. The Einstein molecule, which is the reference state, is an Einstein crystal in which one the molecules does not vibrate. Furthermore instead of performing simulations with fixed centre of mass, Monte Carlo simulations are performed with a molecule fixed in its position. Vega and Noya demonstrated their method on a hard sphere system.

Later Vega and co-workers (2008) published a review on the methods for the calculation of solid-solid and solid-liquid equilibria with a focus mainly on the Einstein crystal and the Einstein molecule approaches, showing how they can be used for calculations on rigid molecules. The configuration integral of the Einstein crystal is split into two contributions, orientational and translational. The orientational contribution, which depends on the geometry, is calculated numerically, although some analytical expressions exist. The orientational configuration integral of the Einstein molecule is the same as that of the Einstein crystal. Vega et al. computed the free energy difference between the solid of interest with fixed centre of mass and the Einstein crystal with fixed centre of mass in two steps:

$$\widehat{\mathcal{A}}_{CM} - \widehat{\mathcal{A}}_{CM}^{Ein} = \left(\widehat{\mathcal{A}}_{CM} - \widehat{\mathcal{A}}_{CM}^{Ein,sol} \right) + \left(\widehat{\mathcal{A}}_{CM}^{Ein,sol} - \widehat{\mathcal{A}}_{CM}^{Ein} \right) \quad (2-26)$$

where $\widehat{\mathcal{A}}_{CM}^{Ein,sol}$ is the free energy of a system whose particles interact with the true potential of the crystal but where the springs of the Einstein crystal are also present. The free energy difference $\widehat{\mathcal{A}}_{CM}^{Ein,sol} - \widehat{\mathcal{A}}_{CM}^{Ein}$ is calculated using the free energy

perturbation method, while the free energy difference $\widehat{\mathcal{A}}_{CM} - \widehat{\mathcal{A}}_{CM}^{Ein,sol}$ is calculated using Hamiltonian integration.

In the molecular version of the Einstein molecule approach (Vega et al. 2008) a thermodynamic cycle is constructed via (a) the crystal of interest, (b) the crystal of interest with a molecule rigidly fixed to its equilibrium position, (c) the interacting Einstein molecule with a fixed molecule, (d) the ideal Einstein molecule with a molecule fixed at its equilibrium position and finally (e) the ideal Einstein molecule. The free energy of the crystal is then:

$$\widehat{\mathcal{A}} = (\widehat{\mathcal{A}} - \widehat{\mathcal{A}}_f) + (\widehat{\mathcal{A}}_f - \widehat{\mathcal{A}}_f^{Em,sol}) + (\widehat{\mathcal{A}}_f^{Em,sol} - \widehat{\mathcal{A}}_f^{Em}) + (\widehat{\mathcal{A}}_f^{Em} - \widehat{\mathcal{A}}^{Em}) + \widehat{\mathcal{A}}^{Em} \quad (2-27)$$

The subscript “f” indicates that a molecule is fixed in space, the superscript “Em” the Einstein molecule, and finally *Em, sol* indicates the interacting Einstein molecule. All the terms are calculated analytically apart from the differences $(\widehat{\mathcal{A}}_f - \widehat{\mathcal{A}}_f^{EM,sol})$ and $(\widehat{\mathcal{A}}_f^{EM,sol} - \widehat{\mathcal{A}}_f^{EM})$, and the overall expression is

$$\begin{aligned} \widehat{\mathcal{A}} = k_B T & \left\{ \frac{1}{N} \ln \left(\frac{\Lambda^3}{\rho} \right) + \frac{3}{2} \left(1 - \frac{1}{N} \right) \ln \left(\frac{\Lambda^2 \alpha'}{\pi k_B T} \right) - \frac{1}{N} \ln(Q_{ori}^{Em}) + U_{latt} \right. \\ & \left. - k_B T \langle e^{-\frac{U_{sol}-U_{lattice}}{k_B T}} \rangle_{Em} - \int_0^{\alpha'} \frac{\langle U_{Em} \rangle_{NVT\lambda}}{\alpha'} d(\lambda \alpha') \right\} \end{aligned} \quad (2-28)$$

where Λ is the de Broglie thermal wave length: $\frac{\hbar}{\sqrt{2\pi m k_B T}}$, α' is the spring constant of the Einstein molecule, Q_{ori}^{Em} is the orientational partition function of the ideal Einstein molecule. The Einstein molecule approach has been used for the determination of the phase diagram of ice (Noya et al., 2008, Vega et al. 2008). Similar free energy calculations had also been performed earlier for ice by Báez and Clancy (1995:a, 1995:b). They also used a molecular version of the Einstein crystal method, similar to that presented by Vega et al. (2008) but they did not use a centre of mass constraint.

Baele in 2002 proposed the *acoustic crystal thermodynamic integration* method, another variation of the Einstein crystal method in which the reference state is the so-called *acoustic crystal*, in which the atoms vibrate harmonically and are coupled only with their nearest neighbours.

A method for the direct calculation of the free energy difference between the solid and the liquid phases is the *constrained λ -integration* (Grochola, 2004). A three stage thermodynamic cycle is employed in which (a) the liquid is transformed into a weakly attractive fluid, (b) the weakly attractive fluid is constrained to the solid configuration space via the insertion of Gaussian wells distributed in a lattice, and finally (c) the Gaussians are turned off, while simultaneously the true potential of the system is reinstated. The free energy differences between all stages are calculated using thermodynamic integration along a Hamiltonian path, an approach referred by Grochola as λ -integration. During the first stage a contraction of the volume is applied simultaneously with the decrease of the attractive forces. The author clarifies that although such a decrease in volume is necessary since the solid is denser, it needs not be done at the first stage. Grochola used this method in conjunction with linear interpolation in order to determine the solid-liquid coexistence of a truncated and shifted Lennard-Jones system.

Eike et al. (2005) used slightly modified constrained λ -integration method together with multiple histogram reweighting and Gibbs-Duhem integration (Kofke, 1993), to determine the solid-liquid coexistence of a Lennard-Jones solid and NaCl. Eike et al. use the term *pseudosupercritical path* (PSCP) instead of the constrained λ -integration, by analogy to the supercritical paths that allow the transformation of the liquid to the gas without a phase transition to occur. In contrast to Grochola the reduction of the simulation cell volume is performed during the second stage of the integration, a choice that is justified by the allowance of more free space for the particle during the early parts of the second stage. Similar calculations were later performed for the crystals of triazole and benzene (Eike & Maginn 2006). The pseudosupercritical path is further modified here and the volume contraction is performed in a separate stage using integration along an isotherm (equation 2-17). Using this methodology the melting point and relative thermodynamic stability of the orthorhombic and monoclinic polymorphs of a salt have also been calculated (Jayaraman & Maginn, 2007).

2.4.3. Expanded ensemble methods

A set of methods that have also been used for the calculation of free energy differences is the so called *expanded ensemble methods*. Lyubartsev et al. (1992) proposed a Monte Carlo scheme in which an expanded canonical ensemble is sampled. The expanded ensemble is a weighted sum of canonical (sub-)ensembles of the same system but at different temperatures. The expanded ensemble is sampled in a single ordinary Monte Carlo simulation, in which additional “moves” are included so that various temperatures are sampled. In this way the free energy of each temperature can be obtained with reference to one of them. Other expanded ensemble techniques exist such as the augmented grand canonical technique of Kaminsky (1994), or the method of Wilding and Müller (1994) for polymers. Those methods do not seem appropriate for solids as they rely on the insertion and deletion of molecules.

The *lattice-switch method* (Bruce et. al., 1997, 2000) is a Monte Carlo technique that allows direct evaluation of the free energy difference between two crystalline states. The configuration space of both states is visited in a single simulation. This is accomplished by Monte Carlo “moves” that involve the switch of the lattice vectors from those of one crystal to those of the other. When such a move is attempted the position of the atoms relative to the origin of the unit cell they belong to does not change. In order for the lattice-switch moves to be accepted *multicanonical Monte Carlo* (Berg & Neuhaus T, 1992), a biased Monte Carlo technique, is used. The method was used for the calculation of the free energy difference between the two closed packed structures, the face centred cubic (fcc) and the hexagonal closed packed (hcp).

2.4.4. Other methods

The method of *metadynamics* (Laio & Parrinello, 2002) can also be used to estimate the free energy of a crystal (Martoňák et al., 2003). In metadynamics a free energy basin is explored in a steepest-decent fashion. The system is prevented from being confined in the basin by a history-dependent term. The history-dependent term is a superposition of Gaussians accumulated while the procedure evolves. Each Gaussian is constructed at every step of the algorithm and prevents the system from

revisiting configurations already visited. In this way all free energy barriers can be overcome and the hyper-surface is explored. The free energy hyper-surface is then obtained (within an additive constant) by using the penalizing history term. Although in principle the free energy can be estimated by metadynamics that is usually not done (Martoňák et al., 2003). The method has found applications in the study of phase transitions (Karamertzanis et al. 2008; Raiteri et al., 2005)

Finally the free energy of a solid can be calculated using the method of *lattice dynamics* under the so-called *harmonic approximation*. In this method an analytical expression is obtained for the free energy of the crystal by approximating its lattice energy with a quadratic function. The fact that no molecular simulation is required significantly reduces the computational cost. This is a considerable advantage over the other methods for the calculation of the free energy, especially in the context crystal structure prediction where it is necessary to evaluate the free energy of a large number of structures (of the order of hundreds). The approximation is valid for a restricted temperature range, but such an approach should nevertheless provide some useful information on temperature effects. Therefore this method is adopted and a detailed description follows in the next chapter.

3. Lattice dynamics

Lattice dynamics is a method that is commonly used for the calculation of the free energy of a crystal and many other properties. Despite the fact that more accurate an-harmonic methods are known (Dove, 1993; Ghatak & Kothari, 1972), we will study lattice dynamics under the widely used *harmonic approximation*. The advantages of simplicity and low computational cost of the harmonic approximation outclass the slightly improved accuracy of the an-harmonic approach. Another widely used option is the *quasi-harmonic* approximation, in which the local minimum of the free energy is obtained.

In order to obtain an analytical solution for the Newton's equations of motion a quadratic approximation of the true potential of the crystal is adopted. In this way the problem is reformulated into an eigenvalue problem, the solution of which allows the calculation of the frequencies of atomic vibrations. This approach has its roots in the work of Born and von Kàrmàn (1912, 1913). Given this information an analytical expression for the free energy can be obtained. A detailed description of the theory of harmonic and quasi-harmonic approximations follows in subsequent sections. The chapter ends with a brief survey of various applications of the method that can be found in the literature.

3.1. Harmonic approximation

We assume that the crystal has M^3 unit cells in the three directions, where M is sufficiently large that the crystal can be considered infinite, i.e. $M^3 \rightarrow \infty$. The unit cell contains Z molecules. Indices $I, I = 1, \dots, Z$, and $I', I' = 1, \dots, Z$, are used to enumerate the Z molecules in the unit cell. The number of atoms in molecules I and I' are denoted by N_I and $N_{I'}$, respectively. Note that any two molecules in the unit

cell can have different numbers of atoms. The indices $i, i = 1, \dots, N_I$, and $i', i' = 1, \dots, N_{I'}$, to enumerate the atoms in molecules I and I' , respectively. Given an arbitrarily chosen unit cell (the reference unit cell), a set \mathbf{L} of vectors $\mathbf{l}, \mathbf{L} = \{\mathbf{l}\}$, can be defined such that exactly one vector corresponds to every unit cell. This vector indicates the translation operation that allows the coordinates of an arbitrary point in an arbitrary unit cell to be obtained from those of the same point in the reference unit cells. Thus the element of a given vector \mathbf{l} are the integer numbers of lattice vectors that must be added to an arbitrary point in the reference unit cell to obtain the completely equivalent point in the unit cell to which the vector corresponds. It is obvious that the reference unit cell has $\mathbf{l}=(0,0,0)$ and that there are M^3 vectors \mathbf{l} . The configuration of the crystal is defined by means of the atomic coordinates:

$$\mathbf{r} = \{\mathbf{r}_{IIi}, \mathbf{l} \in \mathbf{L}, i = 1, 2, \dots, N_I, I = 1, 2, \dots, Z\}$$

where \mathbf{r}_{IIi} is the position vector of the i^{th} atom of the I^{th} molecule of the \mathbf{l}^{th} unit cell. \mathbf{r}_{IIi} can also be expressed as the sum of the position vector of the origin of the \mathbf{l}^{th} unit cell, \mathbf{r}_l , and the position vector of atom IIi with reference to the origin of the unit cell, \mathbf{r}_{IIi} :

$$\mathbf{r}_{IIi} = \mathbf{r}_l + \mathbf{r}_i$$

The lattice energy, U , of the crystal is a function of the configuration, $U=U(\mathbf{r})$, and can be approximated using a Taylor series expansion around any reference point $\hat{\mathbf{r}}$:

$$\begin{aligned} U(\mathbf{r}) &= U(\hat{\mathbf{r}}) + \sum_{\mathbf{l} \in \mathbf{L}} \sum_{I=1}^Z \sum_{i=1}^{N_I} (\mathbf{r}_{IIi} - \hat{\mathbf{r}}_{IIi})^T \frac{\partial U}{\partial \mathbf{r}_{IIi}} \Big|_{\hat{\mathbf{r}}} \\ &\quad + \frac{1}{2} \sum_{\mathbf{l} \in \mathbf{L}} \sum_{I=1}^Z \sum_{i=1}^{N_I} \sum_{\mathbf{l}' \in \mathbf{L}} \sum_{I'=1}^Z \sum_{i'=1}^{N_{I'}} (\mathbf{r}_{IIi} - \hat{\mathbf{r}}_{IIi})^T \cdot \frac{\partial^2 U}{\partial \mathbf{r}_{IIi} \partial \mathbf{r}_{I'I'i'}} \Big|_{\hat{\mathbf{r}}} \\ &\quad \cdot (\mathbf{r}_{I'I'i'} - \hat{\mathbf{r}}_{I'I'i'}) + H.O.T. \end{aligned} \tag{3-1}$$

where *H.O.T.* denotes the higher-order terms. The Taylor expansion of equation (3-1) is valid for any expansion point $\hat{\mathbf{r}}$. The solution of the lattice dynamics equations within the harmonic approximation requires the expansion point to be a minimum with respect to the lattice energy (equilibrium position). At any such point, the forces on all atoms vanish:

$$\mathbf{F}_{\mathbf{l}ii} = -\frac{\partial U}{\partial \mathbf{r}_{\mathbf{l}ii}} \Big|_{\hat{\mathbf{r}}} = \mathbf{0}, \quad \forall \mathbf{l} \in \mathbf{L}, \quad i = 1, 2, \dots, N_l, \quad l = 1, 2, \dots, Z \quad (3-2)$$

In addition, the higher-order terms of equation (3-1) are also ignored and the lattice energy becomes a quadratic function of the displacement:

$$U(\mathbf{r}) \approx U(\hat{\mathbf{r}}) + \frac{1}{2} \sum_{\mathbf{l} \in \mathbf{L}} \sum_{l=1}^Z \sum_{i=1}^{N_l} \sum_{\mathbf{l}' \in \mathbf{L}} \sum_{l'=1}^Z \sum_{i'=1}^{N_{l'}} \mathbf{u}_{\mathbf{l}ii}^T \frac{\partial^2 U}{\partial \mathbf{r}_{\mathbf{l}ii} \partial \mathbf{r}_{\mathbf{l}'i'i'}} \Big|_{\hat{\mathbf{r}}} \mathbf{u}_{\mathbf{l}'i'i'} \quad (3-3)$$

In equation (3-3), $\mathbf{u}_{\mathbf{l}ii}$ is the displacement of atom ii in \mathbf{l}^{th} unit cell from its equilibrium position: $\mathbf{u}_{\mathbf{l}ii} = \mathbf{r}_{\mathbf{l}ii} - \hat{\mathbf{r}}_{\mathbf{l}ii}$.

The vibration of atoms in the crystal can be modeled with Newton's equations of motion. By substituting equation (3-3) into (3-2) and considering that the derivatives of the lattice energy with respect to atomic positions are equal to its derivatives with respect to the displacement, Newton's equations become:

$$\begin{aligned} m_{ii} \frac{d^2 \mathbf{u}_{\mathbf{l}ii}(\mathbf{t})}{dt^2} &= \mathbf{F}_{\mathbf{l}ii} = -\frac{\partial U}{\partial \mathbf{u}_{\mathbf{l}ii}} \Big|_{\hat{\mathbf{r}}} \\ &= -\sum_{\mathbf{l}' \in \mathbf{L}} \sum_{l'=1}^Z \sum_{i'=1}^{N_{l'}} \frac{\partial^2 U}{\partial \mathbf{u}_{\mathbf{l}ii} \partial \mathbf{u}_{\mathbf{l}'i'i'}} \Big|_{\hat{\mathbf{r}}} \mathbf{u}_{\mathbf{l}'i'i'} \quad \forall \mathbf{l}ii \end{aligned} \quad (3-4)$$

where m_{ii} is the mass of the atom characterized by the indices ii , and the symbol \forall followed by one or more indices implies that each of the indices takes all the permissible values.

The solution of equations (3-4), $\mathbf{u}_{\mathbf{l}ii}(\mathbf{t})$, has the general form of a harmonic wave:

$$\mathbf{u}_{IIi}(\mathbf{t}) = \mathbf{U}_{IIi}(\mathbf{k}) e^{i[\mathbf{k}\hat{\mathbf{r}}_{IIi} - \omega(\mathbf{k})t]} \quad (3-5)$$

where $\mathbf{U}_{IIi}(\mathbf{k})$ is the amplitude vector. This does not depend on \mathbf{l} because the differences in the motion of corresponding atoms in different unit cells are described by the exponential phase factor. $\omega(\mathbf{k})$ is the angular frequency and \mathbf{k} is the wave vector which takes values in the reciprocal space:

$$\begin{aligned} \mathbf{k} &= \xi_a \mathbf{a}^* + \xi_b \mathbf{b}^* + \xi_c \mathbf{c}^*, \quad \xi_a, \xi_b, \xi_c \in \mathbb{R} \\ \mathbf{a}^* &= \frac{2\pi}{V} \mathbf{b} \times \mathbf{c} \quad \mathbf{b}^* = \frac{2\pi}{V} \mathbf{a} \times \mathbf{c} \quad \mathbf{c}^* = \frac{2\pi}{V} \mathbf{a} \times \mathbf{b} \end{aligned} \quad (3-6)$$

where \mathbf{a} , \mathbf{b} and \mathbf{c} are the direct space lattice vectors, \mathbf{a}^* , \mathbf{b}^* and \mathbf{c}^* are the reciprocal lattice vectors, ξ_a, ξ_b, ξ_c are the coordinates of the wave vector, \mathbf{k} , and V is the volume of the unit cell: $V = \mathbf{a} \cdot (\mathbf{b} \times \mathbf{c})$.

Every harmonic wave of equation (3-5) must satisfy Newton's system of equations (3-4):

$$\begin{aligned} m_{IIi} \mathbf{U}_{IIi}(\mathbf{k}) e^{i\mathbf{k}\hat{\mathbf{r}}_{IIi}} e^{-i\omega(\mathbf{k})t} \omega^2(\mathbf{k}) \\ = - \sum_{I' \in \mathbf{L}} \sum_{I'=1}^Z \sum_{i'=1}^{N_{I'}} \frac{\partial^2 U}{\partial \mathbf{u}_{IIi} \partial \mathbf{u}_{I'I'i'}} \Big|_{\hat{\mathbf{r}}} \mathbf{U}_{I'I'i'}(\mathbf{k}) e^{i\mathbf{k}\hat{\mathbf{r}}_{I'I'i'}} e^{-i\omega(\mathbf{k})t} \quad \forall IIi \\ \sqrt{m_{IIi}} \mathbf{U}_{IIi}(\mathbf{k}) \omega^2(\mathbf{k}) \\ = - \frac{1}{\sqrt{m_{IIi} m_{I'I'i'}}} \sum_{I' \in \mathbf{L}} \sum_{I'=1}^Z \sum_{i'=1}^{N_{I'}} \frac{\partial^2 U}{\partial \mathbf{u}_{IIi} \partial \mathbf{u}_{I'I'i'}} \Big|_{\hat{\mathbf{r}}} \sqrt{m_{I'I'i'}} \mathbf{U}_{I'I'i'}(\mathbf{k}) e^{i\mathbf{k}(\hat{\mathbf{r}}_{I'I'i'} - \hat{\mathbf{r}}_{IIi})} \quad \forall IIi \\ \mathbf{e}_{IIi}(\mathbf{k}) \omega^2(\mathbf{k}) \\ = - \frac{1}{\sqrt{m_{IIi} m_{I'I'i'}}} \sum_{I' \in \mathbf{L}} \sum_{I'=1}^Z \sum_{i'=1}^{N_{I'}} \frac{\partial^2 U}{\partial \mathbf{u}_{IIi} \partial \mathbf{u}_{I'I'i'}} \Big|_{\hat{\mathbf{r}}} \mathbf{e}_{I'I'i'}(\mathbf{k}) e^{i\mathbf{k}(\hat{\mathbf{r}}_{I'I'i'} - \hat{\mathbf{r}}_{IIi})} \quad \forall IIi \end{aligned}$$

where the vectors $\mathbf{e}_{IIi}(\mathbf{k})$ are defined such that $\mathbf{e}_{IIi}(\mathbf{k}) = \sqrt{m_{IIi}} \mathbf{U}_{IIi}(\mathbf{k})$. Because of the periodicity of the crystal we can concentrate our attention on the reference unit cell $\mathbf{l}=(0,0,0)$ without any loss of generality:

$$\begin{aligned} & e_{Ii}(\mathbf{k}) \omega^2(\mathbf{k}) \\ &= -\frac{1}{\sqrt{m_{Ii} m_{I'i'}}} \sum_{I' \in \mathbf{L}} \sum_{I'=1}^Z \sum_{i'=1}^{N_{I'}} \frac{\partial^2 U}{\partial \mathbf{u}_{0Ii} \partial \mathbf{u}_{I'i'}} \Big|_{\hat{\mathbf{r}}} e_{I'i'}(\mathbf{k}) e^{i\mathbf{k}(\hat{\mathbf{r}}_{I'i'} - \hat{\mathbf{r}}_{0Ii})} \quad \forall Ii \end{aligned} \quad (3-7)$$

We define the *polarization vectors* $\check{\mathbf{e}}(\mathbf{k}) = [e_1(\mathbf{k}), e_2(\mathbf{k}), \dots, e_N(\mathbf{k})]$ and the symmetrical *dynamical matrix*:

$$\mathbf{D}(\mathbf{k}) = \begin{bmatrix} \mathbf{D}_{11} & \mathbf{D}_{21} & \cdots & \mathbf{D}_{N1} \\ \mathbf{D}_{21} & \mathbf{D}_{22} & \cdots & \mathbf{D}_{2N} \\ \vdots & \vdots & \ddots & \vdots \\ \mathbf{D}_{N1} & \mathbf{D}_{N2} & \cdots & \mathbf{D}_{NN} \end{bmatrix} \quad (3-8)$$

containing an $N \times N$ array of 3×3 blocks, each defined as:

$$\mathbf{D}_{Ii,I'i'}(\mathbf{k}) = -\frac{1}{\sqrt{m_{Ii} m_{I'i'}}} \sum_{I \in \mathbf{L}} \frac{\partial^2 U}{\partial \mathbf{u}_{0Ii} \partial \mathbf{u}_{I'i'}} \Big|_{\hat{\mathbf{r}}} e^{i\mathbf{k}(\hat{\mathbf{r}}_{I'i'} - \hat{\mathbf{r}}_{0Ii})}. \quad (3-9)$$

Then equation (3-7) can be written as:

$$\omega^2(\mathbf{k}) \check{\mathbf{e}}(\mathbf{k}) = \mathbf{D}(\mathbf{k}) \check{\mathbf{e}}(\mathbf{k}) \quad (3-10)$$

This last equation describes an eigenvalue problem. Because the elements $\mathbf{D}_{Ii,I'i'}$ of the dynamical matrix are 3×3 matrices, matrix \mathbf{D} is a $3N \times 3N$ matrix. In addition the elements $e_{Ii}(\mathbf{k})$ of the matrix $\check{\mathbf{e}}(\mathbf{k})$ are 3×1 matrices. Thus each polarization vector has $3N$ elements. As a result there are $3N$ eigenvalues, $\omega^2(\mathbf{k})$, and $3N$ eigenvectors, $\check{\mathbf{e}}(\mathbf{k})$, for the eigenvalue problem defined in equation (3-10).

From equation (3-10), it can be seen that the squares of the angular frequencies $\omega_n^2(\mathbf{k})$ (and hence the vibrational frequencies $\nu_n(\mathbf{k}) = \omega_n(\mathbf{k}) / 2\pi$, $n = 1, \dots, 3N$) and the polarization vectors $\check{\mathbf{e}}_n(\mathbf{k})$ (up to a multiplication constant) can be obtained by diagonalizing the dynamical matrix $\mathbf{D}(\mathbf{k})$. It can be seen readily from equation (3-9) that the dynamical matrix is Hermitian as $\mathbf{D}_{ij} = \mathbf{D}_{ji}^*$ and therefore it has real eigenvalues (positive or negative). Negative eigenvalues of the dynamical matrix imply that the structure is unstable.

It is important to note that if a harmonic wave such as that of equation (3-5) were propagating in a continuous medium, then for every wave vector \mathbf{k} there would be infinite number of compatible angular frequencies $\omega(\mathbf{k})$. The discontinuity of the crystal implicitly results in the restriction of the number of compatible wave vectors, so that only $3N$ such vectors exist. The $3N$ corresponding frequencies are those which allow the compatibility of the harmonic wave equation (3-5) with the $3N$ equations of motion (3-4).

It is interesting to point out that the dynamical matrix is closely related to the force constant matrix used by Tan et al. (2010). The dynamical matrix is the mass weighted force constant matrix of the derivative based harmonic system (section 2.4.1).

3.2. Assumptions and necessary conditions

It is worth stressing that the lattice energy U to which we refer in section 3.1 differs from the lattice energy of a single unit cell \bar{U} which is calculated and minimized in the lattice energy minimisation algorithms for crystal structure prediction in that U is the lattice energy of the whole crystal.

The use of the whole crystal rather than the unit cell is necessary for the calculation of second derivatives in equation (3-9), which must be computed without imposing periodicity during differentiation, because the derivative $\left. \frac{\partial^2 U}{\partial \mathbf{u}_{0i} \partial \mathbf{u}_{I'i'}} \right|_{\hat{\mathbf{r}}}$ involves the displacement of atom Ii in the reference unit cell (cell **0**) and the atom $I'i'$ in unit cell **I** only, i.e., with all other atoms fixed at their equilibrium positions. These gradients differ from the gradients of \bar{U} that are used in lattice energy minimisation algorithms. When calculating the gradients of \bar{U} with respect to the atomic positions of any atom in the reference unit cell, all its periodic images are perturbed. This is because in lattice energy minimisation algorithms the periodic structure with minimum energy is sought.

In principle, the conditions implied by equation (3-2) should be true for all the structures on which lattice dynamics calculations are performed. Unfortunately it is not possible to check directly if this condition is fulfilled because (a) the lattice energy U cannot be calculated since an infinite summation is involved, and (b) condition (3-2)

describes an infinite number of gradients that need to be calculated. The validity of conditions (3-2) is checked in an implicit way, using the (periodic) gradients of \bar{U} .

Three further assumptions are adopted, in keeping with many crystal modeling studies:

1. Our crystal extends from minus infinity to infinity in every direction ($M^3 \rightarrow \infty$). This assumption is justified by the fact that we are interested in bulk properties and consequently we want to avoid surface effects.
2. The crystal is perfect (i.e. there are no defects) and periodic in every direction.
3. The *cyclic (or periodic) boundary condition* (Born & Huang, 1954; Dove, 1993; Ghatak & Kothari, 1972), due to Born and von Kàrmàn (1912, 1913) is adopted.

Under the first two assumptions, condition (3-2) is completely equivalent to the condition:

$$\left. \frac{\partial \bar{U}}{\partial \mathbf{r}_{0Ii}} \right|_{\hat{\mathbf{r}}} = \mathbf{0}, \quad i = 1, 2, \dots N_I, I = 1, 2, \dots Z \quad (3-11)$$

It is intuitively understood that if the number of unit cells “approaches” infinity and the crystal is perfect and fully periodic, the environment is the same around every unit cell. As a result, the energy of every atom in a given unit cell will be the same as that of the corresponding atom in every other unit cell. The last assumption (cyclic boundary condition) has no immediate impact, but it will be useful later in the discussion.

Although condition (3-11) is necessary and sufficient for equation (3-2) to be true, a minimization of the lattice energy with respect to the atomic positions and the lattice unit vectors is always performed before every lattice dynamics calculation. At the lattice energy minimum, in addition to condition (3-11), the following condition is true:

$$\frac{\partial \bar{U}}{\partial \mathbf{R}} = \mathbf{0} \quad (3-12)$$

where \mathbf{R} is a matrix whose columns are the lattice vectors of the crystal $\mathbf{R} = [\mathbf{a}, \mathbf{b}, \mathbf{c}]$. Although this condition is not necessary for lattice dynamics calculation to be

performed, in practice it holds for every structure for which such a calculation is carried out. This is because the result of a minimisation which is performed solely with respect to the atomic position is a structure without physical meaning.

Once the minimum lattice energy structure is obtained then the second derivatives of interest, $\frac{\partial^2 U}{\partial \mathbf{u}_{0II} \partial \mathbf{u}_{I'I'} \Big|_{\hat{\mathbf{r}}}}$, are calculated and the lattice dynamics calculation is performed.

3.3. The permissible wave vectors

The translational symmetry of the crystal allows a description of the crystal by means of the formalism of group theory (McWeeny, 1963). The set of all possible translations in the crystal, i.e., mappings of the form:

$$\begin{aligned} T: \mathbf{r} \rightarrow \mathbf{r}' &= \mathbf{r} + \mathbf{t} \quad \text{where} \\ \mathbf{t} &= t^a \mathbf{a} + t^b \mathbf{b} + t^c \mathbf{c} \end{aligned} \tag{3-13}$$

form a group. Under the Born and von Kàrmà̄n cyclic boundary condition adopted here (see section 3.2):

$$t^a, t^b, t^c = M \Rightarrow \mathbf{t} = \mathbf{0}, \tag{3-14}$$

the sub-group of translations becomes a cyclic group, whose representations are those of any ordinary cyclic group (McWeeny, 1963):

$$e^{i \frac{2\pi}{M} (t^a \xi^a + t^b \xi^b + t^c \xi^c)} \quad t^a, t^b, t^c = 0, 1, \dots, M \text{ and } \xi^a, \xi^b, \xi^c = 0, 1, \dots, M - 1 \tag{3-15}$$

In equation (3-15) each combination of the indices ξ^a , ξ^b and ξ^c describes a representation of the (cyclic) sub-group of translations. In this way equation (3-15) provides M^3 representations of the translation sub-group of the crystal. In addition, (ξ^a, ξ^b, ξ^c) represent non-normalized coordinates of the wave vector, \mathbf{k} .

The major conclusion from equation (3-15) is that there are M^3 wave vectors \mathbf{k} permitted for the crystal, i.e., the number of wave vectors is the same as the number of unit cells in the crystal. These have (positive) coordinates ξ^d :

$$\xi^d = \frac{\xi^d}{M} < 1 \quad \xi^d = 0, 1, 2, \dots, M - 1 \quad d = a, b, c \quad (3-16)$$

This suggests that it is sufficient to restrict the wave vector, \mathbf{k} , to the “first” unit cell of the reciprocal lattice. If a wave vector \mathbf{k}' is related by a reciprocal lattice vector, \mathbf{G} , to a wave vector , \mathbf{k} , in the first reciprocal unit cell:

$$\mathbf{k}' = \mathbf{k} + \mathbf{G}, \quad \mathbf{G} = \hat{\xi}^a \mathbf{a}^* + \hat{\xi}^b \mathbf{b}^* + \hat{\xi}^c \mathbf{c}^* \text{ where } \hat{\xi}^a, \hat{\xi}^b, \hat{\xi}^c = 0, 1, 2, \dots,$$

then the wave vector \mathbf{k}' is such that (a) identical motion is described by equation (3-5), (b) identical solutions are obtained to the eigenvalue problem of equation (3-10) and (c) in the language of group theory, an indistinguishable representation is obtained. It is easy to prove that \mathbf{Gt} is equal to $2\pi n$, where n is an integer, and consequently:

$$e^{i\mathbf{k}'\mathbf{t}} = e^{i\mathbf{kt}} e^{i\mathbf{Gt}} = e^{i\mathbf{kt}}. \quad (3-17)$$

A discussion of the issue of permissible wave vector values and their effect on the atomic vibrations can be found in Born & Huang (1954), Dove (1993, 2003) and Ghatak & Kothari (1972). A formal and robust mathematical discussion of this issue based on arguments of group theory can be found in McWeeny (1963).

In the limit of an infinite number of unit cells (see section 3.2) the upper bound for the wave vector coordinates is

$$\lim_{M \rightarrow \infty} \frac{M-1}{M} = 1.$$

This suggests that restricting the wave vector \mathbf{k} to the reciprocal lattice unit cell ,i.e., $\xi^d \in [0,1]$ $d = a, b, c$, would produce sufficient information for the complete study of the dynamical properties of the crystal.

Sometimes, instead of restricting the wave vector to a unit cell of the reciprocal lattice it is confined to the first *Brillouin zone* (Born & Huang, 1954; Dove, 1993,

2003; Ghatak & Kothari, 1972), defined as a section of the reciprocal space that has a volume equal to that of a reciprocal lattice unit cell, therefore containing all the necessary information. A discussion of the construction of the various Brillouin zones can be found in Brillouin (1953). In this thesis calculations are performed within a reciprocal lattice unit cell rather than in the Brillouin zone. The value of the free energy, which is a scalar quantity, is independent of the choice of the period to be studied, and therefore the easiest choice in terms of implementation is adopted.

3.4. Normal modes & dispersion curves

Each of the $3N$ solutions of the eigenvalue problem (3-10), $\omega_n(\mathbf{k})$ and $\epsilon_n(\mathbf{k})$ describes a *mode of vibration* of the crystal. The quantities

$$q_n(\mathbf{k}) = e^{-i\omega_n(\mathbf{k})t}, \quad (3-18)$$

are known as *normal modes* or *normal mode coordinates*. The normal modes can be used as generalized degrees of freedom (“coordinates”) by means of which the system can be described, i.e. the Hamiltonian can be expressed (Born & Huang, 1954; Dove, 1993; Ghatak & Kothari, 1972). In this form of the Hamiltonian each of the terms of the potential energy is a function of the square of one of the normal modes:

$$U(\mathbf{r}) = U(\mathbf{f}) + \frac{1}{2} \sum_{\mathbf{k}} \sum_{n=1}^{3N} \omega_n(\mathbf{k}) [q_n(\mathbf{k})]^* q_n(\mathbf{k}) \quad (3-19)$$

The Cartesian form (equation 3-3) of the potential energy, on the other hand, comprises terms coupling the various degrees of freedom. Equation (3-18) is the complex form of a harmonic wave, therefore it is usually said that the crystal can be analyzed as a set of harmonic waves independent with each other.

The number of normal modes is equal to the number of degrees of freedom of the crystal in its Cartesian representation. The normal modes are connected to the Cartesian displacements of the atoms via a linear transformation:

$$\mathbf{u}_{IIi}(\mathbf{t}) = \frac{1}{\sqrt{Mm_{IIi}}} \sum_{\mathbf{k}} \sum_{n=1}^{3N} \mathbf{e}_n(\mathbf{k}) e^{i\mathbf{k}\hat{\mathbf{r}}_{IIi}} q_n(\mathbf{k}) \Leftrightarrow \\ q_n(\mathbf{k}) = \frac{1}{\sqrt{M}} \sum_{Ii} \sum_{IIi} \sqrt{m_{IIi}} [\mathbf{e}_n(\mathbf{k})]^* e^{-i\mathbf{k}\hat{\mathbf{r}}_{IIi}} \mathbf{u}_{IIi}(\mathbf{t}) \quad (3-20)$$

Equations (3-20) are intuitively understood as an analysis of the true motion of the atoms in the crystal into a set of harmonic waves, or that the true motion of the atoms in the crystal is the superposition of all the harmonic waves that are allowed to propagate in the crystal.

The plot of the frequency of each mode of vibration $\omega_n(\mathbf{k})$ as function of the wave vector \mathbf{k} is called the *dispersion curve* and the curve associated with each mode is known as *branch* of the dispersion curve. In general there are 3 modes of vibration whose frequency vanish at the Γ -point of the Brillouin zone ($\mathbf{k} = \mathbf{0}$), i.e. $\mathbf{k} \rightarrow \mathbf{0} \Rightarrow \omega_{n'}(\mathbf{k}) \rightarrow 0 \quad n' = 1, 2, 3$. These modes are known as *acoustic modes*. The frequency of all the other modes has a non-zero value for $\mathbf{k} = \mathbf{0}$, and are known as *optical modes*. Another distinction of the modes can be made when the crystal consists of polyatomic entities, such as molecules or polyatomic ions. If there are Z molecules in the unit cell and N atoms, then out of the $3N$ branches of the dispersion curve, the $6Z$ lowest frequency represent the so-called *external modes*, and correspond to the motion of the polyatomic entities as rigid objects. The remaining $3N - 6Z$ modes are the so-called *internal modes*. The 3 acoustic modes belong to the set of external modes.

More details on the various types of modes can be found in Born & Huang (1954), Dove (1993, 2003) and Ghatak & Kothari (1972). The formulation of the calculation of the external modes has been presented by Venkataraman & Sahni (1970) and Pawley (1972).

3.5. Calculation of the free energy

In order to calculate the Helmholtz free energy of the crystal a quantum description of the energy states of the system is adopted. The quanta associated with each normal mode are known as *phonons* in analogy with the photons of the electromagnetic theory of light. Each normal mode is described quantum

mechanically via the quantum harmonic oscillator equations. This result can be obtained more formally by applying the commutation relations between the normal mode coordinates and the corresponding momenta, as is done, for example, in Ghatak & Kothari (1972). The total vibrational energy of the crystal is then the sum of the energies of the various independent waves.

Within the quantum mechanical framework the energy states of a harmonic oscillator whose frequency is ν are separated by an energy gap of $h\nu$:

$$E_o(\eta) = \left(\eta + \frac{1}{2}\right) h\nu, \quad \eta \in \mathbb{N} \quad (3-21)$$

where h is Planck's constant and η is the quantum number. It is important to note that the ground state of the quantum harmonic oscillator, which corresponds to $\eta = 0$, is equal to $\frac{1}{2}h\nu$ and not equal to zero.

Equation (3-21) can be used to derive a description of each mode of vibration of the crystal (i.e. each branch of the dispersion curve), as follows:

$$E_o(\eta_n^{\mathbf{k}}) = \left(\eta_n^{\mathbf{k}} + \frac{1}{2}\right) h\nu_n(\mathbf{k}), \quad \eta_n^{\mathbf{k}} \in \mathbb{N} \quad (3-22)$$

This equation describes the energy states of the n^{th} mode of vibration for a given value of the wave vector, \mathbf{k} .

Statistical mechanics can be used to formulate an expression for the Helmholtz free energy of the crystal. This is done in two steps:

1. Initially the canonical partition function Q_{NVT} is constructed.
2. The free energy is formulated, employing the general equation

$$\mathcal{A} = -k_B T \ln(Q_{NVT}).$$

The definition of the partition function of the canonical NVT ensemble is (Allen & Tildesley, 1987; Frenkel & Smit, 2002; Hill, 1986; McQuarrie, 2000):

$$Q_{NVT} = \sum_{\eta} e^{-\frac{E_{\eta}}{k_B T}} \quad (3-23)$$

where the summation is over all energy states of the system E_η , enumerated by the index η . The energy of the crystal is the sum of the static (U) and vibrational (E_{vib}) parts. The vibrational part results from the superposition of all possible waves propagating along the crystal:

$$E_{vib} = \sum_{\mathbf{k}} \sum_{n=1}^{3N} E_o(\eta_n^{\mathbf{k}}) \quad (3-24)$$

The partition function is then given by:

$$\begin{aligned} Q_{NVT} &= e^{-\frac{U}{k_B T}} \sum_{\eta_1^{\mathbf{k}_1}=0}^{\infty} \sum_{\eta_2^{\mathbf{k}_1}=0}^{\infty} \dots \sum_{\eta_{3N}^{\mathbf{k}_1}=0}^{\infty} \sum_{\eta_1^{\mathbf{k}_2}=0}^{\infty} \dots \sum_{\eta_{3N}^{\mathbf{k}_2}=0}^{\infty} e^{-\frac{1}{k_B T} \sum_{\mathbf{k}} \sum_{n=1}^{3N} E_o(\eta_n^{\mathbf{k}})} \\ &= e^{-\frac{U}{k_B T}} \sum_{\eta_1^{\mathbf{k}_1}=0}^{\infty} \sum_{\eta_2^{\mathbf{k}_1}=0}^{\infty} \dots \sum_{\eta_{3N}^{\mathbf{k}_1}=0}^{\infty} \sum_{\eta_1^{\mathbf{k}_2}=0}^{\infty} \dots \sum_{\eta_{3N}^{\mathbf{k}_2}=0}^{\infty} e^{-\frac{1}{k_B T} \sum_{\mathbf{k}} \sum_{n=1}^{3N} (\eta_n^{\mathbf{k}} + \frac{1}{2}) h \nu_n(\mathbf{k})}. \end{aligned} \quad (3-25)$$

When exploiting the properties of the exponential and the distributive property, the partition function takes the form:

$$\begin{aligned} Q_{NVT} &= e^{-\frac{U}{k_B T}} \prod_{\mathbf{k}} \prod_{n=1}^{3N} \sum_{\eta_n^{\mathbf{k}}=0}^{\infty} \left(e^{-\frac{1}{k_B T} (\eta_n^{\mathbf{k}} + \frac{1}{2}) h \nu_n(\mathbf{k})} \right) \\ &= e^{-\frac{U}{k_B T}} \prod_{\mathbf{k}} \prod_{n=1}^{3N} \left(e^{-\frac{h \nu_n(\mathbf{k})}{2 k_B T}} \sum_{\eta_n^{\mathbf{k}}=0}^{\infty} e^{-\frac{h \nu_n(\mathbf{k})}{k_B T} \eta_n^{\mathbf{k}}} \right) \end{aligned} \quad (3-26)$$

Finally using the series expansion:

$$\sum_{\eta=0}^{\infty} x^\eta = \frac{1}{1-x} \quad (3-27)$$

we can convert the last summation in equation (3-26) so that :

$$Q_{NVT} = e^{-\frac{U}{k_B T}} \prod_{\mathbf{k}} \prod_{n=1}^{3N} \left(\frac{e^{-\frac{\hbar v_n(\mathbf{k})}{2k_B T}}}{1 - e^{-\frac{\hbar v_n(\mathbf{k})}{k_B T}}} \right) \quad (3-28)$$

The free energy is then obtained by substitution of the partition function expression in the well-known formula:

$$\mathcal{A} = -k_B T \ln(Q_{NVT}), \quad (3-29)$$

giving as a final expression:

$$\mathcal{A} = U + \sum_{\mathbf{k}} \sum_{n=1}^{3N} \frac{1}{2} \hbar v_n(\mathbf{k}) + k_B T \ln \left(1 - e^{-\frac{\hbar v_n(\mathbf{k})}{k_B T}} \right) \quad (3-30)$$

The last expression for the Helmholtz free energy (equation 3-30) often appears in the literature in other forms (Kopsias & Theodorou, 1998; Westacott & Rodge, 1996, 1998):

$$\begin{aligned} \mathcal{A} &= U + \sum_{\mathbf{k}} \sum_{n=1}^{3N} \frac{1}{2} \hbar \omega_n(\mathbf{k}) + k_B T \ln \left(1 - e^{-\frac{\hbar \omega_n(\mathbf{k})}{k_B T}} \right) \\ &= U + k_B T \sum_{\mathbf{k}} \sum_{n=1}^{3N} \ln \left[2 \sinh \left(e^{-\frac{\hbar \omega_n(\mathbf{k})}{k_B T}} \right) \right], \end{aligned} \quad (3-31)$$

where \hbar is related to Planck's constant $\hbar = \frac{h}{2\pi}$. Note that these expressions for the free energy of the harmonic oscillator differ from the expression used by Tan et al. (2010) and described in section 2.4.1 (equation (2-15)). This is because here we are using the quantum description for the harmonic oscillator while equation (2-15) corresponds to the partition function of the classical harmonic oscillator.

Equation (3-31) is a general equation derived without any approximation other than the quadratic expansion of the lattice energy and is true for every perfect crystal. Of course the number of wave vectors propagating along the crystal is infinite since it

is equal to the number of the unit cells in the crystal (see section 3.4), which we have assumed to tend to infinity, and therefore it is not possible to evaluate it directly. For this reason a number of alternative expressions can be used to evaluate the Helmholtz free energy.

If equation (3-30) is divided by M^3 we obtain an expression for the free energy that involves an average over all possible wave vectors:

$$\begin{aligned}\bar{\mathcal{A}} &= \bar{U} + \frac{1}{M^3} \sum_{\mathbf{k}} \sum_{n=1}^{3N} \frac{1}{2} h\nu_n(\mathbf{k}) + k_B T \ln \left(1 - e^{-\frac{h\nu_n(\mathbf{k})}{k_B T}} \right) \\ \Leftrightarrow \bar{\mathcal{A}} &= \bar{U} + \left\langle \sum_{n=1}^{3N} \frac{1}{2} h\nu_n(\mathbf{k}) + k_B T \ln \left(1 - e^{-\frac{h\nu_n(\mathbf{k})}{k_B T}} \right) \right\rangle_{\mathbf{k}}\end{aligned}\quad (3-32)$$

where $\bar{\mathcal{A}}$ is the Helmholtz free energy per unit cell of the crystal and $\langle \rangle_{\mathbf{k}}$ indicates an average over all possible wave vectors.

As was shown in section 3.3, the feasible wave vectors are infinite, evenly-distributed wave vectors in the unit cube $[0,1] \times [0,1] \times [0,1]$, therefore the average over discrete vectors described in equation (3-32) can be expressed as an integral:

$$\begin{aligned}\bar{\mathcal{A}} &= \bar{U} + \int_0^1 \int_0^1 \int_0^1 \left\{ \sum_{n=1}^{3N} \frac{1}{2} h\nu_n(\mathbf{k}) + k_B T \ln \left(1 - e^{-\frac{h\nu_n(\mathbf{k})}{k_B T}} \right) \right\} d\xi^a d\xi^b d\xi^c \\ \bar{\mathcal{A}} &= \bar{U} + \sum_{n=1}^{3N} \int_0^1 \int_0^1 \int_0^1 \left\{ \frac{1}{2} h\nu_n(\mathbf{k}) + k_B T \ln \left(1 - e^{-\frac{h\nu_n(\mathbf{k})}{k_B T}} \right) \right\} d\xi^a d\xi^b d\xi^c\end{aligned}\quad (3-33)$$

If the free energy of interest is the Gibbs free energy, G , we need to formulate the grand canonical partition function Q_{NPT} . This is done in a completely analogous way to the derivation of equation (3-28) and one obtains:

$$Q_{NPT} = e^{-\frac{U+PV}{k_B T}} \prod_{\mathbf{k}} \prod_{n=1}^{3N} \left(\frac{e^{-\frac{h\nu_n(\mathbf{k})}{k_B T}}}{1 - e^{-\frac{h\nu_n(\mathbf{k})}{k_B T}}} \right)^{-1} \quad (3-34)$$

The Gibbs free energy is then obtained using $G = -k_B T \ln(Q_{NPT})$:

$$\bar{G} = \bar{U} + \left[\sum_{n=1}^{3N} \int_0^1 \int_0^1 \int_0^1 \left\{ \frac{1}{2} h\nu_n(\mathbf{k}) + k_B T \ln \left(1 - e^{-\frac{h\nu_n(\mathbf{k})}{k_B T}} \right) \right\} d\xi^a d\xi^b d\xi^c \right] + P\bar{V} \quad (3-35)$$

where \bar{G} is the Gibbs free energy per unit cell and \bar{V} is the volume per unit cell.

3.6. The density of vibrational states

The density of vibrational states, widely denoted by $g(v)$, is a comprehensive way to characterize the dynamical state of the system. It is also referred to in the literature as *vibrational spectrum* or *normal mode density*. The density of states is defined as follows (Ghatak & Kothari, 1972):

“The frequency distribution function $g(v)$ is the number of vibrational modes per unit frequency around v .”

In mathematical terms, in the limit of an infinite crystal lattice, $g(v)$ is given by (Born & Huang, 1954):

$$g(v) = \frac{1}{V_r} \lim_{\Delta v \rightarrow 0} \frac{1}{\Delta v} \sum_{n=1}^{3N} \iiint_{v < \nu_n(\mathbf{k}) < v + \Delta v} d\xi^a d\xi^b d\xi^c \quad (3-36)$$

Here V_r is the volume of the reciprocal unit cell given by $V_r = \mathbf{a}^* \cdot (\mathbf{b}^* \times \mathbf{c}^*)$. It is easy to prove that $\frac{1}{V_r} = V$.

As a result $g(v)dv$ is the number of modes per unit volume lying between v and $v + dv$. The density of states has the property:

$$\int_0^\infty g(v)dv = 3N \quad (3-37)$$

Using the density of states, the Helmholtz free energy can be written as:

$$\bar{A} = \bar{U} + \int_0^1 \left\{ \left[\frac{1}{2} h\nu + k_B T \ln \left(1 - e^{-\frac{h\nu}{k_B T}} \right) \right] g(\nu) \right\} d\nu \quad (3-38)$$

and the Gibbs free energy as:

$$\bar{G} = \bar{U} + \int_0^1 \left\{ \left[\frac{1}{2} h\nu + k_B T \ln \left(1 - e^{-\frac{h\nu}{k_B T}} \right) \right] g(\nu) \right\} d\nu + P\bar{V} \quad (3-39)$$

There are a number of methods for approximating the density of states (Blackman, 1937; Gilat & Raubenheimer, 1966; Houston, 1948; Montroll, 1942) that are summarized in Born & Huang (1954), De Launay (1956) and Ghatak & Kothari (1972). One can even find analytical expressions for simple systems, such as a one-dimensional crystal of equally spaced identical atoms (Ghatak & Kothari, 1972). The capabilities of modern computers allow the calculation of $g(\nu)$ for complex systems directly via sampling, using its definition (equation 3-36).

In a sampling approach, given a sufficiently large number of wave vectors N_s^{gofn} , the frequencies of atomic vibrations are calculated by solution of the eigenvalue problem given by equation (3-10). Then a “binning” procedure is applied:

$$g(\nu_k) = \frac{N_{\text{int}}^{\text{gofn}}}{\nu_{\text{max}}} \frac{1}{N_s^{\text{gofn}}} \sum_{j=1}^{N_s^{\text{gofn}}} \sum_{n=1}^{3N} \begin{cases} 1 & \text{if } \nu_n(\mathbf{k}_j) \in [\nu_k, \nu_{k+1}] \\ 0 & \text{if } \nu_n(\mathbf{k}_j) \notin [\nu_k, \nu_{k+1}] \end{cases} \quad (3-40)$$

$$\nu_k = \frac{\nu_{\text{max}}}{N_{\text{int}}^{\text{gofn}}} (k - 1), \quad k = 1, 2, \dots, N_{\text{int}}^{\text{gofn}}$$

ν_{max} is an upper bound for the frequencies of the crystal and $N_{\text{int}}^{\text{gofn}}$ is the number of intervals (“bins”) in which the domain $[0, \nu_{\text{max}}]$ is divided.

3.7. Evaluation of the free energy expression

The expression for the free energy (equation 3-33 or 3-35) can be evaluated in many ways. A rather coarse categorization of available methods can be made on the

basis of the following classes: “approximate” methods, non-symmetry based methods, symmetry-based methods and quadrature methods.

There are two widely known approximate methods for the evaluation of the free energy, the Einstein approximation (Dove, 1993; De Launay, 1956) and the Debye approximation (Dove, 1993; Wallace, 1972; De Launay, 1956). Einstein (1907) first used quantum mechanics to describe the vibrations of atoms within a crystal. He assumed that the atoms in the crystal do not interact, and that they all vibrate harmonically and independently with the same frequency. Under those assumptions he obtained a simple analytical expression for the free energy and every other property of the crystal. The frequency of atomic vibrations is usually fitted when applying this approach. On the other hand, Debye ignored the optical modes and considered only acoustic modes which were assumed to be linear and to have the same slope. He assumed an upper bound for the frequencies of the vibrations, obtaining a quadratic expression for the density of the vibrational frequencies (equation 3-36), which could then be used to evaluate the free energy.

Various methods can be found in literature in which the wave vectors are sampled in the first Brillouin zone, the density of states is then constructed on this basis and finally the free energy is evaluated using equations (3-38) and (3-39). We refer to these methods as *non-symmetry based methods*. For example, van Eijk (2001) sampled wave vectors randomly in the primitive reciprocal lattice unit cell, in crystals of glycerol and glycol. He used 50 wave vectors to ensure the density of states converges. One can also construct a grid in the Brillouin zone which can be even (Dove, 1993) or uneven (Filippini et al., 1976). The main advantage of these methods is their simplicity, while their main disadvantage is the limited efficiency.

One can also find in the literature a number of methods that take advantage of the symmetry properties of the crystal in order to improve the efficiency of Brillouin zone sampling. We refer to these methods as *symmetry-based methods*. Bladereschi (1972) proposed a method for the identification of a unique point in the Brillouin zone that has the property that the value of any periodic function of the wave vector at this point is the same as the average of that function over the Brillouin zone. Such a point may be difficult, if not impossible, to identify, and for this reason another method was proposed (Chadi & Cohen, 1973) for the identification of an arbitrarily small number of points in the Brillouin zone, chosen such that the weighted sum of the value of the function at these points is a good approximation of the mean value of the function.

Other methods that take advantage of the symmetry of the crystal include the Monkhorst & Pack (1976) method, and the “special directions” method (Bansil, 1975; Prasad & Bansil, 1980). Although these methods allow the efficient evaluation of the free energy, their applicability to crystals of arbitrary symmetry is questionable.

Finally the triple integral of equation (3-33) can be evaluated using any of the numerical analysis methods that are suitable for this type of integral. We adopt this approach here, and the *Gauss-Legendre quadrature* is chosen for the evaluation of the free energy.

The Gauss-Legendre method is a special case of the Gaussian quadrature class of methods. In Gaussian quadrature, a weighted integral of the function $f(x)$ between limits α and β is approximated as:

$$\int_{\alpha}^{\beta} w(x)f(x)dx = \sum_{i=1}^{N} a_i f(x_i) \quad (3-41)$$

where $w(x)$ is a weighting function, the x_i 's, which are elements of the N -dimensional vector x , are known as the *abscissae* or *nodes* of the quadrature method, a_i are the coefficients of the method and N is a natural number

The various Gaussian quadrature methods, such as Gauss-Jacobi or Gauss-Chebyshev differ in $w(x)$ and in the way the coefficients and the abscissae are chosen. In the Gauss-Legendre quadrature the weighting function is constant and equal to one and the general form of the integral is:

$$\int_{-1}^{1} f(x)dx \quad (3-42)$$

The coefficients in the Gauss-Legendre quadrature method for a specific N are the roots of the N^{th} order Legendre polynomial defined as:

$$P_N(x) = \frac{1}{2^N N!} \cdot \frac{d^N}{dx^N} [(x^2 - 1)^N] \quad (3-43)$$

As soon as the roots of the Legendre polynomial (x_i^*), $i = 1, \dots, N$ have been found, the coefficient of the quadrature formula associated with each root can be calculated using the equation:

$$a_i = -\frac{a_{N+1}}{a_N} \frac{1}{P'_N(x_i^*) P_{N+1}(x_i^*)}, \quad i = 1, \dots, N \quad (3-44)$$

where $P'_N(x_i^*)$ is the gradient of $P_N(x)$ at x_i^* and a_N is the leading coefficient of the normalized N^{th} order Legendre polynomial:

$$\sqrt{\frac{2N+1}{2}} P_{N+1}(x_i).$$

This coefficient can be proven that are equal to:

$$a_N = \sqrt{\frac{2N+1}{2}} \frac{(2N)!}{2^N (N!)^2}. \quad (3-45)$$

If the limits of the integration are different from -1 and 1 , as in equation (3-33), then the same abscissae and coefficients can be used, but the quadrature formula must be modified as follows:

$$\int_{\alpha}^{\beta} f(x) dx = \frac{\beta - \alpha}{2} \sum_{i=1}^N a_i f\left(\frac{\beta - \alpha}{2} x_i + \frac{\beta + \alpha}{2}\right). \quad (3-46)$$

Finally, the extension of the quadrature formula in the case of multiple integrals is straight forward:

$$\int_{\alpha}^{\beta} \int_{\alpha'}^{\beta'} \int_{\alpha''}^{\beta''} w(x, y, z) f(x, y, z) dx dy dz = \sum_{i=1}^N \sum_{j=1}^N \sum_{k=1}^N a_i a_j a_k f(x_i, y_j, z_k) \quad (3-47)$$

In Table 3-1 the abscissae and coefficients of the Gauss-Legendre quadrature for different values of the number of nodes are summarized. Details about the method and extended tables with abscissae and coefficients can be found in literature (Abramowitz & Stegun, 1972; Krylov, 1962; Stroud, 1966).

N	(Coefficient , Abscissa(s))
1	(2,0)
2	(1, ± 0.57735026919)
3	(0.8, 0) $\quad \quad \quad$ (0.5, ± 0.774596669241)
4	(0.652145154863, ± 0.339981043585) \quad (0.347854845137, ± 0.8611363115)

Table 3-1 The coefficients and corresponding abscissas for Gauss-Legendre quadrature. The density of sampling is limited to four nodes per direction.

3.8. The quasi-harmonic approximation

Within the harmonic approximation, the minimum of the free energy coincides with the minimum of the lattice energy function. This is readily understood if we differentiate the expression for the free energy (equation 3-30):

$$\frac{\partial \mathcal{A}}{\partial \chi} = \frac{\partial U}{\partial \chi} + \sum_{\mathbf{k}} \sum_{n=1}^{3N} \hbar \left(\frac{1}{2} + \frac{1}{e^{\frac{\hbar \omega_n(\mathbf{k})}{k_B T}} - 1} \right) \frac{\partial \omega_n(\mathbf{k})}{\partial \chi} \quad (3-48)$$

where χ is any variable of the crystal structure. The derivative can equivalently be written in terms of the derivative of the corresponding eigenvalue of the dynamical matrix $\lambda_n(\mathbf{k})$

$$\frac{\partial \mathcal{A}}{\partial \chi} = \frac{\partial U}{\partial \chi} + \sum_{\mathbf{k}} \sum_{n=1}^{3N} \frac{\hbar}{2\omega_n(\mathbf{k})} \left(\frac{1}{2} + \frac{1}{e^{\frac{\hbar\omega_n(\mathbf{k})}{k_B T}} - 1} \right) \frac{\partial \lambda_n(\mathbf{k})}{\partial \chi} \quad (3-49)$$

Using first-order perturbation theory, it can be proven that the derivative of each eigenvalue of the dynamical matrix is given by (Gale, 1998; Gale & Rohl, 2003; Kantorovich 1995; Taylor, 1997, 1998):

$$\frac{\partial \lambda_n(\mathbf{k})}{\partial \chi} \approx [\mathbf{e}_n(\mathbf{k})]^T \frac{\partial \mathbf{D}(\mathbf{k})}{\partial \chi} \mathbf{e}_n(\mathbf{k}) \quad n = 1, 2, \dots, 3N \quad (3-50)$$

The formalism of the harmonic approximation is built on the assumption that the potential is a quadratic function and that the dynamical matrix is essentially a sum of the second derivatives (equation 3-9), so that the derivative of the dynamical matrix is related to the third derivative of the lattice energy. For a quadratic lattice energy function, this derivative is zero. Therefore the minimum of the free energy within the harmonic approximation coincides with the lattice energy minimum. In addition, any attempt to minimize the free energy derived under the harmonic approximation by moving the system from its minimum lattice energy configuration would violate the necessary condition on which all the formalism has been built (equation 3-2).

In spite of this, it is common practice to minimize a free energy obtained using the harmonic approximation. This is done by calculating the derivative in equation (3-50) using the third derivative of the true lattice energy function, $U(\mathbf{r})$. This derivative had been truncated from the Taylor expansion approximation of $U(\mathbf{r})$ (equation 3-1) in order to simplify the solution of lattice dynamics in the form of the eigenvalue problem (3-10). When reinstating this derivative, the necessary conditions (3-2) no longer hold. For these reasons, minimization schemes that are performed using equations (3-49) and (3-50) are said to adopt a *quasi-harmonic* approximation (Dove, 1993).

It should be also stressed that in the literature (Gale, 1998; Gale & Rohl, 2003; Kantorovich 1995; Taylor et al., 1997, 1998), it is common practice to perform a free energy minimization using a quasi-Newton algorithm, such as the Broyden-Fletcher Goldfarb-Shano (BFGS) algorithm (Press et al., 1986), because it does not require the calculation of the Hessian, which would involve the calculation of the second derivative of the dynamical matrix, and hence the fourth derivative of the lattice energy. Impractically long CPU time would be necessary for a full Newton algorithm, rendering the calculation infeasible.

3.9. Applications of lattice dynamics

Lattice dynamics has been used for many years (Born & von Kàrmàn, 1912, 1913), mainly under the harmonic and quasi-harmonic approximations, in several applications and on various systems, including organic compounds such as naphthalene and inorganic systems such as ArO. In this section, we provide an overview of some of the key applications of lattice dynamics, to illustrate the breadth of systems studied, and the range of properties that have been investigated within this framework. It should be stressed that this is only a brief survey of the literature which is by no means exhaustive.

3.9.1. Inorganic crystals

Rare gas crystals have provided a useful testing ground for lattice dynamics. Using the Lennard-Jones potential (Kaplan, 2006; Lennard-Jones, 1937) for modeling repulsion and dispersion interactions De Wette and co-workers (1971) derived phonon dispersion curves of the Lennard-Jones system in reduced units. Under the quasi-harmonic approximation they calculated the specific heat and thermal expansion of Ar as a function of temperature. The necessary lattice sums in this study were calculated using tabulated values found in the literature (Misra, 1940). Recently lattice dynamic calculations were adopted to study compressed rare gas crystals (Ne, Ar etc.). The calculations were performed within the framework of the Tolpygo model using *ab-initio* potentials (Horbenko et al., 2007, Troitskaya et al., 2005, 2009).

Inorganic solids, for which there is a wealth of data, have also been the subject of numerous investigations with lattice dynamics. One of the early applications of the harmonic theory of lattice dynamics is the calculation of the phonon frequencies and density of states of NaCl, in the pioneering work of Kellermann (1940). This information was later used for the calculation of the specific heat of sodium chloride (Kellermann, 1941). In contrast to Kellermann, who assumed “rigid ions”, Caldwell & Klein (1967) used the “shell model” to include the effect of polarizability in the calculation of the phonon dispersion curves and the density of states of NaCl. The “shell model”, originally proposed by Dick & Overhauser (1958), had earlier been

extended and applied to NaI and KBr crystals (Cowley et al., 1963; Woods et al., 1960, 1963). Another model aiming to model the deformation of the electronic cloud is the “deformation-dipole” (DD) model (Karo & Hardy, 1966). The DD model has been shown by Karo and Harding to give very accurate dispersion curves, density of states, and heat capacity of NaCl. In all these studies, the calculations were performed using the experimentally-determined crystal structure. Permanent electrostatic interactions were usually calculated using the Madelung treatment (Madelung, 1918) while repulsion interactions were calculated considering interactions up to second neighbors only. A variation on this type of model is the so-called “van der Waals three-body force shell model” (VTSM), where three-body and dispersion interactions are also included in the calculations. This has been applied to lattice dynamical calculations of thallous bromide, TlBr, (Tiwari et al., 2009, 2010), thallous chloride, TlCl, (Tiwari et al., 2010) and potassium bromide, KBr, (Srivastava et al., 2010), for which various properties related to the dynamics (such as optical properties, dielectric constant) are available. Jaswal and co-workers have obtained phonon dispersion curves in crystals of lithium deuteride, LiD, (Jaswal & Dilly, 1977:a), magnesium oxide, MgO, (Jaswal & Dilly, 1977:b), zinc sulfide, ZnS, (Jaswal, 1978:a) and copper chloride, CuCl, (Jaswal, 1978:b), using the so called “deformable-ion” model, a generalization of the shell model and the deformation-dipole based on Tolpygo’s theory.

More complex problems can also be tackled using the method of lattice dynamics. Self-diffusion coefficients in MgO crystals that have a defect, a system of geological interest since it is abundant in the Earth’s mantle, have been calculated under the harmonic approximation (Vočadlo et al., 1995). The shell model and the Buckingham potential were used for modeling inter-atomic interactions. The thermal properties and elastic properties of calcite (CaCO_3), a system composed of polyatomic ions, as a function of temperature have also been studied using the quasi-harmonic approximation (Pavese et al., 1996). Electrostatic interactions were modeled using point charges and the shell model was used for modeling the polarizability of the oxygen atom. The repulsive interactions were calculated using an exponential pair potential, while dispersion interactions were included only for the O—O interaction. The deviations from the ideal planar conformation for the $[\text{CO}_3]^{2-}$ ion were modeled using an empirical potential. Many other studies can be found in the literature such as

normal mode analysis in SiO_4 (Patel et.al., 1991) and in $\text{Mg}_3\text{Al}_2\text{Si}_3\text{O}_{12}$, a commonly used gemstone also known as “pyrope garnet” (Chaplin et al., 1998).

3.9.2. Organic molecular crystals

The harmonic approximation method has also been applied to organic crystals. The hexamine crystal (IUPAC name: 1,3,5,7-Tetraazatricyclo[3.3.1.1^{3,7}]decane, with chemical formula $(\text{CH}_2)_6\text{N}_4$) is one of the first organic molecular systems to have been studied (Cochran & Pawley 1964; Rafizadeh & Yip, 1970). Hexamine is used as a hardening additive to resins. In these early works, the external modes of the dispersion curves were derived based on rigid body models. The parameters of the models were fitted to experimental spectroscopic data. The phase transitions between the α - and β - forms of p-dichlorobenzene ($\text{C}_6\text{H}_4\text{Cl}_2$) and those of 1,2,4,5-tetrachlorobenzene ($\text{C}_6\text{H}_2\text{Cl}_4$) were the subject of another early study (Bonadeo et al., 1978). In this work, the lattice dynamics equations were solved using the harmonic approximation and adopting a rigid-body formalism, and therefore ignoring internal modes. No electrostatic contributions were considered and the only inter-atomic interactions considered were of the Buckingham type. The evaluation of the free energy expression was carried out within the Debye approximation for the acoustic modes and the Einstein approximation for the optical modes. The method failed to identify the α - to β - transition in the case of p-dichlorobenzene. Although no phase transition was identified, the free energy between the two polymorphs was found to be very small for the whole temperature range studied. A justification put forward by the authors for this result is the fact that each of the polymorphs can crystallize as a metastable structure (depending on the experimental conditions) in the temperature region in which the other polymorph is stable (Ghelfenstein & Szwarc; 1971). This result suggests that the real free energy difference between the two polymorphs must be very small. In the case of 1,2,4,5-tetrachlorobenzene, a stability shift is identified at 200 K, surprisingly close to the experimental transition temperature (188 ± 2 K) reported by Herbstein (1965).

A much more sophisticated model was used for frequency calculations for the experimentally-determined crystals of ammonia (NH_3) and deuterated ammonia (ND_3) (Righini et al., 1978). The authors calculated the frequencies of the external

modes of vibration at the Γ -point, using the Buckingham potential for the calculation of the repulsion-dispersion interactions. The electrostatic interactions were modeled using molecular multipole moments up to fourth order of interaction (Neto et al., 1978). Experimentally-determined dipole and quadrupole moments were used, while higher moments were determined using *ab-initio* methods. Later, a full dispersion curve was calculated (Della Valle et al., 1979).

Different approaches to the modeling of interactions have been investigated in the application of lattice dynamics to naphthalene (IUPAC name: bicyclo[4.4.0]deca-1,3,5,7,9-pentene, with chemical formula $C_{10}H_8$). The inclusion of a molecular quadrupole moment was found to significantly improve the accuracy of the dispersion curves obtained using lattice dynamics calculations (Righini et al., 1980). Here calculations had been performed for a crystal in which the lattice variables were those measured experimentally at 4.7 K, while the molecular conformation and orientation were those determined at 120 K. Similar dispersion curves had earlier been calculated without including any electrostatic interactions (Natkaniec et al., 1980). In these calculations, the authors calculated the phonon frequencies within the quasi-harmonic approximation by using the experimental unit cell information (at 4.7 K) and by allowing the molecular orientation to vary. For a similar molecule, anthracene ($C_{14}H_{10}$), the external modes and the 4 lowest-energy internal modes have also been calculated (Dorner et.al., 1982), without consideration of electrostatic interactions. The dispersion curves of anthracene and naphthalene have also been calculated using atomic point charges to account for the electrostatic interactions (Criado, 1989). The effects of temperature and pressure on the crystals of naphthalene have also been studied (Della Valle et al., 1995). The authors performed their study within the quasi-harmonic approximation, adopting the Einstein approximation for the optical modes and the Debye approximation for acoustic modes. A rigid body approximation was adopted for the calculation of phonon frequencies and no electrostatic interactions were included in the molecular model.

Ethenetetracarbonitrile, C_6N_4 , (also known as Tetracyanoethylene or TCNE) is another small rigid molecule that has been widely studied both experimentally and theoretically because of its exceptional properties (Chetkina & Bel'skiĭ, 2002) and its rich phase behavior. TCNE finds various applications such as in superconductors and magnets. In 1979 a first study of the dynamics of the two polymorphs of TCNE was published (Luty et al., 1979). A simple “exp-6” potential was used, without any

explicit accounting of the electrostatic interactions. The lattice energies of both polymorphs were minimized and frequency calculations were performed under the harmonic approximation. In later work, the monoclinic phase was studied under strain using the same model, aiming to ascertain whether lattice dynamics could predict a phase transition between the two polymorphs (Munn & Luty, 1980). The authors concluded that since the frequencies associated with certain modes of vibration become imaginary, it is indeed possible that a phase transition occurs. In both these studies the lattice dynamics equations were solved for the external modes (within the rigid-body approximation). The phonon frequencies of TCNE were also calculated by employing an improved model that includes point charges (Criado, 1990). In this study, similar calculations were performed for the crystals of 1,1,2,2-cyclopropanetetracarbonitrile ($C_7H_2N_4$), hexamine, pyrimidine ($C_4H_4N_2$), pyrazine ($C_4H_4N_2$) and s-triazine ($C_3H_3N_3$). The phase diagram for TCNE from 0 K up to 450 K (approaching the normal melting point of 472 K (Funasako et al. 2012; Radomska & Radomski, 1991)) and up to 4 GPa has also been constructed using harmonic lattice dynamics (Chaplot, 1987). The model was based on the Buckingham potential and Coulombic interactions were not considered. The lattice dynamics equations were solved in a semi-rigid fashion. The approach failed to identify the phase transition occurring at ambient pressure and the monoclinic polymorph was calculated to be stable for the whole range of temperatures, contrary to experimental evidence (Mierzejewski & Chaplot, 1980; Mukhopadhyay et al., 1985; Murgich & Pissanetzky, 1972). A similar study of the relative stability of the cubic and monoclinic forms of TCNE was carried out very recently in an *ab-initio* manner (Schatschneider et al., 2012). A dispersion corrected density function theory (DFT+vdw) methodology (Tkatchenko & Scheffler, 2009) was used, with a PBE functional. The phase transition was found to occur at 160 K. This value is lower than both reported experimentally determined temperatures, 320K in Mierzejewski & Chaplot (1980) and Mukhopadhyay et al. (1985) and 292 K in Murgich & Pissanetzky (1972).

Day and co-workers (2003) compared the performance of various models of the repulsion/dispersion and electrostatic interactions in calculations of the harmonic & quasi-harmonic phonon frequencies at the Γ -point for five small organic molecules (hexamethylenetetramine, naphthalene, α -glycine ($C_2H_5NO_2$), imidazole ($C_3H_4N_2$), and pyrazine). Calculations were performed under the rigid body assumption. It was found that both the model for the repulsion/dispersion interactions and the model for

the electrostatics can have a significant effect on the calculated phonon frequencies. Smaller differences in the quasi-harmonic approximation phonon frequencies revealed that the source of error in the harmonic approximation could be partly attributed to the differences in the relaxed structures. Similar calculations have also been performed for 5-azouracil (Gray et al., 2004). A comparison with phonon frequencies obtained using molecular dynamics simulations showed only minor deviations from those obtained by lattice dynamics under harmonic and quasi-harmonic approximation for 5-azouracil and imidazole (Gray et al., 2004)

The Local Harmonic (LH) method of LeSar et al. (1989) is a further simplified variation of the harmonic approximation. In the LH method all the inter-atomic coupling system is neglected, by approximating the dynamical matrix by a 3×3 block diagonal matrix, i.e., by equating the elements that describe the coupling of the motion of different atoms to zero. This approach has been used within a free energy minimization algorithm for the calculation of the free energy of a perfect copper crystal, and the free energy of a copper crystal with a defect. The result was found to be in good agreement with the result obtained via Frenkel & Ladd's thermodynamic integration method (see section 2.4). Similar calculations with the LH model have been performed to obtain the boundary free energy of Au (Najafabadi et al., 1991:a) or Ni-Cu alloys (Najafabadi et al., 1991:b).

Sutton (1989) studied gold grain boundaries in a different way. A second moment approximation was adopted for the local phonon density of states, and approximate expressions were obtained for the free energy gradients. The second moment approximation has also been used for calculations on alloys, with a slightly modified expression for the free energy gradients (Sutton et al., 1992).

A similar methodology has been used for the study of complex hydrate systems. The free energies of hexagonal ice and of the methane hydrate with hexagonal ice were minimized within the “local molecular harmonic model” (LMHM) (Westacott & Rodger, 1996). The LMHM method is a generalization of the LH method that was first presented by LeSar et al. (1989). In the LMHM, all the elements describing the coupling of atoms that do not belong to the same molecule are assumed to be zero. The water molecule was modeled using the SPC model (Berendsen et al., 1981) while a coarse-grained model was adopted for methane, which was represented by a single Lennard-Jones sphere. The minimizations were performed using numerical gradients, and the phonon frequencies were assumed to have no dispersion, i.e. only the zero

reciprocal space vector (Γ -point) was sampled for the evaluation of the free energy expression. Westacott and Rodger investigated the three-phase equilibria between methane hydrate, methane gas and ice and obtained results in good agreement with experimental data for the equilibrium pressure at 270 K and 17% (mol) methane in the hydrate phase. The authors have also used similar models and the LMHM method for the determination of critical nuclei for crystallization for methane hydrates (Westacott & Rodger, 1998).

The quasi-harmonic approximation has also been used to study the amorphous state of a Lennard-Jones system (Kopsias & Theodorou, 1998). Various potential energy minima in the amorphous system hyper-surface are identified, by rapid decrease of the temperature in a molecular dynamics simulation, followed by constant volume steepest decent potential energy minimization. The free energy minimum is then obtained by free energy minimization, which is performed under constant pressure and temperature within the quasi-harmonic approximation. Elementary transitions are then identified among the minima and the rate constant associated with the transition from one minimum to another are calculated based on the multidimensional transition state theory.

Lattice dynamics calculations have also been used to assess the effect of temperature on the result of a crystal structure prediction study (van Eijk, 2001). van Eijk calculated the free energy using the harmonic and quasi-harmonic approximations for hypothetical structures that had been generated by crystal structure prediction studies of glycerol and glycol (Mouij et al., 2000; van Eijk et al., 2001). In this work, no Ewald summation was used and electrostatic interactions were calculated using a direct space sum by application of a cut-off radius for neutral charge groups (see section 5.2). The lattice dynamics calculations were performed in a fully atomistic manner. Free energy minimization was not performed in a rigorous way. The quasi-harmonic free energy was calculated over a grid in the parameter space and a quadratic polynomial was fitted. The minimum was then obtained with the aid of this polynomial. The free energy was calculated using a density of states that had been constructed by random sampling of 50 wave vectors. The density of states was also calculated using Molecular Dynamics for the experimental structure of both molecules. No significant deviation was observed between the density of states obtained by the two methods. This result indicates that the harmonic approximation in lattice dynamics offers good accuracy. Perhaps one of the main findings of this study

is that the result of a crystal structure prediction study can be influenced by including harmonic temperature effects. In the case of glycol, the incorporation of a harmonic free energy correction led to a re-ranking so that the predicted structure corresponding to the experimental crystal became the global minimum, improving its rank by two. Quasi-harmonic free energy minimization had the same effect. In the case of glycerol, although the rank of the minimum corresponding to the experimental structure did not improve, its energy difference from the global minimum decreased. Finally van Eijk (2001) presents a discouraging example of dioxane to give a broader picture. Here no complete prediction was attempted but the calculated relative stability between two known forms deteriorated compared to the static lattice energy calculations.

The methods of harmonic and quasi-harmonic approximation are two of the oldest methods that allow the calculation of the free energy and other thermodynamic properties. They have been widely developed over the past century and have found many applications. The methods are based on a quadratic approximation of the lattice energy of the crystal, but without any other assumptions. Therefore the method is applicable to any model describing the inter-atomic interactions, as is also evident from the survey of the literature presented here. Although experience with this approach has been mixed, the results achieved so far warrant its further exploration in the context of crystal structure prediction. A discussion of the models used in the calculations for this thesis follows in Chapter 4. The form taken by the lattice dynamics equations based on the assumed models is also discussed.

4. Molecular models

As in every computational study it is necessary to assume a model for the description of the inter-atomic interactions. It is evident from section 3.9 that over a long period various models have been used for modeling the crystalline state, and more specifically the organic molecular solid state, which is relevant to this thesis. A wide variety of modeling approaches has also been used in crystal structure prediction. From the AMBER (Bazterra et al., 2004; Cornell et al., 1994) and DREIDING (Kim et al., 2011; Mayo et al. 1990; Panina et al., 2008) force fields to fully periodic density functional theory (DFT) calculations, corrected with a term to account for the dispersion interactions (Neumann & Perrin, 2005; Chan et al., 2011). Several papers review the various modeling approaches that have been used in organic crystal structure prediction endeavors (Day, 2011; Price 2008). The five international blind tests held in the last decade (Bardwell et al., 2010; Day et al., 2005, 2009; Motherwell et al. 2002; Lommerse et al. 2000) also provide a broad overview of the various models and their performance. Furthermore the blind tests have revealed that the accurate modeling of organic crystals requires detailed calculations, whose accuracy reaches the quantum mechanical (QM) level. In addition in a crystal structure prediction study the identification of all the free energy minima of the compound (~ 100.000) of interest need to be identified, thus posing an extra requirement of limited computational cost. The problem of achieving the high accuracy within limited cost is exacerbated in large flexible molecules which are relevant to industrial applications (Bardwell et al., 2010; Kazantsev et al., 2011:b)

Here we assume that the only contributions to the lattice energy come from the electrostatic, U_{ele} , repulsion/dispersion, $U_{rep/dis}$, and the bonding (intra-molecular), U_{intra} interactions. Intra-molecular repulsion/dispersion and electrostatic interactions are assumed to be included within the bonding contribution, so that U_{ele} and $U_{rep/dis}$

contribute to inter-molecular interactions, U_{inter} , exerted only between atoms that belong to different molecules. The total lattice energy of the static crystal (packing energy) is thus approximated in the following way:

$$\begin{aligned} U &= U_{intra} + U_{ele} + U_{rep/dis} + U_{other} \\ &\approx U_{intra} + U_{ele} + U_{rep/dis} \\ &= U_{intra} + U_{inter} \end{aligned} \quad (4-1)$$

In U_{other} all contributions to the intra- and inter-molecular interactions not accounted for in the first three terms are included. A detailed discussion of what those contributions are is found in Stone (1996). Of the various contributions represented by this term the importance of the *induction* contribution for modeling organic crystalline materials has been investigated in particular. It was found that induction is a considerable proportion of total energy (Chipot & Luque, 2000; Welch et al., 2008) and that by including it, it is possible to improve the result of a crystal structure prediction study (Welch et al., 2008).

Simplification of the lattice energy calculation according to equation (4-1) results in a corresponding simplification for the dynamical matrix:

$$\begin{aligned} \mathbf{D}(\mathbf{k}) &\approx \mathbf{D}^{intra}(\mathbf{k}) + \mathbf{D}^{ele}(\mathbf{k}) + \mathbf{D}^{rep/dis}(\mathbf{k}) \\ &= \mathbf{D}^{intra}(\mathbf{k}) + \mathbf{D}^{inter}(\mathbf{k}) \end{aligned} \quad (4-2)$$

It is common practice (Karamertzanis & Price, 2006; Kazantsev et al., 2010, 2011:a; Price, 2008; van Eijk et al. 2000) in molecular crystal studies to choose as a reference state the gas phase energy of the isolated molecule(s), U_{gas} :

$$\Delta U = \Delta U_{intra} + U_{ele} + U_{rep/dis} = (U_{intra} - U_{gas}) + U_{ele} + U_{rep/dis} \quad (4-3)$$

In this way the “intramolecular energy” represents the increase in the energy of the isolated molecule associated with the change in its conformation due to the crystalline environment.

Equivalently, the free energy is normalized also with respect to the vibrational energy of the isolated molecule(s):

$$\begin{aligned}
 \Delta A &= \Delta U_{intra} + U_{ele} + U_{rep/dis} + \Delta U_{ZPE} - TS \\
 &= (U_{intra} - U_{gas}) + U_{ele} + U_{rep/dis} + (U_{ZPE} - U_{ZPE}^{gas}) \quad (4-4) \\
 &\quad - TS
 \end{aligned}$$

4.1. Intra-molecular interactions

The intra-molecular interactions refer to the interactions between atoms bonded within the same molecule. For rigid molecules, the net intra-molecular energy (with reference to the isolated molecule(s)) is by definition zero. However, for flexible molecules, experience shows (Karamertzanis & Price, 2006; Uzoh et al., 2012; van Eijk et al. 2001) that it is a significant contribution to the total lattice energy. Furthermore the balance between intra- and inter-molecular energy plays a decisive role in determining the conformation of the molecule within the crystal. The phenomenon of *conformational polymorphism*, the variation of conformation of the molecule in different polymorphs, is widely known (Mattei & Li, 2011; McCrone 1965; Smith et al., 1998; Yu, 2002). As a consequence it is essential for modeling and predicting the organic solid state that the intra-molecular contribution is calculated at a high level of accuracy and efficiency (Kazantsev et al., 2010, 2011:a, 2011:b, Vasileiadis et.al., 2012). For this reason we calculate the intra-molecular interactions using quantum mechanical (QM) calculations. These normally consist of perturbation theory calculations such as MP2, or density function theory (DFT) calculations such as B3LYP or M06. For computational efficiency reasons these calculations are performed for isolated molecules.

The calculation of the intra-molecular energy via QM consists in isolated molecule geometry optimization. In this thesis geometry optimizations are performed in the *Gaussian 09* package (Frisch et al., 2009). Thus, an outcome of this calculation is the molecular conformation. In the case of rigid molecules it is assumed that the crystalline environment has only a minor effect on the molecular geometry, and therefore the geometry in the crystal is identical to the gas phase conformation (Karamertzanis, 2004; Karamertzanis & Pantelides, 2005). In such a case, the minimization problem solved to determine the molecular geometry is unconstrained. In the case of flexible molecules, the effect of the crystalline environment on the

conformation is determined via a constrained optimization (e.g., Kazantsev et.al., 2010, 2011:a) in which selected degrees of freedom (the most flexible ones) are optimized, while other geometry variables are allowed to relax to the most favourable conformation based on the optimized degrees of freedom.

4.2. Pairwise additive potentials

In general a contribution to the total energy of interaction, U , of the system can be computed as a sum of the interactions of all pairs, triplets etc (Kaplan, 2006):

$$U = \sum_i \sum_{j>i} U_{ij} + \sum_i \sum_{j>i} \sum_{k>j} U_{ijk} + \dots \quad (4-5)$$

where U_{ij} is a function describing the interaction energy of atom i with atom j , U_{ijk} is a function describing the potential energy of the system i, j and k etc. One of the most essential assumptions in almost every computational study is that the energy of the system can be described solely based on the interactions of all possible pairs of atoms, ignoring the interaction of triplets and higher groups. As a consequence equation (4-5) is simplified to:

$$U = \sum_i \sum_{j>i} U_{ij}^{\text{eff.}} = \frac{1}{2} \sum_i \sum_j U_{ij}^{\text{eff.}}, \quad (4-6)$$

where $U_{ij}^{\text{eff.}}$ is an effective potential that is used in the calculations. In this thesis the inter-molecular interactions, i.e. the electrostatic, repulsion and dispersion interactions, are assumed to be pairwise additive. In the following sections the effect of the pairwise additivity assumption on the calculation formulas for these contributions to lattice energy per unit cell, \bar{U} , and the dynamical matrix, $\mathbf{D}_{Ii,Jj}(\mathbf{k})$, are discussed.

4.2.1. Energy

Under the assumption of pairwise additivity any contribution to the inter-molecular component of the lattice energy of the unit cell, \bar{U}^κ , is given by:

$$\begin{aligned}
\bar{U}^\kappa &= \frac{1}{2} \sum_{Ii} \underbrace{\sum_{\substack{\mathbf{l} \in \mathbf{L} \\ \mathbf{l} \neq \mathbf{0} \text{ if } I=J}}}_{\sum_{\substack{\mathbf{l} \in \mathbf{L} \\ \mathbf{l} \neq \mathbf{0}}} \sum_{Jj}} U_{IiJj}^\kappa (\|\mathbf{r}_{0Ii} - \mathbf{r}_{0Jj} + \mathbf{R}\mathbf{l}\|) \\
&= \frac{1}{2} \sum_{Ii} \left[\sum_{\substack{\mathbf{l} \in \mathbf{L} \\ I \neq J}} U_{IiJj}^\kappa (\|\mathbf{r}_{0Ii} - \mathbf{r}_{0Jj} + \mathbf{R}\mathbf{l}\|) \right. \\
&\quad \left. + \sum_{\substack{\mathbf{l} \in \mathbf{L} \\ \mathbf{l} \neq \mathbf{0}}} \sum_j U_{IiIj}^\kappa (\|\mathbf{r}_{0Ii} - \mathbf{r}_{0Ii} + \mathbf{R}\mathbf{l}\|) \right] \quad \kappa = ele, rep/dis,
\end{aligned} \tag{4-7}$$

where the columns of matrix $\mathbf{R} \in \mathbb{R}^3 \times \mathbb{R}^3$ are the unit cell vectors (see section 3.1) and the factor $\frac{1}{2}$ ensures that interactions are not taken into account twice. \bar{U}^κ is any contribution to the potential energy of a unit cell (arbitrarily chosen) of a fully periodic crystal, in which the lattice energy only depends on the coordinates of the atoms in the unit cell $\mathbf{l} = (0,0,0)$ and the unit cell vectors. U_{IiJj}^κ is the potential describing the κ -type interaction between the Ii atom and the Jj atom.

The calculation of the atom-atom energy $U_{IiJj}^\kappa (\|\mathbf{r}_{Ii} - \mathbf{r}_{Jj}\|)$ derivatives with respect to the atomic coordinates is straightforward:

$$\begin{aligned}
\frac{\partial U_{IiJj}^\kappa}{\partial \mathbf{r}_{Ii}} &= \frac{\partial U_{IiJj}^\kappa}{\partial \|\mathbf{r}_{Ii} - \mathbf{r}_{Jj}\|} \cdot \frac{\partial \|\mathbf{r}_{Ii} - \mathbf{r}_{Jj}\|}{\partial \|\mathbf{r}_{Ii}\|} \\
&= \frac{1}{\|\mathbf{r}_{Ii} - \mathbf{r}_{Jj}\|} \frac{\partial U_{IiJj}^\kappa}{\partial \|\mathbf{r}_{Ii} - \mathbf{r}_{Jj}\|} \cdot (\mathbf{r}_{Ii} - \mathbf{r}_{Jj})^T.
\end{aligned} \tag{4-8}$$

The second derivatives are given by:

$$\begin{aligned}
\frac{\partial^2 U_{IiJj}^\kappa}{\partial \mathbf{r}_{Ii}^2} &= \left[\frac{1}{\|\mathbf{r}_{Ii} - \mathbf{r}_{Jj}\|^2} \frac{\partial^2 U_{IiJj}^\kappa}{\partial \|\mathbf{r}_{Ii} - \mathbf{r}_{Jj}\|^2} - \frac{1}{\|\mathbf{r}_{Ii} - \mathbf{r}_{Jj}\|^3} \frac{\partial \|\mathbf{r}_{Ii} - \mathbf{r}_{Jj}\|}{\partial \|\mathbf{r}_{Ii}\|} \right] \\
&\quad \cdot (\mathbf{r}_{Ii} - \mathbf{r}_{Jj})(\mathbf{r}_{Ii} - \mathbf{r}_{Jj})^T \\
&\quad + \frac{1}{\|\mathbf{r}_{Ii} - \mathbf{r}_{Jj}\|} \frac{\partial \|\mathbf{r}_{Ii} - \mathbf{r}_{Jj}\|}{\partial \|\mathbf{r}_{Ii}\|} \mathbf{I}.
\end{aligned} \tag{4-9}$$

In the last equation \mathbf{I} is the unitary 3×3 matrix. Finally it is easy to prove the following properties for any choice of $\mathbf{l}, \mathbf{l}', I, J, i, j$:

$$\begin{aligned}\frac{\partial U_{IiJJ}^{\kappa}}{\partial \mathbf{r}_{\mathbf{I}Ii}} &= -\frac{\partial U_{IiJJ}^{\kappa}}{\partial \mathbf{r}_{\mathbf{I}'Jj}} \\ \frac{\partial^2 U_{IiJJ}^{\kappa}}{\partial \mathbf{r}_{\mathbf{I}Ii}^2} &= \frac{\partial^2 U_{IiJJ}^{\kappa}}{\partial \mathbf{r}_{\mathbf{I}'Jj}^2} \\ \frac{\partial^2 U_{IiJJ}^{\kappa}}{\partial \mathbf{r}_{\mathbf{I}Ii} \partial \mathbf{r}_{\mathbf{I}'Jj}} &= \frac{\partial^2 U_{IiJJ}^{\kappa}}{\partial \mathbf{r}_{\mathbf{I}'Jj} \partial \mathbf{r}_{\mathbf{I}Ii}} = -\frac{\partial^2 U_{IiJJ}^{\kappa}}{\partial \mathbf{r}_{\mathbf{I}Ii}^2}\end{aligned}\quad (4-10)$$

The first derivatives of the lattice energy \bar{U}^{κ} with respect to the positions of the atoms in the unit cell $\mathbf{0}$ are:

$$\frac{\partial \bar{U}^{\kappa}}{\partial \mathbf{r}_{\mathbf{0}Ii}} = \sum_{\mathbf{l} \in \mathbf{L}} \sum_{\substack{j \\ J \neq I \text{ if } \mathbf{l} = \mathbf{0} \\ j \neq i \text{ if } J = I}} \sum_j \frac{1}{\|\mathbf{r}_{\mathbf{0}Ii,\mathbf{l}Jj}\|} \frac{\partial U_{IiJJ}^{\kappa}}{\partial \|\mathbf{r}\|} \Big|_{\mathbf{r}_{\mathbf{0}Ii,\mathbf{l}Jj}} (\mathbf{r}_{\mathbf{0}Ii,\mathbf{l}Jj})^T. \quad (4-11)$$

Equation (4-11) is obtained if all periodic images of atom $\mathbf{0}Ii$ are also “perturbed” during the differentiation process. This type of derivative is useful only in the context of lattice energy minimization schemes. The diagonal elements of the Hessian matrix are given by:

$$\begin{aligned}\frac{\partial^2 \bar{U}^{\kappa}}{\partial (\mathbf{r}_{\mathbf{0}Ii})^2} &= \sum_{\mathbf{l} \in \mathbf{L}} \sum_{\substack{j \\ J \neq I \text{ if } \mathbf{l} = \mathbf{0} \\ j \neq i \text{ if } J = I}} \sum_j \left[\left(\frac{1}{\|\mathbf{r}_{\mathbf{0}Ii,\mathbf{l}Jj}\|^2} \frac{\partial^2 U_{IiJJ}^{\kappa}}{\partial \|\mathbf{r}\|^2} \Big|_{\mathbf{r}_{\mathbf{0}Ii,\mathbf{l}Jj}} \right. \right. \\ &\quad \left. \left. - \frac{1}{\|\mathbf{r}_{\mathbf{0}Ii,\mathbf{l}Jj}\|^3} \frac{\partial U_{IiJJ}^{\kappa}}{\partial \|\mathbf{r}\|} \Big|_{\mathbf{r}_{\mathbf{0}Ii,\mathbf{l}Jj}} \right) \mathbf{r}_{\mathbf{0}Ii,\mathbf{l}Jj} (\mathbf{r}_{\mathbf{0}Ii,\mathbf{l}Jj})^T \right. \\ &\quad \left. + \frac{1}{\|\mathbf{r}_{\mathbf{0}Ii,\mathbf{l}Jj}\|^3} \frac{\partial U_{IiJJ}^{\kappa}}{\partial \|\mathbf{r}\|} \Big|_{\mathbf{r}_{\mathbf{0}Ii,\mathbf{l}Jj}} \mathbf{I} \right]\end{aligned}\quad (4-12)$$

The off-diagonal elements are given by:

$$\begin{aligned} \frac{\partial^2 \bar{U}^\kappa}{\partial \mathbf{r}_{0Ii} \partial \mathbf{r}_{0Jj}} = & - \sum_{\mathbf{l} \in \mathbf{L}} \left[\left(\frac{1}{\|\mathbf{r}_{0Ii,1Jj}\|^2} \frac{\partial^2 U_{IiJj}^\kappa}{\partial \|\mathbf{r}\|^2} \Big|_{\mathbf{r}_{0Ii,1Jj}} \right. \right. \\ & - \frac{1}{\|\mathbf{r}_{0Ii,1Jj}\|^3} \frac{\partial U_{IiJj}^\kappa}{\partial \|\mathbf{r}\|} \Big|_{\mathbf{r}_{0Ii,1Jj}} \Big) \cdot \mathbf{r}_{0Ii,1Jj} (\mathbf{r}_{0Ii,1Jj})^T \\ & \left. \left. + \frac{1}{\|\mathbf{r}_{0Ii,1Jj}\|^3} \frac{\partial U_{IiJj}^\kappa}{\partial \|\mathbf{r}\|} \Big|_{\mathbf{r}_{0Ii,1Jj}} \mathbf{I} \right] \right] \end{aligned} \quad (4-13)$$

The first derivatives with respect to the three lattice vectors are:

$$\frac{\partial \bar{U}^\kappa}{\partial \mathbf{R}} = \sum_{Ii} \sum_{\substack{\mathbf{l} \in \mathbf{L} \\ \mathbf{l} \neq 0}} \sum_{Jj} \frac{1}{\|\mathbf{r}_{0Ii,1Jj}\|} \frac{\partial U_{IiJj}^\kappa}{\partial \|\mathbf{r}\|} \Big|_{\mathbf{r}_{0Ii,1Jj}} (\mathbf{r}_{0Ii,1Jj})^T \mathbf{l} \quad (4-14)$$

The second derivative with respect to the cell and the mixed cell-atom position coordinates are not reported because they are not necessary for lattice dynamics nor for lattice energy minimization if a quasi-Newton algorithm is used.

The first derivatives of a contribution κ to the total lattice energy U , assuming that perturbation of an atom in the unit cell $\mathbf{0}$ does not affect its periodic images, are given as a function of the atom-atom potential U_{IiJj}^κ by:

$$\frac{\partial U^\kappa}{\partial \mathbf{r}_{0Ii}} = \sum_{\substack{\mathbf{l} \in \mathbf{L} \\ \mathbf{l} \neq 0 \text{ if } I=J}} \sum_{Jj} \frac{\partial U_{IiJj}^\kappa (\|\mathbf{r}_{0Ii} - \mathbf{r}_{0Jj} + \mathbf{Rl}\|)}{\partial \mathbf{r}_{0Ii}} \quad (4-15)$$

Under the same assumption, the second derivatives are as follows:

- If we have a diagonal element, i.e. the indices defining the atoms are the same
 $\mathbf{0}Ii = \mathbf{0}Jj$

$$\frac{\partial^2 U^\kappa}{\partial (\mathbf{r}_{0Ii})^2} = \sum_{\substack{\mathbf{l} \in \mathbf{L} \\ \mathbf{l} \neq 0 \text{ if } I=J}} \sum_{Jj} \frac{\partial^2 U_{IiJj}^\kappa (\|\mathbf{r}_{0Ii} - \mathbf{r}_{0Jj} + \mathbf{Rl}\|)}{\partial (\mathbf{r}_{0Ii})^2} \quad (4-16)$$

- In the case where the second derivative is with respect to the atomic positions of two different atoms:

$$\frac{\partial^2 U^\kappa}{\partial \mathbf{r}_{0Ii} \partial \mathbf{r}_{IJj}} = \frac{\partial^2 U_{IJj}^\kappa(\|\mathbf{r}_{0Ii} - \mathbf{r}_{0Jj} + \mathbf{Rl}\|)}{\partial \mathbf{r}_{0Ii} \partial \mathbf{r}_{IJj}}, \mathbf{0}Ii \neq \mathbf{1}Jj \quad (4-17)$$

The second derivatives of the pair potential that are necessary for the evaluation of equations (4-16) and (4-17) are given by equation (4-13).

4.2.2. Dynamical matrix

The pairwise additivity assumption for the inter-molecular interactions determines the formulae for the dynamical matrix. This is of course a consequence of the fact that this assumption determines the form of the second derivatives of the lattice energy (equations (4-16) and (4-17)).

By substitution of equation (4-17) into equation (3-9) we can see that all the off-diagonal 3×3 blocks of equation (3-8) (i.e. those that are associated with the interactions of different atoms) are given by:

$$\mathbf{D}_{II,Jj}^\kappa(\mathbf{k}) = \frac{1}{\sqrt{m_{II} m_{JJ}}} \sum_{\mathbf{l} \in L} \left. \frac{\partial^2 U_{IJj}^\kappa(\|\mathbf{r}_{0Jj} - \mathbf{r}_{0Ii} + \mathbf{Rl}\|)}{\partial \mathbf{r}_{0Ii} \partial \mathbf{r}_{IJj}} \right|_{\hat{\mathbf{r}}} e^{i\mathbf{k}(\hat{\mathbf{r}}_{IJj} - \hat{\mathbf{r}}_{0Ii})} \quad (4-18)$$

while the 3×3 blocks on the diagonal of dynamical matrix (equation 3-8) are given by:

$$\mathbf{D}_{II,II}^\kappa(\mathbf{k}) = -\frac{1}{m_{II}} \sum_{\mathbf{l} \in L} \left. \frac{\partial^2 U}{\partial \mathbf{r}_{0Ii} \partial \mathbf{r}_{IIi}} \right|_{\hat{\mathbf{r}}} e^{i\mathbf{k}(\hat{\mathbf{r}}_{IIi} - \hat{\mathbf{r}}_{0Ii})} \quad (4-19)$$

The equation above is equivalent to:

$$\begin{aligned}
\mathbf{D}_{Ii,Ii}^{\kappa}(\mathbf{k}) &= \frac{1}{m_{Ii}} \left(\sum_{\substack{\mathbf{l} \in \mathbf{L} \\ \mathbf{l} \neq \mathbf{0}}} \frac{\partial^2 U}{\partial \mathbf{r}_{0Ii} \partial \mathbf{r}_{lIi}} \Big|_{\hat{\mathbf{r}}} e^{i\mathbf{k}(\hat{\mathbf{r}}_{lIi} - \hat{\mathbf{r}}_{0Ii})} + \frac{\partial^2 U}{(\partial \mathbf{r}_{0Ii})^2} \Big|_{\hat{\mathbf{r}}} \right) \Leftrightarrow \\
\mathbf{D}_{Ii,Ii}^{\kappa}(\mathbf{k}) &= \frac{1}{m_{Ii}} \left(\sum_{\substack{\mathbf{l} \in \mathbf{L} \\ \mathbf{l} \neq \mathbf{0}}} \frac{\partial^2 U}{\partial \mathbf{r}_{0Ii} \partial \mathbf{r}_{lIi}} \Big|_{\hat{\mathbf{r}}} e^{i\mathbf{k}(\hat{\mathbf{r}}_{lIi} - \hat{\mathbf{r}}_{0Ii})} \right. \\
&\quad \left. + \sum_{\substack{\mathbf{l} \in \mathbf{L} \\ \mathbf{l} \neq \mathbf{0} \text{ if } l=J}} \sum_{JJ} \frac{\partial^2 U_{IiJj}^{\kappa}(\|\mathbf{r}_{0Ii} - \mathbf{r}_{0Jj} + \mathbf{R}\mathbf{l}\|)}{\partial \mathbf{r}_{0Ii} \partial \mathbf{r}_{0Jj}} \right) \tag{4-20}
\end{aligned}$$

Considering the properties listed in equations (4-10) together with equation (3-9), the equation for the diagonal 3×3 blocks of the dynamical matrix becomes:

$$\begin{aligned}
\mathbf{D}_{Ii,Ii}^{\kappa}(\mathbf{k}) &= \frac{1}{m_{Ii}} \sum_{\substack{\mathbf{l} \in \mathbf{L} \\ \mathbf{l} \neq \mathbf{0}}} \frac{\partial^2 U}{\partial \mathbf{r}_{0Ii} \partial \mathbf{r}_{lIi}} \Big|_{\hat{\mathbf{r}}} e^{i\mathbf{k}(\hat{\mathbf{r}}_{lIi} - \hat{\mathbf{r}}_{0Ii})} \\
&\quad - \sqrt{\frac{m_{Jj}}{m_{Ii}}} \frac{1}{\sqrt{m_{Ii} m_{Jj}}} \sum_{Jj} \sum_{\substack{\mathbf{l} \in \mathbf{L} \\ \mathbf{l} \neq \mathbf{0} \text{ if } l=J}} \frac{\partial^2 U_{IiJj}^{\kappa}(\|\mathbf{r}_{0Ii} - \mathbf{r}_{0Jj} + \mathbf{R}\mathbf{l}\|)}{\partial \mathbf{r}_{0Ii} \partial \mathbf{r}_{0Jj}} \tag{4-21}
\end{aligned}$$

At this point, we introduce the matrix $\widehat{\mathbf{D}}_{Ii,Jj}(\mathbf{k})$ defined as

$$\widehat{\mathbf{D}}_{Ii,Ii}^{\kappa}(\mathbf{k}) = \frac{1}{\sqrt{m_{Ii} m_{Jj}}} \sum_{\substack{\mathbf{l} \in \mathbf{L} \\ \mathbf{l} \neq \mathbf{0} \text{ if } l=J}} \frac{\partial^2 U_{IiJj}^{\kappa}(\|\mathbf{r}_{0Ii} - \mathbf{r}_{0Jj} + \mathbf{R}\mathbf{l}\|)}{\partial \mathbf{r}_{0Ii} \partial \mathbf{r}_{0Jj}} e^{i\mathbf{k}(\hat{\mathbf{r}}_{lIi} - \hat{\mathbf{r}}_{0Ii})} \tag{4-22}$$

Then we can calculate the dynamical matrix using the equations:

$$\begin{aligned}
\mathbf{D}_{Ii,Jj}^{\kappa}(\mathbf{k}) &= \widehat{\mathbf{D}}_{Ii,Jj}^{\kappa}(\mathbf{k}) \\
\mathbf{D}_{Ii,Ii}^{\kappa}(\mathbf{k}) &= \widehat{\mathbf{D}}_{Ii,Ii}^{\kappa}(\mathbf{k}) - \sqrt{\frac{m_{Jj}}{m_{Ii}}} \sum_{Jj} \widehat{\mathbf{D}}_{Ii,Jj}^{\kappa}(\mathbf{k}) \tag{4-23}
\end{aligned}$$

These last equations ((4-22) and (4-23)) are valid for any contribution to the dynamical matrix, when the corresponding contribution to the lattice energy is calculated under the pairwise additive assumption. Consequently within this thesis these equations are used for the repulsion/dispersion and electrostatic interactions. The models used for these interactions are introduced in Sections 4.3 and 4.4, respectively.

4.3. Repulsion/dispersion interactions

The repulsion/dispersion interaction is calculated using empirical or semi-empirical potentials, such as the Buckingham or Lennard-Jones potential (Kaplan, 2006; Lennard-Jones, 1937):

$$U_{IiJj}^{rep/is} = U_{IiJj}^{LJ} = 4\varepsilon_{I\iota,\Xi\xi} \left[\left(\frac{\sigma_{I\iota,\Xi\xi}}{\|\mathbf{r}_{IIi,I'Jj}\|} \right)^{12} - \left(\frac{\sigma_{I\iota,\Xi\xi}}{\|\mathbf{r}_{IIi,I'Jj}\|} \right)^6 \right] \quad (4-24)$$

The most popular choice for crystal structure prediction is the Buckingham potential:

$$U_{IiJj}^{dis} = U_{IiJj}^{Buck.} = A_{I\iota,\Xi\xi} e^{-\frac{\|\mathbf{r}_{IIi,I'Jj}\|}{B_{I\iota,\Xi\xi}}} - \frac{C_{I\iota,\Xi\xi}}{\|\mathbf{r}_{IIi,I'Jj}\|^6}, \quad (4-25)$$

mainly because transferable parameters, $A_{I\iota,\Xi\xi}$, $B_{I\iota,\Xi\xi}$ and $C_{I\iota,\Xi\xi}$, for most elements found in organic crystals are available in the literature. The Greek non-italic subscripts, $I\iota$, $\Xi\xi$ represent the chemical element or interaction site of atoms Ii and Jj respectively, i.e. $I\iota$, $\Xi\xi=C$, H, N,... The parameters $A_{I\iota,I\iota}$, $B_{I\iota,I\iota}$ and $C_{I\iota,I\iota}$, which describe same site;element interactions, are usually fitted to experimental data. The parameters for cross-interactions between different sites/elements $I\iota$ and $\Xi\xi$ are obtained by application of the following combining rules (Coombes et al., 1996; Cox et al., 1981 ; Day et al., 2003; Williams & Cox, 1984;) which are of the Lorentz (arithmetic mean) (Lorentz, 1881) and Berthelot (geometric mean) (Berthelot, 1898) forms, for B^{-1} , and A,C respectively:

$$\begin{aligned} A_{I\iota,\Xi\xi} &= \sqrt{A_{I\iota,I\iota} A_{\Xi\xi\Xi\xi}} \\ B_{I\iota,\Xi\xi} &= \frac{2B_{I\iota,I\iota} B_{\Xi\xi\Xi\xi}}{B_{I\iota,I\iota} + B_{\Xi\xi\Xi\xi}} \\ C_{I\iota,\Xi\xi} &= \sqrt{C_{I\iota,I\iota} C_{\Xi\xi\Xi\xi}} \end{aligned} \quad (4-26)$$

The dispersion term $\left(-\frac{c}{\|\mathbf{r}_{IIi,I'Jj}\|^6}\right)$ of the Buckingham potential is semi-empirical, while the repulsive exponential term $\left(e^{-\frac{\|\mathbf{r}_{IIi,I'Jj}\|}{B}}\right)$ is purely empirical (Born & Huang, 1954).

One of the most popular parameterizations is the so-called “FIT” parameters, with parameters for C, N and H (Coombes et al., 1996; Williams & Cox, 1984), O (Cox et al., 1981), Cl (Hsu & Williams, 1980), and F (Williams & Houpt, 1986). One can also find parameters for other elements such as S (Abraha & Williams, 1999; Lommersse, 2000; Motherwell, 2002), or P (Hanke et al., 2001), which have been derived from limited experimental data and whose transferability is therefore questionable.

Another parameterization of the Buckingham potential (equation (4-25)) was proposed by Williams (2001). One of the distinctive characteristics of this parameterization is that the same element is assigned different parameters depending on which atom it is bonded to e.g. the parameters for the hydroxyl group hydrogen are different to the parameters of a hydrogen bonded to nitrogen. Furthermore, hydrogen interaction sites differ from the hydrogen atomic position by 0.1Å along the bond direction. For reasons of simplicity the “FIT” parameterization is used in all the calculations presented in this thesis with the Buckingham potential.

In the context of lattice dynamics calculations we need to evaluate the second derivatives of the lattice energy. Such a calculation requires a knowledge of the derivatives of the repulsion/dispersion pair potential (see section 4.2). The first derivatives of the Buckingham potential with respect to the inter-atomic distances are:

$$\frac{\partial U_{Iijj}^{Buck.}}{\partial \|\mathbf{r}_{IIi,I'Jj}\|} = -\frac{A_{I\iota,\Xi\xi}}{B_{I\iota,\Xi\xi}} e^{-\frac{\|\mathbf{r}_{IIi,I'Jj}\|}{B_{I\iota,\Xi\xi}}} + 6 \frac{C_{I\iota,\Xi\xi}}{\|\mathbf{r}_{IIi,I'Jj}\|^7} \quad (4-27)$$

The second derivatives are:

$$\frac{\partial^2 U_{IiJj}^{Buck.}}{(\partial \|\mathbf{r}_{IIi,I'Jj}\|)^2} = \frac{A_{I\iota,\Xi\xi}}{B_{I\iota,\Xi\xi}^2} e^{-\frac{\|\mathbf{r}_{IIi,I'Jj}\|}{B_{I\iota,\Xi\xi}}} - 42 \frac{C_{I\iota,\Xi\xi}}{\|\mathbf{r}_{IIi,I'Jj}\|^8} \quad (4-28)$$

The first and second derivatives of the Lennard-Jones potential are

$$\frac{\partial U_{IiJj}^{LJ}}{\partial \|\mathbf{r}_{IIi,I'Jj}\|} = -4\varepsilon_{I\iota,\Xi\xi} \left[12 \left(\frac{\sigma_{I\iota,\Xi\xi}}{\|\mathbf{r}_{IIi,I'Jj}\|} \right)^{13} - 6 \left(\frac{\sigma_{I\iota,\Xi\xi}}{\|\mathbf{r}_{IIi,I'Jj}\|} \right)^7 \right] \quad (4-29)$$

$$\frac{\partial^2 U_{IiJj}^{LJ}}{(\partial \|\mathbf{r}_{IIi,I'Jj}\|)^2} = 4\varepsilon_{I\iota,\Xi\xi} \left[156 \left(\frac{\sigma_{I\iota,\Xi\xi}}{\|\mathbf{r}_{IIi,I'Jj}\|} \right)^{14} - 42 \left(\frac{\sigma_{I\iota,\Xi\xi}}{\|\mathbf{r}_{IIi,I'Jj}\|} \right)^8 \right] \quad (4-30)$$

4.4. Electrostatic interactions

The electrostatic interactions between molecules can be modeled in many ways. If one does not follow a full periodic quantum mechanical calculation (Neumann & Perrin, 2005), a popular method for the calculation of the electrostatic interactions is the use of point charges placed on the atoms. The use of multipole moments, also placed on the atoms, has found increasing use in crystal structure prediction (Day 2011; Price 2008).

A common approach in studies of the crystalline solid state is to fit atomic point charges to the electrostatic potential of the molecule. This approach is used, for example, at an early stage of a search for crystal structures, when it is not necessary to use the most accurate model. The electrostatic potential is usually derived using *ab initio* methods. Some of the algorithms designed for this purpose include the Chelp algorithm (Chirlian & Franc, 1987), the ChelpG algorithm (Breneman & Wiberg, 1990), the Merz & Kollman algorithm (Besler et al., 1990), the method proposed by Woods et al. (1990), RESP (Bayly et al, 1993), the method of Spackman (1996), the Chelp-Bow and ChelpMo methods (Sigfridsson & Ryde, 1998), and the REPEAT algorithm (Campaña at al. 2009) and its extension (Chen et al., 2010). The electrostatic energy is then calculated under the pairwise additive assumption. This

approach has been used in various calculations in the organic solid state (Day et al., 2003; Karamertzanis & Pantelides, 2005, 2007; Kazantsev et al., 2011:b; Ismail et al., 2013; Vasileiadis et al., 2012). Another approach is the use of off-atom point charges fitted to the *ab-initio* derived electrostatic potential (Karamertzanis & Pantelides, 2004; Williams, 1994) or derived based on multipole moments (Sokalski et al. 1993). Zhang & Maginn (2012) fitted point charges to the DFT derived electrostatic potential around the molecules in the crystalline phase. This approach showed improved performance in modelling salts where polarizability and charge transfer are important. In the calculations presented in this thesis whenever electrostatic interactions are modeled using point charges the ChelpG algorithm is used and the charges are fitted to the isolated molecule charge density.

Another way to model the electrostatic interactions between molecules is a *multipole expansion*. Here the electrostatic potential created around a continuous or discrete charge distribution, such as that of a molecule, is approximated using a series expansion. In order to overcome problems of convergence and stability (Stone, 1981, 1996) associated with a single-centre multipole expansion, it is common practice to divide the molecule into smaller regions, each one described by a different multipole expansion. The multipole moments are also commonly derived based on the results of *ab-initio* calculations, using one of many methods. Some of these methods are the “*distributed multipole analysis*” (DMA) (Stone, 1981, 1996, 2005:a; Stone & Alderton, 1985), the “*atoms in molecules*” approach (AIM) (Kosov & Popelier, 2000), the “*transferable atom equivalents*” (TAE) (Whitehead et al., 2003), which is a variation of the AIM method, the “*cumulative atomic multipole moments*” (CAMM) method (Sokalski & Poirier, 1983), and its variation the “*correlated cumulative atomic multipole moments*” (CCAMM) method (Sokalski & Sawaryn, 1987).

In this thesis, an atomic multipole representation of the electrostatic interactions is adopted. The multipole moments are derived using the distributed multipole analysis method (Stone, 2005:a) using Stone’s GDMA 2.2 program (Stone, 2005:a). GDMA 2.2 generates atomic multipole moments based on the wave function that had earlier been calculated using the *Gaussian 09* (Frisch et al., 2009). In subsequent sections, the calculation of the electrostatic interactions in a crystal by means of a multipole expansion, for a given description of the electrostatic potential, is described. The equivalent calculation using a point charge representation of the

electrostatic potential is simply the special case in which the multipole expansion is truncated to the 0th order term.

4.4.1. Electrostatic interactions using distributed multipoles

The calculation of the electrostatic interactions between a pair of atoms can be carried out using a multipole expansion. There are two popular variations of the formalism for the description of electrostatics using a multipole expansion, the *Cartesian formalism* and the *Spherical tensor formalism* (Stone, 1996). In the Cartesian formalism the electrostatic potential created by the charge distribution around an atom is approximated by a Taylor series expansion. On the other hand in the spherical tensor formalism the electrostatic potential is expanded in a series of *spherical harmonics*. The formalism for the transition from one of the formalisms to the other and vice versa can be found in Stone (1975, 1976). One can find other definitions in the literature (e.g., Der Chao et al., 2004). Here we adopt the spherical tensor formulation, mainly because the crystal structure prediction technique developed in the Molecular Systems Engineering research group at Imperial College makes use of the spherical tensor formulation (Kazantsev et al., 2010, 2011:a) and this choice allows the lattice dynamics calculations to be consistent with our lattice energy minimization algorithms. In addition, the formalism is less cumbersome and it is easily extended to multipole moments of arbitrarily high order.

Within the spherical tensor formalism the energy arising from the electrostatic interactions of a pair of atoms is given by (Stone, 1996; Stone & Tough 1984):

$$U_{IiIj}^{ele} = \frac{1}{4\pi\epsilon_0} \sum_{l_{II}=0}^{\infty} \sum_{l_{JJ}=0}^{\infty} \sum_{m_{II}m_{JJ}m} (-1)^{l_{II}} \sqrt{\frac{(2l_{II} + 2l_{JJ} + 1)!}{(2l_{II})!(2l_{JJ})!}} Q_{l_{II}}^{m_{II}} Q_{l_{JJ}}^{m_{JJ}} I_{l,m} (\|\mathbf{r}_{II} - \mathbf{r}_{JJ}\|) \cdot \begin{pmatrix} l_{II} & l_{JJ} & l \\ m_{II} & m_{JJ} & m \end{pmatrix} \quad (4-31)$$

where l_{II} enumerates the order of the multipole moment, $Q_{l_{II}}^{m_{II}}$, on atom Ii and m_{II} indicates the components of the multipole moment l_{II} . Each moment takes its name based on its order: charge for $l_{II} = 0$, dipole for $l_{II} = 1$, quadrupole for $l_{II} = 2$, octopole for $l_{II} = 3$ and in general, the $2^{l_{II}}$ -pole moment corresponds to l_{II} . Each

moment has $2l_{II} + 1$ components enumerated as: $m_{II} = -l_{II}, -l_{II} + 1, \dots, 0, \dots, l_{II} - 1, l_{II}$. The order of interaction, l , is equal to $l_{II} + l_{JJ}$. The quantity $\begin{pmatrix} l_{II} & l_{JJ} & l \\ m_{II} & m_{JJ} & m \end{pmatrix}$ is the so-called *Wigner 3j symbol*. It is associated with the Clebsch-Gordan coefficients and analytical expressions for its calculation are available in the literature (Zare, 1988; Stone, 1996). $\|\mathbf{r}_{IIi} - \mathbf{r}_{JJj}\|$ is the distance vector between the two interacting atoms and $I_{l,m}$ is the irregular solid spherical harmonics:

$$I_{l,m}(\|\mathbf{r}\|) = \frac{C_{lm}(\theta, \varphi)}{\|\mathbf{r}\|^{l+1}} \quad (4-32)$$

where $C_{lm}(\theta, \varphi)$ is the normalized spherical harmonics and θ and φ are the polar and azimuthal angles of position vector \mathbf{r} , respectively.

In equation (4-31) the multipole moments are expressed with reference to a global axis system. This reference system is not convenient for calculations in the crystal because different molecules with identical conformation (e.g. molecules related by a point group symmetry operation) have different moments. To avoid this problem, the multipole moments are instead calculated by expressing the molecular conformation with reference to a local axis system which is rigidly fixed to the molecule. Local axis systems are defined in an equivalent way for symmetry-related molecules, so that multipoles are only conformation dependent. A more complete discussion on global and local axis systems and how they are determined can be found elsewhere (Karamertzanis, 2004; Stone 1996). When the multipole moments are calculated with respect to a local axis system the energy of a pair of atoms is given by (Stone, 1996; Stone & Tough 1984; Price et al. 1984):

$$U_{IIiJJj}^{ele} = \frac{1}{4\pi\epsilon_0} \sum_{l_{II}=0}^{\infty} \sum_{l_{JJ}=0}^{\infty} \sum_{m_{II}m_{JJ}} (-1)^{l_{II}} \sqrt{\frac{(2l_{II} + 2l_{JJ} + 1)!}{(2l_{II})!(2l_{JJ})!}} \hat{Q}_{l_{II}}^{m_{II}} \hat{Q}_{l_{JJ}}^{m_{JJ}} \frac{S_{l_{II}l_{JJ}l}^{m_{II}m_{JJ}}(\Omega_I, \Omega_J, \hat{\mathbf{r}}_{II})}{\|\mathbf{r}_{IIi} - \mathbf{r}_{JJj}\|^{l+1}} \quad (4-33)$$

Here the hat symbol is used to indicate the fact that, in contrast to equation (4-31), the multipole moments in equation (4-33), $\hat{Q}_{l_{II}}^{m_{II}}$, are calculated with reference to a local axis system. Different components of the multipole moments are enumerated using

the indices denoted by non-italic symbols, i.e. m_{Ii} (instead of m_{Ii}). The two sets of multipole moments are related via a linear transformation of the form:

$$\hat{Q}_{l_{II}}^{m_{II}} = \sum_{m_{II}} Q_{l_{II}}^{m_{II}} D_{m_{II} m_{II}}^{l_{II}}(\Omega_I) \Leftrightarrow Q_{l_{II}}^{m_{II}} = \sum_{m_{II}} \hat{Q}_{l_{II}}^{m_{II}} [D_{m_{II} m_{II}}^{l_{II}}(\Omega_I)]^*, \quad (4-34)$$

where $D_{m_{II} m_{II}}^{l_{II}}$ is the Wigner rotation matrix (Stone; 1996) and $*$ indicates its complex conjugate. $S_{l_{II} l_{JJ}}^{m_{II} m_{JJ}}(\Omega_I, \Omega_J, \hat{\mathbf{r}}_{IIi, I'Jj})$ denotes a tensor that accounts for the orientation-dependence of the multipole moments (Stone 1978 & 1996; Stone & Tough 1984; Price et al. 1984). Ω_I and Ω_J are matrices defining the local axis system on molecules I and J respectively. $\hat{\mathbf{r}}_{IIi, I'Jj}$ is the unit vector along the direction of the distance vector between IIi and $I'Jj$: $\hat{\mathbf{r}}_{IIi, I'Jj} = \mathbf{r}_{IIi, I'Jj} / \|\mathbf{r}_{IIi, I'Jj}\|^{-1}$.

A last comment that needs to be made is that in order to be consistent with current lattice energy minimization algorithms (Kazantsev et al., 2011:a; Price et al., 2010), we truncate the infinite sums in such a way that interactions up to fourth order only are considered (i.e. the interactions that decay to the inverse fifth power of the distance):

$$U_{IIJ}^{ele} = \frac{1}{4\pi\epsilon_0} \sum_{l_{II}=0}^4 \sum_{l_{JJ}=0}^{4-l_{II}} \sum_{m_{II} m_{JJ}} (-1)^{l_{II}} \sqrt{\frac{(2l_{II} + 2l_{JJ} + 1)!}{(2l_{II})! (2l_{JJ})!}} \hat{Q}_{l_{II}}^{m_{II}} \hat{Q}_{l_{JJ}}^{m_{JJ}} \cdot \frac{S_{l_{II} l_{JJ}}^{m_{II} m_{JJ}}(\Omega_I, \Omega_J, \hat{\mathbf{r}}_{IIi, I'Jj})}{\|\mathbf{r}_{IIi, I'Jj}\|^{l+1}} \quad (4-35)$$

The contributions that are considered if the multipole expansion is truncated in this way are summarized in Table 4-1.

		Order of multipole moment l_{II}				
		0	1	2	3	4
Order of multipole moment l_{II}	0	Charge-Charge	Charge-Dipole	Charge-Quadrupole	Charge-Octopole	Charge-Hexadecapole
	1	Dipole-Charge	Dipole-Dipole	Dipole-Quadrupole	Dipole-Octopole	
	2	Quadrupole-Charge	Quadrupole-Dipole	Quadrupole-Quadrupole		
	3	Octopole-Dipole	Octopole-Dipole			
	4	Hexadecapole-Charge				

Table 4-1 Summary of all the contributions that are included in the electrostatic interactions, when the multipole expansion is truncated at interactions of fourth order.

4.4.2. Orientation dependence of distributed multipoles

The orientation dependence of the distributed multipole moments is described by the tensor, $S_{l_{II}l_{JJ}}^{m_{II}m_{JJ}}(\Omega_I, \Omega_J, \hat{\mathbf{r}}_{IIi,I'Jj})$, defined as (Stone, 1978, 1996; Price et al., 1984):

$$S_{l_{II}l_{JJ}l}^{m_{II}m_{JJ}}(\Omega_I, \Omega_J, \hat{\mathbf{r}}_{IIi,I'Jj}) = (-1)^{l_{II}} \sum_{m_{II}m_{JJ}m} [D_{m_{II}m_{II}}^{l_{II}}(\Omega_I)]^* [D_{m_{JJ}m_{JJ}}^{l_{JJ}}(\Omega_J)]^* C_{lm}(\theta, \varphi) \begin{pmatrix} l_{II} & l_{JJ} & l \\ m_{II} & m_{JJ} & m \end{pmatrix} \quad (4-36)$$

This last equation is not directly useful for calculations because of the appearance of the Wigner rotation matrices and the normalized spherical harmonics. In the literature one can find recurrence relations for its calculation (Hätting, 1996) or for the calculation of the so-called interaction tensor, usually denoted by $T_{l_{II}l_{JJ}}^{m_{II}m_{JJ}}$, which is

essentially the quantity $\frac{S_{l_{II}l_{JJ}l}^{m_{II}m_{JJ}}(\Omega_I, \Omega_J, \hat{\mathbf{r}}_{IIi,I'Jj})}{\|\mathbf{r}_{IIi,I'Jj}\|^{l+1}}$ (Challacombe et al., 1995; Hätting, 1996).

To the best of our knowledge, the most general recurrence relation is (Price et al., 1984):

$$\begin{aligned}
& S_{l'_{II} l''_{JJ} j' j''}^{m'_{II} m''_{JJ}} = \sum_{l_{II} l_{JJ} j} i^{(l'_{II} - l'_{JJ} - j) + (l''_{II} - l''_{JJ} - j'') + (l_{II} - l_{JJ} - j)} (2l_{II} + 1)(2l_{JJ} \\
& + 1)(2j + 1) \\
& \cdot \begin{pmatrix} l'_{II} & l''_{II} & l_{II} \\ m'_{II} & m''_{II} & -m_{II} \end{pmatrix} \begin{pmatrix} l'_{JJ} & l''_{JJ} & l_{JJ} \\ m'_{JJ} & m''_{JJ} & -m_{JJ} \end{pmatrix} \begin{pmatrix} j' & j'' & j \\ 0 & 0 & 0 \end{pmatrix} \\
& \cdot \begin{Bmatrix} l'_{II} & l''_{II} & l_{II} \\ l'_{JJ} & l''_{JJ} & l_{JJ} \\ j' & j'' & j \end{Bmatrix} S_{l_{II} l_{JJ} j}^{m_{II} m_{JJ}}
\end{aligned} \tag{4-37}$$

and it is adopted here. In Price et al. (1984) one can also find that analytical expressions for S_{101}^{00} , $S_{101}^{\pm 10}$, S_{011}^{00} , $S_{101}^{0\pm 1}$, S_{110}^{00} , $S_{110}^{\pm 1\pm 1}$, and S_{111}^{00} as a function of the unit vectors along the local axis systems of the molecules to which the two atoms belong and of the unit vector along the direction of the distance vector between the two atoms. These expressions can be used together with equation (4-37) in order to obtain relations for any other element of the $S_{l_{II} l_{JJ} j}^{m_{II} m_{JJ}}$ tensor that is of interest. In this way, we can obtain equations of the form:

$$S_{202}^{00} = \frac{1}{2\sqrt{5}} [9(S_{101}^{00})^2 - S_{000}^{00}] \tag{4-38}$$

that allow us to calculate the necessary elements of S . The equations that we obtained in this way are presented in detail in Appendix A.

Another way to obtain the orientation dependence of multipole interactions is the ladder operator described in Price et al. (1984). Again the available analytical expressions for low order S elements are used as a starting point and analytical expressions are obtained for the elements of interest. Finally, another strategy (Price et al., 2010) is to use analytical expressions for certain contributions to the electrostatic energy that can be found in the literature (Price et al., 1984; Stone, 1996).

4.4.3. Derivatives of the electrostatic contributions

In order to differentiate the expressions adopted for the electrostatic contribution to the lattice energy (equation 4-33), we make the assumption that infinitesimal changes to the conformation of the molecule do not modify the charge density of the molecule and therefore that the multipole moments do not change. As a consequence of this assumption the derivatives of the multipole moments with respect to the positions of the atoms are zero, and therefore the derivative of the electrostatic contribution is given by:

$$\begin{aligned} & \frac{\partial^{\mu+\lambda} U_{IiJj}^{ele}}{\partial(\mathbf{r}_{IIi})^\mu \partial(\mathbf{r}_{IJj})^\lambda} \\ &= \frac{1}{4\pi\epsilon_0} \sum_{l_{IIi}=0}^4 \sum_{l_{IJj}=0}^{4-l_{IIi}} \sum_{m_{IIi} m_{IJj}} \left[(-1)^{l_{IIi}} \sqrt{\frac{(2l_{IIi} + 2l_{IJj} + 1)!}{(2l_{IIi})! (2l_{IJj})!}} \hat{Q}_{l_{IIi}}^{m_{IIi}} \hat{Q}_{l_{IJj}}^{m_{IJj}} \right. \\ & \quad \left. \cdot \frac{\partial^{\mu+\lambda}}{\partial(\mathbf{r}_{IIi})^\mu \partial(\mathbf{r}_{IJj})^\lambda} \left(\frac{S_{l_{IIi} l_{IJj} l}^{m_{IIi} m_{IJj}} (\Omega_I, \Omega_J, \hat{\mathbf{r}}_{IIi, IJj})}{\|\mathbf{r}_{IIi, IJj}\|^{l+1}} \right) \right] \end{aligned} \quad (4-39)$$

where $\mu, \lambda \in [0, 1, 2, \dots]$. The calculation of the derivative

$$\frac{\partial^{\mu+\lambda}}{\partial(\mathbf{r}_{IIi})^\mu \partial(\mathbf{r}_{IJj})^\lambda} \left(\frac{S_{l_{IIi} l_{IJj} l}^{m_{IIi} m_{IJj}} (\Omega_I, \Omega_J, \hat{\mathbf{r}}_{IIi, IJj})}{\|\mathbf{r}_{IIi, IJj}\|^{l+1}} \right)$$

is carried out using the chain rule. In this calculation, the derivatives of the unit vector $\hat{\mathbf{r}}_{IIi, IJj}$ are required:

$$\frac{\partial^{\mu+\lambda} \hat{\mathbf{r}}_{IIi, IJj}}{\partial(\mathbf{r}_{IIi})^\mu \partial(\mathbf{r}_{IJj})^\lambda} \quad (4-40)$$

The gradient of the unit vector is:

$$\frac{\partial \hat{\mathbf{r}}_{IIi,I'Jj}}{\partial \mathbf{r}_{IIi}} = \mathbf{I} \frac{1}{\|\mathbf{r}_{IIi,I'Jj}\|} - \frac{1}{\|\mathbf{r}_{IIi,I'Jj}\|} \frac{\partial \|\mathbf{r}_{IIi,I'Jj}\|}{\partial \mathbf{r}_{IIi}} (\hat{\mathbf{r}}_{IIi,I'Jj})^T \quad (4-41)$$

Higher-order derivatives of the unit vector are obtained by applying the chain rule to equation (4-41).

4.5. Summary

The modelling approach that is adopted for the calculations to be presented in this work has been described. The intra-molecular interactions are calculated using quantum mechanical calculations, while the repulsion and dispersion interactions are calculated using empirical potentials with transferable parameters available in literature. A distributed multipole approach is used for the electrostatic interactions. Expressions for the calculation of the intermolecular contribution to the lattice energy per unit cell (4-7), and the dynamical matrix (4-22) were derived and found to involve infinite series. In the next chapter an appropriate method for evaluating these series is discussed.

5. Evaluation of lattice sums

5.1. The need for a “lattice sum method”

The term *lattice sum* refers to summations over all the unit cells of a crystal. Under the widely used assumption of an infinite crystal such a summation becomes an infinite sum and a special technique needs to be employed in order to evaluate it. The major common characteristic of the various sums that appear in physical problems is that each term of the summation depends on an inverse power law of the distance:

$$\sim \frac{1}{\|\mathbf{r}_{0Ii,1Jj}\|^l} \quad (5-1)$$

In modeling fluids, it is common practice to apply a *quintic spline* and a *tail correction* (Theodorou & Suter, 1984) in order to facilitate convergence and ensure accuracy when evaluating this type of sums. It is not possible to do this in solids because in order to apply the tail correction it is necessary to assume that the radial distribution function $g(r)$ is equal to one for r greater than the point where the spline applies, an assumption that is not valid in solids. In addition, these types of summations converge slowly for small values of $l < \sim 6$ or conditionally converge for the case of interactions such as charge-charge or charge-dipole ($l \leq 3$). As a consequence it is necessary to find an efficient and accurate method for calculating sums of this kind.

For the purpose of the work described in this thesis, we need special summation techniques in two cases, (a) the calculation of the electrostatic contribution to the

lattice energy and (b) the calculation of the electrostatic contribution to the dynamical matrix.

a) Summation for the electrostatic contribution to the lattice energy

By substitution of equation (4-33) into equation (4-7) we obtain the following expression for the electrostatic contribution to the lattice energy under the pairwise additivity assumption:

$$\begin{aligned} \bar{U}^{ele} = & \frac{1}{2} \frac{1}{4\pi\epsilon_0} \sum_{Ii} \sum_{Jj} \sum_{\substack{l \in L \\ l \neq 0 \text{ if } J=I}} \sum_{l_{ii}=0}^4 \sum_{l_{jj}=0}^{4-l_{ii}} \sum_{m_{Ii} m_{Jj}} (-1)^{l_{ii}} \\ & \cdot \sqrt{\frac{(2l_{ii} + 2l_{jj} + 1)!}{(2l_{ii})! (2l_{jj})!}} \hat{Q}_{l_{ii}}^{m_{Ii}} \hat{Q}_{l_{jj}}^{m_{Jj}} \frac{S_{l_{ii} l_{jj} l}^{m_{Ii} m_{Jj}}(\Omega_I, \Omega_J, \hat{\mathbf{r}}_{IIi, I'Jj})}{\|\mathbf{r}_{0Ii, IJj}\|^{l+1}} \end{aligned} \quad (5-2)$$

which is equivalent to:

$$\begin{aligned} \bar{U}^{ele} = & \frac{1}{2} \frac{1}{4\pi\epsilon_0} \sum_{Ii} \sum_{Jj} \sum_{l_{ii}=0}^4 \sum_{l_{jj}=0}^{4-l_{ii}} \sum_{m_{Ii} m_{Jj}} (-1)^{l_{ii}} \sqrt{\frac{(2l_{ii} + 2l_{jj} + 1)!}{(2l_{ii})! (2l_{jj})!}} \\ & \cdot \hat{Q}_{l_{ii}}^{m_{Ii}} \hat{Q}_{l_{jj}}^{m_{Jj}} \left(\sum_{\substack{l \in L \\ l \neq 0 \text{ if } J=I}} \frac{S_{l_{ii} l_{jj} l}^{m_{Ii} m_{Jj}}(\Omega_I, \Omega_J, \hat{\mathbf{r}}_{IIi, I'Jj})}{\|\mathbf{r}_{0Ii, IJj}\|^{l+1}} \right) \end{aligned} \quad (5-3)$$

It is apparent from equation (5-3) that in order to evaluate the electrostatic contribution to the lattice energy poorly converging (e.g. hexadecapole-charge, i.e. $l_{ii} = 4$ and $l_{jj} = 0$) or conditionally converging (e.g. charge-quadrupole, i.e. $l_{ii} = 2$ and $l_{jj} = 0$) lattice sums are involved. All these sums are of the general form:

$$\sum_{\substack{l \in L \\ l \neq 0 \text{ if } J=I}} \frac{S_{l_{ii} l_{jj} l}^{m_{Ii} m_{Jj}}(\Omega_I, \Omega_J, \hat{\mathbf{r}}_{IIi, I'Jj})}{\|\mathbf{r}_{0Ii, IJj}\|^{l+1}} \quad (5-4)$$

b) Summation for the electrostatic contribution to the dynamical matrix

It is apparent from equations (4-22) and (4-23) that the core part for calculation of the dynamical matrix is a calculation of a lattice sum described in equation (4-22). While this calculation is straightforward for the repulsion/dispersion contribution, it is not at all trivial for the electrostatic contribution. By substitution of equation (4-39) for $\mu, \lambda = 1$ in equation (4-22), the following expression is obtained:

$$\begin{aligned} & \widehat{\mathbf{D}}_{II,Jj}^{ele}(\mathbf{k}) \\ &= \frac{1}{\sqrt{m_{Ii}m_{Jj}}} \frac{1}{4\pi\epsilon_0} \cdot \sum_{l_{II}=0}^4 \sum_{l_{JJ}=0}^{4-l_{II}} \sum_{m_{Ii}m_{Jj}} (-1)^{l_{II}} \sqrt{\frac{(2l_{II} + 2l_{JJ} + 1)!}{(2l_{II})!(2l_{JJ})!}} \widehat{Q}_{l_{II}}^{m_{Ii}} \widehat{Q}_{l_{JJ}}^{m_{Jj}} \\ & \cdot \sum_{\substack{l \in L \\ l \neq 0 \text{ if } I=J}} \left[\frac{\partial^2}{\partial \mathbf{r}_{0Ii} \partial \mathbf{r}_{l'Jj}} \left(\frac{S_{l_{II}l_{JJ}l}^{m_{Ii}m_{Jj}}(\Omega_I, \Omega_J, \hat{\mathbf{r}}_{IIi,l'JJ})}{\|\mathbf{r}_{0Ii,lJJ}\|^{l+1}} \right) e^{i\mathbf{k}(\hat{\mathbf{r}}_{IIi}-\hat{\mathbf{r}}_{0Ii})} \right] \end{aligned} \quad (5-5)$$

This equation shows that we need to evaluate a lattice sum of the form:

$$\sum_{\substack{l \in L \\ l \neq 0 \text{ if } I=J}} \left[\frac{\partial^2}{\partial \mathbf{r}_{0Ii} \partial \mathbf{r}_{l'Jj}} \left(\frac{S_{l_{II}l_{JJ}l}^{m_{Ii}m_{Jj}}(\Omega_I, \Omega_J, \hat{\mathbf{r}}_{IIi,l'JJ})}{\|\mathbf{r}_{0Ii,lJJ}\|^{l+1}} \right) e^{i\mathbf{k}(\hat{\mathbf{r}}_{IIi}-\hat{\mathbf{r}}_{0Ii})} \right] \quad (5-6)$$

This lattice sum also converges conditionally or poorly for small values of l (~ 4).

5.2. Lattice sum methods

The scientific literature is rich in methods that try to tackle the problem of evaluating the lattice sums that appear in several types of calculations in crystalline materials and in which long range Coulomb interactions are present. A first approach widely adopted in the early decades was to assume only nearest neighbours interaction or interaction up to second neighbour need to be taken into account. This approach, a crude truncation of the lattice sum, is of course not accurate and lacks a physical justification. The first effort to formally treat the problem of lattice sums was that of Madelung (1918) followed by Ewald (1917, 1921) and Evjen (1931).

Evjen (1931) suggested a scheme for the calculation of the Coulomb potential of ionic crystals of the NaCl type in direct space. More specifically he suggested that the potential should be calculated directly for the ions inside an arbitrarily chosen volume of the material, containing “N” unit cells. The potential for ions on the surface of that portion of the material should then be added to the sum but weighted with a factor of 1/2 if the ion resides on a face of the chosen volume, a factor of 1/4 if the ion resides on an edge, or with a factor of 1/8 if the ion resides on a vertex. This is a very simple method, whose disadvantage is that it cannot be used for an arbitrary crystal. Evjen (1931) pointed out this problem with the CsCl-type crystal.

The reason why the method of Evjen is not applicable to any crystal was revealed by Dahl (1965), who attributed the issue to the presence of a dipole moment in the chosen “reference” volume for the summation. By directly solving Poisson’s equation Dahl proposed a solution. Later it became clear that in order to have absolute convergence on an arbitrarily chosen “reference” volume, it is necessary for all the multipole moments of the volume up to quadrupole to vanish (Coogan, 1967). Another method that employs different weights for the “surface charges” than those proposed by Evjen has also been put forward (Marathe et.al., 1983). The weights are selected such that the chosen reference volume has zero charge and dipole and thus convergence is guaranteed. The authors demonstrate the method in a one-dimensional lattice of alternating point charges. One can also find methods that attribute weights not only to the charges at the surface but also to those within the chosen volume, such as the method of Derenzo et al. (2000), or the recent method of Gellé & Lepetit (2008), in which volumes with an arbitrarily large number of vanishing multipole moments are constructed.

Another method developed for the calculation of the Coulomb interactions of a system of charges by direct summation is the “Wolf” method (Wolf, 1992; Wolf et al., 1999). Wolf, as Evjen, recognizes the fact that convergence issues arise because the fraction of material included in a cut-off sphere is not neutral, so he suggested that the summation should be performed over “dipolar molecules”, where each “molecule” consists of a pair of opposite ions. In such a way, the necessary lattice sum converges, albeit to an incorrect value. This is because the material within the cut-off sphere is polarized in the presence of the field created by the material outside the sphere. The correct value is then obtained by adding a term accounting for polarization as proposed by de Leeuw et al. (1980). An alternative method to obtain a series that

converges directly to the correct limit is to sum over “quadrupolar molecules” or “octopolar molecules”, where the result obtained is the same as the result of the “dipolar molecule” with the polarization correction (Wolf, 1992; Wolf et al., 1999). The method was demonstrated in the simple NaCl system. The authors also presented a way in which the method can be extended to simulations of disordered phases where it is difficult to identify charge-neutral entities such as the “dipolar molecules”. The extension to disordered phases is based on a term neutralizing the net charge within the cut-off sphere. Wolf’s method has found wide application in various studies such as molecular simulations of electrolyte systems (Avendaño & Gil-Villegas, 2006, Viveros-Méndez & Gil-Villegas, 2012), the study of zeolites (Demontis et al., 2001), thin films of PbTiO₃ (Sepliarsky et al., 2006), simulations of nematic liquid crystals (Goto et al., 2007), and the calculation via Molecular Dynamics simulations of dynamical information (speed of sound and acoustic modes) of 2Ca(NO₃)₂3KNO₃ glass (Ribeiro, 2007).

A modified version of Wolf’s potential with improved dielectric properties via Molecular Dynamics simulation was proposed a few years later (Zhan et al., 2002). Fukuda et al. (2011) presented the “zero-dipole summation method” (ZD) as an extension of Wolf’s method for molecular simulations of disordered phases (Wolf et al., 1999) in order to perform direct space calculations of the electrostatics within a cut-off sphere whose dipole moment is also neutralized. The method has been applied to water (Fukuda et al., 2012) and a biological system (Kamiya et al., 2013).

Another large class of methods consists of those which are based on Ewald’s method for performing a lattice sum in a periodic system. In the early 20th century, Ewald studied the interaction of crystalline solids with light (this early work is reviewed in Ewald (1965, 1979)). Although there was no experimental evidence for the periodicity of crystals at that time¹, Ewald found the “generalized Θ -function transformation”, which is the basis for the summation technique after his name, by studying the field created by an array of dipoles placed on an orthorhombic lattice. It is interesting to mention Ewald’s comments (Ewald, 1979):

¹ “In 1910 when I began to work on my thesis there was no quantitative proof for the internal periodicity of the crystal.” (Ewald, 1979).

“The extraction of one dipole field seemed, however, hopeless because it was thoroughly mixed up with all others. Here a remark of Debye (at the time Sommerfeld’s assistant) at a ski meeting in Mittenland helped. He recalled a method Riemann had used in a similar case.”

He further remarked:

“I often feel embarrassed when the now generally accepted method of summation of potentials in crystals is given my name. True I extended it later to non-orthogonal axes and I gave an explanation why it produces very rapid convergence-but essentially the method seems to go back to Riemann.”

Born, Misra and Fürth published a series of four papers (Born, 1940; Born & Fürth 1940; Born & Misra, 1940; Misra 1940) in which they investigated the stability of crystal lattices. In two of these papers (Born & Misra, 1940; Misra 1940), they presented two methods for the calculation of lattice sums, one based on the Θ -function transformation and one on the generalized Θ -function transformation. The latter is what is widely known as the Ewald summation method. Both methods consist of transforming the lattice sum into two integrals: the first consists of the short range part of the potential while the second corresponds to the long range part, which is evaluated in the reciprocal space, using the generalized Θ -function transformation. The methods and the close connection between them were demonstrated on the simple face centered and body centered cubic lattice in the early papers. Later, other types of lattice sums were evaluated using these methods. These include more complicated lattice sums on the cubic lattice (Born & Bradburn, 1943), and the electric field of a dipole lattice (Born & Huang, 1954). Lattice sums of oscillating functions that are involved in magnetic and electric problems in dipole cubic crystals (simple, face and body centered) were also evaluated using the generalized Θ -function transformation (Cohen & Keffer, 1955).

Nijboer & De Wette (1957) introduced an alternative way to derive the Ewald method of sums. They presented the lattice sum method as a mathematical process of the form:

$$f(x) = f(x) + f(x)g(x) - f(x)g(x) = f(x)g(x) + f(x)[1 - g(x)] \quad (5-7)$$

Here while the lattice sum of $f(x)$ diverges, the lattice sum of $f(x)g(x)$ converges if $g(x)$ is chosen based on criteria the authors define. Then the series of $f(x)[1 - g(x)]$ converges in Fourier space. Apart from presenting this elegant and simple method to prove the summation formulas, the authors derived for the first time, the lattice sum expressions for series of spherical harmonics. Using the principles presented in their 1957 paper, Nijboer & De Wette calculated the field at a lattice point due to the presence of the rest of the lattice in a simple cubic and a monoclinic dipole lattice (Nijboer & De Wette, 1958), later extending this to a general dipole lattice (De Wette & Schacher, 1965). Grant (1965:a,1965:b) later generalized the method presented by Nijboer & De Wette (1957) to include an even wider class of lattice sums.

Soon the method found application in Monte Carlo simulations of plasma (Brush et al., 1966) and salts (Woodcock & Singer, 1971). To the best of my knowledge these were the first studies to present Ewald summations with the aid of screened charges. Later the problem of conditionally converging series was revisited (de Leeuw et al. 1980), and the properties that the screening function should possess were investigated from a mathematical point of view. The authors also presented an Ewald summation technique for the point charge-dipole interactions and the point charge-quadrupole interactions. They did not proceed to higher order multipole interactions because the associated lattice sums converge.

In 1972 Aung & Strauss presented an extended list of the lattice sums involved in various types of calculations, when the inter-atomic and/or inter-molecular interactions are modeled using the Cartesian formalism of a multipole expansion. The authors gave an extended list of various interactions that decay up to inverse 8th power of distance (interactions of 7th order). In 2000 Nymand and Linse presented Ewald type expressions for the electrostatic potential, electrostatic field, electrostatic field gradient and forces, i.e., all the quantities that are necessary for molecular simulations when molecular models that include charge and dipole moment are used. Similar equations for interactions up to quadrupole moment were given later (Aguado & Madden, 2003). The formulas for the real space sum of Aguado & Madden were later

corrected and the reciprocal space sums were presented in a more compact way in the work of Laino & Hutter (2008).

The principles of the Ewald summation were also used to derive the lattice sum arising from the interaction of a multipole moment with a two-dimensional lattice of multipole moments (van der Berg & van der Avoird, 1989). This method is poorly converging when the off-plane multipole is a small distance from the plane of the periodic arrangement of multipole moments, a problem later solved by Stone (2005:b). The extension of the Ewald method to systems that are periodic along only two directions (e.g. surfaces) has also been the subject of extensive research. Some of the published work on the subject can be found in Bródka & Grzybowski (2002), Heyes et al. (1977), Spohr (1997) and Yeh & Berkowitz (1999).

Fuchizaki (1994, 2010) further generalised the Ewald method to lattice sums in spaces of arbitrary dimensionality. Furthermore the lattice sums considered consisted in a scalar, oscillatory function:

$$\sum_{\mathbf{l}} f(\lambda \|\mathbf{r} + \mathbf{l}\|) \frac{e^{i\mathbf{k}\mathbf{l}}}{\|\mathbf{r} + \mathbf{l}\|^l} \quad (5-8)$$

where \mathbf{r} is a direct space vector, \mathbf{l} is a direct space lattice vector, \mathbf{k} is a reciprocal space vector, all of them of arbitrary dimensionality, and λ is the wave number characterising f .

The behaviour of the Ewald summation method as a function of system size motivated the development of a number of variations. The computational cost of the reciprocal sum of the conventional Ewald technique scales as N^2 (where N is the number of particles), thus for large systems the computational cost become prohibitive. “Particle-Particle/Particle-Mesh” (PPPM or P^3M), “Particle Mesh Ewald” (PME) (Darden et al., 1993), and the “Smooth Particle Mesh Ewald” (SPME) (Essmann et al., 1995) summation methods are based on improved numerical algorithms for the calculation of the reciprocal sum, the basis of which is the Fast Fourier Transform (FFT). The direct space sum is calculated normally, with a sufficiently large value of the Ewald convergence parameter so that it converges fast. The reciprocal space sum then becomes the most computationally demanding component and is therefore calculated approximately.

In the various mesh methods, the charge that is distributed in a simulation box is assigned to the nodes of a grid (mesh). In PME (Darden et al., 1993) the barymetric form of the weights of the Lagrangian interpolation is used. The SPME (Essmann et al., 1995) approach is an extension of PME that uses Cardinal *B*-splines instead. This allows direct differentiation of the energy expression to obtain the forces instead of resorting to interpolation as is used in PME. In P^3M an assignment scheme is chosen that distributes the charges onto a user-defined number of nearest mesh nodes (Deserno & Holm, 1998). The “Triangle Shape Charge” (TSC) method (Luty et al., 1995; Toukmaji & Board, 1996) is a specific case of the assignment scheme in P^3M , where each charge is distributed onto the 27 nearest mesh points.

The other major difference between different approaches is the way Poisson’s equation is solved in order to obtain the electrostatic potential created by the discrete distribution of charge. In PME (Darden et al., 1993 ; Deserno & Holm, 1998 ; Luty et al., 1995) the solution of Poisson’s equation is taken to be the same for the mesh and the continuous charge distribution, while in SPME, the solution is modified by a pre-factor (Darden et al., 1993; Deserno & Holm, 1998; Essmann et al., 1995). In P^3E , the solution is optimized in such a way that the resulting potential is as close as possible to the continuous charge distribution (Deserno & Holm, 1998; Luty et al., 1995).

Other variations are also available such as the “Multi-Level Ewald” method (Cerutti & Case, 2010), the variation of SPME for three-dimensional systems exhibiting two-dimensional periodicity (Kawata & Nagashima, 2001), the parallel version of SPME (Oh & Deng, 2007), the variations of SPME (Essman et al., 1995) and P^3M (Isele-Holder et al., 2012) for dispersion interactions, the “Staggered Mesh Ewald” (StME) (Cerutti et al., 2009) and the “Fast Multipole Method” (Greengard & Rokhlin, 1987).

Other methods that are used in the calculation of electrostatic interactions are the “pre-averaging method” of Yakub & Ronchi (2003) and the reaction field method (Fukuda & Nakamura, 2012). The pre-averaging method is suitable only for isotropic systems where the charge is uniformly distributed, such as ionic fluids or plasmas.

It is apparent that the problem of the evaluation of lattice sums of long-range (electrostatic) interaction potentials is a very broad subject; a number of studies comparing and reviewing the various methods have been published and provide a useful overview of the field. Fennell & Gezelter (2006) performed comparisons of the direct space summation methods and the Ewald-type summation schemes. A more

specific comparison between Wolf's method and Ewald's method is also available (Gdoutos et al., 2010). The “traditional” Ewald summation technique has also been compared to the “Mesh” variations of Ewald (Luty et al., 1995). A similar comparison of two Ewald-type summation methods, SPME and StME, in terms of accuracy has also been performed (Wang et al., 2012). Fukuda and Nakamura (2012) published a review of direct summation methods while reviews of the various Ewald type summation techniques are also available (Hünenberger 1999; Toukmaji & Board ; 1995).

The problem of evaluating the lattice sums associated with long range interactions has been the subject of extensive research over the past century. A variety of methods are available, each one designed to tackle different aspects of the problem. The choice of method is mainly related to the specific application of interest. Here we use the method of Ewald. Its efficiency and accuracy in perfect crystal calculations have been widely tested. The systems that are of interest are relatively small (of the order of a few hundred Daltons) and therefore none of the various mesh methods is expected to be significantly more efficient.

5.3. Generalized Ewald summation method

In this section a method for the calculation of the sums necessary to compute the electrostatic contributions to the lattice energy and the dynamical matrix is presented when these are expressed within the spherical tensor formalism of a multipole expansion. Expressions for arbitrarily high order of interaction are derived.

The lattice sums of interest have the general form:

$$\sum_{\substack{\mathbf{l} \in \mathbf{L} \\ \mathbf{l} \neq \mathbf{0} \text{ if } l_i = l_j}} \left[\frac{S_{l_i l_j l}^{m_i m_j}(\Omega_I, \Omega_J, \hat{\mathbf{r}}_{Ii, Ij})}{\|\mathbf{r}_{0Ii, 0Jj}\|^{l+1}} e^{i\mathbf{k}(\hat{\mathbf{r}}_{Ii} - \hat{\mathbf{r}}_{0Ii})} \right], \quad (5-9)$$

$$\sum_{\substack{\mathbf{l} \in \mathbf{L} \\ \mathbf{l} \neq \mathbf{0} \text{ if } l_i = l_j}} \left[\frac{\partial}{\partial \mathbf{r}_{0Ii}} \left(\frac{S_{l_i l_j l}^{m_i m_j}(\Omega_I, \Omega_J, \hat{\mathbf{r}}_{Ii, Ij})}{\|\mathbf{r}_{0Ii, 0Jj}\|^{l+1}} \right) e^{i\mathbf{k}(\hat{\mathbf{r}}_{Ii} - \hat{\mathbf{r}}_{0Ii})} \right], \quad (5-10)$$

and

$$\sum_{\substack{\mathbf{l} \in \mathbf{L} \\ \mathbf{l} \neq \mathbf{0} \text{ if } l=J}} \left[\frac{\partial^2}{\partial \mathbf{r}_{0Ii} \partial \mathbf{r}_{I'Jj}} \left(\frac{S_{lIlJjl}^{m_{II}m_{JJ}}(\Omega_I, \Omega_J, \hat{\mathbf{r}}_{IIi,I'Jj})}{\|\mathbf{r}_{0Ii,IJj}\|^{l+1}} \right) e^{i\mathbf{k}(\hat{\mathbf{r}}_{IIi}-\hat{\mathbf{r}}_{0Ii})} \right]. \quad (5-11)$$

Lattice sums of the form (5-9) can be used for the evaluation of the lattice energy (lattice sum of equation (5-4)), if the wave vector \mathbf{k} is set to zero. Lattice sums of the form given in equation (5-10) are useful in the calculation of the gradients of the lattice energy (again for $\mathbf{k} = \mathbf{0}$) and are a pre-requisite for the derivation of the lattice sums of the general form (5-11).

Leslie (2008) presented fast converging expressions for the calculation of the electrostatic energy using a multipole expansion after transformation of the irregular spherical harmonics to their Cartesian form, following Stone (1975, 1976) and Tough & Stone (1977). However, Leslie's method for deriving his expressions is cumbersome, and very difficult to generalize to sums of the form (5-6) or (5-11).

The methodology presented in Nijboer & De Wette (1957) is adopted. The authors presented a method for the evaluation of lattice sums of the form²:

$$\begin{aligned} \sum_{\substack{\mathbf{l} \in \mathbf{L} \\ \mathbf{l} \neq \mathbf{0}}} \frac{C_{lm}(\theta, \varphi)}{\|\mathbf{r}_{0Ii,IIi}\|^{l+2n}} e^{2\pi i \mathbf{k}(\hat{\mathbf{r}}_{IIi}-\hat{\mathbf{r}}_{0Ii})} \\ = \frac{1}{\Gamma(n+l)} \left[\sum_{\substack{\mathbf{l} \in \mathbf{L} \\ \mathbf{l} \neq \mathbf{0}}} \frac{\Gamma(n+l, \pi \|\mathbf{r}_{0Ii,IIi}\|^2) C_{lm}(\theta, \varphi)}{\|\mathbf{r}_{0Ii,IIi}\|^{l+2n}} e^{2\pi i \mathbf{k}(\hat{\mathbf{r}}_{IIi}-\hat{\mathbf{r}}_{0Ii})} \right. \\ + \frac{i^l \pi^{2n+l-3/2}}{V} \sum_{\mathbf{h}} \|\mathbf{h} - \mathbf{k}\|^{l+2n-3} \\ \cdot \left. \Gamma\left(-n + \frac{3}{2}, \pi \|\mathbf{h} - \mathbf{k}\|^2\right) C_{lm}(\theta_{\mathbf{h}-\mathbf{k}}, \varphi_{\mathbf{h}-\mathbf{k}}) \right] \end{aligned} \quad (5-12)$$

In equation (5-12) n is any real number for which the lattice sum is meaningful and $C_{lm}(\theta, \varphi)$ is the normalized spherical harmonics. $\Gamma(n+l)$ is the gamma

² This equation is valid when the factor 2π is not included in the definition of the reciprocal space basis vectors as we do in this thesis (see equation 3-6).

function, while $\Gamma(n + l, x)$ is the upper incomplete gamma function, which is related to the lower incomplete gamma function, $\gamma(n + l, x)$, and the gamma function by (Abramowitz & Stegun, 1972):

$$\Gamma(n + l) = \Gamma(n + l, x) + \gamma(n + l, x). \quad (5-13)$$

\mathbf{h} is a reciprocal lattice vector, while \mathbf{k} is a reciprocal space vector. The first summation on the right hand side of equation (5-12) is known as a *direct space sum* or *real space sum*, while we refer to the second as a *reciprocal space sum*.

The applicability of equation (5-12) is limited to the case of the sum of a property of periodic images, i.e. $Ii = Jj$. Furthermore in equation (5-12) there is no *Ewald convergence parameter* (Frenkel & Smit, 2002), whose existence is very convenient for optimisation of the relative rate of convergence between the reciprocal and the direct space sums. As a result we propose a modified version of equation (5-12) that can be used for an arbitrary pair of atoms and we also introduce the Ewald convergence parameter α . To do so, we follow the procedure described in Nijboer & De Wette, (1957). A similar generalization of Nijboer & De Wette's method has also been published by Grant (1965:a,1965:b). His result is apparently different and further discussion on this issue will follow after the presentation of the method. Here we do not present in detail all the derivation but only the key intermediate results.

The proof is developed by introducing an auxiliary function, $F(\mathbf{r}_{0Ii,1Jj})$, that transforms the sum of interest in the following way

$$\begin{aligned} & \sum_{\substack{\mathbf{l} \in \mathbb{L} \\ \mathbf{l} \neq \mathbf{0} \\ \text{if } Ii=Jj}} \frac{C_{lm}(\theta, \varphi)}{\|\mathbf{r}_{0Ii,1Jj}\|^{l+2n}} e^{i\mathbf{k}(\hat{\mathbf{r}}_{IIi} - \hat{\mathbf{r}}_{0II})} \\ &= \sum_{\substack{\mathbf{l} \in \mathbb{L} \\ \mathbf{l} \neq \mathbf{0} \\ \text{if } Ii=Jj}} \frac{C_{lm}(\theta, \varphi)}{\|\mathbf{r}_{0Ii,1Jj}\|^{l+2n}} e^{i\mathbf{k}(\hat{\mathbf{r}}_{IIi} - \hat{\mathbf{r}}_{0II})} F(\mathbf{r}_{0Ii,1Jj}) \\ &+ \sum_{\substack{\mathbf{l} \in \mathbb{L} \\ \mathbf{l} \neq \mathbf{0} \\ \text{if } Ii=Jj}} \frac{C_{lm}(\theta, \varphi)}{\|\mathbf{r}_{0Ii,1Jj}\|^{l+2n}} e^{i\mathbf{k}(\hat{\mathbf{r}}_{IIi} - \hat{\mathbf{r}}_{0II})} [1 - F(\mathbf{r}_{0Ii,1Jj})]. \end{aligned} \quad (5-14)$$

The second sum on the right hand of equation (5-14) is the reciprocal sum, because it can only be calculated (after Fourier transformation) in the reciprocal space. We

choose the auxiliary function to be very similar to the original given by Nijboer & De Wette (1957), but it now also contains the convergence parameter α :

$$\gamma(\mathbf{r}_{0Ii,1Jj}) = \frac{\Gamma(n + l, \alpha\pi\|\mathbf{r}_{0Ii,1Jj}\|^2)}{\Gamma(n + l)} \quad (5-15)$$

The remainder of the proof consists in the evaluation of the reciprocal sum:

$$\sum_{\substack{\mathbf{l} \in \mathbf{L} \\ \mathbf{l} \neq \mathbf{0} \\ \text{if } l_i = J_j}} \frac{C_{lm}(\theta, \varphi)}{\|\mathbf{r}_{0Ii,1Jj}\|^{l+2n}} e^{i\mathbf{k}(\hat{\mathbf{r}}_{\mathbf{l}Ii} - \hat{\mathbf{r}}_{0Ii})} \gamma(n + l, \alpha\pi\|\mathbf{r}_{0Ii,1Jj}\|^2) \quad (5-16)$$

This last equation can be written in integral form using Dirac's delta function:

$$I_r = \int_{-\infty}^{\infty} \frac{C_{lm}(\theta, \varphi)}{\|\mathbf{r}\|^{l+2n}} \gamma(n + l, \alpha\pi\|\mathbf{r}\|^2) \sum_{\substack{\mathbf{l} \in \mathbf{L} \\ \mathbf{l} \neq \mathbf{0} \\ \text{if } l_i = J_j}} e^{i\mathbf{k}\mathbf{r}} \delta(\mathbf{r} - \mathbf{r}_{0Ii,1Jj}) d\mathbf{r}. \quad (5-17)$$

The integral in equation (5-17) is then evaluated using *Parseval's formula* (Nijboer & De Wette, 1957; Rudin, 1987):

$$\int_{-\infty}^{\infty} f(\mathbf{r})[g(\mathbf{r})]^* d\mathbf{r} = \int_{-\infty}^{\infty} \hat{f}(\mathbf{h})[\hat{g}(\mathbf{h})]^* d\mathbf{h} \quad (5-18)$$

where $\hat{f}(\mathbf{h})$ and $\hat{g}(\mathbf{h})$ are the Fourier transforms of $f(\mathbf{r})$ and $g(\mathbf{r})$ respectively. The star symbol indicates the complex conjugate. Within the context of evaluating the integral of equation (5-17) using (5-18) we define:

$$\begin{aligned} f(\mathbf{r}) &= \frac{C_{lm}(\theta, \varphi)}{\|\mathbf{r}\|^{l+2n}} \gamma(n + l, \alpha\pi\|\mathbf{r}\|^2) \\ g(\mathbf{r}) &= \sum_{\mathbf{l} \in \mathbf{L}} e^{-i\mathbf{k}\mathbf{r}} \delta(\mathbf{r} - \mathbf{r}_{0Ii,1Jj}) \Leftrightarrow [g(\mathbf{r})]^* = \sum_{\mathbf{l} \in \mathbf{L}} e^{i\mathbf{k}\mathbf{r}} \delta(\mathbf{r} - \mathbf{r}_{0Ii,1Jj}). \end{aligned} \quad (5-19)$$

Following Nijboer & De Wette (1957) we can prove that the Fourier transform, $\hat{f}(\mathbf{h})$, of $f(\mathbf{r})$ as defined by equation (5-19) is:

$$\hat{f}(\mathbf{h}) = i^l 2^{l+2n-3} \pi^{3/2} \|\mathbf{h}\|^{2n+l-3} \Gamma\left(-n + \frac{3}{2}, \frac{\|\mathbf{h}\|^2}{4\alpha\pi}\right) C_{lm}(\theta_{\mathbf{h}}, \varphi_{\mathbf{h}}). \quad (5-20)$$

A crucial step in deriving equation (5-20) is the evaluation of the integral:

$$\int_0^\infty e^{-u^2} u^{l+\frac{3}{2}} J_{l+\frac{1}{2}}(2\|\mathbf{r}\| \sqrt{\alpha\pi} u) du = \frac{(2\|\mathbf{r}\| \sqrt{\alpha\pi})^{l+\frac{1}{2}}}{2^{l+\frac{3}{2}}} e^{-(\|\mathbf{r}\| \sqrt{\alpha\pi})^2}, \quad (5-21)$$

where $J_a(x)$ is the Bessel function (Abramowitz & Stegun, 1972). The equality can be proved using the general expression (Watson, 1944):

$$\int_0^\infty e^{-p^2 u^2} u^{v+1} J_v(au) du = \frac{a^v}{(2p^2)^{v+1}} e^{-\frac{a^2}{4p^2}} \quad (5-22)$$

The evaluation of $\hat{g}(\mathbf{h})$, the Fourier transform of $g(\mathbf{r})$, described in (5-19), is also carried out along the lines described by Nijboer & De Wette (1957):

$$[\hat{g}(\mathbf{h})]^* = e^{-i(\mathbf{h}-\mathbf{k})\mathbf{r}_0} \delta_{Ii,0Jj} \frac{1}{V} \sum_{\mathbf{h}'} \delta(\mathbf{h} - \mathbf{k} - \mathbf{h}') \quad (5-23)$$

Finally by substitution of equations (5-19), (5-20) and (5-23) into equation (5-18), we can obtain an expression for the integral, I_r , of equation (5-17):

$$I_r = \frac{i^l 2^{l+2n-3} \pi^{3/2}}{V} \sum_{\mathbf{h}} \left\{ \|\mathbf{h} + \mathbf{k}\|^{2n+l-3} \Gamma\left(-n + \frac{3}{2}, \frac{\|\mathbf{h} + \mathbf{k}\|^2}{4\alpha\pi}\right) \right. \\ \left. \cdot C_{lm}(\theta_{\mathbf{h+k}}, \varphi_{\mathbf{h+k}}) e^{-i\mathbf{h}\mathbf{r}_{Ii,Jj}} \right\} - \delta_{Ii,Jj} \delta_{\mathbf{l},0} T_s^0(l, m, n), \quad (5-24)$$

where $\delta_{i,i'}$ is the Kronecker delta and $T_s^0(l, m, n)$ is the *self-correction term* given by:

$$T_s^0(l, m, n) = \lim_{\|\mathbf{r}\| \rightarrow 0} \left[\frac{C_{lm}(\theta, \varphi)}{\|\mathbf{r}\|^{l+2n}} \gamma(n + l, \alpha\pi\|\mathbf{r}\|^2) e^{i\mathbf{k}\cdot\mathbf{r}} \right]. \quad (5-25)$$

For our purpose (i.e. the evaluation of summation (5-4)), the suitable sum is that for which $n = \frac{1}{2}$, which is summarized as:

$$\begin{aligned} & \sum_{\substack{\mathbf{l} \in \mathbf{L} \\ \mathbf{l} \neq \mathbf{0} \\ \text{if } l_i = J_j}} \frac{C_{lm}(\theta, \varphi)}{\|\mathbf{r}_{0li, lJj}\|^{l+1}} e^{i\mathbf{k}(\hat{\mathbf{r}}_{li} - \hat{\mathbf{r}}_{0li})} \\ &= \frac{1}{\Gamma\left(\frac{1}{2} + l\right)} \left[\sum_{\substack{\mathbf{l} \in \mathbf{L} \\ \mathbf{l} \neq \mathbf{0} \\ \text{if } l_i = J_j}} \frac{C_{lm}(\theta, \varphi) \Gamma\left(\frac{1}{2} + l, \alpha\pi\|\mathbf{r}_{0li, lJj}\|^2\right)}{\|\mathbf{r}_{0li, lJj}\|^{l+1}} e^{i\mathbf{k}(\hat{\mathbf{r}}_{li} - \hat{\mathbf{r}}_{0li})} \right. \\ &+ \frac{i^l 2^{2-l} \pi^{3/2}}{V} \sum_{\mathbf{h}} \left\{ \|\mathbf{h} + \mathbf{k}\|^{l-2} e^{-\frac{\|\mathbf{h} + \mathbf{k}\|^2}{4\alpha\pi}} C_{lm}(\theta_{\mathbf{h}+\mathbf{k}}, \varphi_{\mathbf{h}+\mathbf{k}}) e^{-i\mathbf{h}\cdot\mathbf{r}_{li, Jj}} \right\} \\ & \left. - \delta_{li, Jj} \delta_{\mathbf{l}, \mathbf{0}} T_s^0\left(l, m, \frac{1}{2}\right) \right] \end{aligned} \quad (5-26)$$

To obtain the last result we have used the identity:

$$\Gamma(1, x) = e^{-x}$$

Finally, it is trivial to derive the necessary expression for sum (5-4) if we substitute equation (4-36) into expression (5-26):

$$\begin{aligned}
& \sum_{\substack{\mathbf{l} \in \mathbf{L} \\ \mathbf{l} \neq \mathbf{0} \\ i \neq l \\ l_i = J_j}} \frac{S_{l_{II}l_{JJ}l}^{m_{II}m_{JJ}}(\Omega_I, \Omega_J, \hat{\mathbf{r}}_{IIi,I'Jj})}{\|\mathbf{r}_{0Ii,1Jj}\|^{l+1}} e^{i\mathbf{k}\mathbf{r}_{0Ii,1Jj}} \\
&= \frac{1}{\Gamma\left(\frac{1}{2} + l\right)} \left[\sum_{\substack{\mathbf{l} \in \mathbf{L} \\ \mathbf{l} \neq \mathbf{0} \\ i \neq l \\ l_i = J_j}} \frac{S_{l_{II}l_{JJ}l}^{m_{II}m_{JJ}}(\Omega_I, \Omega_J, \hat{\mathbf{r}}_{IIi,I'Jj}) \Gamma\left(\frac{1}{2} + l, \alpha\pi\|\mathbf{r}_{0Ii,1Jj}\|^2\right)}{\|\mathbf{r}_{0Ii,1Jj}\|^{l+1}} e^{i\mathbf{k}\mathbf{r}_{0Ii,1Jj}} \right. \\
&+ \frac{i^l 2^{2-l} \pi^{3/2}}{V} \sum_{\mathbf{h}} \left\{ \|\mathbf{h} + \mathbf{k}\|^{l-2} e^{-\frac{\|\mathbf{h} + \mathbf{k}\|^2}{4\alpha\pi}} S_{l_{II}l_{JJ}l}^{m_{II}m_{JJ}}(\Omega_I, \Omega_J, \widehat{\mathbf{h} + \mathbf{k}}) e^{-i\mathbf{h}\mathbf{r}_{IIi,Jj}} \right\} \\
&\left. - \delta_{II,JJ} T_s^0\left(l_{II}, l_{JJ}, m_{II}, m_{JJ}, \frac{1}{2}\right) \right] \tag{5-27}
\end{aligned}$$

In this last expression the self correction term is now given by:

$$\begin{aligned}
& T_s^0(l_{II}, l_{JJ}, m_{II}, m_{JJ}, n) \\
&= \lim_{\|\mathbf{r}\| \rightarrow 0} \left[\frac{S_{l_{II}l_{JJ}l}^{m_{II}m_{JJ}}(\Omega_I, \Omega_J, \hat{\mathbf{r}})}{\|\mathbf{r}\|^{l+2n}} \gamma(n+l, \alpha\pi\|\mathbf{r}\|^2) e^{i\mathbf{k}\mathbf{r}} \right]. \tag{5-28}
\end{aligned}$$

The evaluation of limit (5-28) for the case $n = \frac{1}{2}$, which is the one we are interested in, is straightforward thanks to the definition of the lower incomplete gamma function, $\gamma(s, x) = \int_0^x t^{s-1} e^{-t} dt$:

$$T_s^0\left(l_{II}, l_{JJ}, m_{II}, m_{JJ}, \frac{1}{2}\right) = \delta_{l0} 2\sqrt{\alpha\pi} \tag{5-29}$$

5.3.1. Calculation of the lattice energy of molecular crystals

In the case of molecular crystals modeled according to the approach described in Chapter 4, it is necessary to exclude from the lattice sum in equation (5-27) the term arising from the interactions of atoms that belong to the same molecule. This is necessary in order to avoid the double counting of the electrostatic interactions between these atoms, which are already included in the intra-molecular contribution

computed using *ab-initio* calculations. This is done by means of a *molecular correction term* (Karamertzanis, 2004) that is added to the right side of equation (5-27). Note also that the terms excluded from the lattice sum of equation (5-27) are not the same as those excluded from the required lattice sum (equation 5-9).

The appropriate functional form of the molecular correction term is obtained by subtracting the term to be excluded from both sides of equation (5-27). On the left hand side, this implies removing components of the summation corresponding to the interactions of any two atoms in the same molecule in reference unit cell (i.e., for $\mathbf{l} = \mathbf{0}$, $I=J$ but i not necessarily equal to j). Then we have:

$$\begin{aligned}
& \sum_{\substack{\mathbf{l} \in \mathbf{L} \\ \mathbf{l} \neq \mathbf{0} \\ \text{if } l_i = l_j}} \frac{S_{l_{II}l_{JJ}l}^{m_{II}m_{JJ}}(\Omega_I, \Omega_J, \hat{\mathbf{r}}_{l_{II}, l'_{JJ}})}{\|\mathbf{r}_{0_{II}, l_{JJ}}\|^{l+1}} e^{i\mathbf{k}\mathbf{r}_{0_{II}, l_{JJ}}} \\
&= \frac{1}{\Gamma\left(\frac{1}{2} + l\right)} \left[\sum_{\substack{\mathbf{l} \in \mathbf{L} \\ \mathbf{l} \neq \mathbf{0} \\ \text{if } l_i = l_j}} \frac{S_{l_{II}l_{JJ}l}^{m_{II}m_{JJ}}(\Omega_I, \Omega_J, \hat{\mathbf{r}}_{l_{II}, l'_{JJ}}) \Gamma\left(\frac{1}{2} + l, \alpha\pi\|\mathbf{r}_{0_{II}, l_{JJ}}\|^2\right)}{\|\mathbf{r}_{0_{II}, l_{JJ}}\|^{l+1}} e^{i\mathbf{k}\mathbf{r}_{0_{II}, l_{JJ}}} \right. \\
&+ \frac{i^l 2^{2-l} \pi^{3/2}}{V} \sum_{\mathbf{h}} \left\{ \|\mathbf{h} + \mathbf{k}\|^{l-2} e^{-\frac{\|\mathbf{h} + \mathbf{k}\|^2}{4\alpha\pi}} S_{l_{II}l_{JJ}l}^{m_{II}m_{JJ}}(\Omega_I, \Omega_J, \widehat{\mathbf{h} + \mathbf{k}}) e^{-i\mathbf{h}\mathbf{r}_{l_{II}, l_{JJ}}} \right\} \\
&- \delta_{I,J} (1 - \delta_{i,j}) \frac{S_{l_{II}l_{JJ}l}^{m_{II}m_{JJ}}(\Omega_I, \Omega_J, \hat{\mathbf{r}}_{l_{II}, l'_{JJ}}) \gamma\left(\frac{1}{2} + l, \alpha\pi\|\mathbf{r}_{0_{II}, l_{JJ}}\|^2\right)}{\|\mathbf{r}_{0_{II}, l_{JJ}}\|^{l+1}} e^{i\mathbf{k}\mathbf{r}_{0_{II}, l_{JJ}}} \\
&\left. - \delta_{Ii, Jj} T_s^0\left(l_{II}, l_{JJ}, m_{II}, m_{JJ}, \frac{1}{2}\right) \right] \tag{5-30}
\end{aligned}$$

Equation (5-30) provides a transformation of the general lattice sum (5-9) into two rapidly converging series. This result can be used to evaluate the electrostatic contribution to the lattice energy (equation (5-4)). Equation (5-30) is valid for any wave vector \mathbf{k} , and therefore for $\mathbf{0}$, which if substituted into (5-30) leads directly to lattice sum (5-4). The calculation of the lattice energy by substitution of equation (5-27) or equation (5-30) into (5-3) gives identical results to those obtained when using the formalism presented in Leslie (2008). One difference between the two approaches is that the general form of the lattice sum (5-9) which we use for the

evaluation of the lattice energy represents a wider class of sums than the sums for which Leslie (2008) provides a fast converging expression.

It might seem surprising that in the reciprocal sum of expressions (5-27) and (5-30) the reciprocal space vector $\mathbf{h} + \mathbf{k}$ appears instead of $\mathbf{h} - \mathbf{k}$, which is often found in similar expressions (Aung & Strauss, 1973; Fuchizaki, 1994, 2010; Nijboer & De Wette, 1957; Grant, 1965:a). This is a consequence of our choice of the functions $f(\mathbf{r})$ and $g(\mathbf{r})$ (equation 5-19) for the application of Parseval's formula. This choice was made for convenience and it is trivial to prove that if the opposite definition was chosen then \mathbf{k} would appear with opposite sign. In addition it is easy to prove that for the lattice sums that are of interest in Aung & Strauss (1973), and Fuchizaki (1994, 2010) the sign of the wave vector \mathbf{k} does not affect the value of the reciprocal sum. Furthermore these particular sums are not of interest here so they are not discussed further. On the other hand in the lattice sums (5-27) and (5-30) as well as the very closely related lattice sums presented in Nijboer & De Wette (1957) and in Grant (1965:a), the sign of \mathbf{k} in principle affects the value of the reciprocal sum. These authors seem to have ignored, without stating a reason, the fact that in equation (5-18) the complex conjugate of the Fourier transform of $g(\mathbf{r})$ (equation (5-19)) is required. Finally the wave vector in the reciprocal sum of the Ewald expression for the field of a lattice of dipoles presented in Born & Huang (1954) appears with a positive sign.

A visual demonstration of the way in which the Ewald summation technique operates is presented in this section based on an analysis of the individual contributions to the electrostatic energy of the monoclinic form (Chaplot et al., 1984) of tetracyanoethylene (see Figure 5-1, p.93). The different contributions to the electrostatic energy of the predicted structure, from charge-charge to charge-quadrupole, are plotted against the value of the Ewald convergence parameter “ α ” of equation (5-30). Furthermore the various components of the Ewald method, namely the direct space, reciprocal space, molecular correction and self correction contributions, are also plotted as function of the parameter α . Details of the computational model used and the structure are presented in section 6.4.2, where an in-depth study of tetracyanoethylene is undertaken.

The charge-charge contribution is shown in Figure 5-2, the charge-dipole contribution is shown in Figure 5-3, the charge-quadrupole contribution is shown in

Figure 5-4 and the dipole-dipole contribution is shown in Figure 5-5. The cut-off of the direct space sum is 17 Å, while reciprocal cells up to the 6th are considered in the reciprocal sum. These parameters are sufficiently large to ensure that the sums are converged. It is apparent that for every contribution, although the different components of the sum vary significantly with the value of “ α ”, the total contribution is unaffected by this choice. This is intuitively understood as the cancellation of the error induced in the lattice sum by the auxiliary function (5-15), by the other components (reciprocal space sum, molecular and self correction). This is a validation of equations (5-27) and (5-30). Such a validation can also be achieved by following the approach of Fuchizaki’s (2010), i.e., by proving that the gradient of the right part of equation (5-30) with respect to α vanishes. If the gradient is zero the total contribution is a constant function of α , which implies that the modification incurred in the lattice sum by the presence of the auxiliary function (5-15) in the real space sum is fully compensated by the other terms, namely the reciprocal space sum, the molecular correction, and the self correction (equation 5-14).

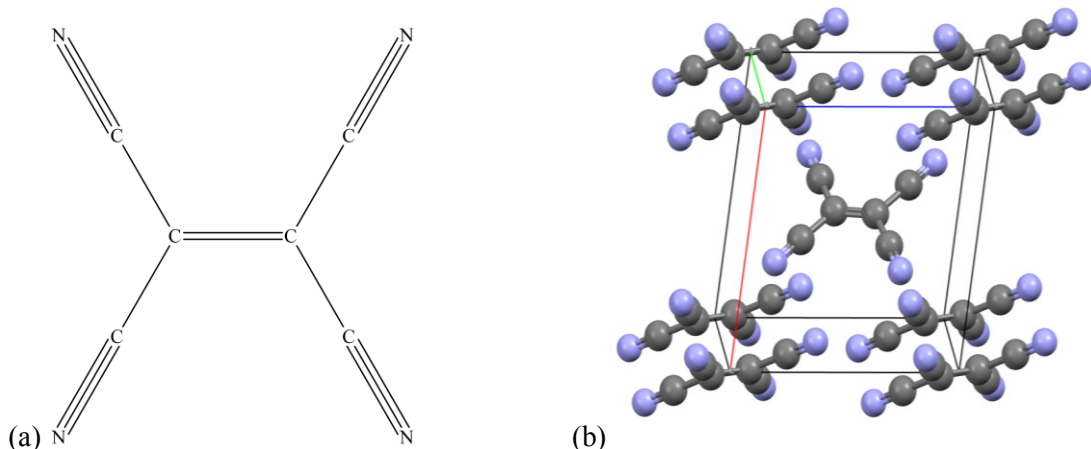


Figure 5-1 (a) The chemical diagram of tetracyanoethylene and (b) the experimental unit cell of the monoclinic form at 298K.

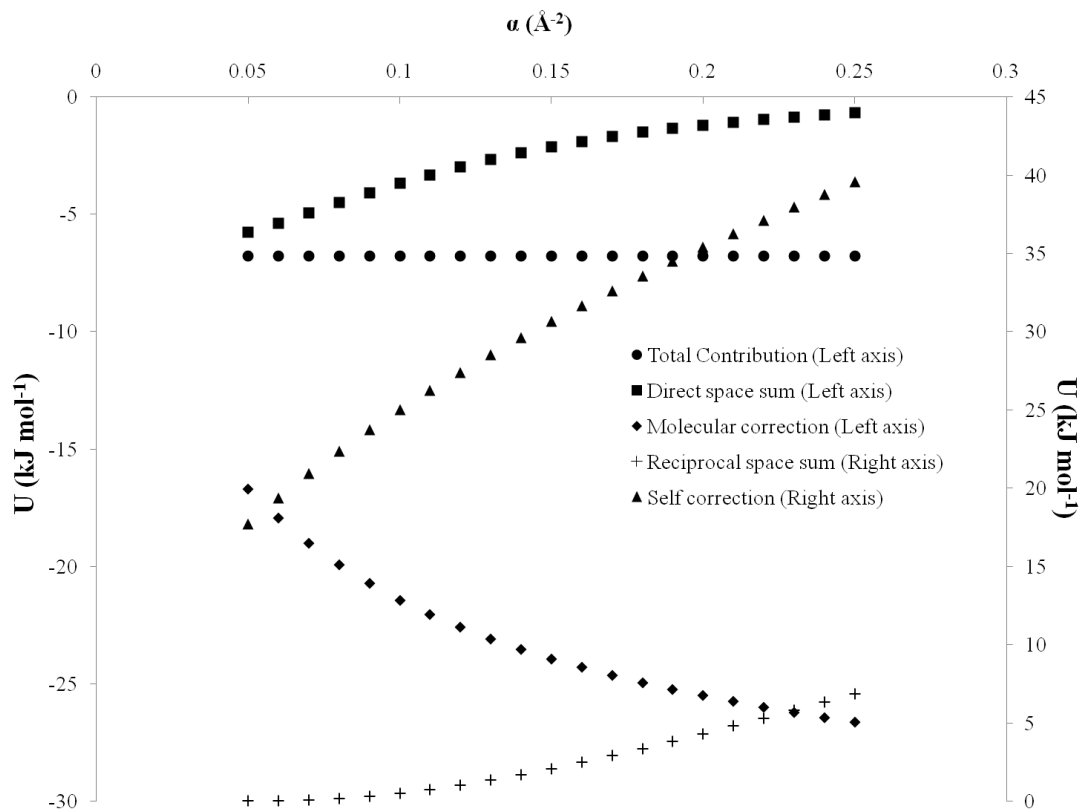


Figure 5-2 The value of the charge-charge contribution to the electrostatic energy of the calculated monoclinic form of tetracyanoethylene, as a function of the Ewald convergence parameter. The direct space sum, the reciprocal space sum, the molecular correction, and the self correction are also presented. Distributed multipoles were derived at the M06/6-31G(d,p) level.

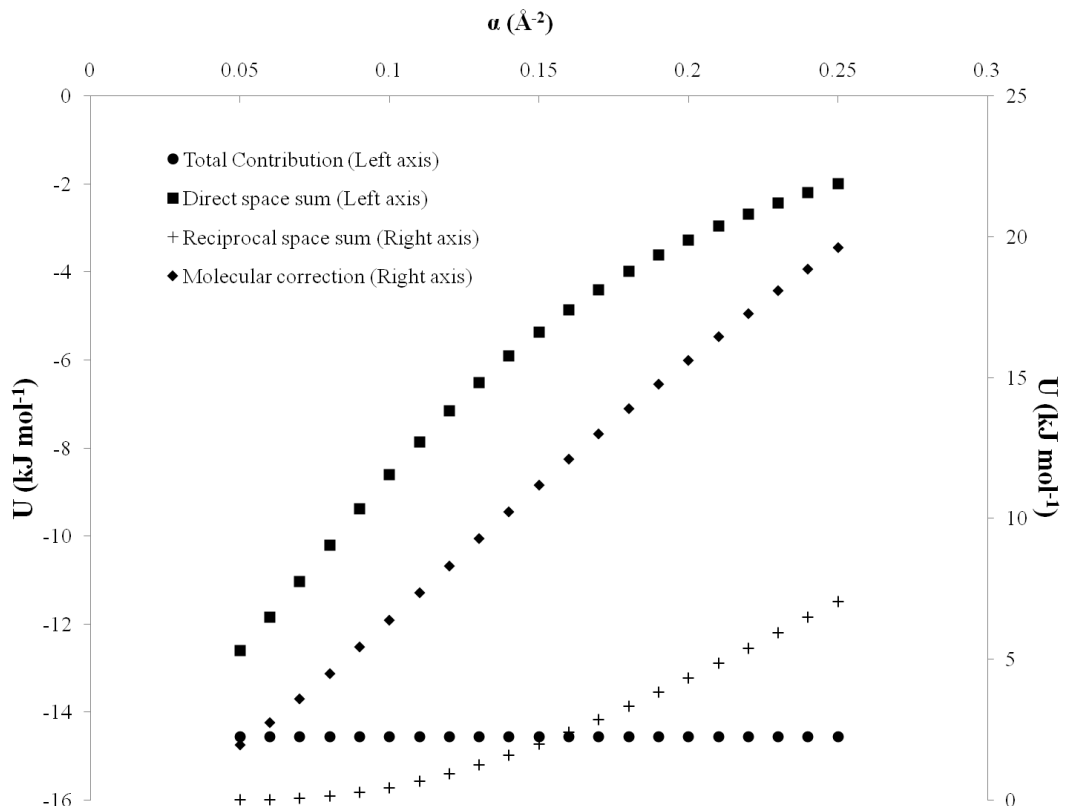


Figure 5-3 The value of the charge-dipole contribution to the electrostatic energy of the calculated monoclinic form of tetracyanoethylene, as function of the Ewald convergence parameter. The direct space sum, the reciprocal space sum, and the molecular correction are also presented. Distributed multipoles were derived at the M06/6-31G(d,p) level.

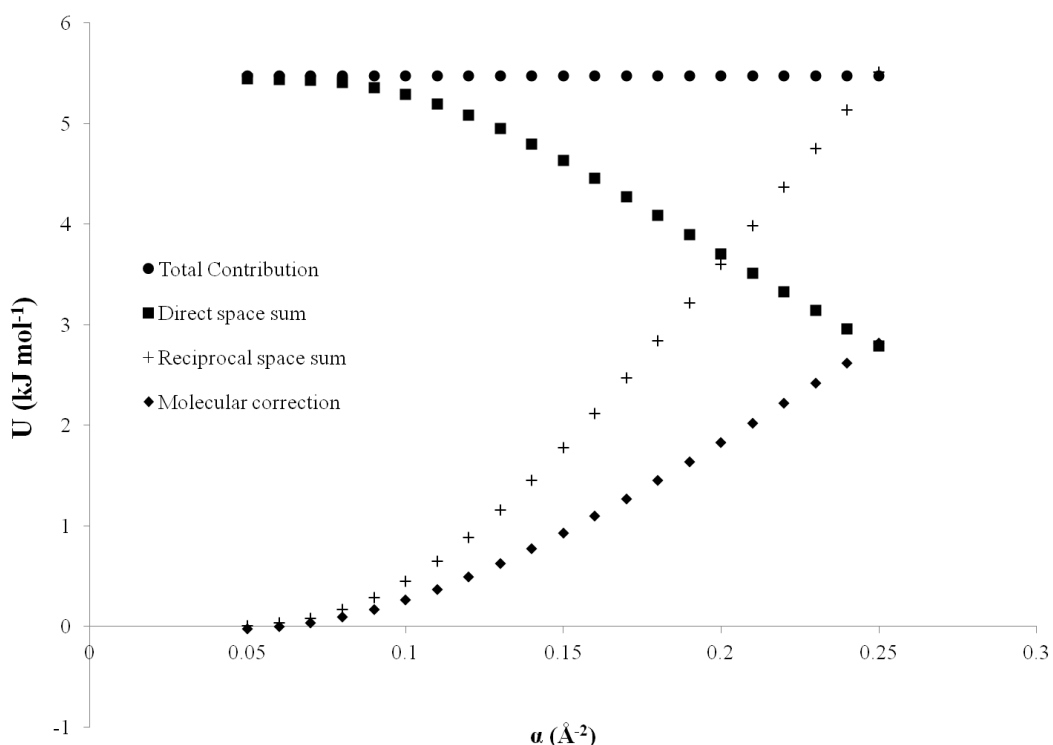


Figure 5-4 The value of the charge-quadrupole contribution to the electrostatic energy of the calculated monoclinic form of tetracyanoethylene, as function of the Ewald convergence parameter. The direct space sum, the reciprocal space sum, and the molecular correction are also presented. Distributed multipoles were derived at the M06/6-31G(d,p) level.

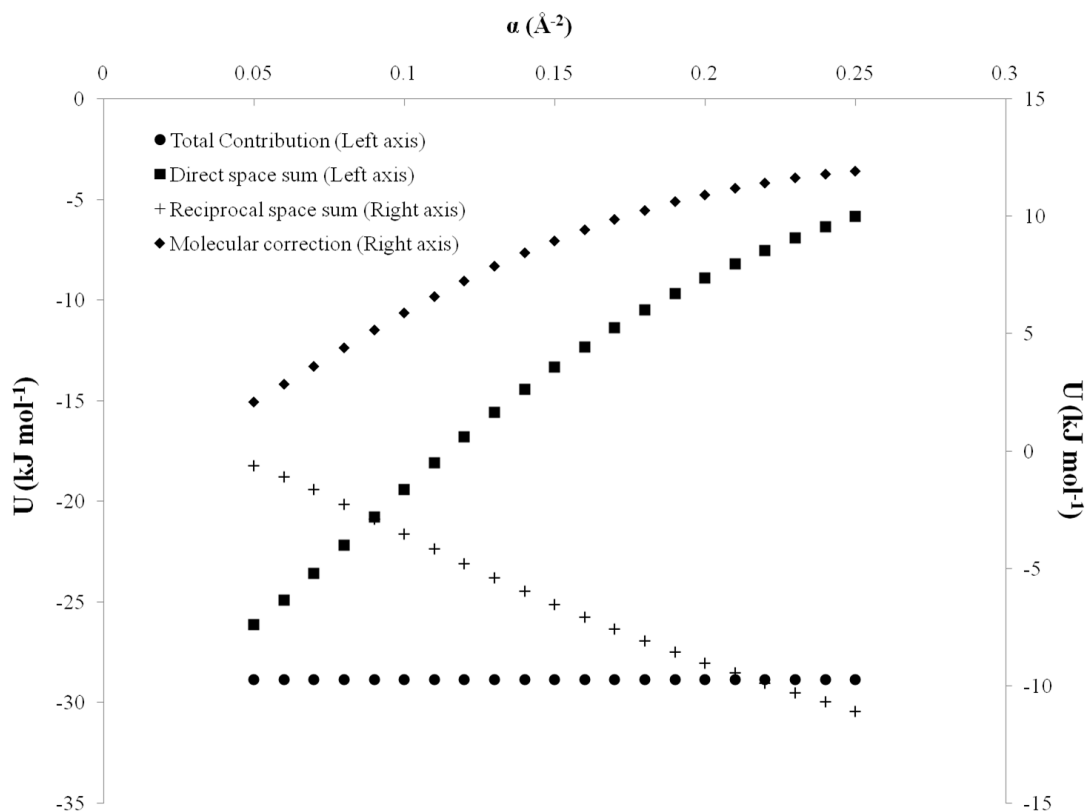


Figure 5-5 The value of the dipole-dipole contribution to the electrostatic energy of the calculated monoclinic form of tetracyanoethylene, as function of the Ewald convergence parameter. The direct space sum, the reciprocal space sum, and the molecular correction are also presented. Distributed multipoles were derived at the M06/6-31G(d,p) level.

5.3.2. Efficient summation scheme for the dynamical matrix

In this section a method for the efficient evaluation of the lattice sums of equations (5-10) and (5-11) is derived. Lattice sum (5-11) is necessary for the efficient evaluation of the electrostatic contribution to the dynamical matrix (essentially the sum of equation (5-6)). On the other hand, lattice sum (5-10) is a necessary intermediate step, which can find use in the evaluation of the gradient of the lattice energy, but it is not used for calculations presented in this thesis. The starting point is the equation derived for the calculation of the lattice energy (equation 5-27). Following Signorini et al. (1991), we differentiate equation (5-27) with respect to \mathbf{r}_{0Ii} , and we subsequently subtract equation (5-27) multiplied by \mathbf{k} .

The following result is obtained:

$$\begin{aligned}
& \sum_{\substack{\mathbf{l} \in \mathbb{L} \\ \mathbf{l} \neq \mathbf{0} \\ \text{if } l_i = J_j}} \frac{\partial}{\partial \mathbf{r}_{0Ii}} \left(\frac{S_{l_{II}l_{JJ}l}^{m_{II}m_{JJ}}(\Omega_I, \Omega_J, \hat{\mathbf{r}}_{IIi,I'Jj})}{\|\mathbf{r}_{0Ii,IJj}\|^{l+1}} \right) e^{i\mathbf{k}\mathbf{r}_{0Ii,IJj}} \\
&= \frac{1}{\Gamma\left(\frac{1}{2} + l\right)} \left[\sum_{\substack{\mathbf{l} \in \mathbb{L} \\ \mathbf{l} \neq \mathbf{0} \\ \text{if } l_i = J_j}} \frac{\partial}{\partial \mathbf{r}_{0Ii}} \left(\frac{S_{l_{II}l_{JJ}l}^{m_{II}m_{JJ}}(\Omega_I, \Omega_J, \hat{\mathbf{r}}_{IIi,I'Jj}) \Gamma\left(\frac{1}{2} + l, \alpha\pi\|\mathbf{r}_{0Ii,IJj}\|^2\right)}{\|\mathbf{r}_{0Ii,IJj}\|^{l+1}} \right) e^{i\mathbf{k}\mathbf{r}_{0Ii,IJj}} \right. \\
&\quad + \frac{i^l 2^{2-l} \pi^{3/2}}{V} \sum_{\mathbf{h}} \left\{ i \frac{-(\mathbf{h} + \mathbf{k})}{\|\mathbf{h} + \mathbf{k}\|^{2-l}} e^{-\frac{\|\mathbf{h} + \mathbf{k}\|^2}{4\alpha\pi}} S_{l_{II}l_{JJ}l}^{m_{II}m_{JJ}}(\Omega_I, \Omega_J, \widehat{\mathbf{h} + \mathbf{k}}) e^{-i\mathbf{h}\mathbf{r}_{IIi,Jj}} \right\} \\
&\quad \left. - \delta_{II,Jj} T_s^1 \left(l_{II}, l_{JJ}, m_{II}, m_{JJ}, \frac{1}{2} \right) \right]. \tag{5-31}
\end{aligned}$$

The self correction term $T_s^1 \left(l_{II}, l_{JJ}, m_{II}, m_{JJ}, \frac{1}{2} \right)$ is equal to:

$$\begin{aligned}
& T_s^1 \left(l_{II}, l_{JJ}, m_{II}, m_{JJ}, \frac{1}{2} \right) \\
&= \frac{\partial}{\partial \mathbf{r}_{0Ii}} T_s^0 \left(l_{II}, l_{JJ}, m_{II}, m_{JJ}, \frac{1}{2} \right) - \mathbf{k} \\
&\quad \cdot T_s^0 \left(l_{II}, l_{JJ}, m_{II}, m_{JJ}, \frac{1}{2} \right). \tag{5-32}
\end{aligned}$$

The derivative involved in expression (5-32) is obtained using the definition of the self correction of the lattice energy (equation 5-28), carrying out the differentiation before the calculation of the limit. If the opposite order is followed, i.e., differentiation of equation (5-29), an invalid result is obtained in which the value of the lattice sum depends on the chosen value of the parameter α , contrary to expectations. The value of the self correction term $T_s^1(l_{Ii}, l_{Jj}, m_{Ii}, m_{Jj}, \frac{1}{2})$ in terms of the local axis system of molecule I defined by the unit vectors $\hat{\mathbf{x}}_I, \hat{\mathbf{y}}_I$ and $\hat{\mathbf{z}}_I$ and the corresponding vectors rigidly fixed on molecule J : $\hat{\mathbf{x}}_J, \hat{\mathbf{y}}_J$ and $\hat{\mathbf{z}}_J$ is summarized in Table 5-1. One very interesting feature of the tabulated values is that none of them depends on the wave vector \mathbf{k} .

$(l_{Ii}, l_{Jj}, m_{Ii}, m_{Jj})$	$T_s^1(l_{Ii} l_{Jj}, m_{Ii}, m_{Jj}, \frac{1}{2})$
(0,0,0,0)	0
(1,0,0,0)	$-\frac{2}{3\sqrt{3}}(\alpha\pi)^{3/2} \cdot \hat{\mathbf{z}}_I$
(1,0,1c, 0)	$-\frac{2}{3\sqrt{3}}(\alpha\pi)^{3/2} \cdot \hat{\mathbf{x}}_I$
(1,0,1s, 0)	$-\frac{2}{3\sqrt{3}}(\alpha\pi)^{3/2} \cdot \hat{\mathbf{y}}_I$
(0,1,0,0)	$-\frac{2}{3\sqrt{3}}(\alpha\pi)^{3/2} \cdot \hat{\mathbf{z}}_J$
(0,1,0,1c)	$-\frac{2}{3\sqrt{3}}(\alpha\pi)^{3/2} \cdot \hat{\mathbf{x}}_J$
(0,1,0,1s)	$-\frac{2}{3\sqrt{3}}(\alpha\pi)^{3/2} \cdot \hat{\mathbf{y}}_J$
$l > 1$	0

Table 5-1 The self correction term for the different components of the various contributions to the electrostatic energy gradient (equation 5-31).

Following the same procedure we obtain the following expression for the lattice sum of second derivatives:

$$\begin{aligned}
& \sum_{\substack{\mathbf{l} \in \mathbf{L} \\ \mathbf{l} \neq \mathbf{0}}} \frac{\partial^2}{\partial \mathbf{r}_{0Ii} \partial \mathbf{r}_{0Jj}} \left(\frac{S_{l_{II} l_{JJ}}^{m_{II} m_{JJ}}(\Omega_I, \Omega_J, \hat{\mathbf{r}}_{IIi, IIj})}{\|\mathbf{r}_{0Ii, IIj}\|^{l+1}} \right) e^{i\mathbf{k}\mathbf{r}_{0Ii, IIj}} \\
&= \frac{1}{\Gamma\left(\frac{1}{2} + l\right)} \left[\sum_{\substack{\mathbf{l} \in \mathbf{L} \\ \mathbf{l} \neq \mathbf{0}}} \frac{\partial^2}{\partial \mathbf{r}_{0Ii} \partial \mathbf{r}_{0Jj}} \left(\frac{S_{l_{II} l_{JJ}}^{m_{II} m_{JJ}}(\Omega_I, \Omega_J, \hat{\mathbf{r}}_{IIi, IIj}) \Gamma\left(\frac{1}{2} + l, \alpha\pi \|\mathbf{r}_{0Ii, IIj}\|^2\right)}{\|\mathbf{r}_{0Ii, IIj}\|^{l+1}} \right) e^{i\mathbf{k}\mathbf{r}_{0Ii, IIj}} \right. \\
&+ \frac{i^l 2^{2-l} \pi^{3/2}}{V} \sum_{\mathbf{h}} \left\{ \frac{(\mathbf{h} + \mathbf{k})(\mathbf{h} + \mathbf{k})^T}{\|\mathbf{h} + \mathbf{k}\|^{2-l}} e^{-\frac{\|\mathbf{h} + \mathbf{k}\|^2}{4\alpha\pi}} S_{l_{II} l_{JJ}}^{m_{II} m_{JJ}}(\Omega_I, \Omega_J, \widehat{\mathbf{h} + \mathbf{k}}) e^{-i\mathbf{h}\mathbf{r}_{IIi, IIj}} \right\} \\
&\left. - \delta_{IIi, IIj} T_s^2 \left(l_{II}, l_{JJ}, m_{II}, m_{JJ}, \frac{1}{2} \right) \right], \tag{5-33}
\end{aligned}$$

where the self correction term $T_s^2 \left(l_{II}, l_{JJ}, m_{II}, m_{JJ}, \frac{1}{2} \right)$ is

$$\begin{aligned}
T_s^2 \left(l_{II}, l_{JJ}, m_{II}, m_{JJ}, \frac{1}{2} \right) &= \frac{\partial}{\partial \mathbf{r}_{0JJ}} T_s^1 \left(l_{II}, l_{JJ}, m_{II}, m_{JJ}, \frac{1}{2} \right) \\
&- \mathbf{k} \cdot T_s^1 \left(l_{II}, l_{JJ}, m_{II}, m_{JJ}, \frac{1}{2} \right). \tag{5-34}
\end{aligned}$$

The values of the self correction term $T_s^2 \left(l_{II}, l_{JJ}, m_{II}, m_{JJ}, \frac{1}{2} \right)$ are presented in detail in Appendix B.

In the case of molecular crystals where the dynamical matrix calculation requires the evaluation of a lattice sum of the form (5-11), it is necessary to include a “molecular correction term” in equation (5-33), in a way that is equivalent to the molecular correction term for the lattice energy that was described in section 5.3.1. This is done as described in section 5.3.1, and the expression that is obtained is:

$$\begin{aligned}
& \sum_{\substack{\mathbf{l} \in \mathbf{L} \\ \mathbf{l} \neq \mathbf{0} \\ i \neq I \\ i \neq I = J}} \frac{\partial^2}{\partial \mathbf{r}_{0Ii} \partial \mathbf{r}_{0Jj}} \left(\frac{S_{l_{II} l_{JJ} l}^{m_{II} m_{JJ}}(\Omega_I, \Omega_J, \hat{\mathbf{r}}_{IIi, I'Jj})}{\|\mathbf{r}_{0Ii, IJj}\|^{l+1}} \right) e^{i\mathbf{k}\mathbf{r}_{0Ii, IJj}} \\
&= \frac{1}{\Gamma\left(\frac{1}{2} + l\right)} \left[\sum_{\substack{\mathbf{l} \in \mathbf{L} \\ \mathbf{l} \neq \mathbf{0} \\ i \neq I \\ i \neq I = J}} \frac{\partial^2}{\partial \mathbf{r}_{0Ii} \partial \mathbf{r}_{0Jj}} \left(\frac{S_{l_{II} l_{JJ} l}^{m_{II} m_{JJ}}(\Omega_I, \Omega_J, \hat{\mathbf{r}}_{IIi, I'Jj}) \Gamma\left(\frac{1}{2} + l, \alpha\pi \|\mathbf{r}_{0Ii, IJj}\|^2\right)}{\|\mathbf{r}_{0Ii, IJj}\|^{l+1}} \right) e^{i\mathbf{k}\mathbf{r}_{0Ii, IJj}} \right. \\
&+ \frac{i^l 2^{2-l} \pi^{3/2}}{V} \sum_{\mathbf{h}} \left\{ \frac{(\mathbf{h} + \mathbf{k})(\mathbf{h} + \mathbf{k})^T}{\|\mathbf{h} + \mathbf{k}\|^{2-l}} e^{-\frac{\|\mathbf{h} + \mathbf{k}\|^2}{4\alpha\pi}} S_{l_{II} l_{JJ} l}^{m_{II} m_{JJ}}(\Omega_I, \Omega_J, \widehat{\mathbf{h} + \mathbf{k}}) e^{-i\mathbf{h}\mathbf{r}_{IIi, IJj}} \right\} \\
&- \delta_{I,J}(1 - \delta_{i,j}) \frac{\partial^2}{\partial \mathbf{r}_{0Ii} \partial \mathbf{r}_{0Jj}} \left(\frac{S_{l_{II} l_{JJ} l}^{m_{II} m_{JJ}}(\Omega_I, \Omega_J, \hat{\mathbf{r}}_{IIi, I'Jj}) \gamma\left(\frac{1}{2} + l, \alpha\pi \|\mathbf{r}_{0Ii, IJj}\|^2\right)}{\|\mathbf{r}_{0Ii, IJj}\|^{l+1}} \right) e^{i\mathbf{k}\mathbf{r}_{0Ii, IJj}} \\
&\left. - \delta_{Ii, Jj} T_s^2 \left(l_{II}, l_{JJ}, m_{II}, m_{JJ}, \frac{1}{2} \right) \right] \tag{5-35}
\end{aligned}$$

The validity of equation (5-35) is assessed graphically in a similar way as equation (5-30) in section 5.3.1. Figure 5-7 shows the value of one component of the charge/dipole contribution to the element of matrix $\widehat{\mathbf{D}}$ associated with the interaction between the third and second atom (and its periodic images) of the first molecule in the unit cell (see Figure 5-6,a), as function of the convergence parameter α . A three-dimensional plot is needed because matrix $\widehat{\mathbf{D}}$ is complex. Figure 5-8 is a projection of matrix $\widehat{\mathbf{D}}$ onto the complex plane. The wave vector was chosen arbitrarily to be

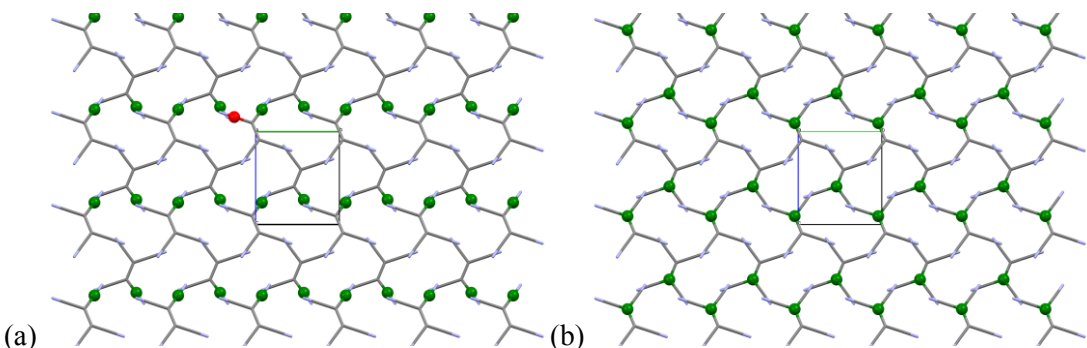


Figure 5-6 (a) The $\widehat{\mathbf{D}}_{13,12}$ element of the dynamical matrix is related to the interaction of the red atom ($Ii = 13$) with the $Jj = 12$ atom and its periodic images (green). (b) The $\widehat{\mathbf{D}}_{11,11}$ element of the dynamical matrix is related to the self-interaction of the green atoms ($Ii, Jj = 11$)

$\mathbf{k} = (0.2, 0, 0)$ Figure 5-9 is obtained in a similar manner to Figure 5-7 but is used to display a component of the charge quadrupole contribution for the element of matrix $\hat{\mathbf{D}}$ related to the self-interaction of the first atom of the first molecule, and its periodic images (see Figure 5-6,b) and for the same wave vector. Since the chosen contribution happens to be real, Figure 5-10 shows a projection on the plane defined by the real part of the dynamical matrix element and the parameter α . All these plots show a behavior independent of the chosen value of parameter α , a result which is identical to that obtained for the lattice energy (see figures in section 5.3.1).

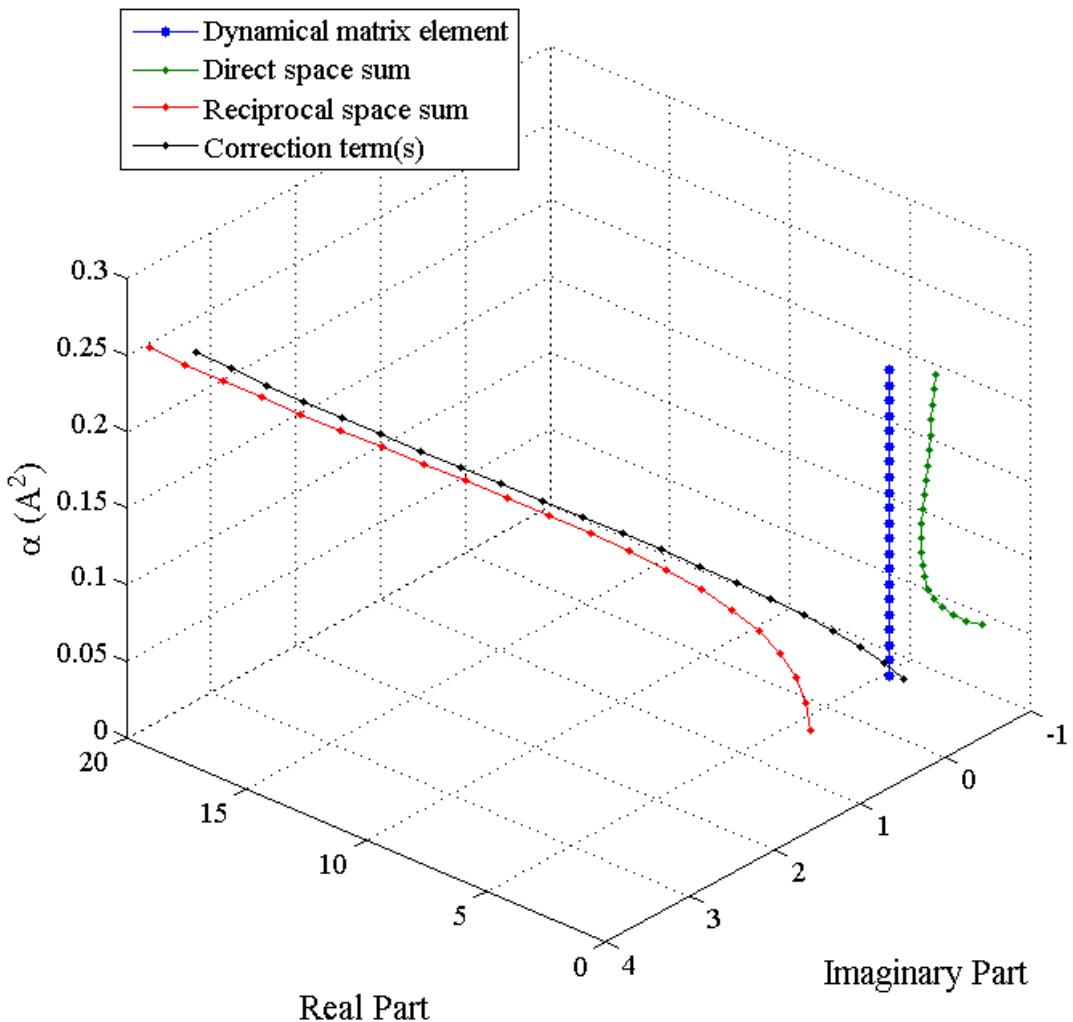


Figure 5-7 The value of the component $(0,1s)$ of the charge-dipole contribution to the element (x,x) of matrix $\hat{\mathbf{D}}_{13,12}$ (defined in equation 4-22, page 63), for $\mathbf{k} = (0.2, 0, 0)$ as function of the Ewald convergence parameter α . The calculation is performed for the predicted structure that corresponds to the monoclinic form of tetracyanoethylene (see section 6.4.2). The quantum mechanical calculations were performed at the M06/6-31G(d,p) level. The direct space sum and the reciprocal space sum are also shown.

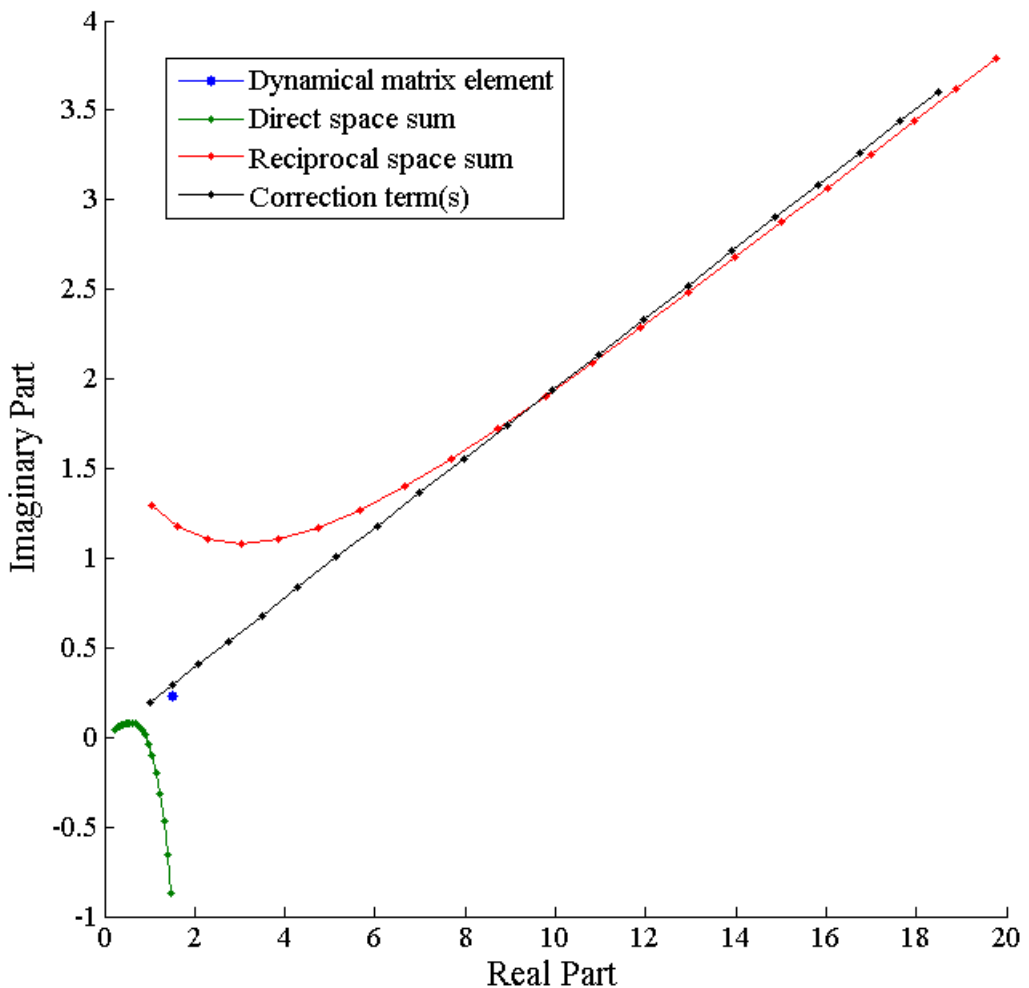


Figure 5-8 A projection onto the complex plane of the dynamical matrix element shown in Figure 5-7. The correction term and the direct and reciprocal space sums are also shown.

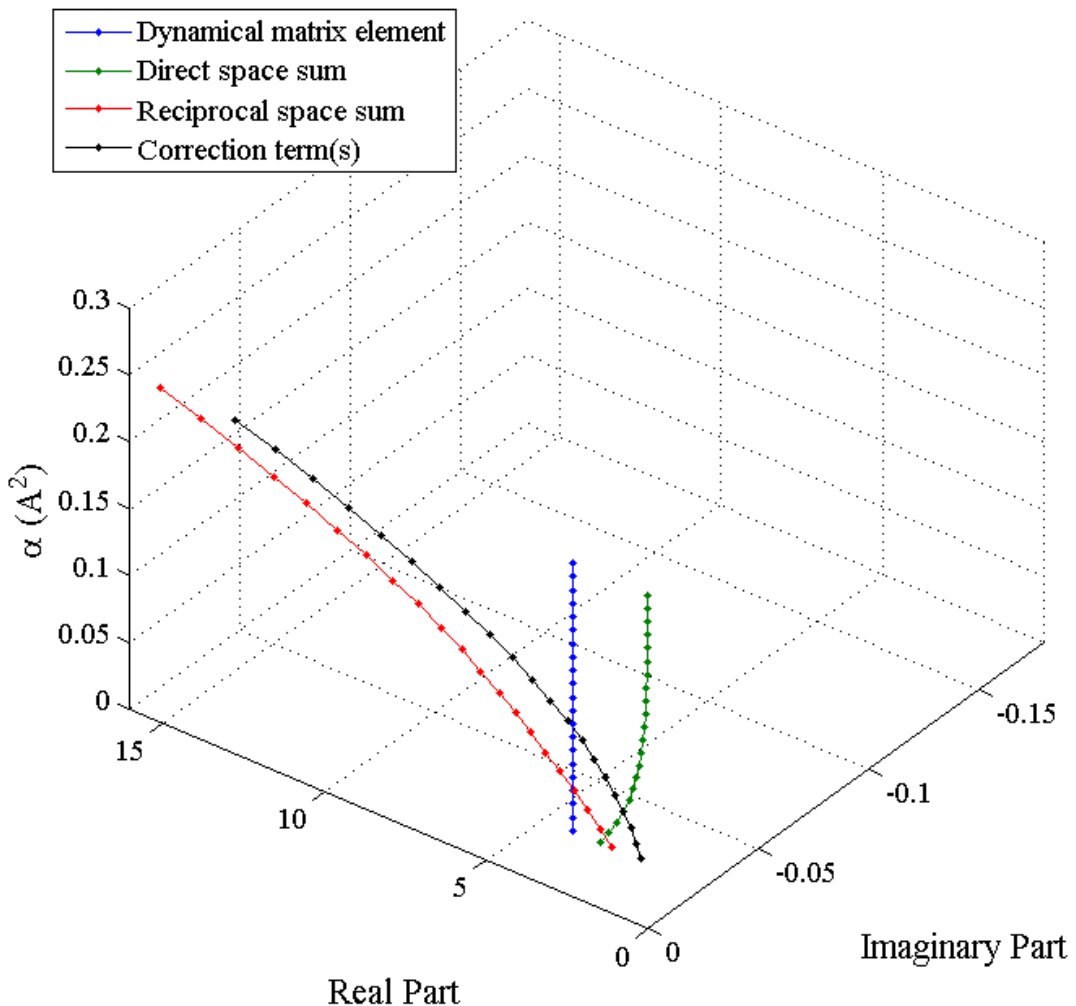


Figure 5-9 The value of the component $(0,2c)$ of the charge-quadruple contribution to the element (x,x) of matrix $\widehat{\mathbf{D}}_{11,11}$ (defined in equation (4-22), page 63), for $\mathbf{k} = (0.2, 0, 0)$ as a function of the Ewald convergence parameter α . The calculation is performed for the predicted structure that corresponds to the monoclinic form of tetracyanoethylene (see section 6.4.2). The quantum mechanical calculations were performed at the M06/6-31G(d,p) level. The direct space sum and the reciprocal space sum are also shown.

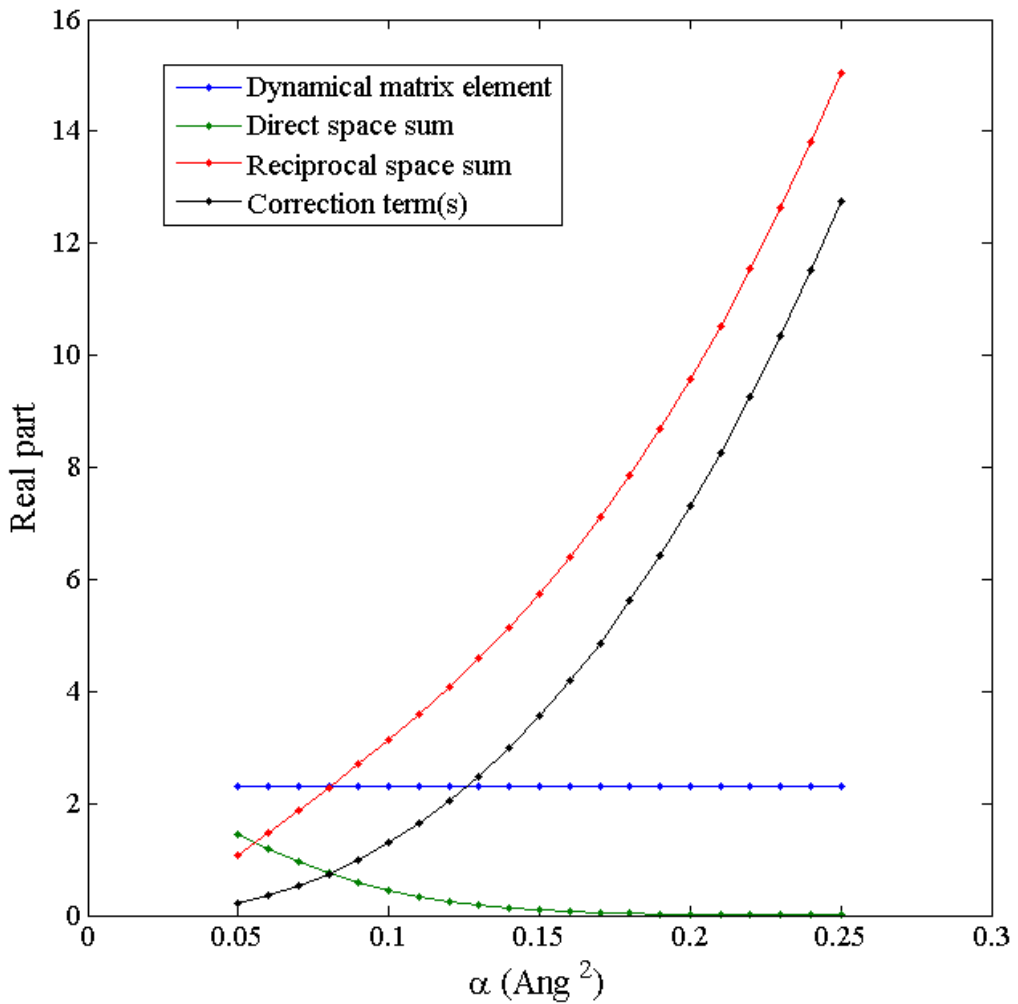


Figure 5-10 A projection onto the plane defined by the real part of the dynamical matrix element shown in Figure 5-9, and the α parameter. The correction term and the direct and reciprocal space sums are also shown.

5.4. The Γ -point in the reciprocal space sum

In equations (5-27), (5-30) the contribution of the Γ -point, $\mathbf{h} = \mathbf{0}$, to the reciprocal lattice sum is undefined if the wave vector $\mathbf{k} = \mathbf{0}$ for $l \leq 2$ and therefore it is omitted. The same behaviour is observed in the reciprocal sum of equations (5-33), (5-35) for $l = 0$. Therefore the lattice sums of interest for the calculation of the lattice energy and the dynamical matrix take the form:

$$\begin{aligned}
& \sum_{\substack{\mathbf{l} \in \mathbf{L} \\ \mathbf{l} \neq \mathbf{0} \\ \text{if } l=J}} \frac{S_{l_{II}l_{JJ}l}^{m_{II}m_{JJ}}(\Omega_I, \Omega_J, \hat{\mathbf{r}}_{IIi,I'Jj})}{\|\mathbf{r}_{0IIi,IJj}\|^{l+1}} e^{i\mathbf{k}\mathbf{r}_{0IIi,IJj}} \\
&= \frac{1}{\Gamma\left(\frac{1}{2} + l\right)} \left[\sum_{\substack{\mathbf{l} \in \mathbf{L} \\ \mathbf{l} \neq \mathbf{0} \\ \text{if } l=J}} \frac{S_{l_{II}l_{JJ}l}^{m_{II}m_{JJ}}(\Omega_I, \Omega_J, \hat{\mathbf{r}}_{IIi,I'Jj}) \Gamma\left(\frac{1}{2} + l, \alpha\pi\|\mathbf{r}_{0IIi,IJj}\|^2\right)}{\|\mathbf{r}_{0IIi,IJj}\|^{l+1}} e^{i\mathbf{k}\mathbf{r}_{0IIi,IJj}} \right. \\
&+ \frac{i^l 2^{2-l} \pi^{3/2}}{V} \sum_{\substack{\mathbf{h} \\ \mathbf{h} \neq \mathbf{0} \text{ if } \mathbf{k}=\mathbf{0}}} \left\{ \|\mathbf{h} + \mathbf{k}\|^{l-2} e^{-\frac{\|\mathbf{h}+\mathbf{k}\|^2}{4\alpha\pi}} S_{l_{II}l_{JJ}l}^{m_{II}m_{JJ}}(\Omega_I, \Omega_J, \widehat{\mathbf{h} + \mathbf{k}}) e^{-i\mathbf{h}\mathbf{r}_{IIi,Jj}} \right\} \\
&- \delta_{I,J} (1 - \delta_{i,j}) \frac{S_{l_{II}l_{JJ}l}^{m_{II}m_{JJ}}(\Omega_I, \Omega_J, \hat{\mathbf{r}}_{IIi,I'Jj}) \gamma\left(\frac{1}{2} + l, \alpha\pi\|\mathbf{r}_{0IIi,IJj}\|^2\right)}{\|\mathbf{r}_{0IIi,IJj}\|^{l+1}} e^{i\mathbf{k}\mathbf{r}_{0IIi,IJj}} \\
&\left. - \delta_{II,JJ} T_s^0\left(l_{II}, l_{JJ}, m_{II}, m_{JJ}, \frac{1}{2}\right) \right] \tag{5-36}
\end{aligned}$$

and

$$\begin{aligned}
& \sum_{\substack{\mathbf{l} \in \mathbf{L} \\ \mathbf{l} \neq \mathbf{0} \\ i \neq I \\ i \neq J}} \frac{\partial^2}{\partial \mathbf{r}_{0Ii} \partial \mathbf{r}_{0Jj}} \left(\frac{S_{l_{II}l_{JJ}l}^{m_{II}m_{JJ}}(\Omega_I, \Omega_J, \hat{\mathbf{r}}_{IIi,I'Jj})}{\|\mathbf{r}_{0Ii,IJj}\|^{l+1}} \right) e^{i\mathbf{k}\mathbf{r}_{0Ii,IJj}} \\
&= \frac{1}{\Gamma\left(\frac{1}{2} + l\right)} \left[\sum_{\substack{\mathbf{l} \in \mathbf{L} \\ \mathbf{l} \neq \mathbf{0} \\ i \neq I \\ i \neq J}} \frac{\partial^2}{\partial \mathbf{r}_{0Ii} \partial \mathbf{r}_{0Jj}} \left(\frac{S_{l_{II}l_{JJ}l}^{m_{II}m_{JJ}}(\Omega_I, \Omega_J, \hat{\mathbf{r}}_{IIi,I'Jj}) \Gamma\left(\frac{1}{2} + l, \alpha\pi \|\mathbf{r}_{0Ii,IJj}\|^2\right)}{\|\mathbf{r}_{0Ii,IJj}\|^{l+1}} \right) e^{i\mathbf{k}\mathbf{r}_{0Ii,IJj}} \right. \\
&+ \frac{i^l 2^{2-l} \pi^{3/2}}{V} \sum_{\mathbf{h}} \left\{ \frac{(\mathbf{h} + \mathbf{k})(\mathbf{h} + \mathbf{k})^T}{\|\mathbf{h} + \mathbf{k}\|^{2-l}} e^{-\frac{\|\mathbf{h} + \mathbf{k}\|^2}{4\alpha\pi}} S_{l_{II}l_{JJ}l}^{m_{II}m_{JJ}}(\Omega_I, \Omega_J, \widehat{\mathbf{h} + \mathbf{k}}) e^{-i\mathbf{h}\mathbf{r}_{IIi,Jj}} \right\} \\
&- \delta_{I,J}(1 - \delta_{i,j}) \frac{\partial^2}{\partial \mathbf{r}_{0Ii} \partial \mathbf{r}_{0Jj}} \left(\frac{S_{l_{II}l_{JJ}l}^{m_{II}m_{JJ}}(\Omega_I, \Omega_J, \hat{\mathbf{r}}_{IIi,I'Jj}) \gamma\left(\frac{1}{2} + l, \alpha\pi \|\mathbf{r}_{0Ii,IJj}\|^2\right)}{\|\mathbf{r}_{0Ii,IJj}\|^{l+1}} \right) e^{i\mathbf{k}\mathbf{r}_{0Ii,IJj}} \\
&\left. - \delta_{II,JJ} T_s^2 \left(l_{II}, l_{JJ}, m_{II}, m_{JJ}, \frac{1}{2} \right) \right] \quad (5-37)
\end{aligned}$$

respectively. The fact that the $(\mathbf{h}, \mathbf{k}) = (\mathbf{0}, \mathbf{0})$ point is omitted in reciprocal sum (5-36) clearly does not affect interactions for which $l > 2$. The same is true in equation (5-37) for interactions for which $l > 0$.

The omitted terms do not have a contribution to the lattice sums of centrosymmetric unit cells crystals, while for non-centrosymmetric unit cells these terms have a finite contribution. The way the contribution of the Γ -point to reciprocal lattice sums (5-36) and (5-37) can be calculated has been discussed by many authors (Born & Huang, 1954; de Leeuw et al., 1980; Deem et al., 1990; Nymand & Linse, 2000; Smith, 1981; van Eijk & Kroon 1997; Minicozzi & Stroot, 1971) for several specific cases. This term is known to have an effect similar to that of an external field (Born & Huang, 1954) and it is associated with non-zero charge at the surface of polar crystals. It is commonly referred to as the *surface correction term*. In contrast to any other term in the lattice sums, this value of this term depends on the crystal's shape. Its dependence on the shape of the crystal has led to some discussions in the literature questioning whether it should be included or not (Pillardy et al., 2000; van Eijk & Kroon, 1997, 2000; Wedemeyer et al., 2000), especially in the course of a crystal structure prediction study based on lattice energy calculations. The main argument

against the use of the term is that “material” external to the crystal needs to accumulate at the surface in order to cancel the surface charge which is responsible for this term (van Eijk & Kroon, 1997, 2000). This is known as the *tin foil boundary condition* and is a reasonable assumption when the crystal is grown from a solvent with a high dielectric constant. Furthermore, in the course of a crystal structure prediction study, the crystal shape is not known and therefore it is challenging to include this term in a meaningful way. On the other hand it is argued that there are some cases where the conditions under which the surface correction term is negligible are not met (Pillardy et al., 2000; Wedemeyer et al., 2000). Therefore, surface correction term cannot be regarded as negligible in all cases, and its importance should in principle be assessed in each new study.

With regards to lattice dynamics calculations, there is evidence suggesting that this term does not significantly affect the result (Aung & Strauss, 1973; van Eijk, 2001). Finally the compatibility of the surface correction term with the Born & von Kàrmàn cyclic boundary condition that is adopted in lattice dynamics calculations is not clear. Here, we omit it following van Eijk & Kroon (1997, 2000).

6. Results

In this chapter the extension of a crystal structure prediction methodology through the integration of a methodology for the calculation of the free energy based on the harmonic approximation is investigated. As a first test of the approach, the fcc crystal of argon (Ar) is studied within the harmonic approximation. The Ar crystal is modeled as an fcc Lennard-Jones crystal. Then the methodology that we adopt for crystal structure prediction is briefly described and is subsequently applied to imidazole and tetracyanoethylene. The free energies, from 0 K to the melting point, of the low-lying lattice energy minima of imidazole and tetracyanoethylene are evaluated as described in chapters 3,4 and 5. A small investigation of the effect of the chosen model on the calculations is also presented. Finally the free energy, from 0 K to 80 K, of the ambient pressure crystal of Ar is calculated using a quasi-harmonic free energy minimisation algorithm. This allows changes in the structure of Ar as a function of temperature to be determined.

6.1. The Lennard-Jones solid; Dispersion curves and density of states

A solid of Lennard-Jones spheres (Choi et al., 1993; Kaplan, 2006; Lennard-Jones, 1937) is a useful model system that allows the initial validation of the harmonic approximation method. In such a system, particles are held together because they interact isotropically via the Lennard-Jones potential (see section 4.3). The Lennard-Jones model system offers a good description of real solids that interact primarily via repulsion and dispersion interactions such as the rare gas solids, such as argon, krypton, xenon. In this work, the Lennard-Jones potential is used to study argon (Ar), whose crystalline form has been extensively studied experimentally at

temperatures up to its melting point (84 K, Dobbs & Jones, 1957) and for which different types of measured data are available. Argon is known to crystallize in a face centered cubic (fcc) lattice at ambient pressure (Born & Huang, 1954).

Many different sets of Lennard-Jones parameters for Ar can be found in the literature (Diemand et al., 2013; Freeman & Doll, 1985; Goharshadi et al., 2007; Özgen et al., 1996; Kittel 2005, Laasonen et al., 2000; Rahman, 1964; Salonen et al., 2007; Singer & Smith, 1987; White 1999). Here we are not interested in the optimal model for the description of argon but in an investigation of the capabilities of method of harmonic approximation. Therefore no assessment of the reliability of the various sets was attempted. We use values proposed by Rahman (1964) in the study of the dynamics of liquid argon, specifically $\varepsilon/k_B = 120$ K and $\sigma = 3.4$ Å. Most of the various other parameters sets differ slightly from these values, with the largest differences observed for ε/k_B , which in the vast majority of cases varies by only $\pm 1\%$. Another popular choice for the σ parameter is only 0.14% higher.

The most stable structure is known qualitatively (fcc), and the lattice constant describing the unit cell has been measured by Barrett & Meyer (1964) as 5.311 Å at 4.2 K and by Peterson et al. (1966) as 5.30017 Å at 4.25 K. Here, the lattice constant is computed by determining the global minimum of the lattice energy function. For comparison with the experimental dispersion curves, it is necessary to use the primitive unit cell, which is rhombohedral (Hawkins et al., 2008). The lattice energy and its derivatives are calculated in a pairwise additive manner as described in section 4.2, without any consideration of the efficiency of convergence of the lattice sum, or any correction for the potential tail region. In order to limit the negative effects of such an approach, a large radial cut-off distance equal to 20σ is used; in the case of Ar, this is equal to the very large value of 68 Å. Lattice energy minimization is performed with respect to the lattice lengths and lattice angles, using the BFGS method, which does not require a calculation of the Hessian. This confirms that a fcc primitive cell ($\alpha, \beta, \gamma = 60^\circ$ and $a=b=c$) is reproduced by the chosen potential. The minimum energy lattice constant of Ar is 5.25 Å. As soon as the lattice energy minimum is obtained, harmonic properties such as the phonon frequencies and the density of vibrational states can be calculated.

The dispersion curves of Ar along three high symmetry directions, $(\xi, 0, 0)$, $(\xi, \xi, 0)$ and (ξ, ξ, ξ) , are shown in Figure 6-1. Because the primitive unit cell of the

fcc crystal contains only one atom, there are three modes of vibration described by three branches on the dispersion curves. Along directions $(\xi, 0, 0)$ and (ξ, ξ, ξ) two modes coincide as a result of the high symmetry of the crystal. Experimental points (Fujii et al., 1974) for every mode and along all directions compare very well with the calculated values.

The density of vibrational states, shown in Figure 6-2, is generated as described in section 3.6, based on one million randomly sampled wave vectors and is normalized to unity. It is found to be in good qualitative agreement (within a multiplicative constant) with the density of states calculated using the method of Gilat & Raubenheimer (1966), as reported in Fujii et al. (1974). A quadratic function is also fitted to the low frequency region of the density of states ($\nu \leq 0.5$ THz). The fit was obtained in MS Excel, and it shows that in this region, the density of states can indeed be approximated by a quadratic function verifying the validity of the Debye approximation (see section 3.7).

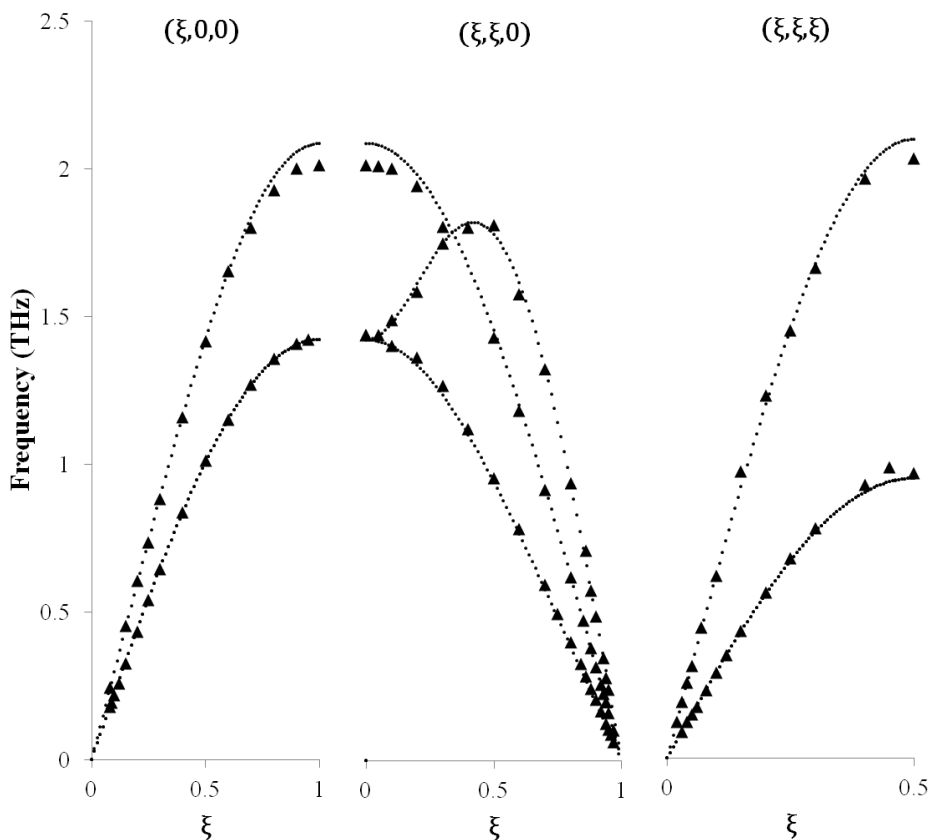


Figure 6-1 Dispersion curves of Argon when the wave vectors vary along three directions $(\xi, 0, 0)$, $(\xi, \xi, 0)$, and (ξ, ξ, ξ) , as a function of the reduced wave vector coordinate ξ . The dots are the calculated points, while the triangles are experimental data (Fujii et al., 1974).

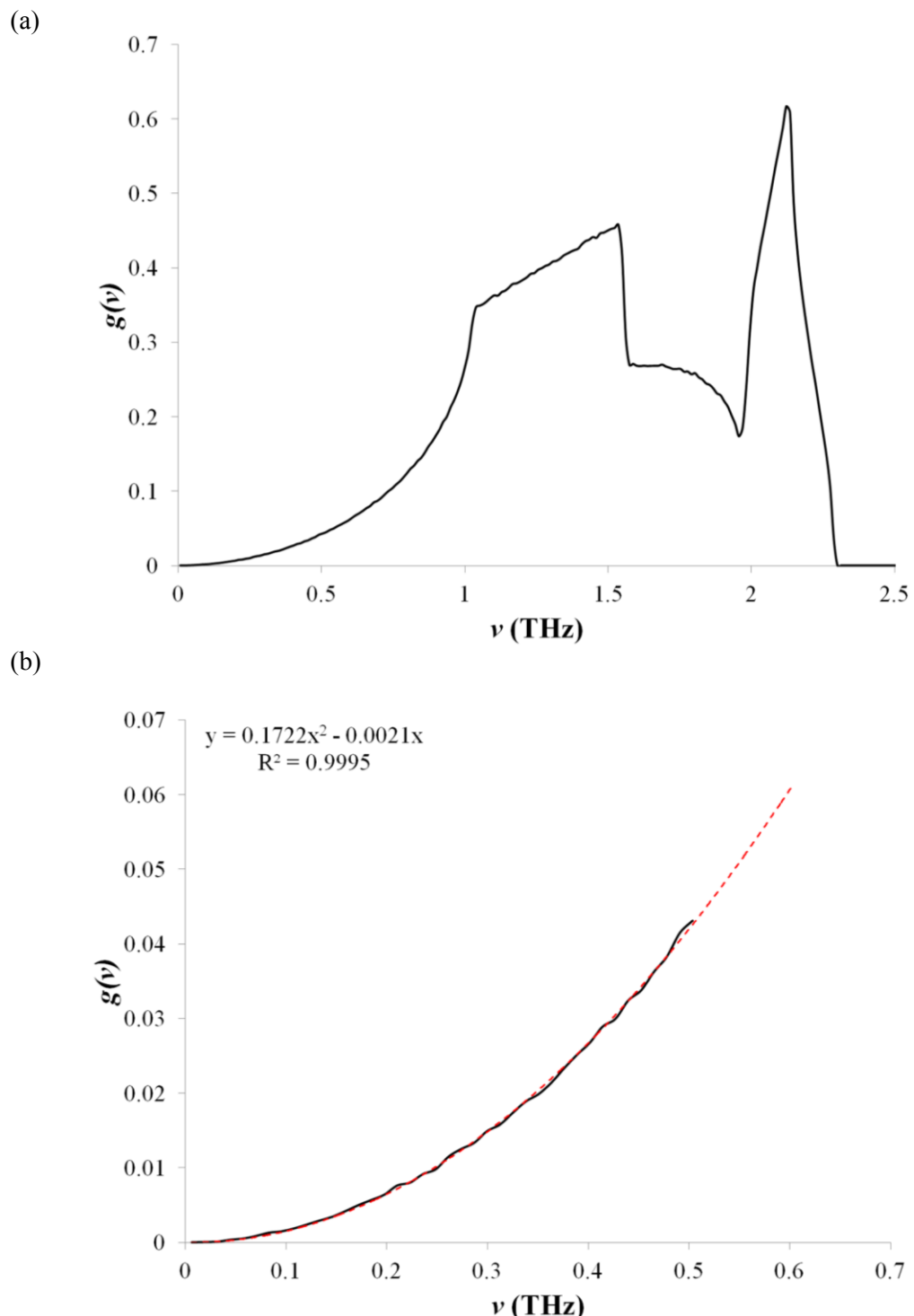


Figure 6-2 (a) Normalized density of vibrational states as a function of frequency; (b) a close-up of the normalized density of states in the low frequency region. A quadratic trend curve is also fitted to the low frequency region and shown in red.

6.2. Crystal structure prediction methodology

It is common practice to perform crystal structure prediction based on optimization algorithms in which the lattice energy function is used as an objective function (Day, 2011; Price, 2008). A distinctive characteristic of crystal structure prediction as an optimization problem is that it is not sufficient to look for the global minimum, but that all low-energy minima are sought. This is because one is interested in metastable polymorphs that are higher in energy than the most stable polymorph, but also because this helps to overcome the limitations of existing techniques, in which model uncertainty may lead to inaccuracies in the relative energies of different structures.

6.2.1. Overview of the approach

From a practical perspective, it is known (Lommerse et al., 2000; Motherwell et al., 2002; Day et al., 2005,2009; Bardwell et al., 2011) that the reliable modeling of the organic solid state requires highly accurate and hence computationally-demanding models. As a consequence, it is necessary to adopt a hierarchical methodology to crystal structure prediction in order to achieve reasonable efficiency. Our group has been performing crystal structure prediction studies over the past years using a multistage methodology, tackling different problems at different stages.

- 1) Stage 1. A conformational analysis is performed based on a survey of the Cambridge Structural Database (CSD), and isolated molecule quantum mechanical calculations. The purpose is to identify the set of intramolecular degrees of freedom that must to be treated as flexible during stage 2, as well as their range of variation. Furthermore, an appropriate model is chosen for the inter-atomic interactions, as specified by a level of theory and a basis set for isolated molecule quantum mechanical calculations, and a semi-empirical model for the repulsion and dispersion interactions with an associated set for parameters.
- 2) Stage 2. A global search is carried out with the aim to identify all low energy minima of the lattice energy hyper-surface. The number of minima identified is of the order of millions and a simplified model is adopted to

achieve this. This stage is performed using the CrystalPredictor algorithm (Karamertzanis & Pantelides, 2005, 2007)

- 3) Stage 3. The most promising minima (i.e., with the lowest lattice energy) identified in the previous stage are further minimized using a much more accurate, and hence computationally-demanding model:
 - a. In the case of rigid molecules, accuracy is increased by using a more detailed model for the electrostatic interactions, based on a distributed multipole expansion. The DMACRYS software is used for this purpose (Price et al., 2010).
 - b. In the case of flexible molecules higher accuracy is achieved in one or more ways: by using a more detailed model for the electrostatic interactions, based on a distributed multipole expansion, by allowing additional molecular flexibility, and by calculating the intra-molecular energy with a higher quantum mechanical level of accuracy. In this case the CrystalOptimizer algorithm (Kazantsev et al., 2010, 2011:a) is used.
- 4) Stage 4: In the final analysis stage, additional criteria can be used to identify the most likely polymorphs from the ranking generating. This may include more accurate calculations on selected structures or the evaluation of additional information. In this work, this stage is extended to include a re-ranking based on the results of free energy calculations under the harmonic approximation.

6.2.2. Comparison of crystal structures

The program COMPACK (Chisholm & Motherwell, 2005) is used for assessing the similarity of any two crystals. The default settings of 15 molecules in the coordination sphere and 20% for the angle and distance tolerance are used. In this way the geometry of a cluster of 15 molecules in one structure is compared with that of the equivalent cluster in the other structure. The quantification of the difference between the two structures is done by a root mean squared deviation of the atomic positions, rms_{15} . The subscript 15 implies that the coordination sphere consists of 15 molecules.

6.3. Imidazole

Imidazole is a small ring molecule, whose chemical diagram is shown in Figure 6-3. It is expected to have a planar conformation and to behave as rigid, i.e. to adopt essentially the same conformation in all crystals. Imidazole is a simple molecule that has already been the subject of successful crystal structure prediction attempts, based on lattice energy minimisation algorithms (Pillardy et al., 2000, 2001; Price et al., 2004), so that it can be modeled with confidence. A broad variety of models has been used in these studies, and in general the results were satisfactory to excellent. Pillardy et al. (2000, 2001) performed an analysis of the suitability of different models based on a number of molecules. Their main conclusion with respect to imidazole is that the AMBER force field, together with a point charge model for the electrostatics, is capable of predicting the most stable polymorph of imidazole at ambient pressure. Price et al. (2004) modeled the electrostatics based on distributed multipoles (calculated at MP2/6-31G**) and used the Buckingham potential (FIT parameterisation) for repulsion/dispersion. They used their own search algorithm for crystal structure prediction. They found the ambient pressure form of imidazole as the global minimum. Based on this reported experience, imidazole is therefore an ideal test case for the proposed approach.

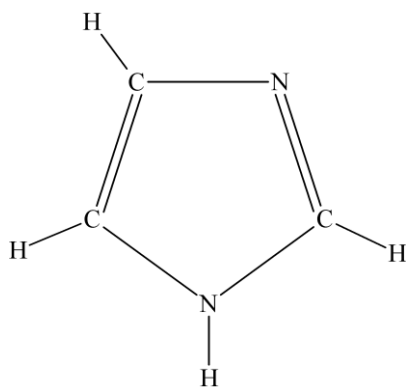


Figure 6-3 The molecular diagram of imidazole.

6.3.1. Experimental information

Imidazole is known to crystallize in two forms, α and β (Craven et al., 1977; Epstein, 1982; Martinez-Carrera, 1966, McMullan et al., 1979; Paliwoda et al., 2012). Form α , a monoclinic form, is known to be the most stable at ambient conditions,

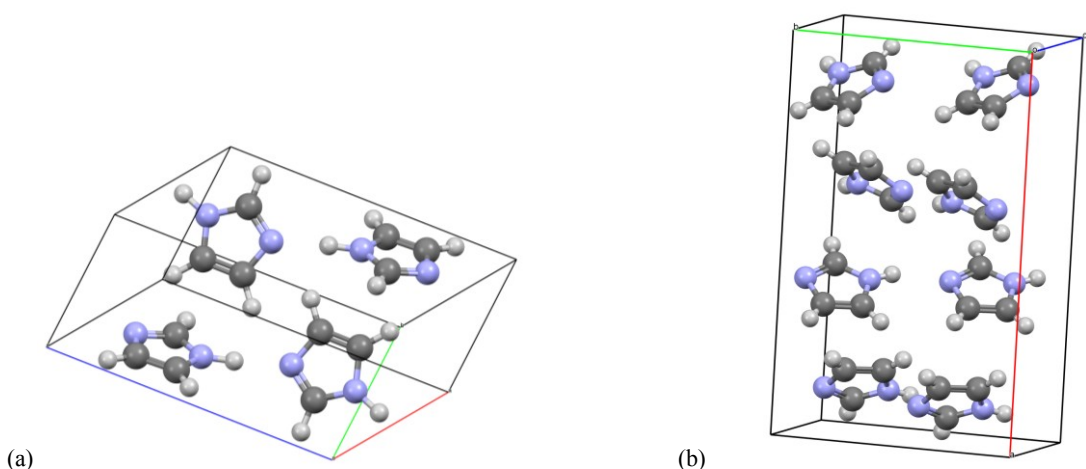


Figure 6-4 Visualisation of the experimental unit cells of the two forms of imidazole
 a) the unit cell of the α -form at 103 K and ambient pressure (McMullan et al., 1979);
 b) the unit cell of the β -form at 298K and 0.8GPa (Paliwoda et al., 2012).

Form	Space group	Z'	Z	a (Å)	b (Å)	c (Å)	β (°)	ρ (g cm ⁻³)
α (103K)	$P2_1/c$	1	4	7.57	5.37	9.79	119.08	1.300
α (293K)	$P2_1/c$	1	4	7.73	5.45	9.78	117.28	1.235
β (298K/0.8GPa)	$Aba2$	1	8	13.91	8.60	5.34	90.00	1.416

Table 6-1 Basic characteristics of the unit cell of the two resolved forms of imidazole. Lattice angles α and γ are equal to 90° for all forms at all temperatures because of symmetry constraints.

while the cubic β form is stable at high pressures (greater than 0.5 GPa). The major characteristics of the two unit cells are summarized in Table 6-1. A visualisation of the unit cell of the two polymorphs of imidazole is found in Figure 6-4.

The normal melting point of imidazole is 364 K; no other form other than α has been observed experimentally from 103 K, the lowest temperature at which experiments have been performed, to the melting point (Paliwoda, 2012). As a consequence we do not expect a polymorphic phase transition to occur in our study. Finally to the best of our knowledge, there are no available dynamical information, i.e., frequencies of vibration.

6.3.2. Crystal structure prediction

The crystal structure prediction methodology described in section 6.2 is applied to imidazole. The molecule is treated as rigid during the search stage and

therefore stage 1 consists only of the determination of the conformation of imidazole, namely the gas phase conformation (the unconstrained global minimum) obtained at the MP2/6-31G(d,p) level. The repulsion and dispersion interactions are calculated using the Buckingham potential with the FIT parameterization described in section 4.3. During stage 2 atomic point charges are used to model the electrostatic interactions. The point charges are derived using the ChelpG method (Breneman & Wiberg, 1990) from the *ab-initio* derived electrostatic potential calculated at the MP2/6-31G(d,p) level of theory for the gas phase conformation.

The search stage is performed with the rigid version of the *CrystalPredictor* algorithm (Karamertzanis & Pantelides, 2005). Half a million crystals are generated in 59 commonly encountered space groups: $P1$, $P\bar{1}$, $P2_1$, $P2_1/c$, $P2_12_12$, $P2_12_12_1$, $Pna2_1$, $Pca2_1$, $Pbca$, $Pbcn$, $C2/c$, Cc , $C2$, Pc , Cm , $P2_1/m$, $C2/m$, $P2/c$, $C222_1$, $Pmn2_1$, $Cmc2_1$, $Aba2$, $Fdd2$, $Iba2$, $Pnna$, $Pccn$, $Pbcm$, $Pnnm$, $Pmmn$, $Pnma$, $Cmcm$, $Cmca$, $Fddd$, $Ibam$, $P4_1$, $P4_3$, $I\bar{4}$, $P4/n$, $P4_2/n$, $I4/m$, $I4_1/a$, $P4_12_12$, $P4_32_12$, $P\bar{4}_22_1/c$, $I\bar{4}2d$, $P3_1$, $P3_2$, $R3$, $P\bar{3}$, $R\bar{3}$, $P3_12_1$, $P3_22_1$, $R3/c$, $R\bar{3}/c$, $P6_1$, $P6_3$, $P6_3/m$, $P2_13$ and $Pa\bar{3}$. It is assumed that there is only one molecule in the asymmetric unit. The global search results in the identification of 811 structures within 10 kJ mol⁻¹ of the global minimum and 3263 structures within 15 kJ mol⁻¹ of the global minimum. The global search identifies the β -form of imidazole as the global minimum with an rms_{15} equal to 0.272 Å, while the α -form corresponds to the 6th lowest energy minimum with a match of the experimental structure quantified by an $rms_{15}=0.200$ Å.

The 200 unique lowest energy structures generated by *CrystalPredictor* are minimised in Stage 3 using the DMACRYS local lattice energy minimisation program (Price et al., 2010), in which a more accurate representation of the electrostatic interactions is used. The gas-phase conformation and energy are re-calculated at the M06/6-31G(d,p) level. Distributed multipoles up to hexadecapole are determined based on the wave function of the resulting gas phase conformation. In general several of the structures obtained at the global search stage may lead to the same minimum during the structure refinement in stage 3. In this case, our final landscape consists of 149 unique structures. Moreover, during 19 of the 200 minimizations, a symmetry reduction was performed because the final structure was found to be a saddle point, giving 19 $Z'=2$ structures. The final lattice energy landscape is shown in Figure 6-5.

The α -form is correctly predicted as the most stable structure with $\text{rms}_{15}=0.133\text{\AA}$, while the β -form, which is unstable at ambient pressure, is found to be 16th lowest-energy structure. The rms_{15} for the β -form is 0.421\AA . These differences can be visualized on Figure 6-6 where the experimental and predicted structures are overlaid.

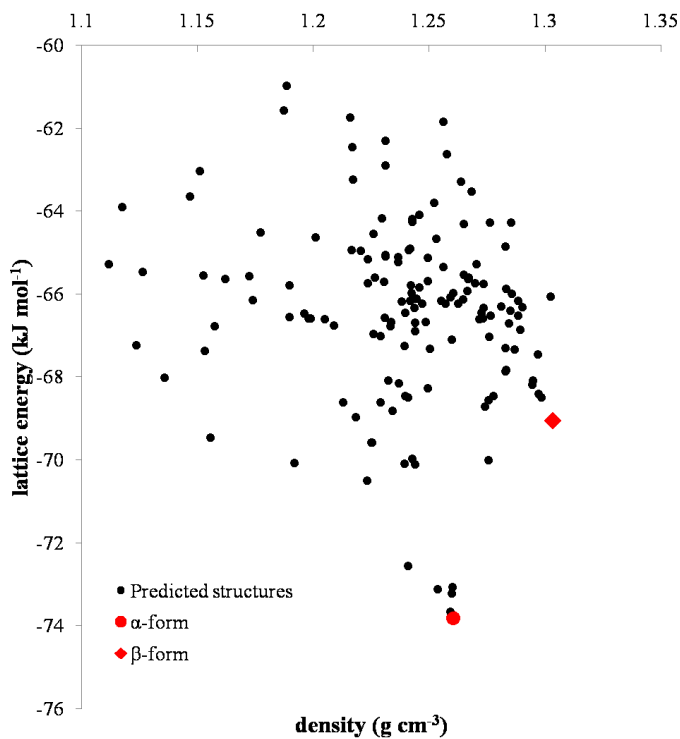


Figure 6-5 Final lattice energy landscape of imidazole. Red dot and diamond represent the experimentally known α and β forms. Quantum mechanical calculations were performed at M06/6-31G(d,p) level.

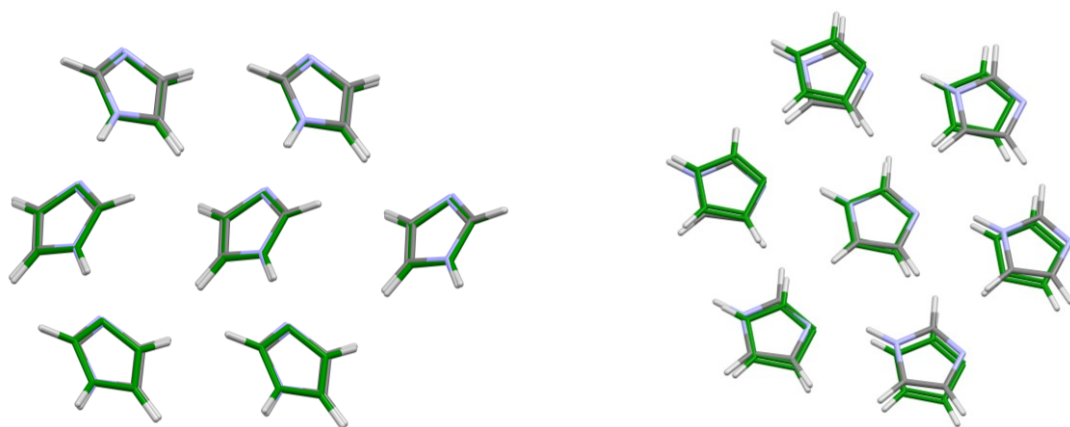


Figure 6-6 Overlay between the predicted (green) and experimental (coloured by element) forms of imidazole. a) the α -form, with $\text{rms}_{15}=0.133\text{\AA}$, b) the β -form, with $\text{rms}_{15}=0.425\text{\AA}$. Quantum mechanical calculations were performed at the M06/6-31G(d,p) level.

It should be pointed out that the β -form is predicted as the densest structure compared to the other predicted structures, in line with the experimental evidence that it is stabilized via pressurisation.

6.3.3. Temperature effects in crystal structure prediction

The free energy landscape is constructed from 0 K to 350 K, very close to the melting point. Integration of the free energy expression (equation 3-33) is carried out using the Gauss-Legendre quadrature (see section 3.7) over a 64-node grid in the reciprocal unit cell. The Helmholtz free energy landscapes at 0 K, 100 K, 200 K, 300 K and 350 K are shown in Figure 6-7, Figure 6-8 and Figure 6-9. The dots in Figure 6-7 to Figure 6-9 are coloured based on the change in rank of the corresponding structure from the lattice energy landscape to that including the vibrational contributions to the free energy, i.e. based on the value of the quantity $R_T - R_{LE}$, where R_T is the rank of the structure in the free energy landscape at temperature T and R_{LE} is the rank in the lattice energy landscape.

Dynamical calculations reveal that 18 structures are unstable, corresponding approximately to 12% of the structures generated in stage 3. This leads to changes in the rank of remaining structures, especially the highest energy ones.

Temperature is found to affect mainly the high free energy structures, while the lowest ranked structures practically remain unaffected. Somewhat unexpectedly at first, the structures that are in the high free energy region appear to achieve an improved rank (they are coloured in blue tones) even at low temperatures. This can in fact be attributed to the elimination of some of the structures with a lower lattice energy as unstable. The stable α -form remains the most stable structure for the whole range of temperatures from 0 K to the melting point. The rank of the unstable β -form deteriorates with increasing temperature.

In order to investigate the effect of the choice of computational model, these calculations are repeated for at the HF/6-31G(d,p) level of theory. The free energy and rank as function of temperature for the two forms, for the HF and M06 level, are summarized in Table 6-2. A similar result is obtained with both models, although some re-ordering of the low energy minima is observed for HF at higher temperatures.

The structure that is the global minimum for 300 K and 350 K in the HF/6-31G(d,p) landscapes is very closely related to the structure that corresponds to the α -

form. Its deviation (rms_{15}) from the experimental structure is 0.442\AA ; from the predicted structure that corresponds to the experimental form, it is 0.234\AA only. The rms_{15} of the β -form for the HF calculation is 0.420\AA . The complete free energy landscapes for the HF calculations are not presented.

T (K)	M06/6-31G(d,p)				HF/6-31G(d,p)			
	α -form		β -form		α -form		β -form	
	\mathcal{A} (kJ mol ⁻¹)	Rank						
0	-68.69	1	-63.95	16	-78.08	1	-69.99	31
50	-69.03	1	-64.23	16	-78.37	1	-70.22	32
100	-70.61	1	-65.68	17	-79.79	1	-71.52	32
200	-76.76	1	-71.55	19	-85.50	1	-76.96	38
300	-85.86	1	-80.38	21	-94.00	2	-85.21	39
350	-91.42	1	-85.80	21	-99.17	2	-91.02	41
U	-73.83	1	-69.06	16	-83.80	1	-75.56	30

Table 6-2 Summary of the lattice energy, rank and the Helmholtz free energy of the α and β forms of imidazole, as function of temperature.

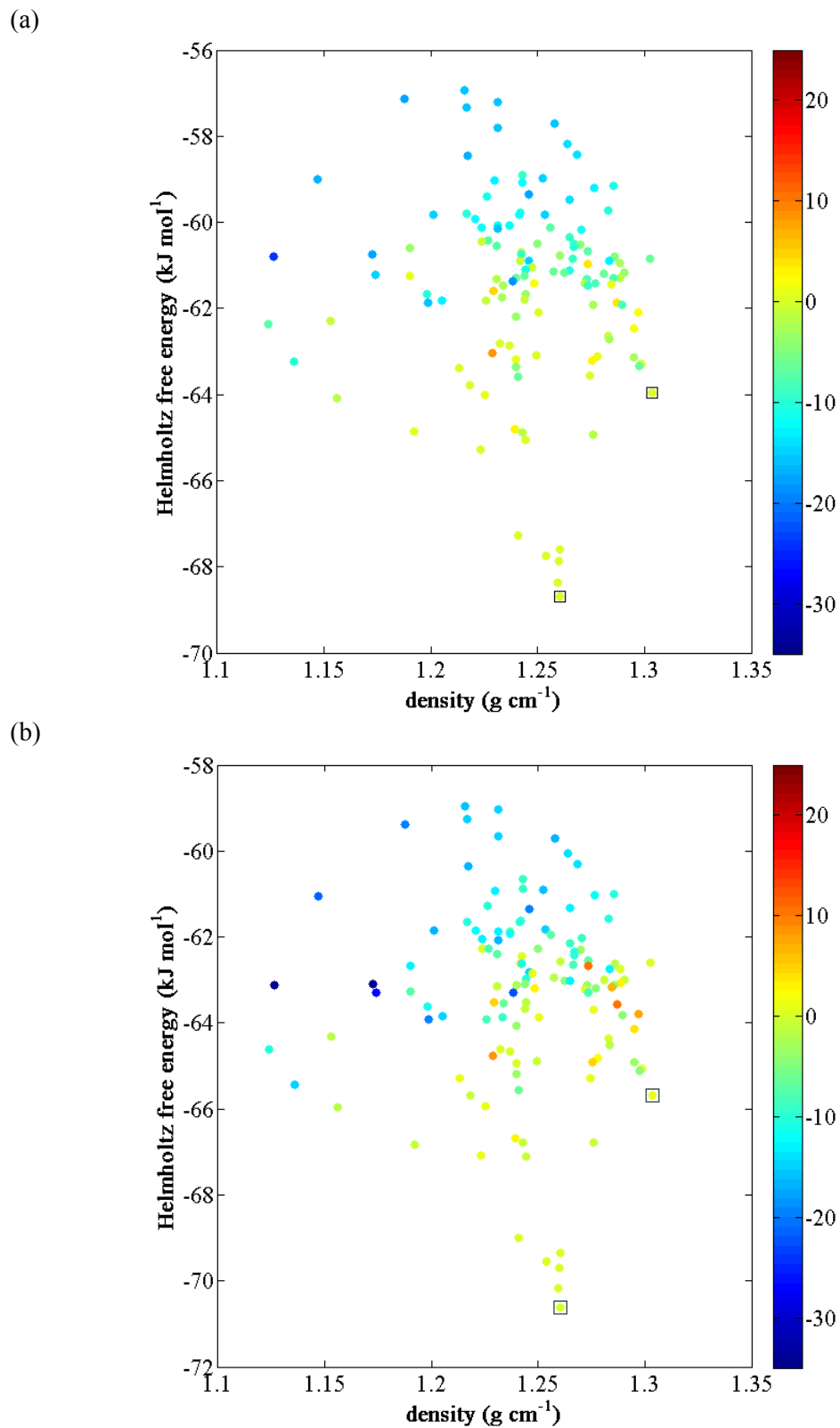


Figure 6-7 The Helmholtz free energy landscape of imidazole at (a) 0 K ; (b) 100 K. All necessary quantum mechanical (charge density and geometry) calculations were performed at M06/6-31G(d,p) level. The colour scale describes the difference in the rank of each structure before and after the vibrational contributions are included.

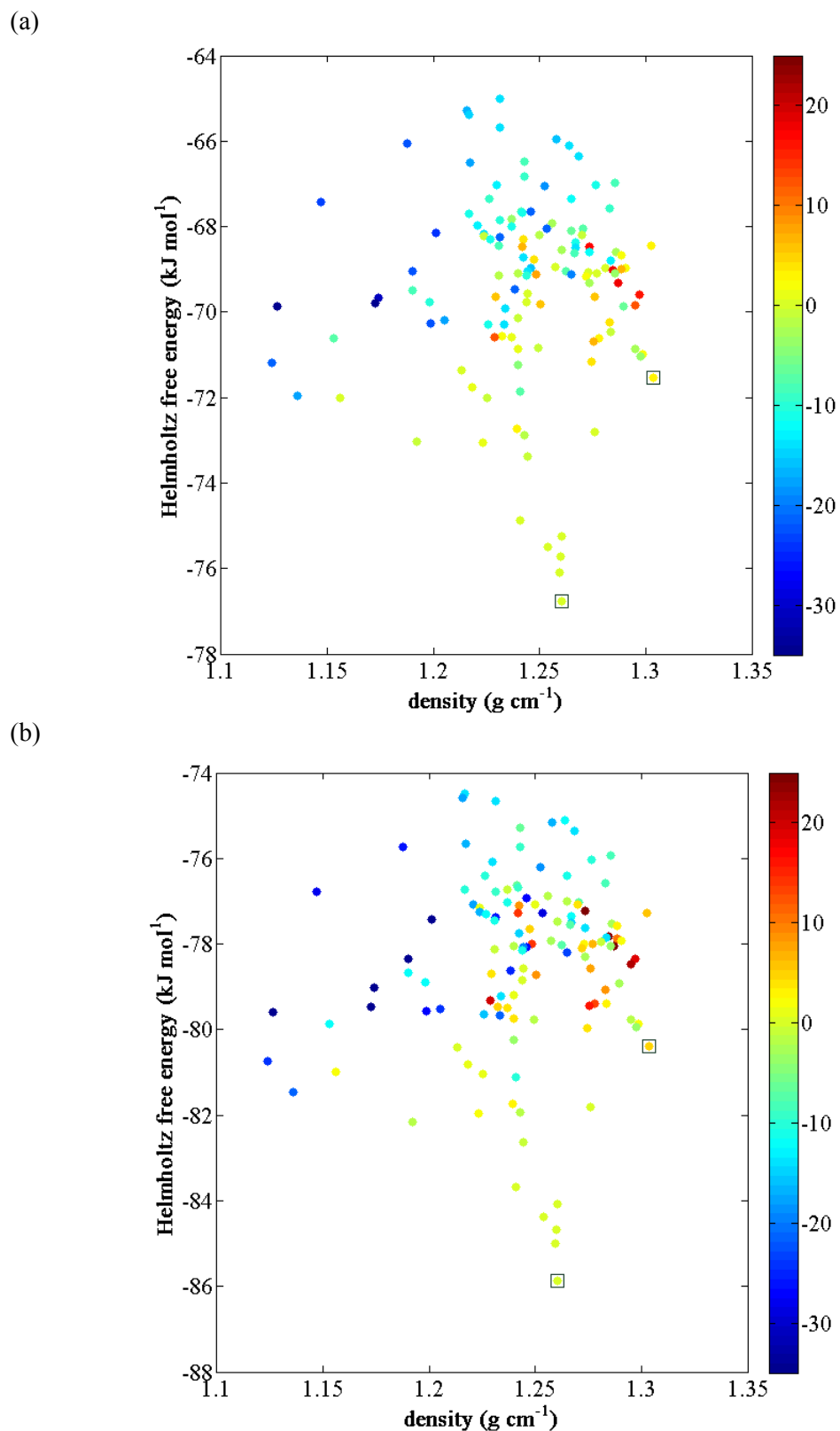


Figure 6-8 The Helmholtz free energy landscape of imidazole at (a) 200K ; (b) 300K. All necessary quantum mechanical (charge density and geometry) calculations were performed at M06/6-31G(d,p) level. The colour scale describes the difference in the rank of each structure before and after the vibrational contributions are included.

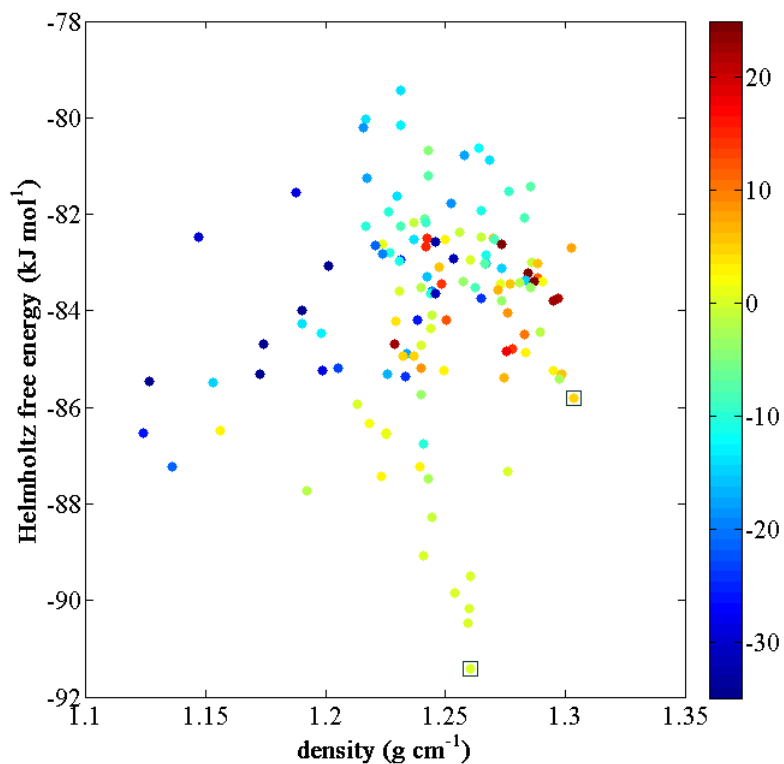


Figure 6-9 The Helmholtz free energy landscape of imidazole at 350K. All necessary quantum mechanical (charge density and geometry) calculations were performed at M06/6-31G(d,p) level. The colour scale describes the difference in the rank of each structure before and after the vibration contributions are included.

6.4. Tetracyanoethylene

The crystal structure prediction methodology described in section 6.2 is applied to tetracyanoethylene (Figure 6-10), a small rigid molecule, whose geometry is expected to be planar. To the best of our knowledge no similar crystal structure prediction study has been performed for this molecule. The geometry of the molecule is obtained by an unconstrained geometry optimisation at various levels of theory: HF, B3LYP, PBE0, M06 and MP2, all with a 6-31G(d,p) basis. A visualisation of the geometry can be found in Figure 6-10, confirming that a planar conformation is favored. Following crystal structure prediction, a free energy calculation is carried out for each of the predicted structures.

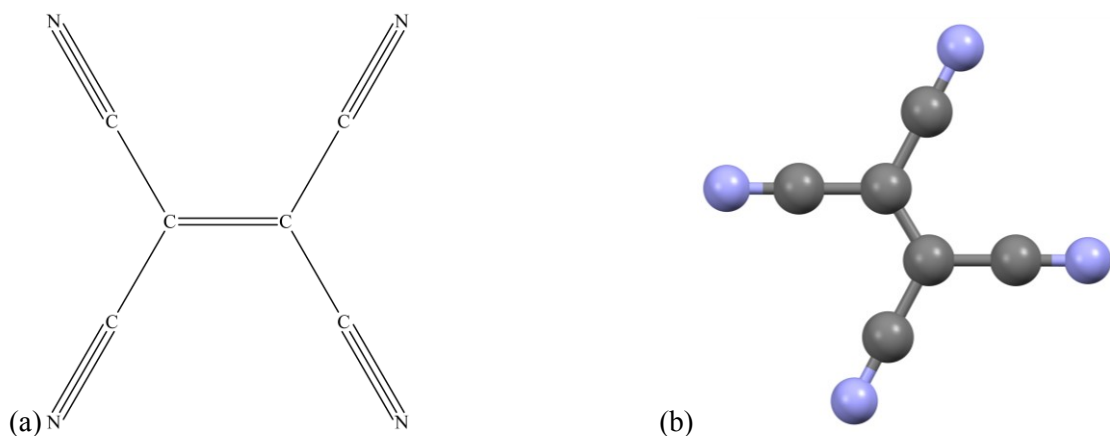


Figure 6-10 a) The molecular diagram of tetracyanoethylene; b) A visualisation of the geometry of the isolated molecule of TCNE obtained by quantum mechanical calculations at MP2/6-31G(d,p) level.

6.4.1. Experimental information

Tetracyanoethylene is known to have a rich polymorphic landscape (Little et al., 1971; Chaplot et al., 1984). The structures of two polymorphs are known: the cubic form (Little et al., 1971) and the monoclinic form (Chaplot et al., 1984). Another polymorph (form III) is reported (Yamawaki et al., 1992, 1996) to be obtained reversibly after pressurization of the monoclinic phase higher than 3GPa but its existence is questioned (Chaplot & Mukhopadhyay 1986; Mukhopadhyay et al., 2009). These authors suggest that when pressurized, an amorphous (Chaplot & Mukhopadhyay 1986) or a disordered crystalline phase (Mukhopadhyay et al., 2009) appears, which leads to the cubic phase after depressurization. Finally a fourth

polymorph is reported to grow from chloride/ethyl-acetate solution at room temperature (Schatsneider et al., 2012), but this structure does not seem to be widely accepted by the crystallographic community. A visualisation of the unit cells of the cubic and monoclinic forms can be found in Figure 6-11. The major characteristics of the unit cells are summarized in Table 6-3. To the best of my knowledge dynamical information is available in the form of dispersion curves only for the monoclinic form (Chaplot et al., 1983) at 5 K. The melting point of tetracyanoethylene is 472 K (Funasako et al., 2012; Radomska & Radomski, 1991). This is likely to be the monoclinic form although no characterisation data are provided. As far as the relative stability of the two polymorphs is concerned, it is widely accepted that the cubic form is more stable at low temperatures than the monoclinic form, but that the monoclinic form becomes more stable than the cubic form at higher temperatures. However, it is difficult to find conclusive evidence in the literature when it comes to determining a

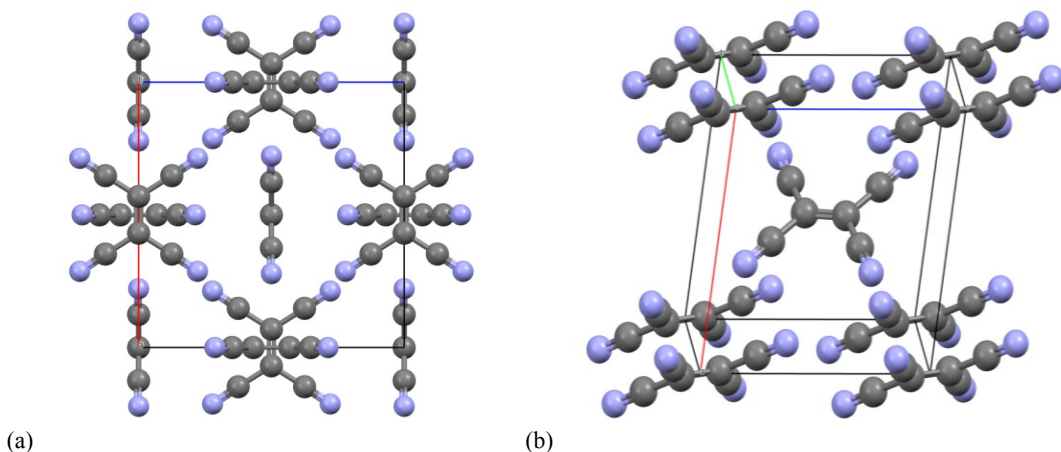


Figure 6-11 Visualization of the experimental unit cells of the two forms of tetracyanoethylene. a) the unit cell of the cubic form at 298K (Little et al., 1971); b) the unit cell of the monoclinic form also at 298K (Chaplot et al., 1984).

Form	Space group	Z'	Z	a (Å)	b (Å)	c (Å)	β (°)	ρ (g cm ⁻³)
Cubic (298K)	$I\bar{m}\bar{3}$	0.13	6	9.74	9.74	9.74	90	1.383
Monoclinic (5K)	$P2_1/n$	1/2	2	7.33	6.11	6.93	97.43	1.380
Monoclinic (298K)	$P2_1/n$	1/2	2	7.51	6.21	7.00	97.17	1.312

Table 6-3 Basic characteristics of the unit cell of the two resolved forms of TCNE. Lattice angles α and γ are equal to 90° for all forms at all temperatures because of symmetry constraints.

transition temperature. Murgich & Pissanetzky (1972) report a reversible transition from the cubic form to the monoclinic form occurring at 292 ± 0.5 K. On the other hand, it is more widely reported (Mierzejewski & Chaplot, 1980; Mukhopadhyay et al., 1985) that an irreversible transition is obtained when heating the cubic form. This transition to the monoclinic form has been found to occur at approximately 320 K. When cooling the monoclinic form, it is reported that it remains stable at least down to 5 K (Chaplot et al., 1983, 1984). This hysteresis in the observed transition behaviour is expected, especially given that the activation energy barrier for the transition is reported to be fairly large, at 230 ± 20 kJ mol⁻¹ (Mukhopadhyay et al., 1985). Thus the transition temperature is expected to lie between 5 and 320 K. The pressure at which the experiments were carried out has not been reported and is assumed to be atmospheric; at moderate pressures, the transition temperature is expected to be relatively insensitive to pressure.

6.4.2. Crystal structure prediction

Since the molecule is rigid, stage 1 of the crystal structure prediction methodology described in section 6.2 simply consists in determining the geometry of the conformation which is subsequently used in stage 2. It is chosen to be the gas phase conformation at the HF/6-31G(d,p) level of theory.

During the search stage the electrostatic interactions are modeled using atomic point charges fitted using ChelpG (Breneman & Wiberg, 1990) to the *ab-initio* derived electrostatic potential at the HF/6-31G(d,p) level. The repulsion and dispersion interactions are calculated using the Buckingham potential with the “FIT” parameters described in section 4.3.

A global lattice energy landscape search (Stage 2 of section 6.2) is performed using the *CrystalPredictor* (Karamertzanis & Pantelides, 2005) algorithm. Molecules are assumed to be rigid and 500,000 structures are generated in 59 common space groups: *P1*, *P* $\bar{1}, *P2*₁, *P2*₁/c, *P2*₁2₁2, *P2*₁2₁2₁, *Pna*2₁, *Pca*2₁, *Pbc*a, *Pbcn*, *C*2/c, *Cc*, *C*2, *Pc*, *Cm*, *P2*₁/m, *C*2/m, *P2*/c, *C*222₁, *Pmn*2₁, *Cmc*2₁, *Aba*2, *Fdd*2, *Iba*2, *Pnna*, *Pccn*, *Pbcm*, *Pnnm*, *Pmmn*, *Pnma*, *Cmcm*, *Cmca*, *Fddd*, *Ibam*, *P4*₁, *P4*₃, *I* $\bar{4}$, *P4/n*, *P4*₂/n, *I4/m*, *I4*₁/a, *P4*₁2₁2, *P4*₃2₁2, *P* $\bar{4}$ ₂2₁/c, *I* $\bar{4}$ 2d, *P3*₁, *P3*₂, *R*3, *P* $\bar{3}$, *R* $\bar{3}$, *P3*₁2₁, *P3*₂2₁, *R3/c*, *R* $\bar{3}$ /c, *P6*₁, *P6*₃, *P6*₃/m, *P2*₁3 and *Pa* $\bar{3}$.$

The 200 lowest energy structures are further minimized using the DMACRYS program (Price, 2010). At this stage electrostatic interactions are modeled using distributed multipoles up to 4th order of interactions. The multipoles have been calculated based on the optimal HF/6-31G(d,p) wave function using the *distributed multipole analysis* proposed by Stone (1981, 2005) and Stone & Alderton (1985). The final lattice energy landscape is shown in Figure 6-12. An overlay between the predicted and experimental structures can be found in Figure 6-13. The final lattice

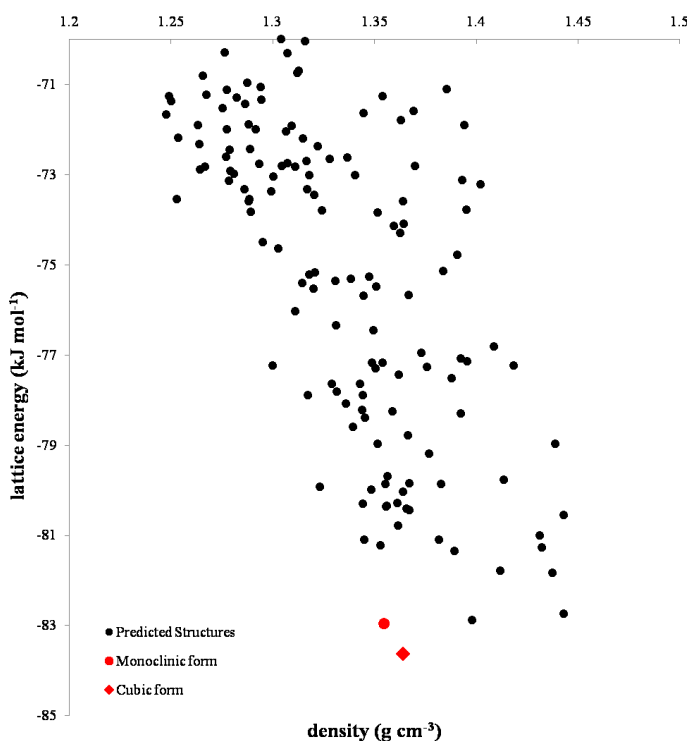


Figure 6-12 Final lattice energy landscape of TCNE. The red dot and diamond represent the monoclinic and cubic experimentally known forms. Quantum mechanical calculation were performed at HF/6-31G(d,p) level.

energy landscape contains 148 unique minima, 122 with $Z'=1$, 25 with $Z'=2$ and 1 with $Z'=8$. The number of minima obtained is smaller than the number of starting points because structures obtained as minima of the global search stage model may merge into the same minimum after DMACRYS minimization. Minima having higher Z' values are obtained as a result of re-minimization after symmetry reduction of the structures corresponding to saddle points instead of minima. These saddle points had been obtained as a consequence of the fact that the minimization is performed under space group symmetry constraints.

This approach results in a successful prediction of the polymorphic landscape of TCNE. Both polymorphs are predicted as lattice energy minima. Furthermore the experimental structures occupy the first and second place among the predicted

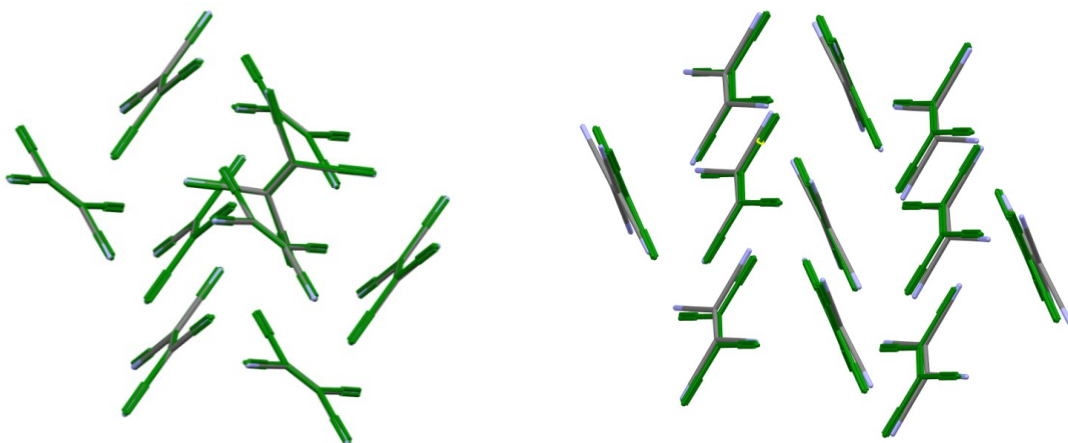


Figure 6-13 Overlay of the two known experimental forms of TCNE (coloured by element) and the corresponding predicted structures (green). a) the cubic form compares to the experimental with an $\text{rms}_{15}=0.039\text{\AA}$; b) the predicted monoclinic form is different from the experimental by an $\text{rms}_{15}=0.285\text{\AA}$. Quantum mechanical calculations were performed at the HF/6-31G(d,p) level.

structures, with the cubic form being first and the monoclinic form being second by the small difference of 0.669 kJ mol^{-1} . Quantification of the difference between these two predicted structures and the actual experimental structures (Figure 6-13) indicates a high predictive accuracy has been achieved with the chosen computational model.

6.4.3. Calculation of the dispersion curves

Dispersion curves for the monoclinic form are available at 5 K (Chaplot et al., 1983). This temperature is sufficiently low so that the dispersion curves calculated for the predicted structure (which correspond to 0 K) are comparable with the experimental data. The experimental data are available for the wave vectors varying along three directions $(\xi, 0, 0)$, $(0, \xi, 0)$ and $(0, 0, \xi)$. In the experimental data only the 24 modes of vibrations with the lowest energy (and therefore frequency) are included. These refer to the 12 external modes of vibration and the 12 lowest internal modes.

The dispersion curves are calculated for the minimum lattice energy form, which corresponds to the monoclinic crystal ($\text{rms}_{15}=0.285\text{\AA}$). The necessary quantum mechanical calculations were performed at the HF/6-31G(d,p) level of theory.

The complete calculated dispersion curves are presented in Figure 6-14 while a comparison between the calculated and predicted external modes is presented in Figure 6-15 and Figure 6-16. The calculated dispersion curves are in good qualitative agreement with the experimentally-determined ones. The values of the calculated phonon frequencies are also found to be of the correct order of magnitude. Quantitatively, the agreement between experimental and calculated frequencies is satisfactory, with errors up to about 0.5THz to 1THz (approximately 16.5 cm^{-1} to 33 cm^{-1}). This level of accuracy is typical in phonon frequency calculations (Day et al., 2003; Della Valle et al., 1995; Gray et al., 2004; Natkaniec et al., 1980; Righini et al., 1980) and therefore it is considered acceptable for the calculation of the free energy. Equivalent calculations are not presented for the cubic form because there are no experimental data available for comparison.

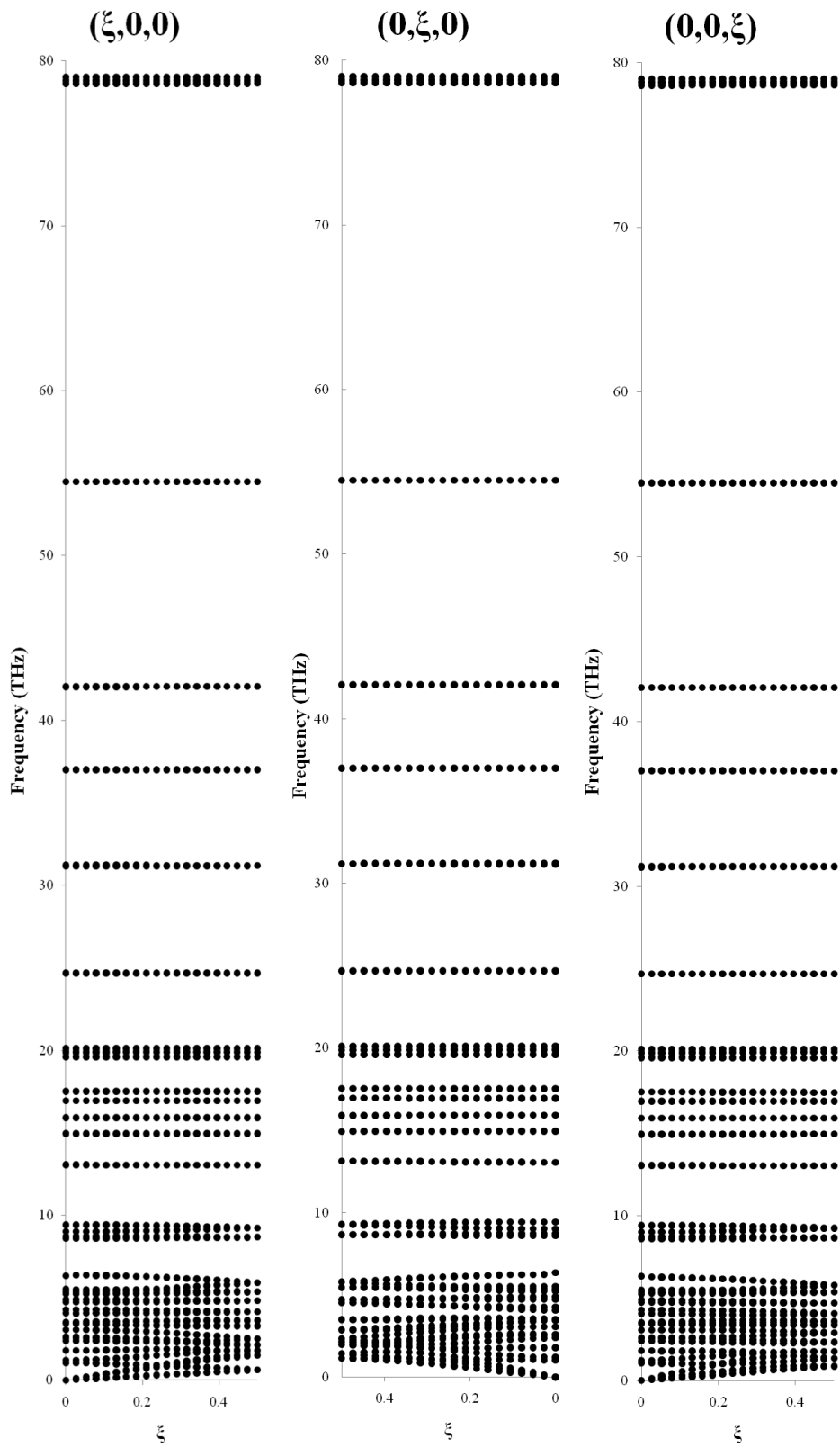


Figure 6-14 Dispersion curves of TCNE. The three panels correspond to different wave vectors as indicated at the top. The 12 lowest energy branches represent the external modes of vibration while the remaining branches represent the internal modes.

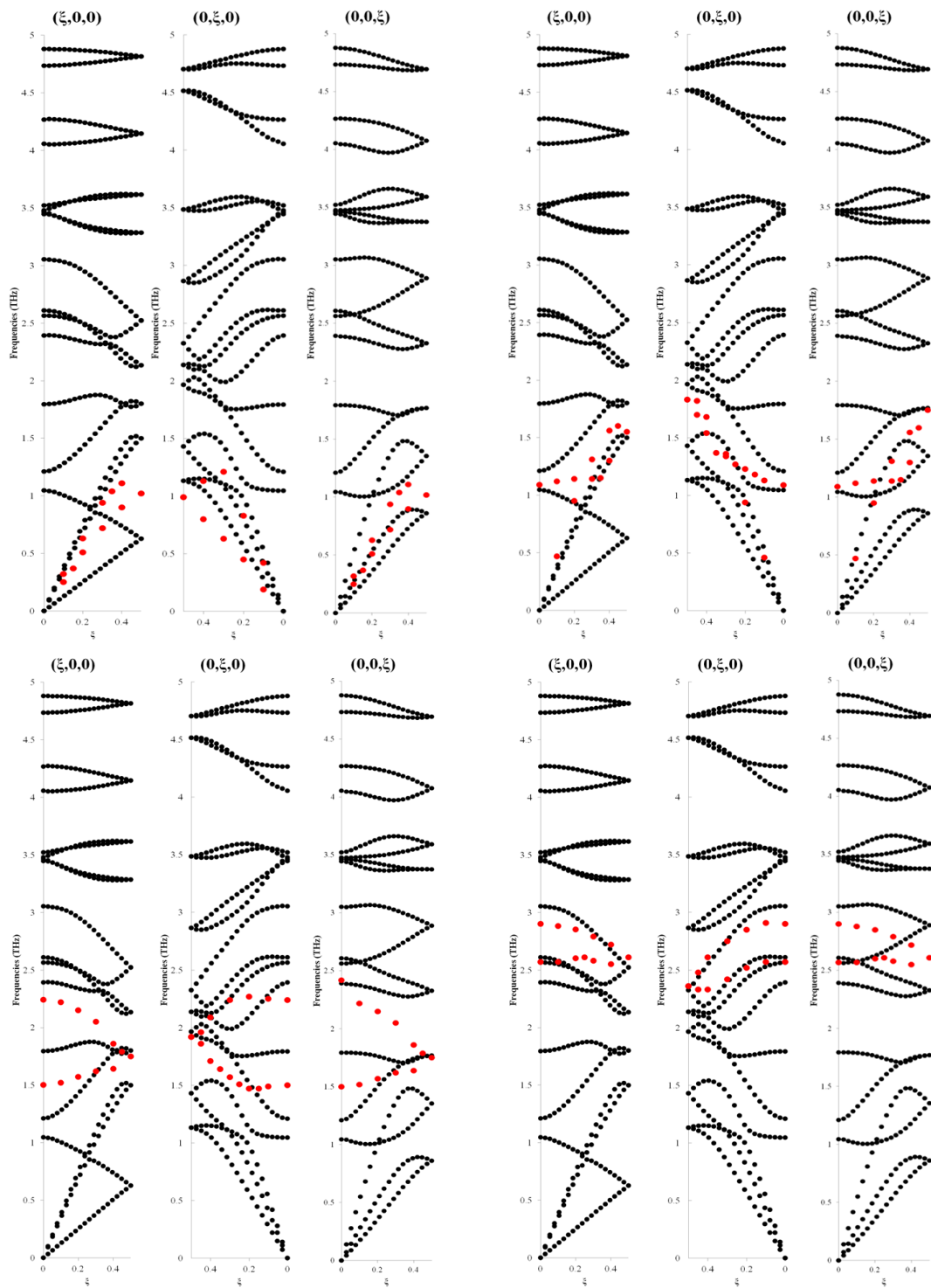


Figure 6-15 Comparison of the 8 experimentally determined lowest frequency modes of vibration of TCNE (in red) with the corresponding calculated modes (in black). The wave vector varies along directions $(\xi, 0, 0)$, $(0, \xi, 0)$ and $(0, 0, \xi)$.

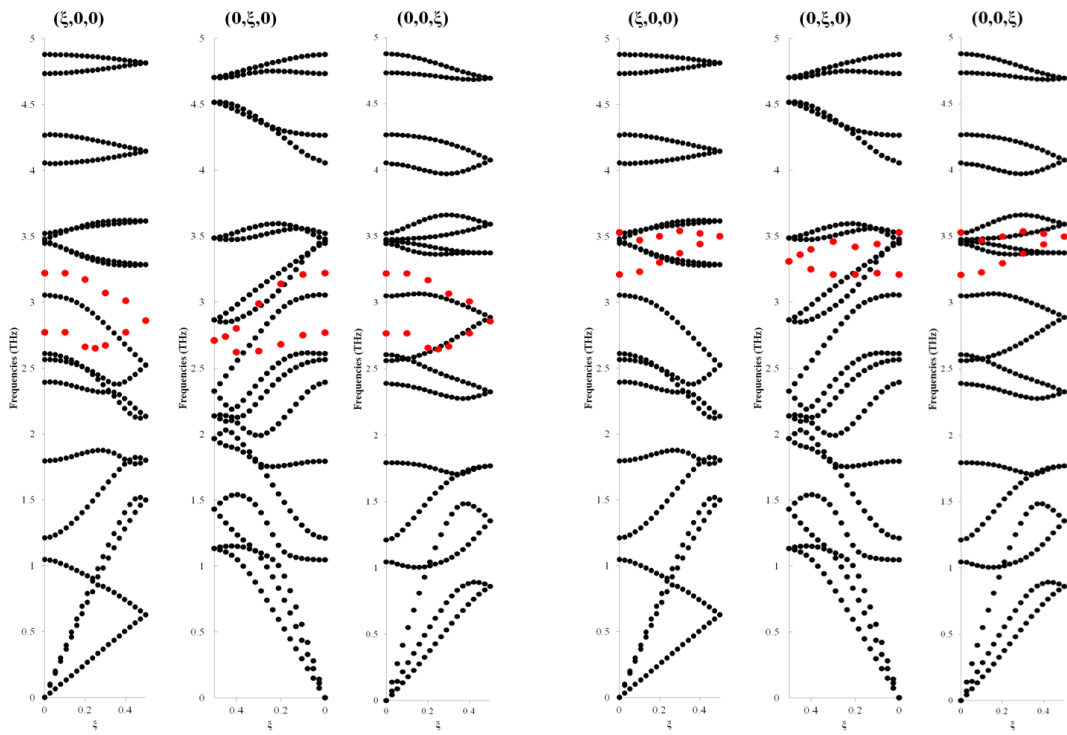


Figure 6-16 Comparison of the 4 experimentally determined highest frequency external modes of vibration of TCNE (in red) with the corresponding calculated modes (in black). The wave vector varies along directions $(\xi, 0, 0)$, $(0, \xi, 0)$ and $(0, 0, \xi)$.

6.4.4. Temperature effects in crystal structure prediction

The free energy of each structure in the landscape shown in Figure 6-12 is calculated using lattice dynamics under the harmonic approximation from 0 K up to 500 K. The evaluation of integrals of the free energy expression (equation 3-33, page 39) is carried out using the Gauss-Legendre quadrature (see subsection 3.7), with 64 wave vector samples (4 nodes for each direction in the reciprocal space). The landscapes obtained for 0 K, 50 K, 100 K, 200 K, 300 K, 400 K, 450 K and 500 K are shown in Figure 6-17 (0 K and 50 K), Figure 6-18 (100 K and 200 K), Figure 6-19 (300 K and 400 K), and finally in Figure 6-20 (450 K and 500K).

During the calculation of the free energy 36 structures out of the 148 structures of Figure 6-12 (approximately 24%) are found to be unstable as imaginary frequencies of atomic vibrations are obtained for at least one wave vector. These unstable structures are therefore eliminated from Figure 6-17 to 6-20. The colour of

the dots in Figure 6-17 to Figure 6-20 has the same significance as in the landscapes of imidazole (section 6.3.3) i.e. it describes the change of the rank of the structures compared to the lattice energy landscape (Figure 6-12).

It is apparent from the energy landscapes that all major qualitative changes that could be expected as temperature increases are indeed observed. The Helmholtz free energy of the structures decreases with increasing temperature. The impact of the contributions of the atomic vibrations increases at higher temperatures. In fact there is only a minor effect on the rank of all structures of in low and medium free energy regions for up to 50 K to 100 K. Finally it should be stressed that we also observe that in general vibrational contributions favour the less dense structures as has been pointed out in the literature (Chaplot, 1987 ; Day, 2011; Dunitz et al., 2000; Dunitz & Gavezzotti, 1998), although this is not the case for all crystals (van Eijk, 2000). This is indicated by the fact that the low density region of all plots of Figure 6-17, Figure 6-18, Figure 6-19 and Figure 6-20 are mainly populated by structures coloured in blue tones while the red tones are seen in the high density region.

The Helmholtz free energy and rank for the predicted structures corresponding to the experimental cubic and monoclinic forms are presented in Table 6-4. The cubic form is found to be more stable at lower temperatures and subsequently, at medium temperatures the monoclinic form is the most stable. The transition between the cubic and monoclinic form occurs at approximately 74 K, based on a linear interpolation of the free energy difference between the two forms (see Figure 6-21). The free energy is interpolated between 60 K and the melting point. This calculated transition temperature is in line with available experimental (Mierzejewski & Chaplot, 1980; Mukhopadhyay et al., 1985) and calculated data (Schatschneider et al., 2012). When the temperature is increased further the rank of the cubic form deteriorates while other structures are stabilised over the monoclinic form. Particularly from 368 K (obtained in a similar way, as shown in Figure 6-22) to the melting point the 24th structure of the lattice energy landscape, hereafter referred as S_{24}^{HF} , becomes the global minimum structure in terms of free energy as shown in Table 6-4. To the best of my knowledge there are no available experimental data (Murgich & Pissanetzky, 1972; Mukhopadhyay et al., 1985) to agree or disagree with such a result. On the other hand, the harmonic approximation is known to have a validity which is limited to low temperatures and therefore this observation cannot be considered to be reliable.

T (K)	Cubic Form		Monoclinic Form		Global minimum
	\mathcal{A} (kJ mol ⁻¹)	Rank	\mathcal{A} (kJ mol ⁻¹)	Rank	\mathcal{A} (kJ mol ⁻¹)
0	-79.60	1	-79.38	2	-79.60 (Cubic)
50	-80.04	1	-79.94	2	-80.04 (Cubic)
100	-82.43	2	-82.62	1	-82.62 (Monoclinic)
200	-92.75	3	-93.63	1	-93.63 (Monoclinic)
300	-109.02	11	-110.62	1	-110.62 (Monoclinic)
400	-130.15	18	-132.46	4	-132.71
450	-142.28	25	-144.96	6	-145.61
500	-155.36	25	-158.41	7	-159.45
\bar{U}	-83.63	1	-82.96	2	-83.63 (Cubic)

Table 6-4 The Helmholtz free energy \mathcal{A} and rank of the cubic and monoclinic forms of TCNE, as function of temperature T . The value of the global minimum free energy is presented in the last column for comparison. In the bottom, the lattice energy \bar{U} and rank of the relevant structures are also presented. Quantum mechanical calculations were performed at the HF/6-31G(d,p) level.

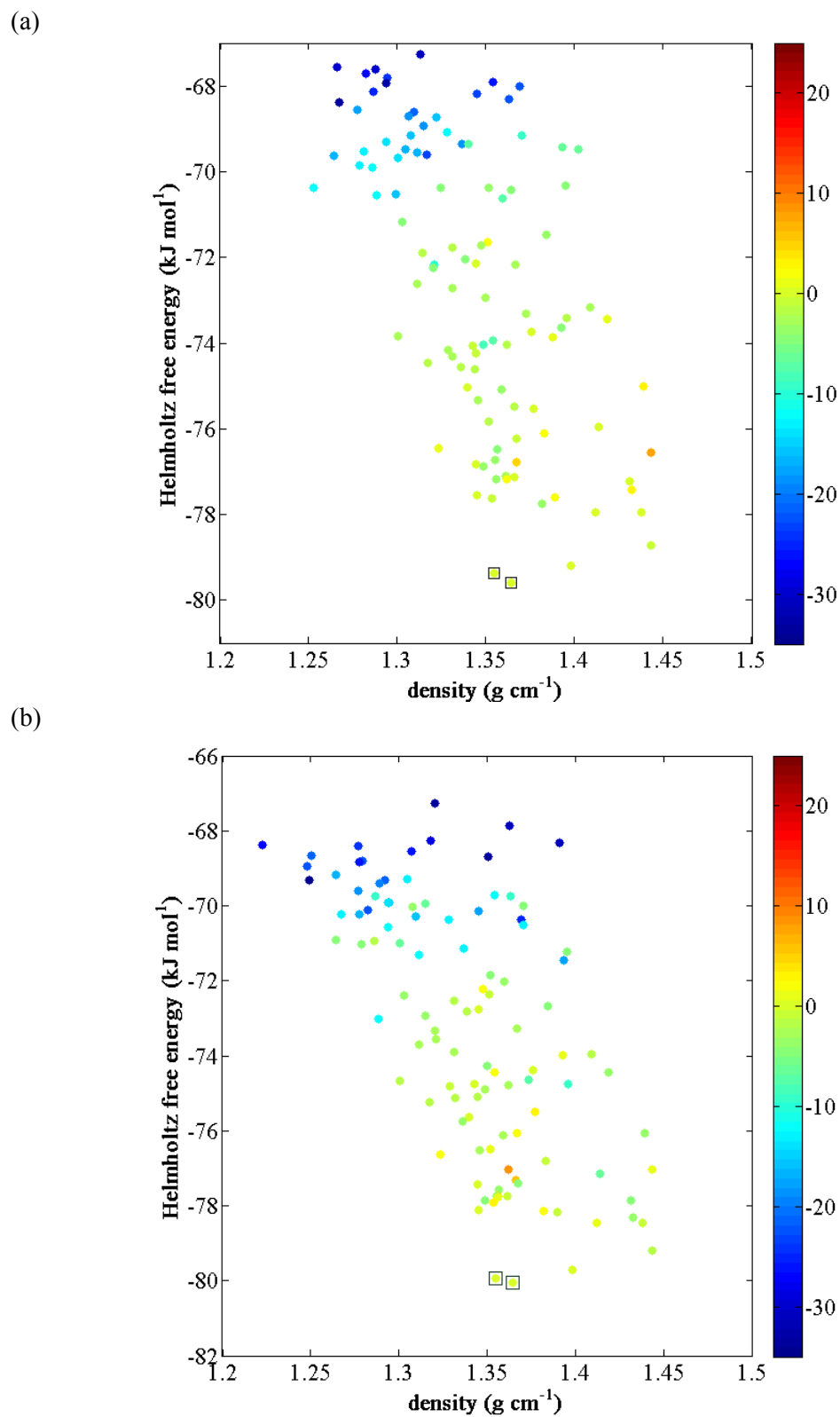


Figure 6-17 The Helmholtz free energy landscape of tetracyanoethylene at (a) 0 K ; (b) 50 K. All necessary quantum mechanical (charge density and geometry) calculations were performed at HF/6-31G(d,p) level. The colour scale describes the difference in the rank of each structure before and after the vibrational contributions are included.

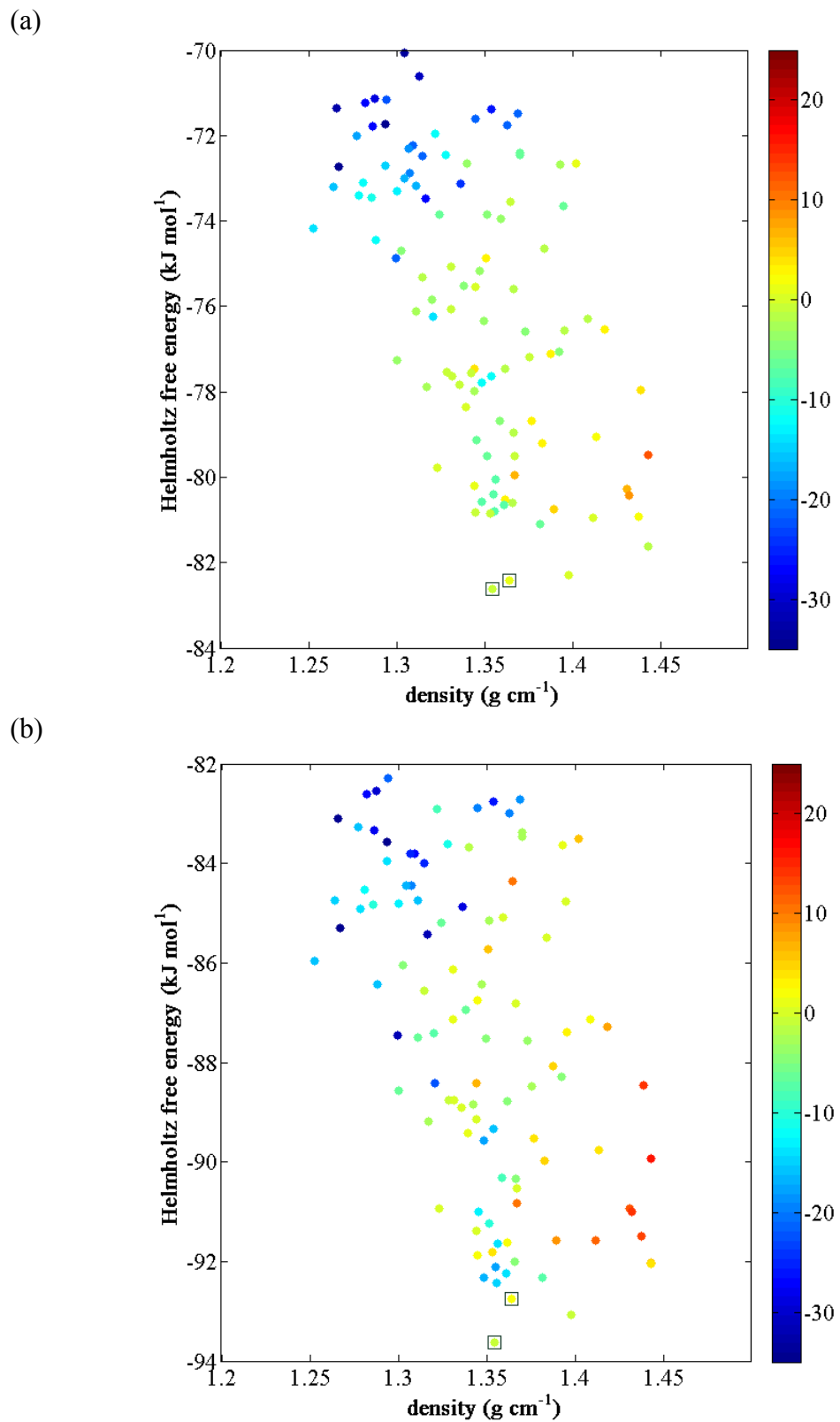
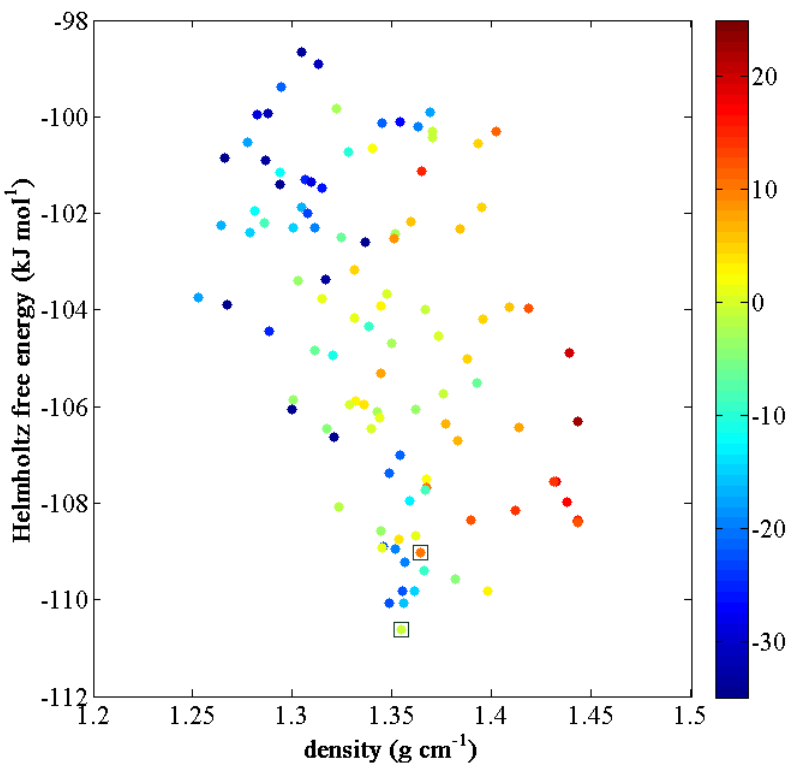


Figure 6-18 The Helmholtz free energy landscape of tetracyanoethylene at (a) 100 K ; (b) 200 K. All necessary quantum mechanical (charge density and geometry) calculations were performed at HF/6-31G(d,p) level. The colour scale describes the difference in the rank of each structure before and after the vibrational contributions are included.

(a)



(b)

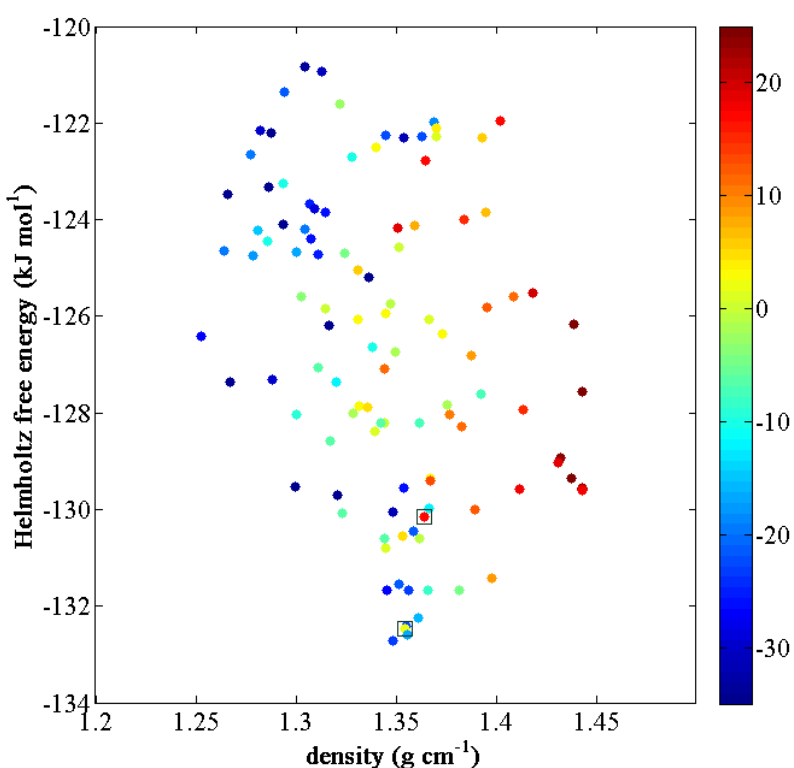


Figure 6-19 The Helmholtz free energy landscape of tetracyanoethylene at (a) 300 K ; (b) 400 K. All necessary quantum mechanical (charge density and geometry) calculations were performed at HF/6-31G(d,p) level. The colour scale describes the difference in the rank of each structure before and after the vibrational contributions are included.

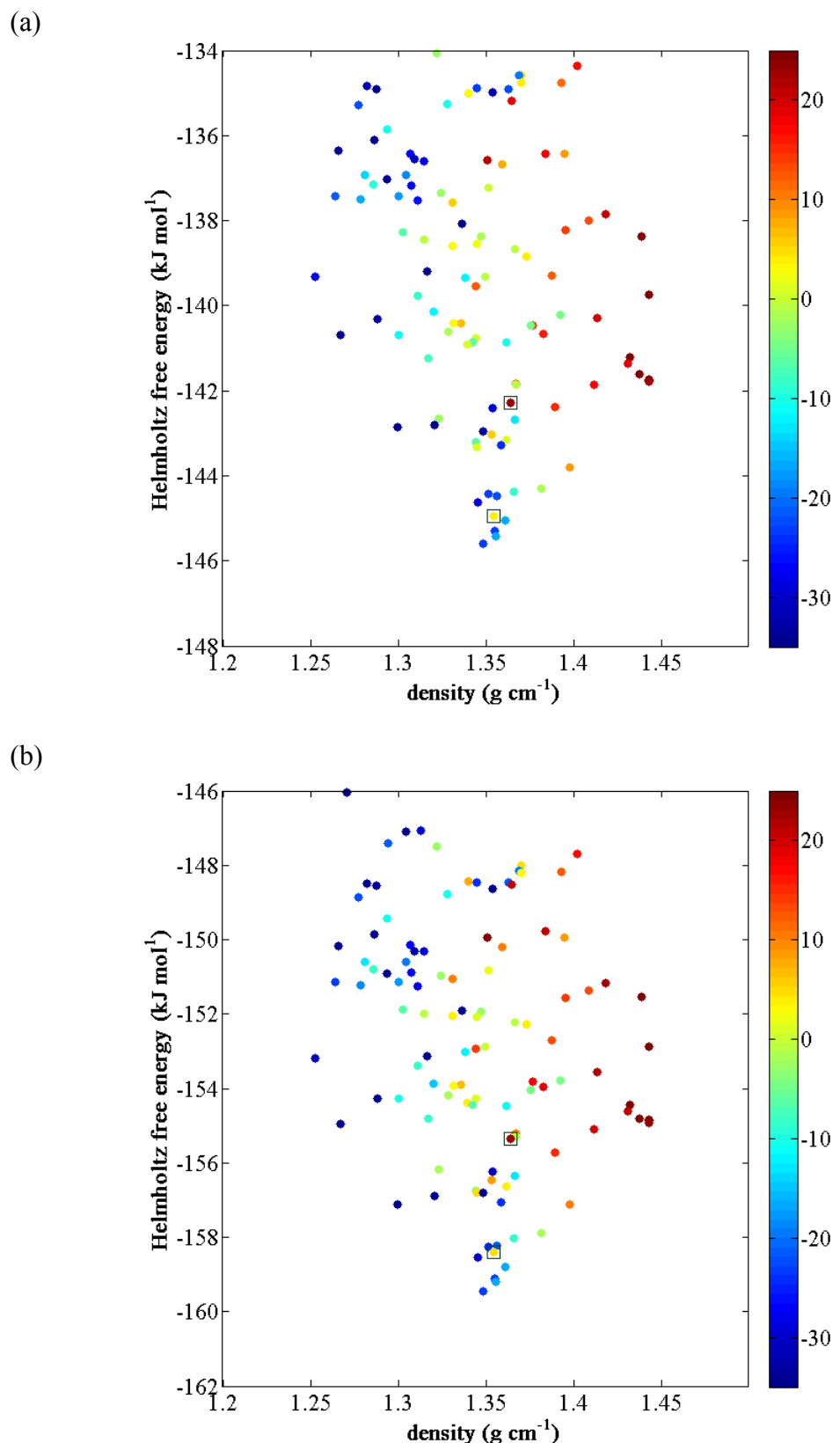


Figure 6-20 The Helmholtz free energy landscape of tetracyanoethylene at (a) 450 K (b) 500 K. All necessary quantum mechanical (charge density and geometry) calculations were performed at HF/6-31G(d,p) level. The colour scale describes the difference in the rank of each structure before and after the vibrational contributions are included.

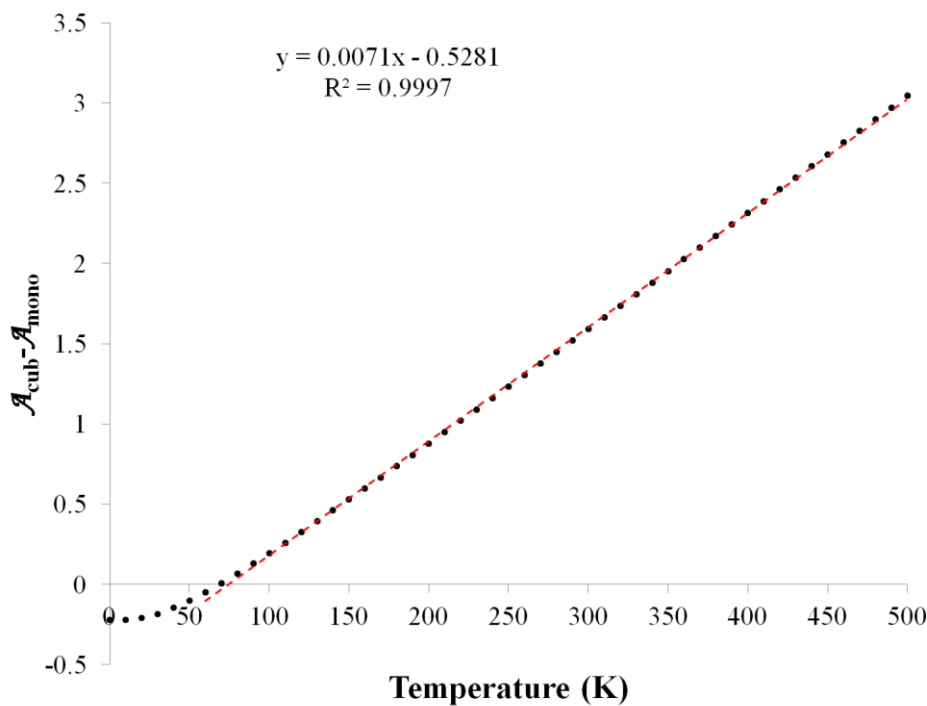


Figure 6-21 The free energy difference between the cubic and monoclinic forms of TCNE as function of temperature. The red dashed line is a linear interpolation of the free energy difference in the region of temperatures between 60K and the melting point. The transition temperature is obtained as the solution of the equation on the plot, setting y to 0.

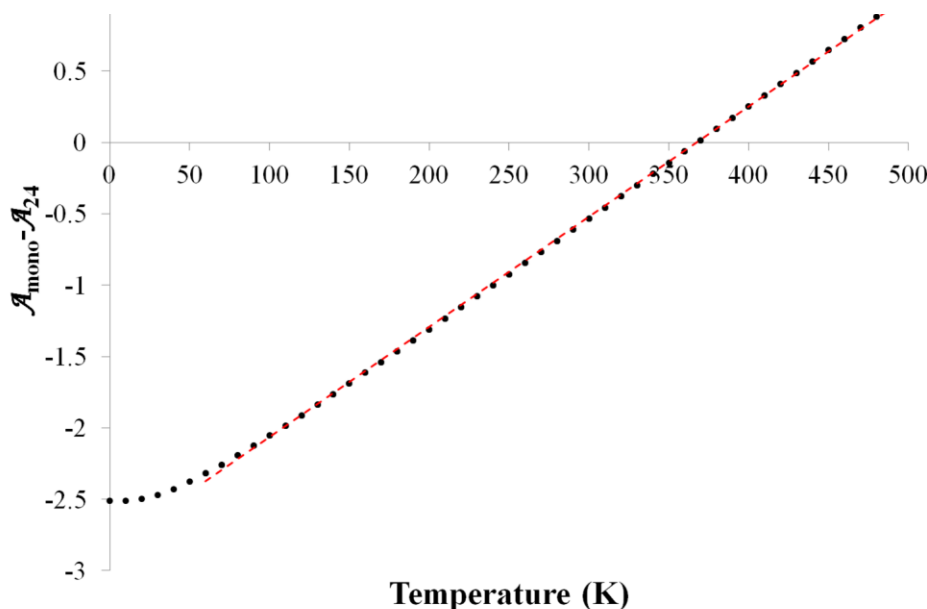


Figure 6-22 The free energy difference between the structure that corresponds to the monoclinic form and structure #24 as a function of temperature. The red dashed line is a linear interpolation of the free energy difference in the region of temperatures between 60K and the melting point. The transition temperature is obtained as solution of the equation on the plot setting y to 0.

6.4.5. The effect of the molecular model on the lattice energy calculation

In this section the effect of the choice of level of theory for the quantum mechanical calculations and on the free energy landscapes is investigated. Calculations are performed using the M06 functional with a 6-31G(d,p) basis set. In order to perform a free energy calculation under the harmonic approximation, it is necessary for the structure to be a minimum of the corresponding model. As a consequence each of the structures of the lattice energy landscape obtained during the search stage described in section 6.4.2 is minimised again with DMACRYS but the distributed multipoles and the geometry of the molecules in the gas phase are obtained at the M06/6-31G(d,p) level and the multipole moments to be used are derived again at the new level of theory. Following the minimization of 200 structures, 151 unique structures were obtained, 123 with $Z'=1$, 27 with $Z'=2$ and 1 with $Z'=8$.

The lattice energy landscape obtained is shown in Figure 6-24. The structure corresponding to the cubic form is ranked second while the monoclinic form corresponds to the 6th predicted structure. The cubic form structure is reproduced with an rms_{15} equal to 0.103Å, while the monoclinic form is predicted with an rms_{15} equal to 0.299Å. While the structure of the monoclinic form is reproduced with similar accuracy to the HF calculation, the reproduction of the structure of the cubic form is significantly worse, although still within acceptable limits. An overlay of the experimental and predicted structures is shown in Figure 6-23. The significantly better reproduction of the structure of the cubic polymorph and its stabilization with the HF level of theory may be due to the way in which the Buckingham potential parameters were derived. The parameters were fitted to reproduce a number of experimental azahydrocarbon structures using a model based on atomic point charges, where the atomic point charges had been fitted to reproduce the HF-derived electrostatic potential around the molecules (Williams & Cox, 1984). In addition, one of the structures to which the potential parameters were fitted is the cubic polymorph of TCNE. It can thus be expected that the cubic form of TCNE is best reproduced using HF. A comparison of the predicted unit cells of the monoclinic and cubic forms at the M06 and HF levels is found in Table 6-5.

The dispersion curves are once again calculated for the monoclinic form only. The full set of dispersion curves is shown in Figure 6-25. The external modes are

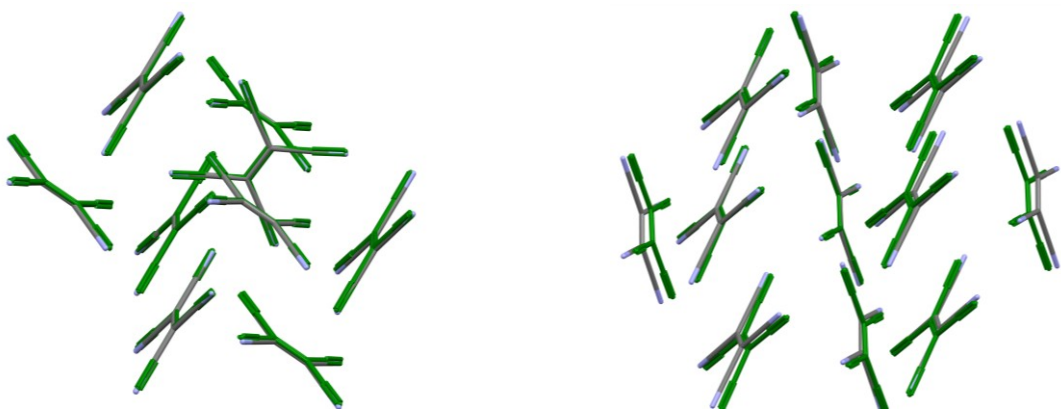


Figure 6-23 Overlay of the predicted and experimental forms of TCNE. a) the cubic form matches the experimental with an $\text{rms}_{15}=0.103\text{\AA}$, b) the predicted monoclinic form matches the experimental form with an $\text{rms}_{15}=0.299\text{\AA}$. Quantum mechanical calculations were performed at the M06/6-31G(d,p) level of theory.

compared with the experimental data (Chaplot et al., 1983). The comparison is shown in Figure 6-26 (the 8 lowest energy modes) and in Figure 6-27 (the remaining four modes). Qualitatively, the dispersion curves obtained are practically the same as those obtained using the HF level of theory. The absolute values of the frequencies are significantly different, however. For example the highest energy mode in the HF level

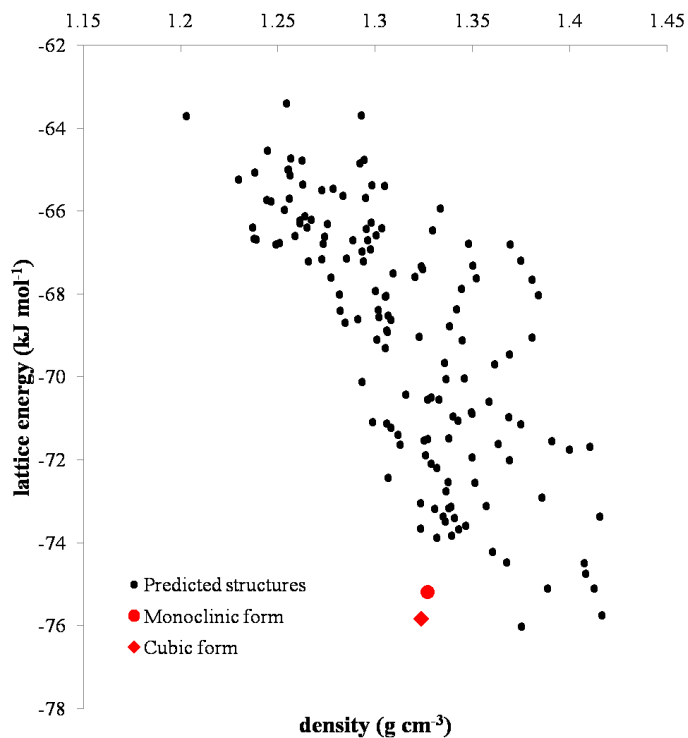


Figure 6-24 Final lattice energy landscape of TCNE. Red dot and diamond represent the monoclinic and cubic experimentally known forms. Quantum mechanical calculation were performed at M06/6-31G(d,p) level.

of theory has a frequency of 79.02 THz while at the M06 level of theory, the frequency obtained is 71.38 THz.

The comparison of the computed external modes of the monoclinic form with the available experimental results shows a deterioration in the agreement when moving to the M06 functional. This effect is more obvious for the lowest 4 modes. That can be attributed partly in the change of the level of theory for quantum mechanical calculations and the fact that the minimum obtained at the M06 level is not identical to the minimum obtained at the HF level.

The free energy landscape is again calculated in the same way it was calculated for the HF/6-31G(d,p) level (see section 6.4.4), again for the temperature range 0 K to 500 K. The landscapes for temperatures 0 K, 100 K, 200 K and 300 K are shown in Figure 6-28 and Figure 6-29. The general qualitative observations regarding the free energy landscapes at the HF level (see section 6.4.4) are equally applicable. The variation of the free energy and rank as a function of temperature for the two polymorphs and that of the global minimum are summarized in Table 6-6, and several differences are evident from this table.

In contrast to the calculations at the HF/6-31G(d,p) level of theory, the cubic form here is never predicted as the thermodynamically most stable structure. Furthermore, the cubic form is predicted to be less dense than the monoclinic form when using the M06 functional, in contrast to the experimental result. For a wide range of temperatures (up to approximately 100 K) it remains one of the most stable structures and is ranked within the 5 lowest free energy structures. The most stable structure in the low temperature range corresponds to the third-ranked structure on the HF lattice energy landscape (with an $\text{rms}_{15}=0.105\text{\AA}$), and is hereafter referred to as S_3^{HF} . The transition from this postulated structure to the monoclinic form occurs at

Form	Space group	QM level	Z	a (Å)	b (Å)	c (Å)	β (°)	γ (°)	ρ (g cm⁻³)
Cubic	$R\bar{3}$	HF	18	13.82	13.82	16.94	90	120	1.364
	$R\bar{3}$	M06	18	13.97	13.97	17.11			1.324
Monoclinic	$P2_1$	HF	2	6.74	6.00	7.86	80.87	90	1.355
	$P2_1$	M06	2	6.76	6.05	7.95	80.83		1.326

Table 6-5 Comparison of the unit cells of the two predicted forms of TCNE at M06 and HF level of theory. Lattice angle α is equal to 90° for all forms because of symmetry constraints.

163 K, while the cubic form becomes less stable than the monoclinic form at a temperature of 79.5K, which is very close to the value we calculated using the HF level. Finally, in the region between 276 K and the melting point, another structure is stabilized over the monoclinic form. It is the same structure as S_{24}^{HF} that was predicted to be stable at high temperatures at the HF level of theory (within $\text{rms}_{15}=0.066\text{\AA}$). The transition temperatures reported here are determined by linear interpolation, in the same way as in section 6.4.4.

The results obtained using this level of theory are to a large extent different from the results obtained using the HF level of theory revealing, as expected, the large degree of dependence of the final result on the chosen computational model. The choice of functional for the DFT calculations has a pronounced effect on the relative lattice energy and free energy of the structures. On the other hand the actual structures obtained are much less sensitive on this choice. Calculations using both functionals reveal a polymorphic landscape that is dense in structures separated by very small lattice energy and free energy differences. Although the existence of the high pressure form cannot be verified by these calculations (performed at 0 atm), the results are consistent with the puzzling experimental evidence suggesting that at least one more polymorph may exist. The overall better performance of the HF level of theory may be due to the fact that a description of the electrostatic potential at this level of theory was used for the parameterization of the Buckingham potential.

T (K)	Cubic Form		Monoclinic Form		Global minimum
	\mathcal{A} (kJ mol ⁻¹)	Rank	\mathcal{A} (kJ mol ⁻¹)	Rank	\mathcal{A} (kJ mol ⁻¹)
0	-71.87	3	-71.62	6	-72.11
50	-72.39	3	-72.26	5	-72.68
100	-75.06	4	-75.21	2	-75.45
200	-86.28	10	-87.07	1	-87.07 (Monoclinic)
300	-103.70	18	-105.16	4	-110.62
400	-126.15	24	-128.28	8	-132.71
450	-138.99	26	-141.46	10	-145.61
500	-152.80	30	-155.62	10	-159.45
\bar{U}	-75.84	2	-75.19	6	-75.17

Table 6-6 The Helmholtz free energy \mathcal{A} and rank of the cubic and monoclinic forms of TCNE, as function of temperature T . The value of the global minimum free energy is presented in the last column for comparison. In the bottom, the lattice energy \bar{U} and rank of the relevant structures are also presented. Quantum mechanical calculations were performed at the M06/6-31G(d,p) level.

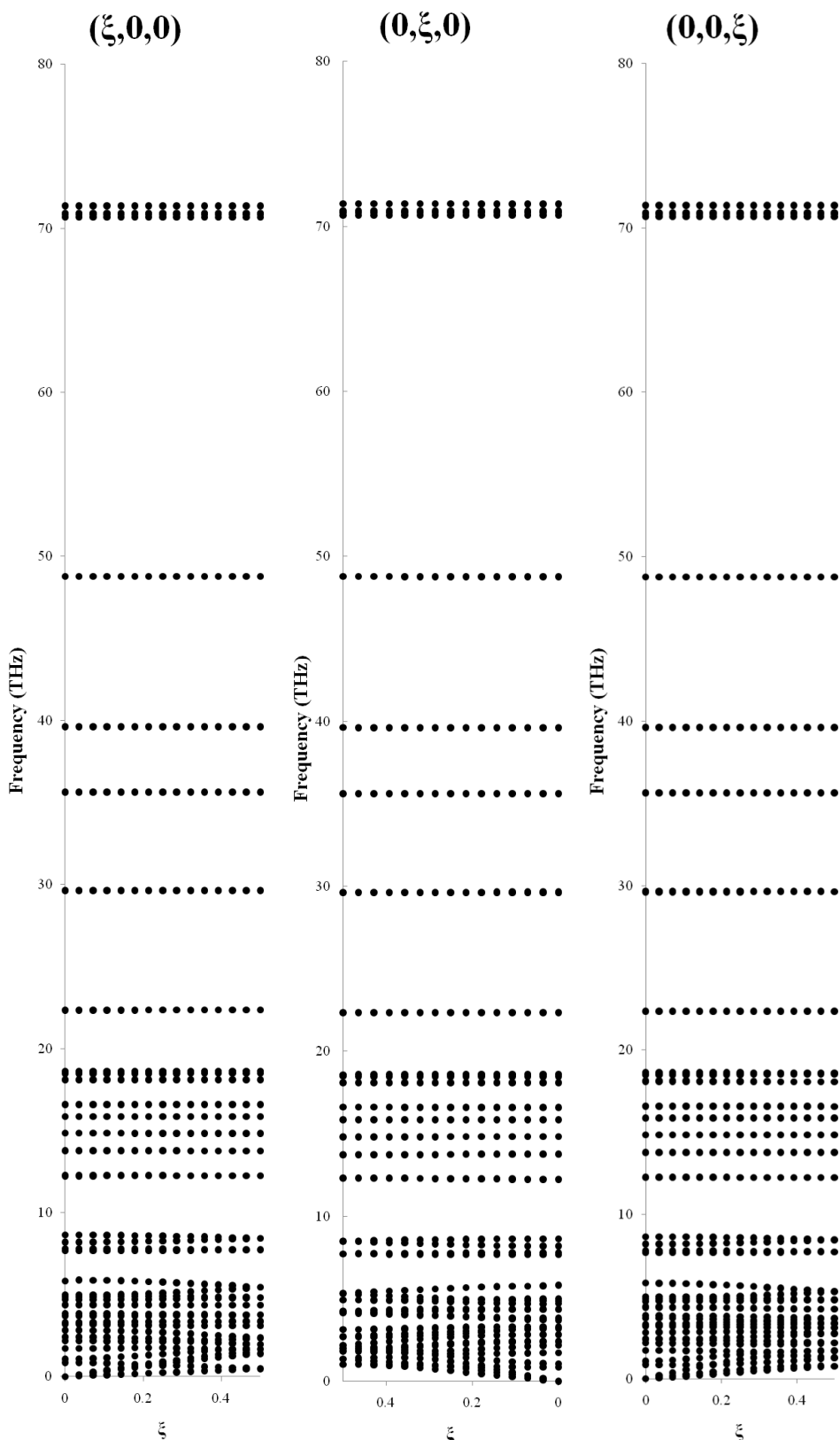


Figure 6-25 Dispersion curves of TCNE. The 12 lowest energy branches represent the external modes of vibration while the remaining branches represent the internal modes. Quantum mechanical calculations were performed at the M06/6-31G(d,p) level of theory.

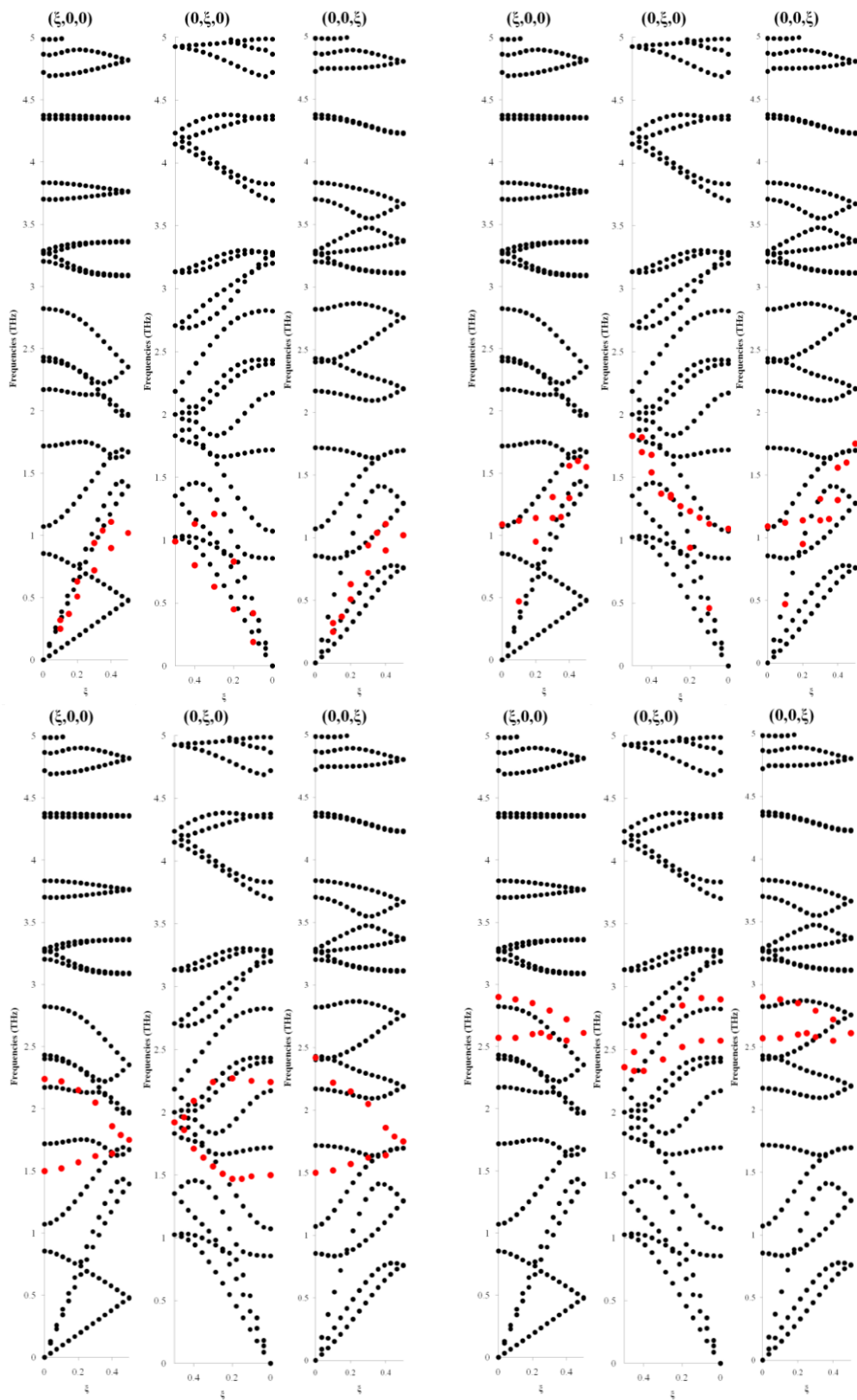


Figure 6-26 Comparison of the 8 experimentally determined lowest frequency modes of vibration of TCNE (in red) with the corresponding calculated modes (in black). The wave vector varies along directions $(\xi, 0, 0)$, $(0, \xi, 0)$ and $(0, 0, \xi)$. Calculations were carried out at the M06/6-31G(d,p) level of theory.

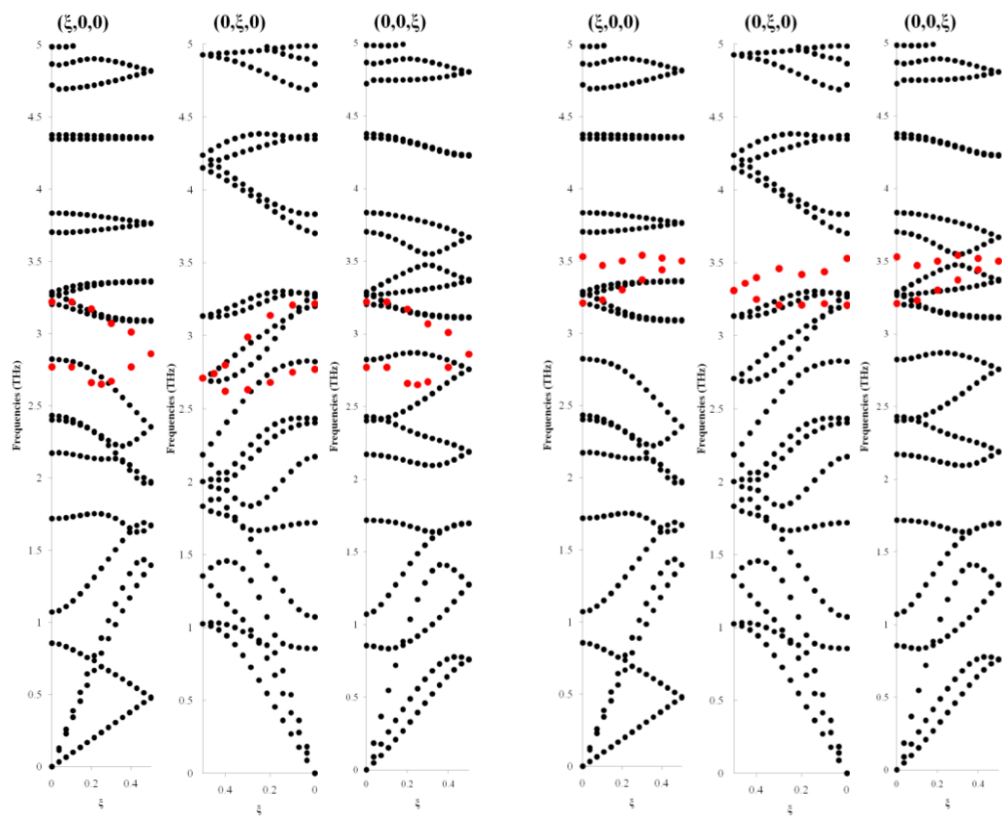


Figure 6-27 Comparison of the 4 experimentally determined highest frequency external modes of vibration of TCNE (in red) with the corresponding calculated modes (in black). The wave vector varies along directions $(\xi, 0, 0)$, $(0, \xi, 0)$ and $(0, 0, \xi)$. Calculations were carried out at the M06/6-31G(d,p) level of theory.

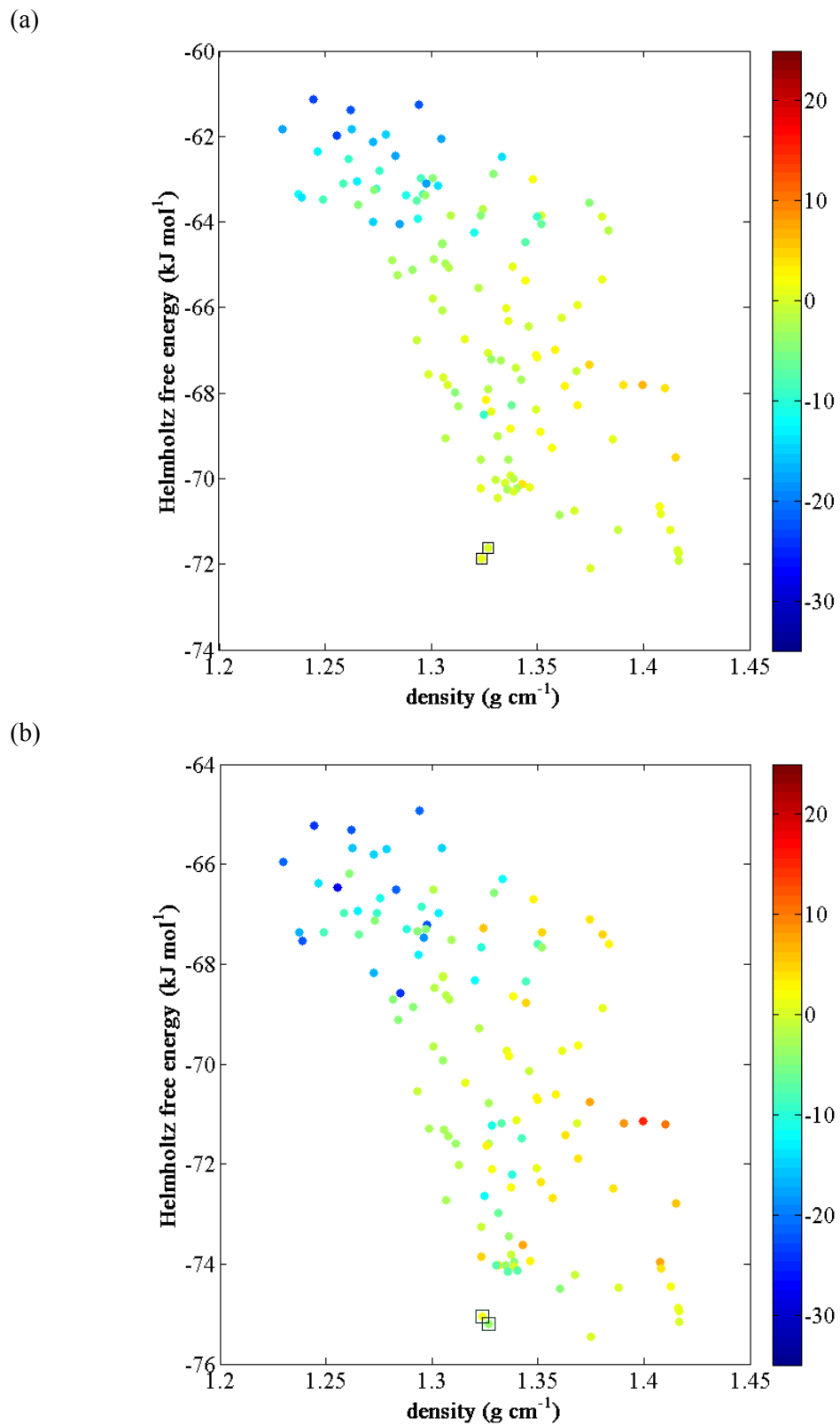


Figure 6-28 The Helmholtz free energy landscape of tetracyanoethylene at (a) 0 K ; (b) 100 K. All necessary quantum mechanical (charge density and geometry) calculations were performed at M06/6-31G(d,p) level. The colour scale describes the difference in the rank of each structure before and after the vibrational contributions are included.

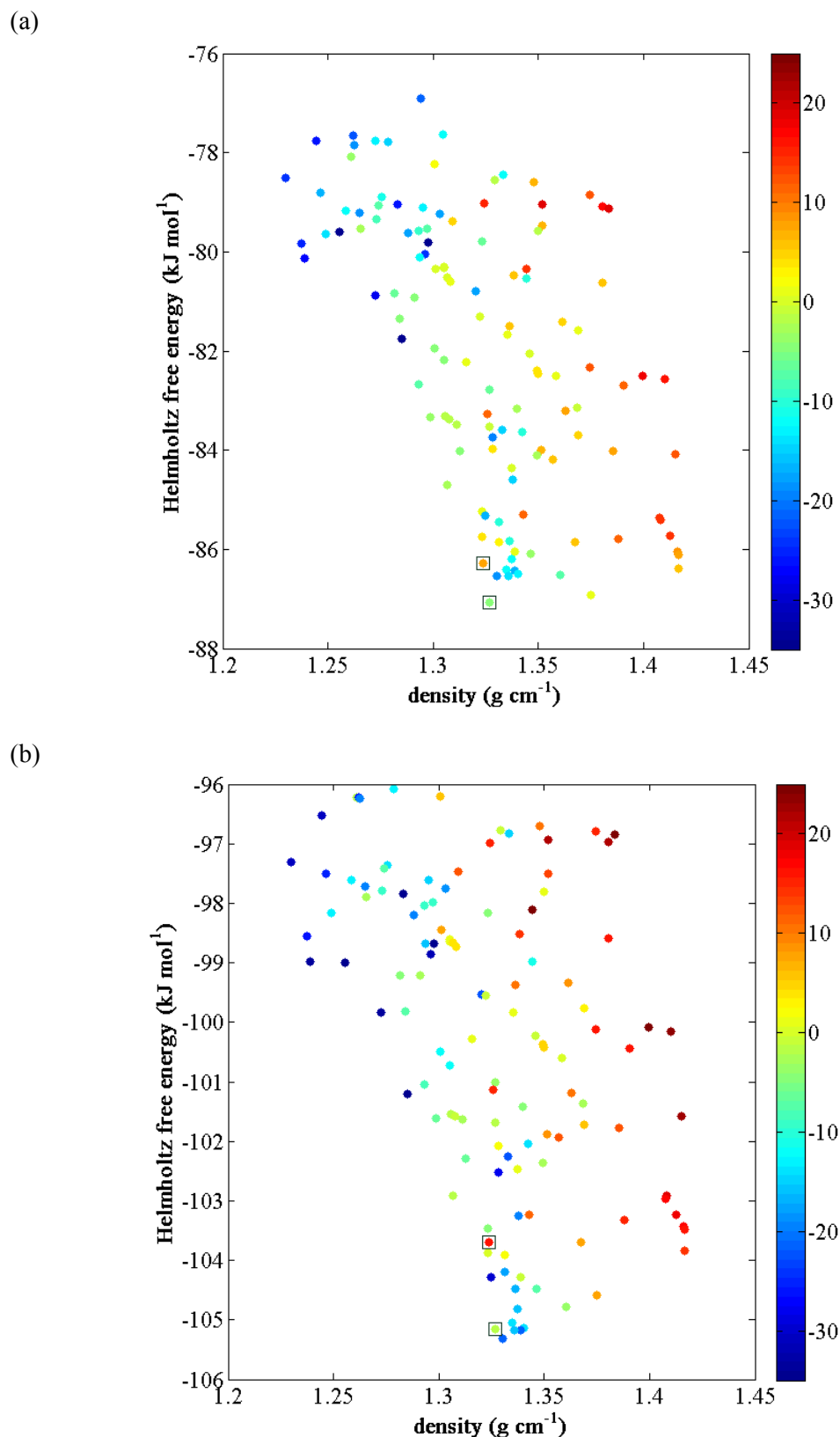


Figure 6-29 The Helmholtz free energy landscape of tetracyanoethylene at (a) 200 K ; (b) 300 K. All necessary quantum mechanical (charge density and geometry) calculations were performed at M06/6-31G(d,p) level. The colour scale describes the difference in the rank of each structure before and after the vibration contributions are included.

6.5. Quasi-harmonic free energy minimisation; Argon example revisited

In order to investigate the effect of temperature on the structure of the argon fcc crystal, free energy minimization is performed within the quasi-harmonic approximation, as described in section 3.8. The necessary integrals for the calculation of the vibrational part of the Helmholtz free energy (equation 3-33) and the free energy gradient (equation 3-49) are calculated using the Gauss-Legendre quadrature (subsection 3.7) by sampling 512 wave vectors (8 points for each direction).

The quasi-harmonic approximation is found to provide an accurate estimate of the effect of temperature on the structure of argon. In Figure 6-30 the lattice constant of the face centred cubic unit cell α_{fcc} of argon is plotted as function of temperature. This quantity is related to the lattice length of the primitive unit cell α_p which is obtained by the minimization via the relation:

$$\alpha_{\text{fcc}} = \sqrt{2}\alpha_p \quad (6-1)$$

The lattice constant α_{fcc} compares very well with the experimental values (Berrett & Jones, 1964; Dobbs et al., 1956; Dobbs & Jones, 1957; Peterson et al., 1966) up to 50 K and the error is satisfactorily low for 15 to 20 K beyond this temperature. This corresponds to a temperature range that is more than half the melting point. A similar behavior is observed for the coefficient of thermal expansion α_v :

$$\alpha_v\% = \frac{\alpha_{\text{fcc}}(T) - \alpha_{\text{fcc}}(0)}{\alpha_{\text{fcc}}(0)} \cdot 100 \quad (6-2)$$

The coefficient α_v is shown in Figure 6-31. For the thermal expansion coefficient there are one set of experimental data (Peterson et al., 1966). For comparison reasons equation (6-2) is used to convert the experimentally available lattice constants presented in Figure 6-30 to the coefficient $\alpha_v\%$. For that conversion the value for $\alpha_{\text{fcc}}(0)$ accepted by each author was used. Good agreement is observed at low temperatures, and the computational model tends to overestimate the extent of the variation. It is reasonable to expect that an adjustment of the Lennard-Jones potential

parameters would allow an even better representation of the temperature dependence of the geometry of the lattice.

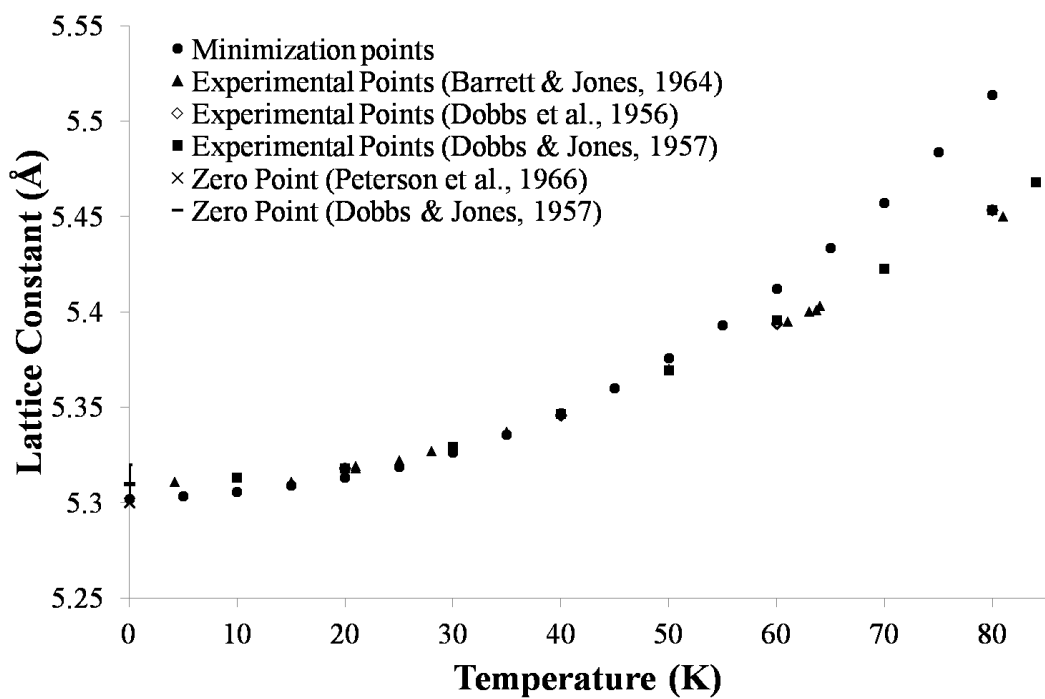


Figure 6-30 The lattice constant of argon as function of temperature.

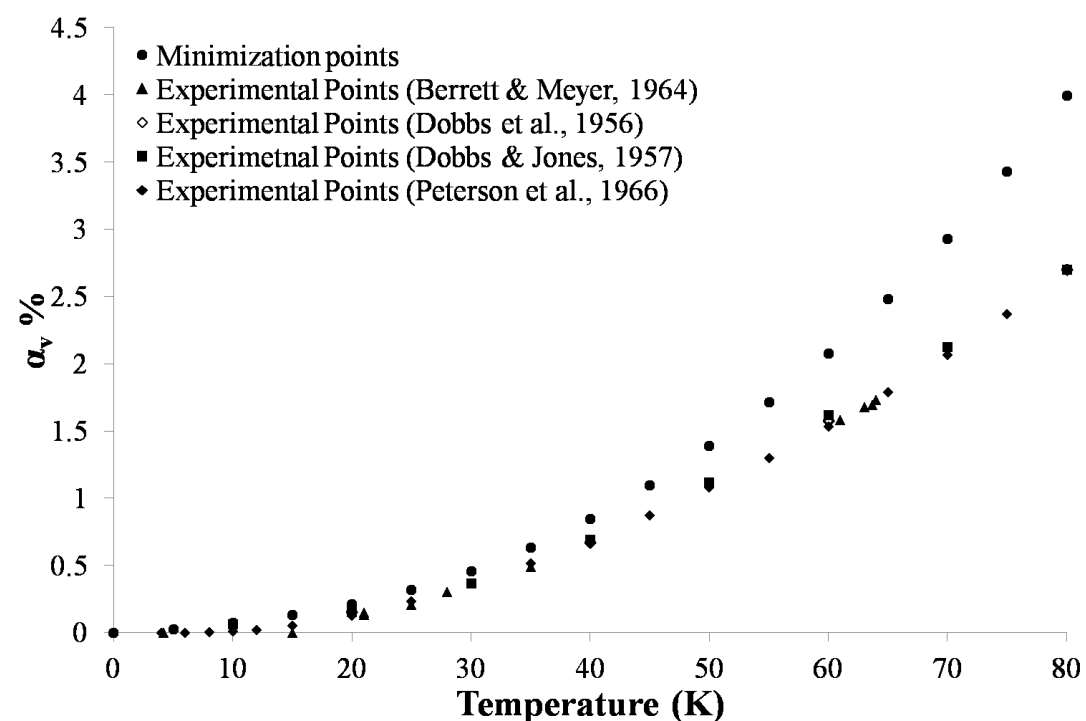


Figure 6-31 The thermal expansion coefficient of argon as function of temperature.

7. Conclusion and Perspectives

7.1. Summary

A method for the incorporation of temperature effects in crystal structure prediction has been described. The interaction potential of the crystal is approximated via a Taylor series expansion truncated at second order. The approximate potential allows the analytical solution of Newton's equations of motion, in the general form of a harmonic plane wave. The indeterminate parameters of the harmonic wave equation i.e. the frequency of atomic vibrations, and the amplitude of the wave can be obtained as eigenvalues and eigenvectors of the dynamical matrix. The eigenvalues and eigenvectors are obtained by diagonalization of the dynamical matrix. In this way the problem of solving Newton's equations of motion is reformulated as an eigenvalue problem. This method, known as the harmonic approximation in lattice dynamics, has been widely used in the literature, but has not yet found widespread use in crystal structure prediction.

Once the frequencies of vibration of the atoms within the crystal have been obtained, the energy states of the crystal can be calculated by using the equations for the energy states of the quantum harmonic oscillator. An analytical expression for the total canonical partition function of the crystal can then be formulated. The canonical partition function is then used within the framework of statistical mechanics in order to derive an analytical expression for the Helmholtz free energy of the crystal. In a similar way, the isothermal-isobaric ensemble partition function can also be constructed and the Gibbs free energy can be obtained. Under the widely used assumption of an infinite periodic crystal, the resulting free energy expressions take an integral form. The efficient evaluation of this integral plays a decisive role in

determining the computational cost of the method. The main obstacle to overcome then is the non-trivial task of calculating the dynamical matrix.

The formalism of the harmonic approximation is applicable to any choice of computational model. Long experience has shown that an accurate representation of the crystalline solid state requires very detailed models. The intra-molecular interactions are typically modeled using *ab-initio* methods. In order to manage the computational cost of the structure search in a crystal prediction study, such calculations are often performed for isolated molecules, ignoring the effects of the crystalline environment. The electrostatic interactions between the molecules are calculated using multipole expansions truncated at the fourth order. Atomic multipole moments up to hexadecapole are derived based on the *ab-initio* derived wave function, by means of a distributed multipole analysis. In such a way, the applicability of the method is not restricted by the requirement of experimental data, and high accuracy is maintained. Finally the repulsion and dispersion interactions are modelled using the semi-empirical Buckingham potential together with transferable sets of parameters that are available in the literature for the atoms that are most commonly found in organic compounds. A detailed description of the molecular models used was presented in Chapter 4 and a major part of the work was dedicated to the challenge of calculating the dynamical matrix when using such models.

A major implication of the assumption of an infinite periodic crystal on the dynamical matrix calculations is that the lattice sums (i.e. the sums over all unit cells of the crystal) that appear in the calculations are infinite series. When these series exhibit good convergence properties, such as in the case of the repulsion interactions, the evaluation of lattice sums is trivial. On the other hand, the infinite series associated with the electrostatic interactions are not only poorly convergent but also in some cases converge under conditions. A method for the efficient calculation of the electrostatic contribution to the lattice energy and the dynamical matrix was developed in Chapter 5, based on a generalization of the method of Ewald.

The method of harmonic approximation was tested for three compounds, starting with crystalline argon. The crystal was modeled using a Lennard-Jones potential with parameters from the literature. The structure of the crystal is known to be face-centred cubic, and calculations were performed for the primitive unit cell of the fcc crystal. The primitive unit cell contains only one atom, and the lattice angles are known to be 60°. The lattice lengths are equal, and they were determined via lattice energy

minimization. Dispersion curves were calculated and found to be in excellent agreement with the experimentally-determined curves at 5 K. The density of vibrational states was also calculated based on one million randomly sampled wave vectors. It was found to be in qualitative agreement with other calculated density of states. The low frequency region (<0.5THZ) of the density of states is found to have a quadratic form in line with Debye's theory.

To assess the potential for the integration of free energy calculations based on the harmonic approximation in a crystal structure prediction study, the free energy of computationally-generated crystal structures was calculated at temperatures from absolute zero to the melting point for two molecules. An *ab-initio* crystal structure prediction methodology based on the *CrystalPredictor* and DMACRYS algorithms was applied to imidazole and tetracyanoethylene. Both polymorphs of imidazole were identified as lattice energy minima. The stable α -form was found as the global minimum while the β -form, which is unstable at ambient pressure, was found a few kJ mol⁻¹ higher in lattice energy. The free energy was calculated under the harmonic approximation from 0 K to the melting point using the 64-node Gauss-Legendre quadrature method for the evaluation of the free energy integrals. The α -form was found to remain the global minimum for the whole range of temperatures, while the free energy difference between the β -form and the global minimum increased as function of temperature. The calculations were performed using M06/6-31G(d,p) and HF/6-31G(d,p) level for all the necessary quantum mechanical calculations (intra-molecular interactions, conformation and charge density). The results obtained are similar for both *ab-initio* levels of theory and in good agreement with experimental data.

Similar calculations were carried out for tetracyanoethylene. TCNE is known to form four crystals, and structural information is available for two of these: the monoclinic polymorph and the cubic polymorph. Both of these crystals were predicted as minima of the lattice energy hypersurface (at the HF/6-31G(d,p) and M06/6-31G(d,p) levels of theory for the quantum mechanical calculations). With the HF functional, the cubic form was found to be the global minimum, while the second lowest energy minimum was found to correspond to the monoclinic form. There was a small energy difference between these two structures. Dispersion curves were calculated for the monoclinic form, for which experimental data are available. The calculated dispersion curves compare very well qualitatively with the experimental

data. The quantitative differences between the experimentally-determined and calculated dispersion curves were found to be satisfactorily low. The free energy calculations indicate that a polymorphic phase transition from the cubic to the monoclinic form occurs at 74 K. As the temperature was further increased the structure that corresponds to the 24th lowest lattice energy minimum became stable. The transition occurred at 368 K and the structure remained the most stable until the melting point. This result is in qualitative agreement with the experimental evidence, although there is some uncertainty about the transition temperature.

The effect of the choice of quantum mechanical model was also investigated for TCNE. In contrast to imidazole, when calculations were performed using the M06/6-31G(d,p) level of theory the final result was significantly different from the HF calculations. Although the shape of the dispersion curve remains the same, quantitatively, the agreement with experimental data deteriorates slightly. In the free energy landscapes the cubic form was not found to be the most stable at any temperature. The structure that was found to be the global minimum of the lattice energy landscape, S_3^{HF} , remains the most stable up to 163 K, at which temperature the monoclinic form becomes the most stable. Finally at 276 K the same structure that was found to be the most stable at high temperatures in the HF/6-31G(d,p) free energy landscapes, becomes the most stable. The cubic form was found to be a low-energy form, more stable at 0 K than the monoclinic form, but becoming less stable at 79.5 K.

Finally the effect of temperature on the structure of the Ar crystal was investigated within the quasi-harmonic approximation. The free energy of the crystal was minimized within the quasi-harmonic approximation. The necessary integrals for the free energy and its gradient were calculated using a 512-node Gauss-Legendre quadrature. The free energy was minimized from 0 K to 80 K, very close to the melting point of Ar, which is 84 K. The calculated lattice constant is found to be in excellent agreement with the experimental constant up to 60K. The thermal expansion coefficient is exactly the same as the experimental for low temperatures and in very good agreement in the medium temperature range (30 K to 50 K). When the temperature increases further the calculations deviate from experimental results.

The results in the studies of imidazole and TCNE suggest that vibrational contributions to the free energy in principle cannot be neglected, especially in cases such as TCNE. The effect of temperature on the various landscapes is profound.

Many structures are eliminated as unstable and extensive rearrangement of the structures can be achieved. Even if the effect of temperature were overestimated under the harmonic approximation, the small energetic differences among the putative structures indicate that entropic contributions cannot be ignored. The harmonic approximation is thus an excellent first estimate of the effect that temperature may have on putative crystal structures, especially in the low temperature region. Its relatively small computational cost allows the evaluation of the free energy of a large number of structures that are described with detailed but computationally-expensive models. This approach can be applied as a post-processing stage, following a crystal structure prediction based on already available lattice energy-based algorithms. The success of the harmonic approximation in the example of Ar, where an accurate and widely tested model is used, and other reports that are found in the literature (Falter et al., 1999; Day et al., 2003; Natkanienc et al, 1980; Righini et al., 1980) suggest that the errors that are observed in the other examples, e.g., in the calculation of dispersion curves of TCNE, can to a large extent be attributed to the assumptions in the chosen model, and secondarily, to an-harmonic effects. This is in accordance with the finding that the choice of level of theory has a large effect on the calculations for TCNE. The example of the minimisation of the free energy of Ar under the quasi-harmonic approximation is an encouraging start for a more comprehensive approach to modeling temperature effects on the structure of predicted crystals.

7.2. Future work

Lattice dynamics under the harmonic approximation has been shown to be a promising method for the estimation of the effect of temperature on putative crystal structures. The work presented in this thesis can be the starting point for many other advances. A few possible avenues of research are presented in this section.

Issues associated with the computational cost of the method were not addressed in the thesis. The computations reported here are of the order of one hour per structure on a single processor (usually an Intel Xeon 5150 2.66GHz). The CPU time consumed can be significantly reduced in one of many ways. A parallel implementation of the integration algorithm that is used to evaluate the free energy expression is a natural step that would significantly reduce the computational cost. Furthermore the symmetry properties of the crystal impose constraints that allow

much faster evaluation of the dynamical matrix since it is necessary to calculate only a portion of the complete matrix. The current implementation does not take symmetry effects into account. Apart from the computational cost associated with the actual calculation of the dynamical matrix, this would also reduce the time spent on the evaluation of the second derivatives of lattice energy. An optimization of the relative computational cost between the direct space sum and the reciprocal sum by means of the choice of the Ewald convergence parameter can also be carried out. The computational cost of the evaluation lattice sums can also be reduced by a factorization of the orientation dependence of distributed multipoles as described by Leslie (2008). Although in principle not necessary, it is worth investigating the possible computational cost savings when evaluating the dispersion contribution in an Ewald-type manner, as has been done by other authors (in't Veld et al., 2007; Isele-Holder et al., 2012)

The reduced computational cost would allow the use more accurate and detailed models. The effect that the assumption that atomic vibrations have a negligible effect on the charge density (described in section 4.4.3) is worth investigating. Adding more terms in the multipole expansion may also facilitate the determination of the correct relative stability in cases where many predicted crystals are separated by small, almost indistinguishable, energy and free energy differences. More accurate repulsion/dispersion potential parameters can also be obtained by fitting to experimental data for the vibrations in the crystal, e.g., IR spectra. One must also bear in mind that these parameters were obtained using a specific level of theory, atomic point charges, and without accounting for any entropic contributions. Thus, the derivation of a revised set of parameters, taking into account the use of different levels of theory, more detailed electrostatics, and entropic contributions, may yield improved agreement with experimental data.

Harmonic free energy calculations were performed for the hypothetical and experimental crystal structures of two small rigid molecules, imidazole and tetracyanoethylene. It is necessary to further validate and investigate the method on other examples. Comparison with other available dispersion curves would allow a broader understanding of the capabilities and limitations of the method. The estimation of the effect of temperature on the computationally generated polymorphic landscapes of other molecules is also necessary for further assessment of the harmonic approximation. The method can also be extended to other classes of systems that are

of interest, such as co-crystals, hydrates, and salts. The method also needs to be tested on molecules of varying size and flexibility.

The structure of the fcc Ar crystal as function of temperature was determined with satisfactory accuracy up to half the melting point by free energy minimisation using the quasi-harmonic approximation. This encouraging result suggests that it is worth extending the method to organic molecular crystals modeled as described in chapter 4. This can first be done within a rigid-molecule minimization algorithm. In this way the effect of temperature on the various predicted structures would also be estimated, in addition to its effect on their relative stability, as obtained within the harmonic approximation.

In the second chapter a number of methods were discussed in which the harmonic crystal was used as a reference state for the calculation of free energy differences in which anharmonic effects are also included. The calculations presented in this thesis are an excellent basis for calculation of free energy differences using methods such as the method of Tan et al. (2010) or the method of Hoover et al. (1970).

Although the methodology presented here does not provide a complete account of the effect of temperature on crystals, it is a step towards a better understanding of the organic solid state and brings us closer to the overall objective of determining *ab initio* the phase diagram of organic compounds.

Conference presentations & publication

M. Vasileiadis, C.S. Adjiman, & C.C. Pantelides, “Ab initio prediction of crystal structure and the effect of temperature on the relative stability of enantiotropic polymorphs”, AIChE annual meeting, San Francisco, USA, November 2013 - (talk)

M. Vasileiadis, C.S. Adjiman, & C.C. Pantelides, “Temperature effects in crystal structure prediction”, PPEPPD, Iguazu Falls, Argentina, May 2013 - (talk)

M. Vasileiadis, P.G. Karamertzanis, C.S. Adjiman, & C.C. Pantelides, “Computation of entropic effects in crystal structures”, AIChE annual meeting, Pittsburgh, USA, October/November 2012 - (talk)

M. Vasileiadis, P.G. Karamertzanis, C.S. Adjiman, & C.C. Pantelides, “Computation of entropic effects in crystal structures”, 5th FOMMS, Mt. Hood, Oregon, USA, July 2012 - (poster)

M. Vasileiadis, A.V. Kazantsev, P.G. Karamertzanis, O. Lyngverg, C.S. Adjiman, & C.C. Pantelides, “*Ab initio* crystal structure prediction; Methodology & applications to flexible molecules”, 6th CF@Bo, Bologna, Italy, January 2012 - (poster)

M. Vasileiadis, A.V. Kazantsev, P.G. Karamertzanis, C.S. Adjiman, & C.C. Pantelides, “The polymorphs of ROY: Application of crystal structure prediction techniques”, AIChE annual meeting, Minneapolis, USA, October 2011 - (talk)

M. Vasileiadis, P.G. Karamertzanis, C.S. Adjiman, & C.C. Pantelides, “Towards lattice dynamics in crystal structure prediction”, Thermodynamics conference, Athens, Greece, September 2011 - (short oral presentation/poster)

M. Vasileiadis, A.V. Kazantsev, P.G. Karamertzanis, C.S. Adjiman, & C.C. Pantelides, “Polymorph prediction of a challenging molecule”, CAPE Forum, Bradford, UK, March 2011 - (talk)

M. Vasileiadis, E. Siougkrou, D.N. Theodorou, “MC simulation of a polyethylene melt: Prediction of volumetric properties under negative pressure. Local density-cavitation.”, Thermodynamics conference, London, United Kingdom, September 2009 - (poster)

M. Vasileiadis, A.V. Kazantsev, P.G. Karamertzanis, C.S. Adjiman & C.C. Pantelides, "The polymorphs of ROY: application of a systematic crystal structure prediction technique", *Acta Cryst.*, B68, (2012), 677-685

8. Bibliography

- Abraha A., & Williams D.E., "Spherical and aspherical intermolecular force fields for sulphur allotropes", Inorg. Chem., 38, 19, (1999), 4224-4228
- Abramowitz M., & Stegun I.A., "Handbook of mathematical functions with formulas, graphs, and mathematical tables", Dover Publications, New York, 1972
- Aguado A., & Madden P. A., "Ewald summation of electrostatic multipole interactions up to the quadrupolar level", J. Chem. Phys., 119, 14, (2003), 7471-7482
- Allen M.P., & Tildesley D.J., "Computer simulation of liquids", Clarendon Press, Oxford, (1987)
- Aung S., & Strauss H.L., "Lattice sum transformations and potential function expansions in lattice dynamics", J. Chem. Phys., 58, 7, (1973), 2737-2745
- Avendaño C., & Gil-Villegas A., "Monte Carlo simulations of primitive models for ionic systems using the Wolf method", Molecular Physics, 104, 9, (2006), 1475-1486
- Baele P.D., "Acoustic crystal thermodynamic integration method", Phys. Rev. E., 66, (2002), 036132
- Báez L.A., & Clancy P., "Calculation of free energy for molecular crystals by thermodynamic integration", Molecular Physics, 86, 3, (1995:a), 385-396
- Báez L.A., & Clancy P., "Phase equilibria in extended simple point charge ice-water systems", J. Chem. Phys., 103, 22, (1995:b), 9744-9755
- Bansil A., "Special directions in the Brillouin zone", Solid State Communications, 16, (1975), 885-889
- Bardwell D.A., Adjiman C.S., Arnaudova Y.A., Bartashevich E., Boerrigter S.X.M., Braun D.E., Cruz-Cabeza A.J., Day G.M., Della Valle R.G., Desiraju G.R., van Eijk B.P., Facelli J.C., Ferraro M.B., Grillo D., Habgood M., Hofmann D.W.M., Hofmann F., Jose K.V.J., Karamertzanis P.G., Kazantsev A.V., Kendrick J., Kuleshova L.N., Leisen F.J.J., Maleev A.V., Misquitta A.J., Mohamed S.,

- Needs R.J., Neumann M.A., Nikylov D., Orendt A.M., Pantelides C.C., Pickard C.J., Price L.S., Price S.L., Scheraga H.A., van de Streek J., Thakur T.S., Tiwari S., venuti E., & Zhitkov I.K., "Towards crystal structure prediction of complex organic compounds—a report on the fifth blind test", *Acta Cryst.*, B67, (2011), 535-551
- Barrett C.S., & Meyer L., "X-Ray diffraction study of solid argon", *J. Chem. Phys.*, 41, 4, (1964), 1078-1081
- Bauer J., Spanton S., Henry R., Quick J., Dziki W., Porter W., & Morris J., "Ritonavir: An extraordinary example of conformational polymorphism", *Pharmaceutical Research*, 18, 6, (2001), 859-866
- Bayly C.I., Cieplak P., Cornell W.D., & Kollman P.A., "A well-behaved electrostatic potential based method using charge restraints for deriving atomic charges: The RESP model", *J. Phys. Chem.*, 97, 40, (1993), 10269-10280
- Bazterra V.E., Ferraro M.B., & Facelli J.C., "Modified genetic algorithm to model crystal structures: III. Determination of crystal structures allowing simultaneous geometry relaxation.", *International Journal of Quantum Chemistry*, 96, 4, (2004), 312-320
- Bennett C.H., "Efficient estimation of free energy differences from Monte Carlo data", *J. Comput. Phys.*, 22, (1976), 245-268
- Berendsen H.J.C., Postma J. P.M., van Gasteren W.F., & Hermans J.: in *Intermolecular forces*, edited by Pullman B., (1981), Reidel, Dordrecht, 331
- Berg B.A., & Neuhaus T., "Multicanonical ensemble: a new approach to simulate first-first order phase transitions", *Phys. Rev. Lett.*, 68, 1, (1992), 9-12
- Berthelot D., *Compte rendus hebdomadaires des séances de l'academie des sciences, Academie des sciences* (Bechelier, Paris), 126, (1898), 1703-1706
- Besler B.H., Merz Jr. K.M., & Kollman P.A., "Atomic charges derived from semiempirical methods", *J. Comput. Chem.*, 11, 4, (1990), 431-439
- Blackman M., "On the vibrational spectrum of a three-dimensional lattice", *Proc. Roy. Soc. Lond. A*, 159, (1937), 416-431

Bladereschi A., “Mean-value point in the Brillouin zone”, Phys. Rev. B, 7, 12, (1973), 5212-5215

Bonadeo H., D’ Alessio E., Halac E., & Burgos E., “Lattice dynamics, thermodynamic function, and phase transitions of p-dichloro and 1,2,4,5-tetrachlorobenzene”, J. Chem. Phys., 68(10), (1978), 4714-4721

Born M., “On the stability of crystal lattices. I”, Proc. Cambridge Phil. Soc., 36, 2, (1940), 160-172

Born M., & Bradburn M., “The thermodynamics of crystal lattices II. Calculation of certain lattice sums occurring in thermodynamics”, Proc. Cambridge Phil. Soc., 39, (1943), 104-113

Born M., & Fürth, “The stability of crystal lattices. III”, Proc. Cambridge Phil. Soc., 36, 4, (1940), 454-465

Born M., & Huang K., “Dynamical theory of crystal lattices”, Clarendon Press-Oxford, (1954)

Born M., & Misra R.D., “On the stability or crystal lattices.IV”, Proc. Cambridge Phil. Soc., 36, (1940), 466-478

Born M., & von Kármán Th., “Über schwingungen in raumgittern”, Phys. Zeit., 13, (1912), 297-309

Born M., & von Kármán Th., “Über die verteilung der eigenschwingungen von Punktgittern”, Phys. Zeit., 14, (1913), 65-71

Breneman C.M., & Wiberg K.B., “Determining atom-centered monopoles from molecular electrostatic potentials. The need of high sampling density in formamide conformational analysis”, J. Comput. Chem., 11, 3, (1990), 361-373

Brillouin L., “Wave propagation in periodic structures; electric filters and crystal lattices”, Dover publications Inc., (1953)

Bródka A., & Grzybowski A., “Electrostatic interactions in computer simulations of three-dimensional system periodic in two directions: Ewald-type summation”, J. Chem. Phys., 117, (2002), 8208

- Broughton J.Q., & Gilmer G.H., “Molecular dynamics investigation of the crystal fluid interface. I., Bulk properties”, *J. Chem. Phys.*, 79, 10, (1983), 5095-5104
- Bruce A.D., Jackson A.N., Ackland G.J., & Wilding N.B., “Lattice-switch Monte Carlo method”, *Phys. Rev. E*, 61, 1, (2000), 906-919
- Bruce A.D., Wilding N.B., & Ackland G.J., “Free energy of crystalline solids: a lattice-switch Monte Carlo method”, *Phys. Rev. Lett.*, 79, 16, (1997), 3002-3005
- Brush S.G., Sahlin H.L., & Teller E., “Monte Carlo study of a one-component plasma. I”, *J. Chem. Phys.*, 45, 6, (1966), 2102-2118
- Caldwell R.F., & Klein M.V., “Experimental and theoretical study of phonon scattering from simple point defects in sodium chloride”, *Phys. Rev.*, 158, 3, (1967), 851-875
- Campaña C., Mussard B., & Woo T.K., “Electrostatic potential derived atomic charges for periodic systems using a modified error functional”, *J. Chem. Theory Comput.*, 5, 10, (2009), 2866-2878
- Campeta A.M., Chekal B.P., Abramov Y.A., Meenan P.A., Henson M.J., Shi B., Singer R.A., & Horspool K.R., “Development of targeted polymorph screening approach for a complex polymorphic and highly solvating API”, *J. Pharm. Sci.*, 99, 9, (2010), 3874-3886
- Cerutti D.S., & Case D.A., “Multi-Level Ewald: A hybrid multigrid/Fast Fourier transform approach to the electrostatic particle-mesh problem”, *J. Chem. Theory Comput.*, 6, (2010), 443-458
- Cerutti D.S., Duke R.E., Darden T.A., & Lybrand T.P., “Staggered mesh Ewald: an extension of the smooth particle-mesh Ewald adding great versatility”, *J. Chem. Theory Comput.*, 5, 9, (2009), 2322-2338
- Chadi D.J., & Cohen M.L., “Special points in the Brillouin zone”, *Phys. Rev. B*, 8, 12, (1973), 5747-5753
- Challacombe M., Schwegler E., & Almlöf J., “Recurrence relations for calculation of the Cartesian multipole tensor”, *Chemical Physics Letters*, 241, (1995), 67-72

- Chan H.C.S., Kendrick J., & Leusen F.J.J., "Molecule VI, a benchmark crystal-structure-prediction sulfonimide: Are its polymorphs predictable?", *Angew. Chem. Int. Ed.*, 50, (2011), 2979-2981
- Chaplin T., Price G.D., & Ross N.L., "Computer simulation of the infrared and Raman activity of pyrope garnet and assignment of calculated modes to specific atomic motions" *American Mineralogist*, 83, (1998), 841-847
- Chaplot S.L., "Free energy and the relative stability of the phases of solid tetracyanoethylene with pressure and temperature", *Phys. Rev. B*, 36, 16, (1987), 8471-8477
- Chaplot S.L., Mierzejewski A., & Pawley G.S., "The monoclinic structure of tetracyanoethylene (TCNE), C₆N₄, at 5, 150 and 295K; Powder diffraction analysis", *Acta Cryst.*, C40, (1984), 663-666
- Chaplot S.L., Mierzejewski A., Pawley G.S., Lefebvre J., & Luty T., "Phonon dispersion of external and low-frequency internal vibrations in monoclinic tetracyanoethylene at 5K", *J. Phys. C: Solid State Phys.*, 16, (1983), 625-644
- Chaplot S.L., & Mukhopadyay R., "Monoclinic-amorphous-cubic phase transitions in tetracyanoethylene under high pressure", *Phys. Rev. B*, 33, 7, (1986), 5099-5101
- Chaplot S.L., Pawley G.S., Bokhenkov E.L., Sheka E.F. Dorner B., Kalus J., Jindal V.K., & Natkaniec I., "Eigenvectors of low frequency internal phonons in crystalline anthrcene-d₁₀", *Chem. Phys.*, 57, (1981), 407-414
- Chekal B.P, Campeta A.M., Abramov Y.A., Feeder N., Glynn P.P., McLaughlin R.W., Meenan P.A., & Singer R.A., "The challenges of developing an API crystallization process for a complex polymorphic and highly solvating system. Part I", *Org. Process Res. & Dev.*, 13, (2009), 1327-1337
- Chemburkar S.R., Bauer J., Deming K., Spiwek H., Patel K., Morris J., Henry R., Spanton S., Dziki W., Porter W., Quick J., Bauer P., Donaubauer J., Narayanan B.A., Soldani M., Riley D., & McFarland K., "Dealing with the impact of ritonavir polymorphs on the late stages of bulk drug process development", *Org. Process Res. Dev.*, 4, (2000), 413-417

- Chen D.-L., Stern A.C., Space B., & Johnson J.K., "Atomic charges derived from electrostatic potentials for molecular and periodic systems", *J. Phys. Chem. A*, 114, (2010), 10225-10233
- Chetkina L.A., & Bel'skiĭ V.K., "Structures of tetracyanoethylene and its tricyanovinyl derivatives with intramolecular charge transfer: a review", *Crystallography Reports*, 47, 4, (2002), 581-602
- Chipot C., & Luque F.J., "Fast evaluation of induction energies: a second-order perturbation theory approach", *Chem. Phys. Lett.*, 332, (2000), 190-198
- Chirlian L.E., & Franci M.M., "Atomic charges derived from electrostatic potentials: A detailed study", *J. Comput. Chem.*, 8, 6, (1987), 894-905
- Chisholm J.A., & Motherwell S., "COMPACK: a program for identifying crystal structure similarity using distances", *J. Appl. Cryst.*, 38, (2005), 228-231
- Choi Y., Ree T., & Ree F.H., "Phase diagram of a Lennard-Jones solid", *J. Chem. Phys.*, 99, 12, (1993), 9917-9919
- Cochran W., & Pawley G.S., "The theory of diffuse scattering of X-rays by a molecular crystal", *Proc. Roy. Soc. Lond. A*, 280, (1964), 1-22
- Cohen M.H., & Keffer F., "Dipolar sums in the primitive cubic lattices", *Phys. Rev.*, 99, 4, (1955), 1128-1134
- Conrad P.B., & de Pablo J.J., "Comparison of histogram reweighting techniques for a flexible water model", *Fluid Phase Equilibria*, 150-151, (1998), 51-61
- Coogan C.K., "Some simple theorems concerning crystal lattice sums of electric potential, electric field, and electric field gradient in crystals", *Aust. J. Chem.*, 20, (1967), 2551-2565
- Coombes D.S., Price S.L., Willock D.J., & Leslie M., "Role of electrostatic interactions in determining the crystal structures of polar organic molecules. A distributed multipole study", *J. Chem. Phys.*, 100, 18, (1996), 7352-7360
- Cornell W.D., Cieplak P., Bayly C.I., Gould I.R., Merz Jr. K.M., Ferguson D.M., Spellmeyer D.C., Fox T., Caldwell J.W., & Kollman P.A., "A second

- generation force field for the simulation of proteins, nucleic acids, and organic molecules”, J. Am. Chem. Soc., 117, (1995), 5179-5197
- Cowley R.A., Cochran W., Brockhouse B.N., & Woods A.D.B., “Lattice dynamics of alkali halide crystals. III. Theoretical”, Phys. Rev., 131, 3, (1963), 1030-1039
- Cox S.R., Hsu L.-Y., & Williams D.E., “Nonbonded potential function models for crystalline oxyhydrocarbons”, Acta Cryst., A37, (1981), 293-301
- Craven B.M., McMullan R.K., Bell J.D., & Freeman H.C., “The crystal structure of imidazole by neutron diffraction at 20 °C and -150°C”, Acta Cryst., B33, (1977), 2585-2589
- Criado A., “The influence of Coulombic interactions on thermal parameters for naphthalene and anthracene: a lattice-dynamical approach”, Acta Cryst., A45, (1989), 409-415
- Criado A. “Lattice dynamics and thermal parameters in azahydrocarbons”, Acta Cryst., A46, (1990), 489-494
- Dahl J.P., “Correction and extension of Evjen’s method for evaluating crystal potential by means of lattice sums”, J. Phys. Chem. Solids, 26, (1965), 33-40
- Darden T., Darrin Y., & Pedersen L., “Particle mesh Ewald: An $N \cdot \log(N)$ method for Ewald sums in large systems”, J. Chem. Phys., 98, 12, (1993), 10089-10092
- Day G.M., “Current approaches to predicting molecular organic crystal structures”, Cryst. Rev., 17, 1, (2011), 3-52
- Day G.M., Cooper T.G., Cruz-Cabeza A.J., Hejczyk K.E., Ammon H.L., Boerrigter S.X.M., Tan J.S., Della Valle R.G., venuti E., Jose J., Gadre S.R., Desiraju G.R., Thakur T.S., van Eijk B.P., Facelli J.C., Bazterra V.E., Ferraro, V.E., Hofmann D.W.M., Neumann M.A., Leusen F.J.J., Jendrick J., Price S.L., Misquitta A.J., Karamertzanis P.G., Welch G.W.A., Scheraga H.A., Arnautova Y.A., Schmidt M.U., van de Streek J., Wolf A.K., & Schweizer B., “Significant progress in predicting the crystal structures of small organic molecules—a report on the fourth blind test”, Acta Cryst., B65, (2009), 107-125

- Day G.M., Motherwell W.D.S., Ammon H.L., Boerrigter S.X.M., Della Valle R.G., Venuti E., Dzyabchenko A., Dunitz J.D., Schweizer B., van Eijk B.P, Erk P., Facelli J.C., Bazterra V.E., Ferraro M.B., Hofmann D.W.M., Leusen F.J.J., Liang C., Pantelides C.C., Karamertzianis P.G., Price S.L., Lewis T.C., Nowell H., Torrisi A., Scheraga H.A., Arnautova Y.A., Schmidt M.U., & Verwer P., “A third blind test of crystal structure prediction”, *Acta Cryst.*, B61, (2005), 511-527
- Day G.M., Price S.L., & Leslie M., “Atomistic calculations of phonon frequencies and thermodynamic quantities for crystals of rigid organic molecules”, *J. Phys. Chem. B*, 107, 39, (2003), 10919-10933
- De Launay J. “Theory of specific heat and lattice vibrations”, *Solid state physics*, 2, (1956), 219-304
- De Leeuw S.W., Perram J.W., & Smith E.R., “Simulation of electrostatic systems in periodic boundary conditions. I. Lattice sums and dielectric constants”, *Proc. R. Soc. Lond. A*. 373, (1980), 27-56
- De Wette F.W., Fowler L.H., & Nijboer B.R.A., “Lattice dynamics, thermal expansion and specific heat of a Lennard-Jones solid in the quasi-harmonic approximation”, *Physica*, 54, (1971), 292-304
- De Wette F.W., & Schacher G.E., “The internal field in general dipole lattices”, *Phys. Rev.*, 137, 1A, (1965), 78-91
- Deem M.W., Newsam J.M., & Sinha S.K., “The h=0 term in Coulomb sums by the Ewald transformation”, *J. Phys. Chem.*, 94, (1990), 8356-8359
- Della Valle R.G., Fracassi P.F., Righini R., Califano S., & Walmsley S.H., “Phonon dispersion curves and phonon lifetimes in crystalline ammonia”, *Chem. Phys.*, 44, (1979), 189-196
- Della Valle R.G., Venuti E., & Brillante A., “Pressure and temperature effects in lattice dynamics: the case of naphthalene”, *Chem. Phys.*, 198, (1995), 79-89

- Demontis P., Spanu S., & Suffritti G.B., "Application of the Wolf method for the evaluation of Coulombic interactions to complex condensed matter systems: Aluminosilicates and water", *J. Chem. Phys.*, 114, (2001), 7980
- Der Chao S., Kress J. D., & Redondo A., "An alternative multipolar expansion for intermolecular potential functions", *J. Chem. Phys.*, 120, 12, (2004), 5558-55765
- Derenzo S.E., Klintenberg M.K., & Weber M.J., "Determining point charge arrays that produce accurate ionic crystal fields for atomic cluster calculations", *J. Chem. Phys.*, 112, 5, (2000), 2074-2081
- Deserno M., & Holm C., "How to mesh up Ewald sums. I. A theoretical and numerical comparison of various particle mesh routines", *J. Chem. Phys.*, 109, 18, (1998), 7678-7693
- Desikan S., Parsons Jr. R.L., Davis W.P., Ward J.E., Marshall W.J., & Toma P.H., "Process development challenges to accommodate a late-appearing stable polymorph: A case study on the polymorphism and crystallization of a fast-track drug development compound", *Org. Process Res. Dev.*, 9, (2005), 933-942
- Dick B.G. Jr., & Overhauser A.W., "Theory of the dielectric constants of alkali halide crystals", *Phys. Rev.*, 112, 1, (1958), 90-103
- Diemand J., Angélil R., Tanaka K.K., & Tanaka H., "Large scale molecular dynamics simulations of homogeneous nucleation", *J. chem. Phys.*, 139, (2013), 074309
- Dobbs E.R., Figgins B.F., Jones G.O., Piercy D.C., & Riley D.P., "Density and expansivity of solid argon", *Nature*, 178, (1956), 483
- Dobbs E.R., & Jones G.O., "Theory and properties of solid argon", *Rep. Prog. Phys.* 20, (1957), 516
- Dorner B., Bokhenkov E.L., Chaplot S.L., Kalus J., Natkaniec I., Pawley G.S., Schmelzer U., & Sheka E.F., "The 12 external and the 4 lowest internal phonon dispersion branched in d_{10} – anthracene at 12K", *J. Phys. C: Solid State Phys.*, 15 (1982), 2353-2365
- Dove M.T., "Introduction to lattice dynamics", Cambridge University Press, (1993)

- Dove M.T., “Structure and dynamics: an atomic view of materials”, Oxford University Press, (2003)
- Dunitz J.D., Filippini G., & Gavezzotti A., “Molecular shape and crystal packing: a study of C₁₂H₁₂ isomers, real and imaginary”, *Helv. Chim. Acta.*, 83, (2000), 2317-2335
- Dunitz J.D., & Gavezzotti A., “Attractions and repulsions in molecular crystals: What can be learned from the crystal structures of condensed ring aromatic hydrocarbons?”, *Acc. Chem. Res.*, 32, (1999), 677-684
- Eike D.M., & Maginn E.J., “Atomistic simulation of solid-liquid coexistence for molecular systems: application to triazole and benzene”, *J. Chem. Phys.*, 124, (2006), 164503
- Eike D.M., Brennecke J.F., & Maginn E.J., “Towards a robust and general molecular simulation method for computing solid-liquid coexistence”, *J. Chem. Phys.*, 122, (2005), 014115
- Einstein A. “Die Plancksche theorie der strahlung und die theorie der spezifischen wärme”, *Ann. Phys.*, 22, (1907), 180-190
- Epstein J., Ruble R. J., & Craven B.M., “The charge density in imidazole by X-ray diffraction at 103 and 293K”, *Acta Cryst.*, B38, (1982), 140-149
- Essmann U., Perera L., Berkowitz M.L., Darden T., Lee H., & Pedersen L.G., “A smooth particle mesh Ewald method.” *J. Chem. Phys.*, 103, (19), (1995), 8577-8593
- Evjen H.M., “On the stability of certain heteropolar crystals”, *Phys. Rev.*, 39, (1972), 675-687
- Ewald P.P., *Ann. D. Phys.*, 54, (1917), 519
- Ewald P.P., “Die berenchnung optischer und elektrostatischer gitterpotentiale.”, *Ann. D. Phys.*, 64, (1921), 253-287
- Ewald P.P., “Crystal optics for visible light and X-Rays”, *Rev. Mod. Phys.*, 37, 1, (1965), 46-56

- Ewald P.P., “A review of my papers on crystal optics 1912 to 1968”, *Acta Cryst.*, A35, (1979), 1-9
- Falter C., Klenner M., Hoffmann G.A., & Schnetgöke F., “Dipole polarization and charge transfer effects in the lattice dynamics and dielectric properties of ionic crystals”, *Phys. Rev. B*, 60, 17, (1999), 12051-12060
- Fenell C.J., & Gezelter J.D., “Is Ewald summation still necessary? Pairwise alternatives to the accepter standard for long-range electrostatics”, *J. Chem. Phys.*, 124, (2006), 234104
- Ferrenberg A.M., & Swendsen R.H., “New Monte Carlo technique for studying phase transitions”, *Phys. Rev. Lett.*, 61, 23, (1988), 2635-2638
- Ferrenberg A.M., & Swendsen R.H., “Optimized Monte Carlo data analysis”, *Phys. Rev. Lett.*, 63, 12, (1989), 1195-1198
- Filippini G., Gramaccioli C.M., Simonetta M., & Suffritti G.B., “Lattice-dynamical applications to crystallographic problems: Consideration of the Brillouin zone sampling”, *Acta Cryst.*, A32, (1976), 259-264
- Freeman D.L., & Doll J.D., “Quantum Monte Carlo study of the thermodynamic properties of argon clusters: The homogenous nucleation of argon in argon vapour and “magic number” distributions in argon vapor”, *J. Chem. Phys.*, 82, (1985), 462
- Frenkel D., & Ladd A.J.C., “New Monte Carlo method to compute the free energy of arbitrary solids. Application to the fcc and hcp phases of hard spheres”, *J. Chem. Phys.*, 81, 7, (1984), 3188-3191
- Frenkel D., & Mulder B.M., “The hard ellipsoid-of-revolution fluid I. Monte Carlo simulations”, *Molecular Physics*, 100, 1, (2002), 201-217
- Frenkel D., & Smimt B., “Understanding molecular simulation”, Academic Press, (2002)
- Frisch M. J., Trucks G. W., Schlegel H. B., Scuseria G. E., Robb M. A., Cheeseman J. R., Scalmani G., Barone V., Mennucci B., Petersson G. A., Nakatsuji H., Caricato M., Li X., Hratchian H. P., Izmaylov A. F., Bloino J., Zheng G.,

Sonnenberg J. L., Hada M., Ehara M., Toyota K., Fukuda R., Hasegawa J., Ishida M., Nakajima T., Honda Y., Kitao O., Nakai H., Vreven T., Montgomery Jr. J. A., Peralta J. E., Ogliaro F., Bearpark M., Heyd J. J., Brothers E., Kudin K. N., Staroverov V. N., Kobayashi R., Normand J., Raghavachari K., Rendell A., Burant J. C., Iyengar S. S., Tomasi J., Cossi M., Rega N., Millam J. M., Klene M., Knox J. E., Cross J. B., Bakken V., Adamo C., Jaramillo J., Gomperts R., Stratmann R. E., Yazyev O., Austin A. J., Cammi R., Pomelli C., Ochterski J. W., Martin R. L., Morokuma K., Zakrzewski V. G., Voth G. A., Salvador P., Dannenberg J. J., Dapprich S., Daniels A. D., Farkas O., Foresman J. B., Ortiz J. V., Cioslowski J. & Fox D. J. (2009), ‘Gaussian 09 Revision C.1’, Gaussian, Inc., Wallingford, CT

Fuchizaki K., “Towards generalization of Ewald sum”, *J. Phys. Soc. Jap.*, 63, 11, (1994), 4051-4059

Fuchizaki K., “Application of the Generalized Ewald method to a molecular system”, *J. Phys. Soc. Jap.*, 79, 2, (2010), 024004

Fujii Y., Lurie N.A., Pynn, R., & Shirane G., “Inelastic neutron scattering from solid ^{36}Ar ”, *Phys. rev. B*, 10, 8, (1974), 3647-3659

Fukuda I., & Nakamura H., “Non-Ewald methods: theory and applications to molecular systems”, *Biophys. Rev.*, 4, (2012), 161-170

Fukuda I., Kamiya N., Yonezawa Y., & Nakamura H., “Simple and accurate scheme to compute electrostatic interaction: Zero-dipole summation technique for molecular system and application to bulk water”, *J. Chem. Phys.*, 137, (2012), 054314

Fukuda I., Yonezawa Y., & Nakamura H., “Molecular dynamics scheme for precise estimation of electrostatic interaction via zero-dipole summation principle”, *J. Chem. Phys.*, 134, (2011), 164107

Funasako Y., Abe K.-i., & Mochida T., “Thermal properties of alkyloctamethylferrocenium salts with TFSA and TCNE (TFSA = bis(trifluoromethylsulfonyl)amide and TCNE = tetracyanoethylene)”, *Thermochimica Acta*, 532, (2012), 78-82

Gale J.D., “Analytical free energy minimisation of silica polymorphs”, *J. Phys. Chem. B*, 102, (1998), 5423-5431

Gale J.D., & Rohl A.L., “The general utility lattice program”, *Molecular Simulation*, 29, 5, (2003), 291-341

Gdoutos E.E., Agrawal R., & Espinosa H.D., “Comparison of the Ewald and Wolf methods for modelling electrostatic interactions in nonwires”, *Int. J. Numer. Meth. Eng.*, 84, (2010), 1541-1551

Gellé A. & Lepetit M.-B., “Fast calculation of the electrostatic potential in ionic crystals by direct summation method”, *J. Chem. Phys.*, 128, (2008), 244716

Ghatak A.K., & Kothari L.S., “An introduction to lattice dynamics”, Addison-Wesley, (1972)

Ghelfenstein M., & Szwarc H., “Raman spectra in molecular solids II. Low frequency Raman spectroscopy as a means to study phase changes: More about the “anomalous” γ -phase of p-dichlorobenzene”, *Mol. Cryst. Liq. Cryst.*, 14, 3-4, (1971), 283-288

Gilat G., & Raubenheimer L.J., “Accurate numerical method for calculating frequency-distribution functions in solids”, *Phys. Rev.*, 144, 2, (1966), 390-395

Goharshadi E.K., Morsali A., & Mansoori G.A., “A molecular dynamics study on the role of attractive and repulsive forces in internal energy, internal pressure and structure of dense fluids”, *Chem. Phys.*, 331, (2007), 332-338

Goto M., Takezoe H., & Ishikawa K., “Carrier transport simulation of anomalous temperature dependence in nematic liquid crystals”, *Phys. Rev. E*, 76, (2007), 040701

Grant W.J.C, “Computation of lattice sums: Generalization of the Ewald method”, *B.S.T.J.*, 44, (1965:a), 427-437

Grant W.J.C, “Computation of lattice sums: Generalization of the Ewald method II”, *B.S.T.J.*, 44, (1965:b), 2433-2446

- Gray A.E., Day G.M., Leslie M., & Price S.L, "Dynamics in crystals of rigid organic molecules: contrasting the phonon frequencies calculated by molecular dynamics with harmonic lattice dynamics for imidazole and 5-azauracil", Molecular Physics, 102, 9-10, (2004), 1067-1083
- Greengard L., & Rokhlin V., "A fast algorithm for particle simulations", J. Comput. Phys., 73, (1987), 325-348
- Grochola G., "Constrained fluid λ -integration: Constructing a reversible thermodynamic path between the solid and the liquid state", J. Chem. Phys., 120, 5, (2004), 2122-2126
- Hanke C.G., Price S.L., & Lynden-Bell R.M., "Intermolecular potentials for simulation of liquid imidazolium salts", Molecular Physics, 99,10, (2001), 801-809
- Hätting C., "Recurrence relations for the direct calculation of spherical multipole interaction tensors and Coulomb-type interaction energies", Chem. Phys. Lett., 260, (1996), 341-351
- Hawkins J.A., Rittenhouse J.L, Soper L.M., & Rittenhouse R.C., "Use of the primitive unit cell in understanding subtle features of the cubic closest-packed structure", J. Chem. Educ., 85, 1, (2008), 90-92
- Herbstein F.H., "Twinned crystals. II. a-1,2:4,5-tetrachlorobenzene", Acta Cryst., A18, (1965), 997-1000
- Herrero C.P., & Ramírez R., "Configurational entropy of ice from thermodynamic integration", Chem. Phys. Lett., 568-569, (2013), 70-74
- Heyes D.M., Barber M., & Clarke J.H.R., "Molecular dynamics computer simulation of surface properties of crystalline potassium chloride", J. Chem. Soc. Faraday Trans II., 73, (1977), 1485-1496
- Hilfiker R., "Polymorphism in the pharmaceutical industry", (2006), Wiley-VCH: New York
- Hill T.L., "An introduction to statistical thermodynamics", Dover Publications, (1986), New York

- Hoover W.G., & Ree F.H., "Use of computer experiments to locate the melting transition and calculate the entropy in solid phase", *J. Chem. Phys.*, 47,12, (1967), 4873-4878
- Hoover W.G., & Ree F.H., "Melting transition and communal entropy for hard spheres", *J. Chem. Phys.*, 49, 8, (1968), 3609-3617
- Hoover W.G., Ross M., Johnson K.W., Henderson D., Barker J.A., & Brown B.C., "Soft-sphere equation of state", *J. Chem. Phys.*, 52,10, (1970), 4931-4941
- Horbenko E.E., Troitskaya E.P., & Chabanenko V.V., "Lattice dynamics of cryocrystals at high pressure", *Low Temp. Phys.*, 33, 6-7, (2007), 573-577
- Houston W.V., "Normal vibrations of a crystal lattice", *Rev. Mod. Phys.* 20, 1, (1948), 161-165
- Hsu L.-Y., & Williams D.E., "Intermolecular potential-function models for crystalline perchlorohydrocarbons", *Acta Cryst.*, A36, (1980), 277-281
- Hünenberger P.H., "Lattice-sum methods for computing electrostatic interactions in molecular simulations", *AIP Conf. Proc.*, 492, 17 (1999), 17-83
- in't Veld P.J., Ismail A., & Grest G.S., "Application of Ewald summations to long range dispersion forces", *J. Chem. Phys.*, 127, 14, (2007), 144711
- Isele-Holder R.E., Mitchell W., & Ismail A.E., "Development and application of a particle-particle particle-mesh Ewald method for dispersion interactions", *J. Chem. Phys.*, 137, (2012), 174107
- Ismail S.Z., Anderton C.L., Copley R.C.B., Price L.S., & Price S.L., "Evaluating the lattice energy landscape in the context of industrial polymorph screening", *Cryst. Growth Des.*, 13(6), (2013), 2396-2406
- Jaswal S.S., "Deformable-ion model and the lattice dynamics of II-IV compounds: ZnS", *J. Phys. C: Solid State Phys.*, 11, (1978:a), 3559-3563
- Jaswal S.S., "Lattice dynamics of CuCl at 4.2 °K", *Solid State Communications*, 27, 10, (1978:b), 969-971

- Jaswal S.S., & Dilly V.D., “Deformable-ion model and lattice dynamics of ^7LiD ”, Phys. Rev. B, 15, 4, (1977:a), 2366-2370
- Jaswal S.S., & Dilly V.D., “Second order Raman scattering in MgO”, Solid state communications, 24, 8, (1977:b), 577-581
- Jayaraman S., & Maginn E. J., “Computing the melting point and thermodynamic stability of the orthorhombic and monoclinic crystalline polymorphs of the ionic liquid 1-n-butyl-3-methylimidazolium chloride”, J. Chem. Phys., 127, (2007), 214504
- Kaminsky R.D., “Monte Carlo evaluation of ensemble averages involving particle number variations in dense fluid systems”, J. Chem. Phys., 101, 6, (1994), 4986-4994
- Kamiya N., Fukuda I., & Nakamura H., “Application of the zero-dipole summation method to molecular dynamics simulations of a membrane protein system”, Chem. Phys. Lett., 568-569, (2013), 26-32
- Kantorovich L.N., “Thermoelastic properties of perfect crystals with nonprimitive lattices. I. General theory”, Phys. Rev. B, 51, 6, (1995), 3520-3534
- Kaplan I.G., “Intermolecular interactions: physical picture, computational methods, model potentials”, Wiley, (2006), Hoboken, NJ
- Karamertzanis P.G., Raiteri P., Parrinello M., Leslie M., & Price S.L., “The thermal stability of lattice-energy minima of 5-fluorouracil: Metadynamics as an aid to polymorph prediction”, J. Phys. Chem. B., 112, (2008), 4298-4308
- Karamertzanis P.G., “Prediction of crystal structure of molecular solids”, Ph.D. Thesis, Imperial College London, (2004)
- Karamertzanis P.G., & Pantelides C.C., “Optimal site charge models for molecular electrostatic potentials”, Molecular Simulation, 30, 7, (2004), 413-436
- Karamertzanis P.G., & Pantelides C.C., “*Ab-initio* Crystal Structure Prediction—I. Rigid Molecules”, J. Comput. Chem., 26, 3, (2005), 304-323

- Karamertzanis P.G., & Pantelides C.C., “*Ab-initio* Crystal Structure Prediction—II. Flexible Molecules”, Molecular Physics, 105, 2-3, (2007), 273-291
- Karamertzanis P.G., & Price S.L., “Energy minimization of crystal structures containing flexible molecules”, J. Chem. Theory Comput., 2, (2006), 1184-1199
- Karo A.M., & Hardy J.R., “Precise vibrational frequency distributions and the second-order Raman spectrum and specific heat of NaCl”, Phys. Rev., 141, 2, (1966), 696-710
- Kawata M., & Nagashima U., “Particle mesh Ewald method for three-dimensional systems with two-dimensional periodicity”, Chem. Phys. Lett., 340, (2001), 165-172
- Kazantsev A.V., Karamertzanis P.G., Adjiman C.S., & Pantelides C.C., “CrystalOptimizer: An efficient algorithm for lattice energy minimisation of organic crystals using quantum mechanical calculations”, Molecular Systems Engineering, (2010), edited by C.S. Adjiman & A. Galindo. Germany: Wiley-VCH
- Kazantsev A.V., Karamertzanis P.G., Adjiman C.S., & Pantelides C.C., “Efficient handling of molecular flexibility in lattice energy minimization of organic crystals”, J. Chem. Theory Comput., 7, 6, (2011: a), 1998-2016
- Kazantsev A.V., Karamertzanis P.G., Adjiman C.S., Pantelides C.C., Price S.L., Galek P.T.A., Day G.M., & Cruz-Cabeza A.J., “Successful prediction of a model pharmaceutical in the fifth blind test of crystal structure prediction”, Int. J. Pharmaceuticals, 418, 2, (2011: b), 168-178
- Kellermann E.W., “Theory of the vibrations of the sodium chloride lattice”, Phil. Trans. R. Soc. Lond. A, 238, (1940), 513-548
- Kellermann E.W., “On the specific hear of the sodium chloride crystal”, Proc. Roy. Soc. A, 178, (1941), 17-24
- Kim K.-H., Jung D.H., Kim D., Lee A., Choi K., Kim Y., & Choi S.-H., “Crystal structure prediction of organic materials: Tests on the 1,4-diketo-3,6-

- diphenylpyrrolo(3,2-c)pyrrole and 1,4-diketo-3,6-bis(4'-dipyridyl)-pyrrolo-[3,4-c]pyrrole”, Dyes and pigments, 89, 1, (2011), 37-43
- Kirkwood J.G., “Statistical mechanics of fluid mixtures”, J. Chem. Phys., 3 (1935), 300-313
- Kirkwood J.G., “Critique of the free volume theory of the liquid state”, J. Chem. Phys., 18, 3,(1950), 380-382
- Kittel C., “Introduction to solids state physics”, John Wiley & Sons Inc., (2005),
- Kiyohara K., Gubbins K.E., & Panagiotopoulos Z., “Phase coexistence properties of polarisable Stockmayer fluids”, J. Chem. Phys., 106, 8, (1997), 3338-3347
- Kofke D.A., “Direct evaluation of phase coexistence by molecular simulation via integration along a saturation line”, J. Chem. Phys., 98, (1993), 4149
- Kofke D.A., & Cummings P.T., “Quantitative comparison and optimization of methods for evaluating the chemical potential by molecular simulation”, Molecular Physics, 92,6, (1997), 973-996
- Kofke D.A., & Cummnings P.T., “Precision and accuracy of staged free-energy perturbation methods for computing the chemical potential by molecular simulation”, Fluid Phase Equilibria, 150-151, (1998), 41-49
- Kopsias N.P., & Theodorou D.N., “Elementary structural transitions in the amorphous Lennard-Jones solid using multidimensional transition state theory”, J. Chem. Phys., 109, 19, (1998), 8573-8582
- Kosov D.S., & Popelier P.L.A., “Atomic partitioning of molecular electrostatic potentials”, J. Phys. Chem. A, 104, (2000), 7339-7345
- Krylov V.I., “Approximate calculation of integrals”, Macmillian, (1962)
- Laasonen K., Wonczak S., Strey R., & Laaksonen A., “Molecular dynamics simulations of gas-liquid nucleation of Lennard-Jones fluid”, J. Chem. Phys., 113, (2000), 9741-9747

- Laino T., & Hutter J., “Notes on “Ewald summation of electrostatic multipole interaction up to quadrupolar level” [J. Chem. Phys., 119, 74171, (2003)]”, J. Chem. Phys., 129, (2008), 074102
- Laio A., & Parrinello M., “Escaping free energy minima”, Proc. Nat. Ac. Sci USA, 99, 20, (2002), 12562-12566
- Lennard-Jones J.E., “The equation of state of gases and critical phenomena”, Physica IV, (1937), 941-956
- Lennard-Jones J.E., & Devonshire A.F., “Critical phenomena in gases. I”, Proc. Roy. Soc. A, 163, (1937), 53-70
- LeSar R., Najafabadi R., & Srolovitz D.J., “Finite-temperature defect properties from free-energy minimisation”, Phys. Rev. Lett., 63, 6, (1989), 624-627
- Leslie M., “DL_MULTI—A molecular dynamics program to use distributed multipole electrostatic models to simulate the dynamics of organic crystals”, Molecular Physics, 106, 12-13, (2008), 1567-1578
- Little R.G., Pautler D., & Coppens P., “X-ray structure analysis of cubic Tetracyanoethylene and the length of the $\text{C}\equiv\text{N}$ bond. Application of a double-atom refinement method”, Acta Cryst., B27, (1971), 1493-1499
- Lommerse J.P.M., Motherwell W.D.S., Ammon H.L., Dunitz J.D., Gavezzotti A., Hofmann D.W.M., Leusen F.J.J., Mooij W.T.M., Price S.L., Schwizer B., Schmidt M.U., van Eijk B.P., Verwer P., Williams D.E., “A test of crystal structure prediction of small organic molecules”, Acta Cryst., B56, (2000), 697-714
- Lorentz H.A., “Über die anwendung des statez vom virial in der kinetischen theorie der gase”, Ann. Phys., 248, 1, (1881), 127-136
- Lu N., & Kofke D.A., “Optimal intermediates in staged free energy calculations”, J. Chem. Phys., 111, 10, (1999), 4414-4423
- Luty B.A., Tironi I.G., & van Gunsteren W.F., “Lattice-sum methods for calculating electrostatic interactions in molecular simulations”, J. Chem. Phys., 103, 22, (1995), 3014-3021

- Luty T., Van Der Avoird A., & Mierzejewski A., "Lattice dynamics of tetracyanoethylene", *Chem. Phys. Lett.*, 61, 1,(1979), 10-14
- Lyubartsev A.P., Martsinovski A.A., Shevkunov S.V., & Vorontsov-Velyaminov P.N., "New approach to Monte Carlo calculation of the free energy: Method of expanded ensembles", *J. Chem. Phys.*, 96, 3, (1992), 1776-1783
- Madelung E. *Phys. Z.*, (1918), 524
- Marathe V.R., Lauer S., & Trautwein A.X., "Electrostatic potentials using direct-lattice summations", *Phys. Rev. B.*, 27, 8, (1983), 5162-5165
- Marsh R.E., "A refinement of the crystals structure of glycine", *Acta Cryst.* 11, 9,(1958), 654-663
- Martinez-Carrera S., "The crystal structure of imidazole at -150 °C", *Acta Cryst.*, 20, (1966), 783-789
- Martoňák R., Laio A., & Parrinello M., "Predicting crystal structures: The Parrinello-Rahman method revisited", *Phys. Rev. Lett.*, 90, 7, (2003), 075503
- Mattei A., & Li T., "Interplay between molecular conformation and intermolecular interactions in conformational polymorphism: A molecular perspective from electronic calculations of tolfenamic acid", *Int. J. Pharm.*, 418, (2011), 179-186
- Mayo S.L., Olafson B.D., & Goddard W.A., "DREIDING: A generic force field for molecular simulations", *J. Phys. Chem.*, 94, (1990), 8897-8909
- McCrone W.C., "Polymorphism", in "Physics and chemistry of the organic solid state", vol. 2, edited by Fox D., (1965)
- McMullan R.K., Epstein J., Ruble J.R., & Craven B.M., "The crystal structure of imidazole at 103K by neutron diffraction", *Acta Cryst.*, B35, (1979), 688-691
- McQuarrie D.A., "Statistical Mechanics", University Science Books, (2000), Sausalito, California
- McWeeny R., "Symmetry-introduction to group theory", (1963), The international encyclopedia of physical chemistry and chemical physics, Topic I, Vol. 3., edited by: Jones H., Pergamon Press

- Meijer E.J., Frenkel D., LeSar R.A, & Ladd A.J.C., “Location of melting point at 300K of nitrogen by Monte Carlo simulation”, *J. Chem. Phys.*, 92, 12, (1990), 7570-7575
- Mierzejewski A., & Chaplot S.L., “Raman scattering study of phase transition in tetracyanoethylene”, *Conf. Int. Raman. Spectrosc.* 7th (1980), 46-47
- Minicozzi W.P., & Stroot M.T., “Solutions for the indeterminate term occurring in infinite multipole cubic lattice sums”, *Physica*, 51, (1971), 503-508
- Misra R.D., “On the stability of crystal lattices.II”, *Proc. Cambridge Phil. Soc.*, 36, (1940), 173-182
- Monkhorst H.J., & Pack J.D., “Special points for Brillouin-zone integrations”, *Phys. Rev. B*, 13, 12, (1976), 5188-5192
- Montroll E.W., “Frequency spectrum of crystalline solids”, *J. Chem. Phys.*, 10, (1942), 218-229
- Mooij W.T.M., van Eijk B.P., & Kroon J., “Ab initio crystal structure predictions for flexible hydrogen-bonded molecules”, *J. Am. Chem. Soc.*, 122, (2000), 3500-3505
- Motherwell W.D.S., Ammon H.L., Dunitz J.D., Dzyabchenko A., Erk P., Gavezzotti A., Hofmann D.W.M., Leusen F.J.J., Lommerse J.P.M., Mooij W.T.M., Price S.L., Scheraga H., Schweizer B., Schmidt M.U., van Eijk B.P., Verwer P., Williams D.E., “Crystal structure prediction of small organic molecules: a second blind test”, *Acta Cryst.*, B58, (2002), 647-661
- Mukhopadhyay R., Chaplot S.L., & Rao K.R., “Phase transition in tetracyanoethylene”, *Physica Status Solidi A.*, 92, (1985), 467-474
- Mukhopadhyay R., Deb S.K., Das A., & Chaplot S.L., “Phase transitions at high pressure in tetracyanoethylene”, *Solid State Communications*, 149, (2009), 1914-1918
- Munn R.W., & Luty T., “Theoretical studies of phase transitions in tetracyanoethylene”, *Faraday Discuss. Chem. Soc.*, 69, (1980), 107-114

- Murgich J., & Pissanetzky S., “Temperature dependence of the ^{14}N nuclear quadrupole resonance and the observation of the phase transition in cubic tetracyanoethylene”, *J. Chem. Phys.*, 62, (1975), 92-93
- Najafabadi R., Srolovitz D.J., & LeSar R., “Thermodynamic and structural properties of [001] twist boundaries in gold”, *J. Mater. Res.*, 6, 5, (1991:a), 999-1011
- Najafabadi R., Wang H.Y., Srolovitz D.J., & LeSar R., “A new method for the simulation of alloys: Application to interfacial segregation”, *Acta metall. Mater.*, 39, 12, (1991:b), 3071-3082
- Natkaniec I., Bokhenkov E.L., Dorner B., Kalus J., Mackenzie G.A., Pawley G.S., Schmelzer U., & Sheka E.F. “Phonon dispersion in d₈-naphthalene crystal at 6K”, *J. Phys. C: Solid State Phys.*, 13, (1980), 4265-4283
- Nayhouse M., Amlani A.M., & Orkoulas G., “A Monte Carlo study of the freezing transition of hard spheres”, *J. Phys.: Condens. Matter*, 23, (2011:a), 325106
- Nayhouse M., Amlani A.M., & Orkoulas G., “Precise simulation of the freezing transition of supercritical Lennard-Jones”, *J. Chem. Phys.*, 135, (2011:b), 154103
- Nayhouse M., Amlani A.M., Heng V.R., & Orkoulas G., “Simulation of fluid-solid coexistence via thermodynamic integration using a modified cell model”, *J. Phys.: Condens. Matter*, 24, (2012), 155101
- Neto N., Righini R., Califano S., & Walmsley S.H., “Lattice dynamics of molecular crystals using atom-atom and multipole-multipole potentials”, *Chem. Phys.*, 29, (1978), 167-179
- Neumann M.A., & Perrin M.-A., “Energy ranking of molecular crystals using density functional theory calculations and an empirical van der Waals correction”, *J. Phys. Chem. B.*, 109, (2005), 15531-15541
- Nijboer B.R.A., & De Wette F.W., “On the calculation of lattice sums”, *Physica XXIII*, (1957), 309-321
- Nijboer B.R.A., & De Wette F.W., “The internal field in dipole lattices”, *Physica XXIV*, (1958), 422-431

- Noya E.G., Conte M.M., & Vega C., “Computing the free energy of molecular solids by the Einstein molecule approach: Ices XIII and XIV, hard-dumbbells and a patchy model or proteins”, *J. Chem. Phys.*, 129, (2008), 104704
- Nymand T.M., & Linse P., “Ewald summation and reaction field methods for potentials with atomic charges, dipoles and polarizabilities”, *J. Chem. Phys.*, 112, (2000), 6152-6160
- Oh K.J., & Deng Y., “An efficient parallel implementation of the smooth particle mesh Ewald method for molecular dynamics simulations”, *Computer Physics Communications*, 177, (2007), 426-431
- Özgen S., Kuzucu V., & Adigüzel, “Investigation of solid argon crystal by means of isobaric isoenthalpic MD method”, *Erc. Ünv. Fen. Bil. Derg.*, 12, 1-2, (1996), 60-74
- Paliwoda D., Dziubek K.F., & Katrusiak A., “Imidazole hidden polar phase”, *Cryst. Growth Des.*, 12,9, (2012), 4302-4305
- Panagiotopoulos A.Z., “Direct determination of phase coexistence properties of fluids by Monte Carlo simulation in a new ensemble”, *Molecular Physics*, 61, 4, (1987), 813-816
- Panina N., van de Ven R., Verwer P., Meekes H., Vileg E., & Deroover G., “Polymorph prediction of organic pigments”, *Dyes and Pigments*, 79, (2008), 183-192
- Patel A., Price G.D., & Mendelssohn, M.J., “A computer simulation of approach to modelling the structure thermodynamics and oxygen isotope equilibria in silicates”, *Phys. Chem. Minerals*, 17, (1991), 690-699
- Pavese A., Catti M., Parker S.C., & A. Wall, “Modelling of the thermal dependence of structural and elastic properties of calcite, CaCO_3 ”, *Phys. Chem. Minerals*, 23, (1996), 89-93
- Pawley G.S., “Analytic formulation of molecular lattice dynamics based on pair potential functions”, *Physica Status Solidi B*, 49, (1972), 475-488

- Peterson O.G., Batchelder D.N., & Simmons R.O., "Measurements of X-Ray lattice constant, thermal expansivity, and isothermal compressibility of argon crystals", Phys., Rev., 150, 2, (1966), 703-711
- Pillardy J., Arnautova Y.A., Czaplewski C., Gibson K.D., & Scheraga H.A., "Conformation-family Monte Carlo: A new method for crystal structure prediction", PNAS, 98, 22, (2001), 12351-12356
- Pillardy J., Wawak R.J., Arnautova Y.A., Czaplewski C., & Scheraga H.A., "Crystal structure prediction by global optimization as a tool for evaluating potentials: role of the dipole moment correction term in successful predictions", J. Am. Chem. Soc., 122, (2000), 907-921
- Polson J.M., Trizac E., Pronk S., & Frenkel D., "Finite-size corrections to the free energies of crystalline solids", J. Chem. Phys., 112, 12, (2000), 5339-5342
- Prasad R., & Bansil A. "Special directions for Brillouin-zone integration: Application to density-of-states calculations", Phys. Rev. B, 21, 2, (1980), 496-503
- Press W.H., Teukolsky S.A., Vetterling W.T., & Flannery B.P., "Numerical recipies: the art of scientific computing", Cambridge University Press, (1986), Cambridge
- Price S.L., "Computational prediction of organic crystal structures and polymorphism", International Reviews in Physical Chemistry, 27, 3, (2008), 541-568
- Price S.L., Leslie M., Welch G.W.A., Habgood M., Price L.S., Karamertzanis P.G., & Day G.M., "Modelling organic crystal structures using distributed multipole and polarizability-based model intermolecular potentials", Phys. Chem. Chem. Phys., 12, (2010), 8478-8490
- Price S.L., Patel B., Pridhanani-Jethani P., & Torrisi A., "Crystal structure prediction and polymorphism-some mutual insights", ACA Transactions, 39, (2004), 2-13
- Price S.L., Stone A.J., & Alderton M., "Explicit formulae for the electrostatic energy, forces and torques between a pair of molecules of arbitrary symmetry", 52, 4, (1984), 987-1001

- Radomska M., & Radomski R., “Phase diagrams in the binary systems of tetracyanoethylene with mesitylene, durene and pentamethylbenzene”, *J. Therm. Anal.*, 37, (1991), 693-704
- Rafizadeh H.A., & Yip S., “Lattice dynamics of hexamine—A rigid molecule approximation”, *J. Chem. Phys.*, 53, 1, (1970), 315-325
- Rahman A., “Correlations in the motion of atoms in liquid argon” *Phys. Rev.*, 136, 2A, (1964), A405-A411
- Raiteri P., Martoňák R., & Parrinello M., “Exploring polymorphism: The case of benzene”, *Angew. Chem. Int. Ed.*, 44, (2005), 3769-3773
- Ribeiro M.C.C., “High frequency sound velocity in the glass former $2\text{Ca}(\text{NO}_3)_2 \cdot 3\text{KNO}_3$: Molecular dynamics simulations”, *Phys. Rev. B*, 75, 14, (2007), 144202
- Righini R., Califano S., & Walmsley S.H., “Calculated phonon dispersion curves for fully deuterated naphthalene crystals at low temperature”, *Chem. Phys.*, 50, (1980), 113-117
- Righini R., Neto N., Califano S., & Walmsley S.H., “Lattice dynamics of crystalline ammonia and deutero-ammonia”, *Chem. Phys.*, 33, (1978), 345-353
- Rudin W., “Real & Complex analysis”, McGraw-Hill, (1987)
- Salonen M., Napari I., Vehkämäki H., “Molecular dynamics simulation of atomic clusters in equilibrium with a vapour”, *Molecular Simulation*, 33, 3, (2007), 245-251
- Sandler S.I., “Chemical engineering and thermodynamics”, John Wiley& Son Inc., (1999)
- Schatschneider B., Liang J.J., Jezowski S., & Tkatchenko A., “Phase transition between cubic and monoclinic polymorphs of the tetracyanoethylene crystal: the role of temperature and kinetics”, *CrystEngComm*, 14, (2012), 4656-4663

- Sepliarsky M., Stachiotti M.G., & Migoni R.L., "Interface effects in ferroelectric PbTiO₃ ultrathin films on a paraelectric substrate", Phys. Rev. Lett., 96, (2006), 137603
- Shi W., & Johnson J.K., "Histogram reweighting and finite-size scaling study of the Lennard-Jones fluids", Fluid Phase Equilibria, 187-188, (2001), 171-191
- Sigfridsson E., & Ryde U., "Comparison of methods for deriving atomic charges from the electrostatic potential and moments", J. Comput. Chem., 19, 4,(1998), 377-395
- Signorini G.F., Righini R., & Schettino V., "Lattice dynamics of the orthorhombic phase of KClO₄: Ewald's method in molecular coordinates", Chem. Phys., 154, (1991), 245-261
- Singer K., & Smith W., "The classical and quantum-mechanical free energy of solid (Lennard-Jones) argon", Chem. Phys. Lett., 140, 4, (1987), 406-410
- Smith E.R., "Electrostatic energy in ionic crystals", Proc. R. Soc. Lond. A, 375, (1981), 475-505
- Smith J., MacNamara E., Raftery D., Borchardt T., & Byrn S., "Application of two-dimensional ¹³C solid-state NMR to the study of conformational polymorphism", J. Am. Chem. Soc., 120, (1998), 11710-11713
- Sokalski W.A., & Poirier R.A., "Cumulative atomic multipole representation of the molecular charge distribution and its basis set dependence", Chem. Phys. Lett., 98, 1, (1983), 86-92
- Sokalski W.A., & Sawaryn A., "Correlated molecular and cumulative atomic multipole moments", 87, 1, (1987), 526-534
- Sokalski W.A., Shibata M., Ornstein R.L., & Rein R., "Point charge representation of multicenter multipole moments in calculation of electrostatic properties", Theor. Chim. Acta, 85, (1993), 209
- Spackman M.A., "Potential derived charges using a geodesic point selection scheme", J. Comput. Chem., 17, 1,(1996), 1-18

- Spohr E., "Effect of electrostatic boundary conditions and system size on the interfacial properties of water and aqueous solutions", *J. Chem. Phys.*, 107, (1997), 6342-6348
- Srivastava U.C., Pandey R.S., & Upadhyaya K.S., "Lattice dynamical study of potassium bromide using theoretical approach", *Int. J. Phys. Sci.*, 5,7, (2010), 972-977
- Stone A.J., "Transformation between Cartesian and spherical tensors", *Molecular Physics*, 29, 5, (1975), 1461-1471
- Stone A.J., "Properties of Cartesian-spherical transformation coefficients", *J. Phys. A: Math. Gen.*, 9, 4, (1976), 485-497
- Stone A.J., "The description of bimolecular potentials, forces and torques: the S and V function expansions", *Molecular Physics*, 36, 1, (1978), 241-256
- Stone A.J., "Distributed multipole analysis, or how to describe a molecular charge distribution", *Chem. Phys. Lett.*, 83, 2, (1981), 233-239
- Stone A. J., "The theory of intermolecular interactions", Clarendon Press, Oxford, (1996)
- Stone A.J., "Distributed multipole analysis: Stability for large basis sets", *J. Chem. Theory Comput.*, 1, 6, (2005:a), 1128-1132
- Stone A.J., "Lattice sums and their derivatives for surface adlayers", *Molecular Physics*, 103, 18, (2005:b), 2427-2481
- Stone A.J., & Alderton M., "Distributed multipole analysis; Methods and applications", *Molecular Physics*, 100, 1, (2002), 221-233
- Stone A.J., & Tough R.J.A., "Spherical tensor theory of long-range intermolecular forces", *Chem. Phys. Lett.*, 110, 2, (1984), 123-129
- Stroud A.H. "Gaussian quadrature formulas", Prentice-Hall, (1966)
- Sutton A.P., "Temperature-dependent interatomic forces", *Philosophical Magazine A*, 60, 2, (1989), 147-159

- Sutton A.P., Mulheran P.A., & Stoneham A.M., “Direct free energy minimisation methods: application to grain boundaries”, *Phil. Trans. R. Soc. Lond. A*, 341, (1992), 233-245
- Tan T.B., Schultz A.J., & Kofke D.A., “Suitability of umbrella- and overlap-sampling methods for calculation of solid-phase free energies by molecular simulation”, *J. Chem. Phys.*, 132, (2010), 214103
- Taylor M.B., Barrera G.D., Allan N.L., & Barron T.H.K., “Free energy derivatives and structure optimization within quasiharmonic lattice dynamics”, *Phys. Rev. B*, 56, 22, (1997), 14380- 14390
- Taylor M.B., Barrera G.D., Allan N.L., Barron T.H.K. & Mackrodt W.C., “Shell: a code for lattice dynamics and structure optimisation of ionic crystals”, *Comput. Phys. Comm.*, 109, (1998), 135-143
- Theodorou D.N., & Suter U.W., “Detailed molecular structure of a vinyl polymer glass”, *Macromolecules*, 18, 7, (1985), 1467-1478
- Tiwari S.K., Pandey L.K., Shukla L.J., & Upadhyaya K.S., “van der Walls three body force shell model (VTSM) for the lattice dynamical studies of thallous bromide”, *Phys. Scr.*, 80, (2009), 065603
- Tiwari S.K., Shukla L.J., & Upadhyaya K.S., “Harmonic dynamical behaviour of thallous halides”, *Pramana—J. Phys.*, 74, 5, (2010), 793-804
- Tkatchenko A., & Scheffler M., “Accurate molecular van der Waals interaction from ground-state electron density and free-atom reference data”, *Phys. Rev. Lett.*, 102, (2009), 073005
- Torrie G.M. & Valleau J.P., “Monte Carlo free energy estimates using non-Boltzmann sampling: Application to sub-critical Lennard-Jones fluid”, *Chem. Phys. Lett.*, 28, 4, (1974), 578-581
- Torrie G.M. & Valleau J.P., “Nonphysical sampling distributions in Monte Carlo free-energy estimation: Umbrella sampling”, *J. Comput. Phys.*, 23, (1977), 187-199
- Tough R.J.A., & Stone A.J., “Properties of the regular and irregular solid harmonics”, *J. Phys. A., Math. Gen.*, 10, 8, (1977), 1261-1269

- Toukmaji A.Y., & Board J.A. Jr., “Ewald summation techniques in perspective: a survey”, Computer Physics Communications, 95, (1996), 73-92
- Troitskaya E.P., Chabanenko V.V., & Horbenko E.E., “Nonadiabatic effects in the lattice dynamics of compressed rare-gas crystals”, Phys. Sol. State, 47, 9, (2005), 1748-17584
- Troitskaya E.P., Chabanenko V.V., & Horbenko E.E., “Lattice dynamics in light rare-gas crystals under pressure”, Phys. Sol. State, 51, 10, (2009), 2121-2128
- Uzoh O.G., Cruz-Cabeza A.J., & Price S.L., “Is the fenamate group a polymorphophore? Contrasting the crystal energy landscapes of fenamic acid and tolfenamic acids”, Crys. Growth. Des., 12, 8, (2012), 4230-4239
- Valleau J. P., & Card D.N., “Monte Carlo estimation of the free energy by multistage sampling”, J. Chem. Phys., 57, 12, (1972), 5457-5462
- Van Der Berg T.H.M., & Van Der Avoird A., “Analytical two- and three-dimensional lattice sums for general multipole interactions”, Chem. Phys. Lett., 160, 2, (1989), 223-227
- van Eijk B.P., “Ab initio crystal structure predictions for flexible hydrogen-bonded molecules. Part III. Effect of lattice vibrations”, J. Comput. Chem., 22, 8, (2001), 816-826
- van Eijk B.P., & Kroon J., “Coulomb energy of polar crystals”, J. Phys. Chem. B, 101, (1997), 1096-1100
- van Eijk B.P., & Kroon J., “Comment on “Crystal structure prediction by global optimization as a tool for evaluating potentials: role of the Dipole moment correction term in successful predictions””, J. Chem. Phys. B, 104, (2000), 8089-1100
- van Eijk B.P., Mooij W.T.M., & Kroon J., “Ab initio crystal structure predictions for flexible hydrogen-bonded molecules. Part II. Accurate energy minimization”, J. Comput. Chem., 22, 8, (2001), 805-815

- Vasileiadis M., Kazantsev A.V., Karamertzanis P.G., Adjiman C.S., & Pantelides C.C., “The polymorphs of ROY: application of a systematic crystal structure prediction technique”, *Acta Cryst.*, B68, (2012), 677-685
- Vega C., & Noya E.G., “Revisiting the Frenkel-Ladd method to compute the free energy of solids: The Einstein molecule method”, *J. Chem. Phys.*, 127, (2007), 154113
- Vega C., Paras E.P.A., & Monson P.A., “Solid-fluid equilibria for hard dumbbells via Monte Carlo simulation”, *J. Chem. Phys.*, 96, 12, (1992), 9060-9072
- Vega C., Sanz E., Abascal J.L.F., & Noya E.G., “Determination of phase diagrams via computer simulation: Methodology and applications to water, electrolytes and proteins”, *J. Phys. Condens. Matter*, 20, (2008), 153101
- Venkataraman G., & Sahni V.C., “External vibrations in complex crystals”, *Rev. Mod. Phys.*, 42, 4, (1970), 409-470
- Viveros-Méndez P.X., & Gil-Villegas A., “Computer simulation of sedimentation of ionic systems using the Wolf method”, *J. Chem. Phys.*, 136, (2012), 154507
- Vočadlo L., Wall A., Parker S.C., & Price G.D., “Absolute ionic diffusion in MgO—computer simulations via lattice dynamics”, *Physics of the Earth and Planetary Interiors*, 88, (1995), 193-210
- Wallace D.C., “Thermodynamics of crystals”, Dover Publications, New York, 1972
- Wang H., Zhang P., & Schütte C., “On the numerical accuracy of Ewald, Smooth Particle Mesh Ewald and Staggered Mesh Ewald methods for correlated molecular systems”, *J. Chem. Thoery Comput.*, 8, (2012), 3243-4256
- Watson G.N., “A treatise on the theory of Bessel functions”, Cambridge University Press, (1944)
- Wedemeyer W., Arnautova Y.A., Pillardy J. Wawak R.J., Czaplewski C., & Scheraga H.A., “Reply to ‘Comment on ‘Crystal structure prediction by global optimization as a tool for evaluating potentials: Role of the dipole moment correction term in successful predictions’’ by B.P. van Eijk and J. Kroon”, *J. Chem. Phys.* B, 104, (2000), 8090-8092

- Welch G.W.A., Karamertzanis P.G., Misquitta A.J., Stone A.J., & Price S.L., "Is the induction energy important for modelling organic crystals?", *J. Chem. Theory Comput.*, 4, 3, (2008), 522-532
- Westacott R.E., & Rodger P.M., "Full-coordinate free-energy minimisation for complex molecular crystals: type I hydrates", *Chem. Phys. Lett.*, 262, (1996), 47-51
- Westacott R.E., & Rodger P.M., "A local harmonic study of clusters of water and methane", *J. Chem. Soc. Faraday Trans.*, 94, (1998), 3421-3426
- White J.A., "Lennard-Jones as a model for argon and test of extended renormalization group calculations" *J. Chem. Phys.*, 111, 20, (1999), 9352
- Whitehead C.E., Breneman C.M., Sukumar N., & Ryan M.D., "Transferable atom equivalent multicentered multipole expansion method", *J. Comput. Chem.*, 24, 4, (2003), 512-529
- Widom B., "Some topics in the theory of fluids", *J. Chem. Phys.*, 39, 11, (1963), 2808-2812
- Wilding N.B., and Müller M., "Accurate measurements of the chemical potential of polymeric systems by Monte Carlo simulation", *J. Chem. Phys.*, 101, (1994), 4324-4330
- Williams D.E., "Failure of net atomic charge models to represent the van der Waals envelope electric potential of n-alkanes", *J. Comput. Chem.*, 15, 7, (1994), 719-732
- Williams D.E., "Improved intermolecular force field for molecules containing H, C, N and O atoms with application to nucleoside and peptide crystals", *J. Comput. Chem.*, 22, 11, (2001), 1154-1166
- Williams D.E., & Cox S.R., "Nonbonded potentials for azahydrocarbons: the Importance of the Coulombic interaction", *Acta Cryst.*, B40, (1984), 404-417
- Williams D.E., & Houpt D.J., "Fluorine nonbonded potential parameters derived from crystalline perfluorocarbons", *Acta Cryst.*, B42, (1986), 286-295

- Wolf D., "Reconstruction of NaCl surfaces from a dipolar solution to the Madelung problem", Phys. Rev. Lett., 68, 22, (1992), 3315-3318
- Wolf D., Kebinski P., Phillipot S.R., & Eggebrecht J., "Exact method for the simulation of Coulombic systems by spherically truncated, pairwise r^{-1} summation", J. Chem. Phys., 110, 17, (1999), 8254-8282
- Woodcock L.V., & Singer K., "Thermodynamic and structural properties of liquid ionic salts obtained by Monte Carlo computation. Part 1.-Potassium chloride", Trans. Faraday Soc., 67, (1971), 12-30
- Woods A.D.B., Brockhouse B.N., Cowley R.A., & Cochran W., "Lattice dynamics of alkali halide crystals. II. Experimental studies of KBr and NaI", Phys. Rev., 131, 3, (1963), 1025-1029
- Woods A.D.B., Cochran W., & Brockhouse B.N., "Lattice dynamics of alkali halide crystals", Phys. Rev., 119, 3, (1960), 980-999
- Woods R.J., Khalil M., Pell W., Moffat S.H., & Smith V.H. Jr., "Derivation of net atomic charges from molecular electrostatic potentials", J. Comput. Chem., 11, 3, (1990), 297-310
- Yamawaki H., Aoki K., Kakudate Y., Yoshida M., Usuba S., & Fujiwara S., "Infrared study of phase transition and chemical reaction in tetracyanoethylene under high pressure", Chem. Phys. Lett., 198, 1-2, (1992), 183-187
- Yamawaki H., Sakashita M., Aoki K., & Takemura K., "Reversible phase transition between the metastable phases of tetracyanoethylene under high pressure", Phys. Rev. B, 53, 17, (1996), 11403-11407
- Yakub E., & Ronchi C., "An efficient method for computation of long-ranged Coulomb forces in computer simulation of ionic fluids", J. Chem. Phys., 119, 22, (2003), 11556-11560
- Yeh I.-C., & Berkowitz M.L., "Ewald summation for systems with slab geometry", J. Chem. Phys., 111, 7, (1999), 3155-3162

- Yu L., “Color changes caused by conformational polymorphism: optical – crystallography single-crystal spectroscopy, and computational chemistry”, J. Phys. Chem. A, 106, (2002), 544-550
- Zahn D., Schilling B., & Kast S. M., “Enhancement of the Wolf damped Coulomb potential: static, dynamic, and dielectric properties of liquid water from molecular simulation”, J. Phys. Chem. B., 106, (2002), 10725-10732
- Zare R.N., “Angular momentum”, Wiley Interscience, (1988)
- Zhang Y., & Maginn E.J., “A simple AIMD approach to derive atomic charges for condensed phase simulation of ionic liquids”, J. Phys. Chem. B, 116, (2012), 10036-10048
- Zwanzig R.W., “High-temperature equation of state by a perturbation method. I., Nonpolar gases”, J. Chem. Phys., 22, 8, (1954), 1420-1426

Appendix A—Relations for the $S_{l_I l_J l}^{m_I m_J}$ tensor

The equations obtained using the recurrence relation for the $S_{l_I l_J l}^{m_I m_J}$ are reported here for all the contributions to the electrostatic energy considered in our calculations for which analytical expressions were not available. These are the charge/quadruple, quadruple/charge, dipole/dipole, charge/octopole, octopole/charge, dipole/quadruple, quadruple/dipole, charge/hexadecapole, hexadecapole/charge, octopole/dipole, dipole/octopole and quadruple/quadruple.

Charge/Quadruple & Quadrupole Charge

$$S_{022}^{00} = (S_{011}^{00})^2 \cdot 2.0124611797481 - 0.223606796649979$$

$$S_{022}^{0\pm 1} = S_{011}^{0\pm 1} S_{011}^{00} \cdot 2.32379000772445$$

$$S_{022}^{0\pm 1} = S_{011}^{0\pm 1} S_{011}^{0\pm 1} \cdot 1.64316766725155$$

$$S_{202}^{00} = (S_{101}^{00})^2 \cdot 2.0124611797481 - 0.223606796649979$$

$$S_{202}^{\pm 10} = S_{101}^{\pm 10} S_{101}^{00} \cdot 2.32379000772445$$

$$S_{022}^{\pm 20} = S_{101}^{\pm 10} S_{101}^{\pm 10} \cdot 1.64316766725155$$

Dipole/Dipole

$$S_{112}^{m_I m_J} = S_{011}^{0m_{JJ}} S_{101}^{m_{II} 0} \cdot 1.6431676725155 - S_{110}^{m_I m_{JJ}} 0.316227766016837$$

Charge/Octopole & Octopole/Charge

$$S_{033}^{00} = S_{011}^{00} S_{022}^{00} \cdot 2.43975018237133 - S_{011}^{00} 0.436435780471984$$

$$S_{033}^{0\pm 1} = S_{011}^{00} S_{022}^{0\pm 1} \cdot 2.58774584753383 - S_{011}^{0\pm 1} 0.40089186286868638$$

$$S_{033}^{0\pm 2} = S_{011}^{00} S_{022}^{0\pm 2} \cdot 3.2732683535989$$

$$S_{033}^{0\pm 3} = S_{011}^{0\pm 1} S_{022}^{0\pm 2} \cdot 1.88982236504614$$

$$S_{303}^{00} = S_{101}^{00} S_{202}^{00} \cdot 2.43975018237133 - S_{101}^{00} 0.436435780471984$$

$$S_{303}^{\pm 10} = S_{101}^{00} S_{202}^{\pm 10} \cdot 2.58774584753383 - S_{101}^{\pm 10} 0.40089186286868638$$

$$S_{303}^{\pm 20} = S_{101}^{00} S_{202}^{\pm 20} \cdot 3.2732683535989$$

$$S_{303}^{\pm 30} = S_{101}^{\pm 10} S_{202}^{\pm 20} \cdot 1.88982236504614$$

Dipole /Quadruple & Quadruple/Dipole

$$S_{123}^{m_{li} m_{jj}} = S_{101}^{m_{li} 0} S_{022}^{0 m_{jj}} \cdot 1.88982265 - S_{121}^{m_{li} m_{jj}} 0.534522484$$

Where $S_{121}^{m_{li} m_{jj}}$ is obtained using the following equations:

$$S_{121}^{m_{li} 0} = S_{110}^{m_{li} 0} S_{011}^{00} 1.643167673 - S_{101}^{m_{li} 0} 0.316227766$$

$$S_{121}^{m_{li} \pm 1} = S_{110}^{m_{li} \pm 1} S_{011}^{00} 1.89736659610103 \mp i \cdot S_{111}^{m_{li} \pm 1} 0.774596669241485$$

$$S_{121}^{m_{li} \pm 2} = S_{110}^{m_{li} \pm 1} S_{011}^{0 \pm 1} 1.34164078649987$$

$$S_{213}^{m_{li} m_{jj}} = S_{011}^{m_{li} 0} S_{202}^{0 m_{jj}} \cdot 1.88982265 - S_{211}^{m_{li} m_{jj}} 0.534522484$$

Where $S_{211}^{m_{li} m_{jj}}$ is obtained using the following equations:

$$S_{211}^{0 m_{jj}} = S_{110}^{0 m_{jj}} S_{101}^{00} 1.643167673 - S_{011}^{0 m_{jj}} 0.316227766$$

$$S_{211}^{\pm 1 m_{jj}} = S_{110}^{\pm 1 m_{jj}} S_{101}^{00} 1.89736659610103 \mp i \cdot S_{111}^{\pm 1 m_{jj}} 0.774596669241485$$

$$S_{211}^{\pm 2 m_{jj}} = S_{110}^{\pm 1 m_{jj}} S_{101}^{\pm 10} 1.34164078649987$$

Charge/Hexadecapole & Hexadecapole/Charge

$$S_{044}^{00} = S_{033}^{00} S_{011}^{00} \cdot 2.67316915539091 - S_{022}^{00} 0.559016994374947$$

$$S_{044}^{0 \pm 1} = S_{033}^{0 \pm 1} S_{011}^{00} \cdot 2.76083723211315 - S_{022}^{0 \pm 1} 0.544331053951817$$

$$S_{044}^{0 \pm 2} = S_{033}^{0 \pm 2} S_{011}^{00} \cdot 3.08670986290868 - S_{022}^{0 \pm 2} 0.481125224324686$$

$$S_{044}^{0 \pm 3} = S_{033}^{0 \pm 3} S_{011}^{00} \cdot 4.04145188432738$$

$$S_{044}^{0 \pm 4} = S_{033}^{0 \pm 3} S_{011}^{0 \pm 1} \cdot 2.02072594216369$$

$$S_{404}^{00} = S_{303}^{00} S_{101}^{00} \cdot 2.67316915539091 - S_{022}^{00} 0.559016994374947$$

$$S_{404}^{\pm 10} = S_{303}^{\pm 10} S_{101}^{00} \cdot 2.76083723211315 - S_{202}^{\pm 10} 0.544331053951817$$

$$S_{404}^{\pm 20} = S_{303}^{\pm 20} S_{101}^{00} \cdot 3.08670986290868 - S_{202}^{\pm 20} 0.481125224324686$$

$$S_{404}^{\pm 30} = S_{303}^{\pm 30} S_{101}^{00} \cdot 4.04145188432738$$

$$S_{404}^{\pm 40} = S_{303}^{\pm 30} S_{101}^{\pm 10} \cdot 2.02072594216369$$

Dipole/Octopole & Octopole/Dipole

$$S_{134}^{m_{li} m_{jj}} = S_{033}^{0m_{jj}} S_{101}^{m_{li} 0} \cdot 2.0207259421639 - S_{132}^{m_{li} m_{jj}} 0.645497224367902$$

Where $S_{132}^{m_{li} m_{jj}}$ is calculated in the following way:

$$\begin{aligned} S_{132}^{m_{li} 0} &= S_{121}^{m_{li} 0} S_{011}^{00} \cdot 2.314550249431380 - S_{110}^{m_{li} 0} 0.281718084909506 \\ &\quad - S_{112}^{m_{li} 0} 0.890870806374748 \end{aligned}$$

$$\begin{aligned} S_{132}^{m_{li} \pm 1} &= S_{121}^{m_{li} \pm 1} S_{011}^{00} \cdot 2.45495126515491 - S_{110}^{m_{li} \pm 1} 0.258774584753383 \\ &\quad - S_{112}^{m_{li} \pm 1} 0.0818317088384969 \mp i \cdot S_{122}^{m_{li} \pm 1} 0.2362277956307670 \end{aligned}$$

$$S_{132}^{m_{li} \pm 2} = S_{121}^{m_{li} \pm 2} S_{011}^{00} \cdot 3.1052950170406 \mp i \cdot S_{122}^{m_{li} \pm 2} 0.597614304667197$$

$$S_{132}^{m_{li} \pm 3} = S_{121}^{m_{li} \pm 2} S_{011}^{0 \pm 1} \cdot 1.79284291400159$$

$$S_{314}^{m_{li} m_{jj}} = S_{303}^{m_{li} 0} S_{011}^{0m_{jj}} \cdot 2.0207259421639 - S_{312}^{m_{li} m_{jj}} 0.645497224367902$$

Where $S_{312}^{m_{li} m_{jj}}$ is calculated in the following way:

$$\begin{aligned} S_{312}^{0m_{jj}} &= S_{211}^{0m_{jj}} S_{101}^{00} \cdot 2.314550249431380 - S_{110}^{0m_{jj}} 0.281718084909506 \\ &\quad - S_{112}^{0m_{jj}} 0.890870806374748 \end{aligned}$$

$$\begin{aligned} S_{312}^{\pm 1m_{jj}} &= S_{211}^{\pm 1m_{jj}} S_{101}^{00} \cdot 2.45495126515491 - S_{110}^{\pm 1m_{jj}} 0.258774584753383 \\ &\quad - S_{112}^{\pm 1m_{jj}} 0.0818317088384969 \mp i \cdot S_{212}^{\pm 1m_{jj}} 0.2362277956307670 \end{aligned}$$

$$S_{312}^{\pm 2m_{jj}} = S_{211}^{\pm 2m_{jj}} S_{101}^{00} \cdot 3.1052950170406 \mp i \cdot S_{212}^{\pm 2m_{jj}} 0.597614304667197$$

$$S_{312}^{\pm 3m_{jj}} = S_{211}^{\pm 2m_{jj}} S_{101}^{\pm 1m_{jj}} \cdot 1.79284291400159$$

Quadruple/Quadruple

$$S_{224}^{m_{Ii}m_{Jj}} = S_{202}^{m_{Ii}0} S_{022}^{0m_{Jj}} \cdot 2.32405562926132 - S_{220}^{m_{Ii}m_{Jj}} 0.207869854820774 - S_{222}^{m_{Ii}m_{Jj}} 0.5$$

Where $S_{220}^{m_{Ii}m_{Jj}}$ and $S_{222}^{m_{Ii}m_{Jj}}$ are calculated as:

$$S_{220}^{00} = (S_{110}^{00})^2 2.012461179749810 - 0.223606797749979$$

$$S_{220}^{0\pm 1} = S_{110}^{0\pm 1} S_{110}^{00} 2.32379000772445$$

$$S_{220}^{0\pm 2} = S_{110}^{0\pm 1} S_{110}^{0\pm 1} 1.6431676725155$$

$$S_{220}^{\pm 10} = S_{110}^{\pm 10} S_{110}^{00} 2.32379000772445$$

$$S_{220}^{\pm 1\pm 1} = S_{110}^{\pm 1} S_{110}^{\pm 10} 2.683281572999750 + S_{110}^{\pm 1\pm 1} m_{Ii} m_{Jj} 0.774596669241484$$

$$S_{220}^{\pm 1\pm 2} = S_{110}^{\pm 1\pm 1} S_{110}^{0\pm 1} 1.89736659610103$$

$$S_{220}^{\pm 20} = S_{110}^{\pm 10} S_{110}^{\pm 10} 1.6431676725155$$

$$S_{220}^{\pm 2\pm 1} = S_{110}^{\pm 1\pm 1} S_{110}^{\pm 10} 1.89736659610103$$

$$S_{220}^{\pm 1\pm 2} = S_{110}^{\pm 1\pm 1} S_{110}^{0\pm 1} 1.34164078649987$$

$$S_{222}^{00} = S_{110}^{00} S_{112}^{00} 3.40168025708304 - (S_{202}^{00} + S_{022}^{00}) 0.534522483824847$$

$$S_{222}^{\pm 10} = S_{110}^{00} S_{112}^{\pm 10} 3.92792202424786 - S_{202}^{\pm 10} 0.534522483824847 \mp i \\ \cdot S_{122}^{\pm 10} 1.13389341902768$$

$$S_{222}^{\pm 20} = S_{110}^{\pm 1} S_{112}^{\pm 10} 2.77746029931765 - S_{202}^{\pm 20} 0.534522483824847$$

$$S_{222}^{0\pm 1} = S_{110}^{00} S_{112}^{0\pm 1} 3.92792202424786 - S_{022}^{0\pm 1} 0.534522483824847 \mp i \\ \cdot S_{212}^{0\pm 1} 1.13389341902768$$

$$S_{222}^{\pm 1\pm 1} = S_{110}^{00} S_{112}^{\pm 1\pm 1} 4.53557367611073 + m_{Ii} m_{Jj} S_{112}^{\pm 1\pm 1} 0.654653670707976 - m_{Ii} i \\ \cdot S_{122}^{\pm 1\pm 1} 1.13389341902786 - m_{Jj} i S_{212}^{\pm 1\pm 1} 1.13389341902786$$

$$S_{222}^{\pm 2\pm 1} = S_{110}^{\pm 10} S_{112}^{\pm 1\pm 1} 3.20713490294909 - \frac{m_{Ii}}{2} S_{212}^{\pm 2\pm 1} 1.13389341902786$$

$$S_{222}^{0\pm 2} = S_{110}^{0\pm 1} S_{112}^{0\pm 1} 2.77746029931765 - S_{022}^{0\pm 2} 0.534522483824847$$

$$S_{222}^{\pm 1\pm 2} = S_{110}^{0\pm 1} S_{112}^{\pm 1\pm 1} 3.20713490294909 - \frac{m_{Jj}}{2} S_{122}^{\pm 1\pm 2} 1.13389341902786$$

$$S_{222}^{\pm 2\pm 2} = S_{110}^{\pm 1\pm 1} S_{112}^{\pm 1\pm 1} 2.26778683805537$$

The components $S_{212}^{m_{Ii}m_{Jj}}$ and $S_{122}^{m_{Ii}m_{Jj}}$ that are necessary for the calculation of some components of $S_{222}^{m_{Ii}m_{Jj}}$ are calculated in the following way:

$$S_{212}^{0m_{Jj}} = S_{111}^{0m_{Jj}} S_{101}^{00} 2.32379000772445$$

$$\begin{aligned} S_{212}^{\pm 1m_{Jj}} &= S_{111}^{\pm 1m_{Jj}} S_{101}^{00} 2.68328157299975 \pm i \cdot S_{112}^{\pm 1m_{Jj}} 0.577350269189627 \mp i \\ &\quad \cdot S_{110}^{\pm 1m_{Jj}} 0.365148371670112 \end{aligned}$$

$$S_{212}^{\pm 2m_{Jj}} = S_{111}^{\pm 1m_{Jj}} S_{101}^{+10} 1.89736659610103$$

$$S_{122}^{m_{Ii}0} = S_{111}^{m_{Jj}0} S_{011}^{00} 2.32379000772445$$

$$\begin{aligned} S_{122}^{m_{Ii}\pm 1} &= S_{111}^{m_{Ii}\pm 1} S_{011}^{00} 2.68328157299975 \pm i \cdot S_{112}^{m_{Ii}\pm 1} 0.577350269189627 \mp i \\ &\quad \cdot S_{110}^{m_{Ii}\pm 1} 0.365148371670112 \end{aligned}$$

$$S_{122}^{m_{Ii}\pm 2} = S_{111}^{m_{Ii}\pm 1} S_{011}^{0+1} 1.89736659610103$$

It should be stressed here that the expressions given here are not unique equation (4-37) gives also other, completely equivalent, expressions for the calculation of the same $S_{l_il_jl}^{m_{Ii}m_{Jj}}$.

Appendix B—The term $T_s^2(l_{Ii}, l_{Jj}, m_{Ii}, m_{Jj}, \frac{1}{2})$

The calculation of the self correction term $T_s^2(l_{Ii}, l_{Jj}, m_{Ii}, m_{Jj}, \frac{1}{2})$ given by equation (5-34) requires the knowledge of the orientation dependence for all interactions up second order: charge/charge, charge/dipole, dipole/charge, charge/quadruple, quadruple/charge and dipole/dipole. While the value of the S_{000}^{00} is known equal to 1 (i.e. there is no orientation dependence for the charge/charge interaction) and analytical expressions are available for $S_{101}^{m_{Ii}m_{Jj}}$ and $S_{011}^{m_{Ii}m_{Jj}}$ (Price et al., 1984), there are no available analytical expressions for the second order interactions i.e. charge/quadruple ($S_{022}^{m_{Ii}m_{Jj}}$), quadruple/charge ($S_{202}^{m_{Ii}m_{Jj}}$) and dipole/dipole $S_{112}^{m_{Ii}m_{Jj}}$. Those are derived using the ladder operator method (Price et al., 1984) using as starting points the available analytical expressions for S_{022}^{00} , S_{202}^{00} and S_{112}^{00} (Stone, 1978).

Charge/quadrupole

$$\begin{aligned} S_{022}^{00} &= \frac{1}{2\sqrt{5}} [3(\hat{\mathbf{z}}_J \hat{\mathbf{r}})^2 - 1] \\ S_{022}^{01c} &= \sqrt{\frac{3}{5}} (\hat{\mathbf{x}}_J \hat{\mathbf{r}})(\hat{\mathbf{z}}_J \hat{\mathbf{r}}) \\ S_{022}^{01s} &= \sqrt{\frac{3}{5}} (\hat{\mathbf{y}}_J \hat{\mathbf{r}})(\hat{\mathbf{z}}_J \hat{\mathbf{r}}) \\ S_{022}^{02c} &= \frac{1}{2} \sqrt{\frac{3}{5}} [(\hat{\mathbf{x}}_J \hat{\mathbf{r}})^2 - (\hat{\mathbf{y}}_J \hat{\mathbf{r}})^2] \\ S_{022}^{02s} &= \sqrt{\frac{3}{5}} (\hat{\mathbf{x}}_J \hat{\mathbf{r}})(\hat{\mathbf{y}}_J \hat{\mathbf{r}}) \end{aligned}$$

Quadrupole /Charge

$$\begin{aligned} S_{202}^{00} &= \frac{1}{2\sqrt{5}} [3(\hat{\mathbf{z}}_I \hat{\mathbf{r}})^2 - 1] \\ S_{202}^{1c0} &= \sqrt{\frac{3}{5}} (\hat{\mathbf{x}}_I \hat{\mathbf{r}})(\hat{\mathbf{z}}_I \hat{\mathbf{r}}) \\ S_{202}^{1s0} &= \sqrt{\frac{3}{5}} (\hat{\mathbf{y}}_I \hat{\mathbf{r}})(\hat{\mathbf{z}}_I \hat{\mathbf{r}}) \\ S_{202}^{2c0} &= \frac{1}{2} \sqrt{\frac{3}{5}} [(\hat{\mathbf{x}}_I \hat{\mathbf{r}})^2 - (\hat{\mathbf{y}}_I \hat{\mathbf{r}})^2] \\ S_{202}^{2s0} &= \sqrt{\frac{3}{5}} (\hat{\mathbf{x}}_I \hat{\mathbf{r}})(\hat{\mathbf{y}}_I \hat{\mathbf{r}}) \end{aligned}$$

Dipole /Dipole

$$\begin{aligned} S_{112}^{00} &= \frac{1}{\sqrt{30}} [(\hat{\mathbf{z}}_I \hat{\mathbf{z}}_J) - 3(\hat{\mathbf{z}}_I \hat{\mathbf{r}})(\hat{\mathbf{z}}_J \hat{\mathbf{r}})] \\ S_{112}^{01c} &= \frac{1}{\sqrt{30}} [(\hat{\mathbf{z}}_I \hat{\mathbf{x}}_J) - 3(\hat{\mathbf{z}}_I \hat{\mathbf{r}})(\hat{\mathbf{x}}_J \hat{\mathbf{r}})] \\ S_{112}^{01s} &= \frac{1}{\sqrt{30}} [(\hat{\mathbf{z}}_I \hat{\mathbf{y}}_J) - 3(\hat{\mathbf{z}}_I \hat{\mathbf{r}})(\hat{\mathbf{y}}_J \hat{\mathbf{r}})] \\ S_{112}^{1c0} &= \frac{1}{\sqrt{30}} [(\hat{\mathbf{x}}_I \hat{\mathbf{z}}_J) - 3(\hat{\mathbf{x}}_I \hat{\mathbf{r}})(\hat{\mathbf{z}}_J \hat{\mathbf{r}})] \\ S_{112}^{1c1c} &= \frac{1}{\sqrt{30}} [(\hat{\mathbf{x}}_I \hat{\mathbf{x}}_J) - 3(\hat{\mathbf{x}}_I \hat{\mathbf{r}})(\hat{\mathbf{x}}_J \hat{\mathbf{r}})] \\ S_{112}^{1c1s} &= \frac{1}{\sqrt{30}} [(\hat{\mathbf{x}}_I \hat{\mathbf{y}}_J) - 3(\hat{\mathbf{x}}_I \hat{\mathbf{r}})(\hat{\mathbf{x}}_J \hat{\mathbf{r}})] \\ S_{112}^{1s0} &= \frac{1}{\sqrt{30}} [(\hat{\mathbf{y}}_I \hat{\mathbf{z}}_J) - 3(\hat{\mathbf{y}}_I \hat{\mathbf{r}})(\hat{\mathbf{z}}_J \hat{\mathbf{r}})] \\ S_{112}^{1s1c} &= \frac{1}{\sqrt{30}} [(\hat{\mathbf{y}}_I \hat{\mathbf{x}}_J) - 3(\hat{\mathbf{y}}_I \hat{\mathbf{r}})(\hat{\mathbf{x}}_J \hat{\mathbf{r}})] \end{aligned}$$

$$S_{112}^{1s1s} = \frac{1}{\sqrt{30}} [(\hat{\mathbf{y}}_I \hat{\mathbf{y}}_J) - 3(\hat{\mathbf{y}}_I \hat{\mathbf{r}})(\hat{\mathbf{x}}_I \hat{\mathbf{r}})]$$

Using those expressions equation (5-34) can be evaluated and the result is summarised on the table

$(l_{ii}, l_{jj}, m_{ii}, m_{jj})$	$T_s^2 \left(l_{ii} l_{jj}, m_{ii}, m_{jj}, \frac{1}{2} \right)$
(0,0,0,0)	$\frac{4}{3}(\alpha\pi)^{3/2}$
(1,0, m_{ii} , m_{jj})	0
(0,1, m_{ii} , m_{jj})	0
(0,2,0,0)	$-\frac{6}{5\sqrt{5}}(\alpha\pi)^{5/2} \cdot \hat{\mathbf{z}}_J (\hat{\mathbf{z}}_J)^T + \mathbf{I} \frac{2}{5\sqrt{5}}(\alpha\pi)^{5/2}$
(0,2,0,1c)	$-\frac{2}{5}\sqrt{\frac{3}{5}}(\alpha\pi)^{5/2} \cdot [\hat{\mathbf{x}}_J (\hat{\mathbf{z}}_J)^T + \hat{\mathbf{z}}_J (\hat{\mathbf{x}}_J)^T]$
(0,2,0,1s)	$-\frac{2}{5}\sqrt{\frac{3}{5}}(\alpha\pi)^{5/2} \cdot [\hat{\mathbf{y}}_J (\hat{\mathbf{z}}_J)^T + \hat{\mathbf{z}}_J (\hat{\mathbf{y}}_J)^T]$
(0,2,0,2c)	$-\frac{2}{5}\sqrt{\frac{3}{5}}(\alpha\pi)^{5/2} \cdot [(\hat{\mathbf{x}}_J + \hat{\mathbf{y}}_J)(\hat{\mathbf{x}}_J - \hat{\mathbf{y}}_J)^T + (\hat{\mathbf{x}}_J - \hat{\mathbf{y}}_J)(\hat{\mathbf{x}}_J + \hat{\mathbf{y}}_J)^T]$
(0,2,0,2s)	$-\frac{2}{5}\sqrt{\frac{3}{5}}(\alpha\pi)^{5/2} \cdot [\hat{\mathbf{x}}_J (\hat{\mathbf{y}}_J)^T + \hat{\mathbf{y}}_J (\hat{\mathbf{x}}_J)^T]$
(2,0,0,0)	$-\frac{6}{5\sqrt{5}}(\alpha\pi)^{5/2} \cdot \hat{\mathbf{z}}_I (\hat{\mathbf{z}}_I)^T + \mathbf{I} \frac{2}{5\sqrt{5}}(\alpha\pi)^{5/2}$
(2,0,1c,0)	$-\frac{2}{5}\sqrt{\frac{3}{5}}(\alpha\pi)^{5/2} \cdot [\hat{\mathbf{x}}_I (\hat{\mathbf{z}}_I)^T + \hat{\mathbf{z}}_I (\hat{\mathbf{x}}_I)^T]$
(2,0,1s,0)	$-\frac{2}{5}\sqrt{\frac{3}{5}}(\alpha\pi)^{5/2} \cdot [\hat{\mathbf{y}}_I (\hat{\mathbf{z}}_I)^T + \hat{\mathbf{z}}_I (\hat{\mathbf{y}}_I)^T]$
(2,0,2c,0)	$-\frac{2}{5}\sqrt{\frac{3}{5}}(\alpha\pi)^{5/2} \cdot [(\hat{\mathbf{x}}_I + \hat{\mathbf{y}}_I)(\hat{\mathbf{x}}_I - \hat{\mathbf{y}}_I)^T + (\hat{\mathbf{x}}_I - \hat{\mathbf{y}}_I)(\hat{\mathbf{x}}_I + \hat{\mathbf{y}}_I)^T]$
(2,0,2s,0)	$-\frac{2}{5}\sqrt{\frac{3}{5}}(\alpha\pi)^{5/2} \cdot [\hat{\mathbf{x}}_I (\hat{\mathbf{y}}_I)^T + \hat{\mathbf{y}}_I (\hat{\mathbf{x}}_I)^T]$

Table 8-1 The self correction term for the different components of the contributions up to second order to the electrostatic energy hessian (equation 5-34).

$(l_{Ii}, l_{Jj}, m_{Ii}, m_{Jj})$	$T_s^2 \left(l_{Ii} l_{Jj}, m_{Ii}, m_{Jj}, \frac{1}{2} \right)$
(1,1,0,0)	$-\frac{2}{5\sqrt{30}}(\alpha\pi)^{5/2} \cdot [\hat{\mathbf{z}}_I(\hat{\mathbf{z}}_J)^T + \hat{\mathbf{z}}_J(\hat{\mathbf{z}}_I)^T] + \mathbf{I} \frac{4}{5\sqrt{40}} \hat{\mathbf{z}}_I \hat{\mathbf{z}}_J (\alpha\pi)^{5/2}$
(1,1,0,1c)	$-\frac{2}{5\sqrt{30}}(\alpha\pi)^{5/2} \cdot [\hat{\mathbf{z}}_I(\hat{\mathbf{x}}_J)^T + \hat{\mathbf{x}}_J(\hat{\mathbf{z}}_I)^T] + \mathbf{I} \frac{4}{5\sqrt{40}} \hat{\mathbf{z}}_I \hat{\mathbf{x}}_J (\alpha\pi)^{5/2}$
(1,1,0,1s)	$-\frac{2}{5\sqrt{30}}(\alpha\pi)^{5/2} \cdot [\hat{\mathbf{z}}_I(\hat{\mathbf{y}}_J)^T + \hat{\mathbf{y}}_J(\hat{\mathbf{z}}_I)^T] + \mathbf{I} \frac{4}{5\sqrt{40}} \hat{\mathbf{z}}_I \hat{\mathbf{y}}_J (\alpha\pi)^{5/2}$
(1,1,1c, 0)	$-\frac{2}{5\sqrt{30}}(\alpha\pi)^{5/2} \cdot [\hat{\mathbf{x}}_I(\hat{\mathbf{z}}_J)^T + \hat{\mathbf{z}}_J(\hat{\mathbf{x}}_I)^T] + \mathbf{I} \frac{4}{5\sqrt{40}} \hat{\mathbf{x}}_I \hat{\mathbf{z}}_J (\alpha\pi)^{5/2}$
(1,1,1c, 1c)	$-\frac{2}{5\sqrt{30}}(\alpha\pi)^{5/2} \cdot [\hat{\mathbf{x}}_I(\hat{\mathbf{x}}_J)^T + \hat{\mathbf{x}}_J(\hat{\mathbf{x}}_I)^T] + \mathbf{I} \frac{4}{5\sqrt{40}} \hat{\mathbf{x}}_I \hat{\mathbf{x}}_J (\alpha\pi)^{5/2}$
(1,1,1c, 1s)	$-\frac{2}{5\sqrt{30}}(\alpha\pi)^{5/2} \cdot [\hat{\mathbf{x}}_I(\hat{\mathbf{y}}_J)^T + \hat{\mathbf{y}}_J(\hat{\mathbf{x}}_I)^T] + \mathbf{I} \frac{4}{5\sqrt{40}} \hat{\mathbf{x}}_I \hat{\mathbf{y}}_J (\alpha\pi)^{5/2}$
(1,1,1c, 0)	$-\frac{2}{5\sqrt{30}}(\alpha\pi)^{5/2} \cdot [\hat{\mathbf{y}}_I(\hat{\mathbf{z}}_J)^T + \hat{\mathbf{z}}_J(\hat{\mathbf{y}}_I)^T] + \mathbf{I} \frac{4}{5\sqrt{40}} \hat{\mathbf{y}}_I \hat{\mathbf{z}}_J (\alpha\pi)^{5/2}$
(1,1,1c, 1c)	$-\frac{2}{5\sqrt{30}}(\alpha\pi)^{5/2} \cdot [\hat{\mathbf{y}}_I(\hat{\mathbf{x}}_J)^T + \hat{\mathbf{x}}_J(\hat{\mathbf{y}}_I)^T] + \mathbf{I} \frac{4}{5\sqrt{40}} \hat{\mathbf{y}}_I \hat{\mathbf{x}}_J (\alpha\pi)^{5/2}$
(1,1,1c, 1s)	$-\frac{2}{5\sqrt{30}}(\alpha\pi)^{5/2} \cdot [\hat{\mathbf{y}}_I(\hat{\mathbf{y}}_J)^T + \hat{\mathbf{y}}_J(\hat{\mathbf{y}}_I)^T] + \mathbf{I} \frac{4}{5\sqrt{40}} \hat{\mathbf{y}}_I \hat{\mathbf{y}}_J (\alpha\pi)^{5/2}$
$l \geq 3$	0

Table 8-2 The self correction term for the different components of the contributions from the third order to the electrostatic energy hessian (equation 5-34).